A DISTANCE ADAPTABLE BRAIN–COMPUTER INTERFACE BASED ON STEADY–STATE VISUAL EVOKED POTENTIAL

CHI-HSU WU

This thesis is submitted in partial fulfilment of the requirements for the **Degree of Doctor of Philosophy** in

Biomedical Engineering

Biomedical Engineering Department

University of Strathclyde

Glasgow, UK

Supervisor: Dr. Heba Lakany

April 2017

Declaration

This thesis is the result of the author′s original research. It has been composed by the author and has not been previously submitted for examination which has led to the award of a degree. 'The copyright of this thesis belongs to the author under the terms of the United Kingdom Copyright Acts as qualified by University of Strathclyde Regulation 3.50. Due acknowledgement must always be made of the use of any material contained in, or derived from, this thesis.

Signed:

Date:

Acknowledgements

First of all, I would like to thank my supervisor, Dr. Heba Lakany, for her time and valuable guidance for these years. I also would like to thank all colleagues in neurophysiology lab, all subjects participating the experiments and people who help me through this study. Finally, I want to thank Engineering and Physical Science Research Council (EPSRC) for funding this study and my families for their support and encouragement.

Abstract

Brain–computer interfaces (BCI) provide an alternative communication channel which does not rely on the brain′s normal output pathway between patients suffering from neuromuscular diseases and their external environment. BCI requires at least one brain signal as input in order to interpret the intent of the user. Non–invasive electroencephalography (EEG) is the most common and favourite method for acquiring brain signals. In the last two decades, several EEG based BCIs have been developed to help these patients. The brain signals which can be recorded in EEG and used as the input for BCIs include motor sensory rhythm, slow cortical potential, P300 and steady–state visual evoked potential (SSVEP). Compared to the other EEG based BCI paradigms, SSVEP based BCI has the advantage of high information transfer rate, high detection rate, less user training time required and commands scalability. Furthermore, SSVEP based BCI is normally operated in the self paced mode which is more intuitive and practical for real world applications. Recently, SSVEP based BCIs have attracted great attention in the field of BCI research.

While most SSVEP BCI studies focus on the improvement of signal detection and classification accuracy, there is a need to bridge the gap between BCI research and practice in the real world. SSVEP based BCI requires an external visual stimulator to elicit SSVEP response. Currently, for most SSVEP based BCIs, the viewing distances between the visual stimulator and the users are less than 100cm, limiting the usability and flexibility of BCI and its potential applications and users. This study proposes a novel distance adaptable SSVEP BCI paradigm which allows its users to operate the system from a range of viewing distances between the user and the visual stimulator. Unlike the conventional SSVEP BCI where users can only operate the system when they are sitting in front of the visual stimulator at a fixed distance which is normally less than 100cm, in our proposed system, users can operate the BCI at any viewing distance within the range in this proposed BCI. It is hoped that the proposed BCI system can improve the usability and the flexibility of BCI and also broaden the range of potential applications and users. For example, it can be used by older people with degenerating mobility or by patients with impaired mobility in the care environment to support their independence. Moreover, it can also be used by healthy people in a smart home or for a game control environment.

The primary goal of the present study is to investigate the feasibility of the proposed distance adaptable SSVEP based BCI. This study first investigates the

impact of the viewing distance on SSVEP response and compensates the deteriorated SSVEP resulting from the viewing distance by changing the intensities of the visual stimuli. 10 healthy subjects participate in the experiment to assess the feasibility of the distance adaptable SSVEP based BCI. The feasibility of the system is evaluated by the classification performance of off–line experiments at different viewing distances. The classification accuracies of the proposed BCI are examined by different EEG time window lengths, number of SSVEP harmonics and the number of recording electrodes employed. This study also investigates the sources of deterioration of SSVEP detection in BCI setup and proposes an electrode ranking method to select the recording electrodes for the implementation of the real time on line system.

The experimental results demonstrate that a distance adaptable SSVEP BCI is achievable and that electrodes chosen by the proposed electrode ranking method outperform electrodes chosen by random selection in classification performance.

List of Abbreviations

ANOVA	Analysis of Variance
AUC	Area Under Curve
BBCI	Berlin Brain–Computer Interface
BCI	Brain–Computer Interface
CAR	Common Average Reference
CCA	Canonical Correlation Analysis
CSP	Common Spatial Patterns
c–VEP	code modulated Visual Evoked Potential
ECG	Electrocardiography
ECoG	Electrocorticography
EEG	Electroencephalography
EMG	Electromyography
EOG	Electrooculography
ERD	Event–Related De–synchronisation
ERP	Event Related Potential
ERS	Event–Related Synchronisation
ERSP	Event Related Spectral Perturbation
FFT	Fast Fourier Transform
fMRI	functional Magnetic Resonance Imaging
fp(r)	False Positive Rate
fTCD	functional Transcranial Doppler Sonography
hBCI	hybrid Brain–Computer Interface

HCI	Human Computer Interface
IC	Intentional Control
ICA	Independent Component Analysis
ITC	Inter–Trial Coherence
ITR	Information Transfer Rate
LED	Light Emitting Diode
LFP	Local Field Potential
MCC	Maximum Contrast Combination
MEA	Micro Electrode Array
MEC	Minimum Energy Combination
MEG	Magnetoencephalography
MFSC	Multiple Frequencies Sequential Coding
MI	Motor Imagery
MON	Minimal Optimal Number
m–VEP	motion Visual Evoked Potential
NC	No Control
NIRS	Near Infrared Spectroscopy
PBR	Practical Bit Rate
PCA	Principle Component Analysis
PET	Positron Emission Tomography
PI	Performance Index
PSDA	Power Spectral Density based Analysis
ROC	Receiver Operating Characteristic
SCP	Slow Cortical Potential
SLIC	Stimulus Locked Inter–trace Correlation
SMR	Sensor Motor Rhythm
SNR	Signal to Noise Ratio
SR	Symbol Rate

SSVEP	Steady—State Visual Evoked Potential
TBR	Theoretical Bit Rate
tp(r)	True Positive Rate
TWL	Time Window Length
VEP	Visual Evoked Potential
WSR	Written Symbol Rate

Contents

List of Figures

Page

List of Tables

Chapter 1

Introduction

Brain–computer interfaces (BCI) provide an alternative communication channel which does not rely on the normal motor output of the nervous system between users and their external environment (Wolpaw et al., 2000; Shih et al., 2012; Xu et al., 2013; Lesenfants et al., 2014). BCI requires at least one brain signal associated with a task from the user in order to interpret the user's intent. BCIs can use invasive or non–invasive methods to obtain the brain signal. Non–invasive (surface) electroencephalography (EEG) is the most common and preferred method to acquire the brain signal due to its low risk, low cost and easy setup (Wolpaw et al., 2002). Brain signals, such as sensor motor rhythms (SMR), slow cortical potentials (SCP), visual evoked potentials (VEP), steady–state visual evoked potentials (SSVEP) and P300, can be used as the input of BCIs. These BCI paradigms have successfully translated brain signals into control commands (Wolpaw et al., 2000; Martinez et al., 2007). Compared to other BCI paradigms, SSVEP based BCI can offer a higher accuracy rate, a higher information transfer rate, better scalability and requires less training time (Martinez et al., 2007; Bin et al., 2009b; Kelly et al., 2005d). SSVEP is the brain response to the repetitive visual stimulus of frequencies over 6Hz and can be recorded in EEG (Bin et al., 2009b; Kelly et al., 2005d; Lin et al., 2006; Piccini et al., 2005).

1.1 Aims of this study

SSVEP based BCI has demonstrated that it can provide a reliable channel to the users to communicate and control an external device in several studies. For example, Volosyak (2011) proposed a speller based on SSVEP. The mean classification accuracies and information transfer rates (ITR) were over 95% and over 60 bits/min. An environment controller comprising 48 commands was implemented by Gao et al. (2003) and achieved ITR 68 bits/min. A mental speller, also based on SSVEP, which allowed spelling one letter by one selection utilising 30 LEDs to present a conventional QWERTY keyboard of 26 letters and 4 symbols, was developed by Hwang et al. (2012). The reported ITR exceeded 40 bits/min. These aforementioned studies have shown that high ITR and classification accuracies can be achieved by SSVEP based BCIs. They also demonstrated that the superior performance of SSVEP BCI can be achieved by single or sequential selection

tasks.

Recently, SSVEP has been incorporated with other BCI paradigms to form the hybrid BCI system. For example, Edlinger et al. (2011) used a hybrid BCI comprising of SSVEP and P300 paradigms in an application for smart home control in a virtual reality environment. SSVEP was used to turn on/off the P300 component BCI which was used to select control commands. Savić et al. (2014) used a hybrid BCI combining SSVEP and SMRs paradigms in a functional electrical therapy for stroke patients. These studies also demonstrated the versatility of SSVEP based BCI.

Meanwhile, great effort has been made to overcome the obstacle of the number of frequencies available to encode visual stimuli. Four stimulating frequencies can present 6 to 10 visual stimuli by using dual frequencies to present one stimulus (Shyu et al., 2010; Hwang et al., 2013). Jia et al. (2011) encoded the visual stimulus by including phase information. In their study, 15 visual stimuli were created by 3 distinct frequencies. Furthermore, the stimulus was presented by multiple frequencies in a serial order in multiple frequencies sequential coding (MFSC) (Zhang et al., 2012). The number of stimuli can be up to 9 in combinations of 2 coding epochs and 3 distinct frequencies by MFSC.

There are few SSVEP based BCI studies which attempted to improve SSVEP detection rates and reduce the calibration phase. Lin et al. (2006) proposed a SSVEP detection method based on canonical correlation analysis (CCA). Their proposed CCA SSVEP detection method estimated the CCA correlation coefficients between EEG signals and the reference signal corresponding to one stimulating frequency. The reference signal producing the largest CCA correlation coefficient was regarded as the attended target. Friman et al. (2007) proposed a SSVEP detection method which combined multiple electrodes signals into a channel signal to enhance SSVEP response and cancel noise. Both methods outperformed the conventional power spectral density analysis.

Currently, a few commercial EEG headsets are available, e.g. EMOTIV, which provides user friendly EEG acquisition, easy setup feature, wireless recording and have been evaluated and used in BCI studies (Lin et al., 2014). The aforementioned studies have offered a solid theoretical background in demonstrating the feasibility of SSVEP based BCI, from the fundamental visual stimuli to SSVEP detection. Therefore, there is a need to bridge the gap between BCI studies and real world applications.

SSVEP based BCI is an exogenous system which relies on an external visual stimulator in order to elicit the required SSVEP response. These visual stimulators are normally set close to the users at a distance less than 100cm (Hwang et al., 2012; Muller-Putz and Pfurtscheller, 2008; Savić et al., 2014) which limits the application of the BCI system. This study proposes a novel SSVEP based BCI which can adapt to the change in viewing distance between users and visual stim-

uli and allows its users to access BCI at a range of distances. In a conventional SSVEP based BCI system, the users have to be in front of the visual stimuli in order to operate the BCI. Such setup limits its flexibility and usability. The proposed new paradigm can improve accessibility, versatility and flexibility. It is hoped that this new proposed paradigm can broaden the potential target users and applications.

The distance adaptable feature can take advantage of a self paced system to enhance flexibility, increase potential applications and widen the range of potential users. SSVEP response is affected by the types, stimulating frequencies and colours of of visual stimulator. SSVEP response is sensitive to modulation depth of visual stimulator which is related to stimulus intensity. This study starts by investigating the impact of the viewing distance between the visual stimulator and the users on SSVEP response. The primary goals of the present study include:

1. Investigation of the impact of the viewing distance on SSVEP response.
2. Evaluation of the feasibility of a distance adaptable SSVEP based BCI allowing users to operate the BCI system at any given distance ($\leq$ 350cm).
3. Inspection of the practicality and reliability of a distance adaptable SSVEP based BCI.

1.2 Requirements of this study

From a functionality and design point of view, the proposed SSVEP based BCI should have the following features and requirements:

1. To provide a stable and reliable visual stimulator to elicit a SSVEP response.
2. To be able to adapt to the change in viewing distance so that the users can operate the system in a range of viewing distances.
3. To be able to detect SSVEP in a relatively short time.
4. To be user friendly and easy to use.

In order to evaluate the above requirements, the following have been developed in this study:

1. A visual stimulator consists of two modules, a visual stimulator module and a control module. The control module can provide stable and reliable visual stimulation. The number of stimuli and the frequencies are adjustable by custom–built software and hardware.
2. The intensity of the visual stimulator can be adjusted by changing the value of the resistor connected to it.
3. The implemented classification algorithms can classify EEG data efficiently, in terms of the accuracies and time required.

1.3 Achievements of this study

The primary goal of this study is to investigate the feasibility of the proposed distance adaptable SSVEP based BCI which can adapt to the change of the viewing distance between users and the visual stimulator and allows its users to operate the BCI in a range of distances. The following have been developed, implemented and evaluated:

1. A portable visual stimulator module: The visual stimulator module consists of a stimulating panel which contains four red LEDs and a control module based on a programmable microcontroller. The main functions of the control module include:

    - A stable and reliable square wave generator to control LEDs. Each square wave has a different frequency with 50% duty cycle: The frequency, the duty cycle of the square wave and the number of the visual stimuli can be modified by programming the microcontroller.
    - Synchronising the visual stimulator with the EEG acquisition equipment: Synchronisation is implemented by sending the event trigger signal to the EEG acquisition equipment.
    - Time control of the whole experiment.

2. Implementation of three classification methods: Three classification algorithms based on canonical correlation analysis (CCA), minimum energy combination (MEC) and maximum contrast combination (MCC) have been implemented using MATLAB. They are all multiple electrode based classification methods. The classification performance of three methods is compared. The result shows the performance of these three methods, CCA, MEC and MCC, is very similar in terms of the classification accuracy.

3. Investigation of impact of viewing distance on SSVEP: Inspecting the impact of viewing distance on SSVEP response in terms of power spectrum and the time– and phase–locking to stimulus properties. When the intensity of visual stimuli is the same, SSVEP power decreases and the time– and phase–locking to the stimulus become less prominent as the viewing distances increase.

4. Investigation of impact of EEG time window length and the number of SSVEP harmonics on the classification performance: It was found that in the proposed paradigm, the longer EEG recording time can improve the classification accuracies and the number of SSVEP higher harmonics has no significant impact on the classification accuracies.

5. Exploring the impact of the electrode number employed on classification performance: This study employed 11 electrodes for EEG acquisition. A comprehensive classification performance analysis based on all possible electrode combinations (over 2000 combinations) was performed.

6. Analysis of inter–subject variance: A comprehensive analysis on inter–subject variance in terms of the highest classification rates, the minimum number required to achieve the highest classification rates and the composite of optimal electrodes was conducted.

7. Identifying the source of deterioration of SSVEP classification accuracies: This study identified the sources which affect SSVEP detection.

8. Proposing a method to rank and select the electrodes: This study proposed a method to rank 11 pre–selected electrodes. The electrode rankings were used as the order/priority in selecting the electrodes. The results show that the electrodes selected via the proposed ranking method outperform the electrodes by random selection. The proposed method provides a quick and efficient way to select electrodes for data acquisition.

1.4 Contributions of this study

The main contributions of this study include:

1. Propose and demonstrate of the feasibility of a novel distance adaptable SSVEP based BCI. To the author′s best knowledge, this is the first study that evaluates and confirms the feasibility of a distance adaptable SSVEP based BCI.

2. Investigate the impact of viewing distance on SSVEP response in terms of power strength and other properties and how to compensate it. To the author′s best knowledge, this is the first study that investigates and confirms the impact of the viewing distance on SSVEP response.

3. Investigate the relationship between SSVEP response and the intensity of the visual stimulus.

4. Perform comprehensive analysis to investigate the impact of the number of electrodes over BCI classification accuracies. To the author′s best knowledge, this study provides the most comprehensive analysis for investigating the impact of the number of electrodes over BCI applications.

5. Propose and implement a simple, effective and flexible electrode selection method.

6. Investigate and identify the source of deterioration of SSVEP classification accuracies in BCI setup.

1.5 List of publications

1. Wu, Chi-Hsu, and Heba Lakany. "Evaluation of the feasibility of a novel distance adaptable steady–state visual evoked potential based brain–computer interface." Neural Engineering (NER), 2015 7th International IEEE/EMBS Conference on. IEEE, 2015.

2. Wu, Chi-Hsu, and Heba Lakany. "The Effect of the Viewing Distance of Stimulus on SSVEP Response for Use in Brain–Computer Interfaces." In Systems, Man, and Cybernetics (SMC), 2013 IEEE International Conference on, pp. 1840–1845. IEEE, 2013.

3. Wu, Chi-Hsu, and Heba Lakany. "Impact of Stimulus Configuration on Steady State Visual Evoked Potentials (SSVEP) Response." In COGNITIVE 2012, the Fourth International Conference on Advanced Cognitive Technologies and Applications, pp. 77–82. 2012.

1.6 Organisation of the thesis

The rest of this thesis is organised as follows: Chapter 2 gives an overview of BCI, in terms of its components, paradigms, users, applications, current limitations and challenges. It also provides an overview of the visual pathway of the eyes and the genesis of event related potentials. Chapter 3 describes the design of the experiments, including the visual stimuli, experiment protocols and the data recording and processing methods. The data analysis methods are also explained in Chapter 3.

Chapter 4 explores the impact of viewing distances on SSVEP response. In this chapter, power spectrum and time– and phase–locking properties of SSVEP are analysed and discussed. The classification performance with/without intensities of visual stimuli is also investigated.

Chapter 5 is the core of this thesis. The feasibility of a distance adaptable SSVEP based BCI is evaluated in this chapter. The classification performances corresponding to different EEG recording time and the number of SSVEP harmonics at different viewing distances are computed and compared. Practical BCI designing issues are also considered, such as the minimum number of electrodes required and the thresholds in the classification process.

Chapter 6 discusses the data analysis results. Chapter 7 is the conclusion of this study and also outlines the limitations, contributions and the future work of this study.

The pin–out diagram of the microcontroller, data sheets of LEDs used in this study and more figures and tables of the analysis results are included in Appendices.

Chapter 2

Overview of Brain–Computer Interface

Brain–computer interface (BCI) is a multi–disciplinary research collaborating the fields of neurology, physiology, mathematics, computer science, bio–signal processing and electronics engineering. This chapter starts by presenting a brief overview of BCI constituents and how BCI works.

Next we will focus on Electroencephalography (EEG) based BCI and review different EEG based BCI paradigms and their potential users and applications. EEG was discovered by Hans Berger in 1929 (Wolpaw et al., 2002). In 1973, Jaques Vidal published a paper which evaluated the feasibility to communicate directly between the brain and a computer (Vidal, 1973). In 1988, Farwell and Donchin (1988) proposed a P300 based mental speller. In 1999, short cortical potentials (SCP) based BCI allowed the users to type the letter after they underwent intensive training to learn to regulate their SCP (Birbaumer et al., 1999). Meanwhile, the research group in Wadsworth center (Shih et al., 2012) demonstrated that cursor movement can be controlled using mu rhythm in one and two dimensions. Finally, the limitations and challenges of SSVEP based BCI are discussed.

2.1 Components of BCI

Figure 2.1 illustrates a typical EEG based BCI block diagram which consists of modules for signal acquisition, signal pre–processing, signal feature extraction, classification, command translation and command execution (van Gerven et al., 2009). The classification result and the output of BCI are used to provide the feedback to the users. This loop starts off from the user who exerts an effort (i.e. performs a task) to generate a brain signal as an input to the BCI and closes with the feedback. Different BCI paradigms will require the users to perform different tasks. For example, in motor imagery paradigm, it requires the users to perform motor imagery task (1 in mental task/stimulation). For P300 BCI, users are required to attend a visual stimulator in matrix (2 in mental task/stimulation). For SSVEP based BCI, users are required to attend to the flickering of a visual stimuli (3 in mental task/stimulation).

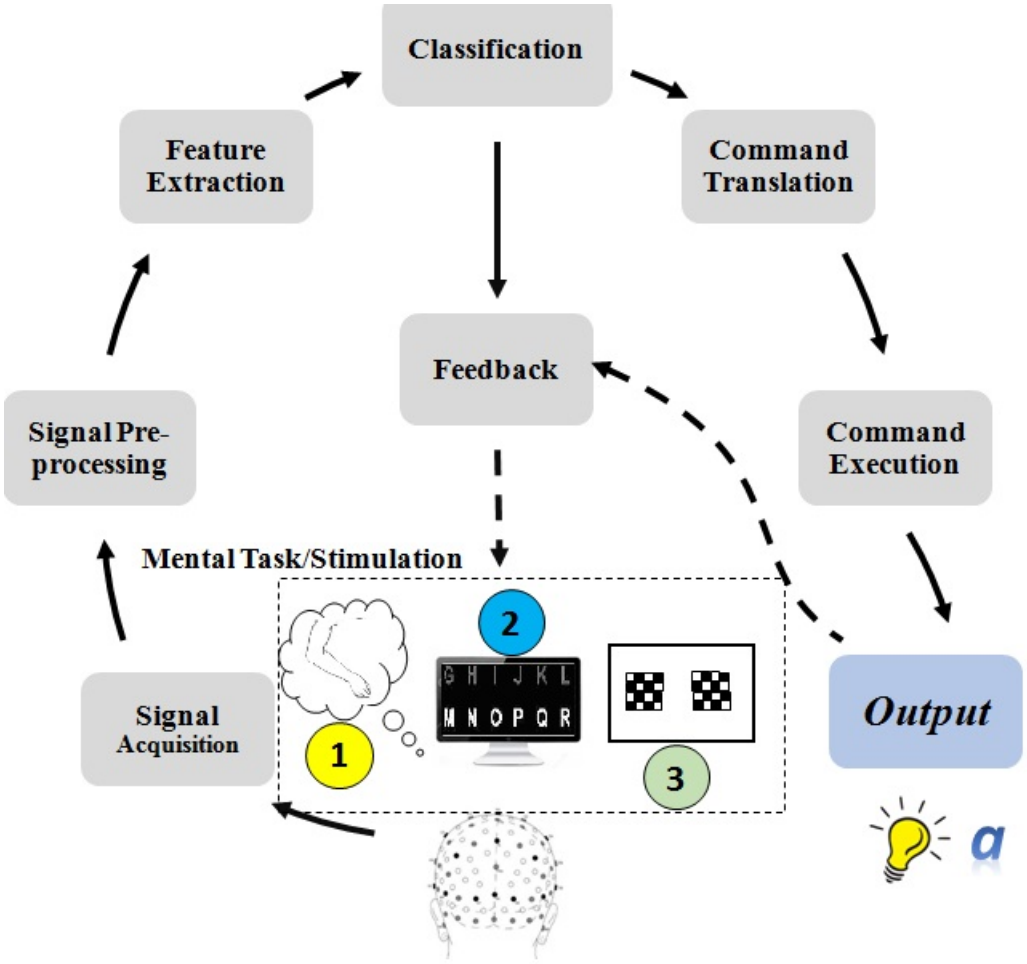

Figure 2.1: **A typical EEG based BCI block diagram.** BCI consists of modules for signal acquisition, signal pre-processing, feature extraction, classification, command translation, command execution and application output. The BCI loop starts when the user performs a task to generate a change in his/her brain signal which is used as the input of BCI and is closed by feedback to the user. **This figure is reprinted and modified from van Gerven et al. (2009) with permission from the publisher.**

- Signals: BCI could be classified to invasive or non–invasive systems according to the method of recording the brain signal from the users as input (Lebedev and Nicolelis, 2006). Invasive methods record the activity of single neuron, multiple neurons spiking and the local field potentials (LFP) directly from the surface of the cortex or intra–cortex. Invasive methods, such as electrocorticography (ECoG) and micro–electrode array (MEA), require to implant the electrodes inside the brain (van Gerven et al., 2009; Vallabhaneni et al., 2005). Although the invasive method is able to provide higher signal to noise ratio (SNR), higher temporal and spatial resolution, there are some concerns about the long term use of the implanted electrodes, in terms of stability, reliability and quality of the signal. Also there is the risk of infection during or after surgery (Vallabhaneni et al., 2005; Min et al., 2010).

The non–invasive methods include electroencephalography (EEG), magnetoencephalography (MEG), functional MRI (fMRI), near infrared spectroscopy (NIRS) and functional transcranial doppler sonography (fTCD) and positron emission tomography (PET) (Min et al., 2010). These methods are different in terms of the signal recorded, temporal resolution, spatial resolution, portability and cost but all record the brain activities. MEG, fMRI and PET are relatively expensive and technically demanding. NIRS detects the changes in the concentrations of oxyhemoglobin (HbO2) and deoxyhemoglobin (Hb). This measurement limits the temporal resolution of NIRS. fTCD is an ultrasound technique that detects the change of the cerebral blood flow velocity in major cerebral arteries. It has a limitation on the penetration depth and on targeting only major vessels (Min et al., 2010). Compared to invasive BCI, non–invasive BCIs require training. SNR and ITR are lower. It also requires intensive professional support (Birbaumer, 2006). Figure 2.2 compares the corresponding spatial and temporal resolutions using different signal acquisition techniques.

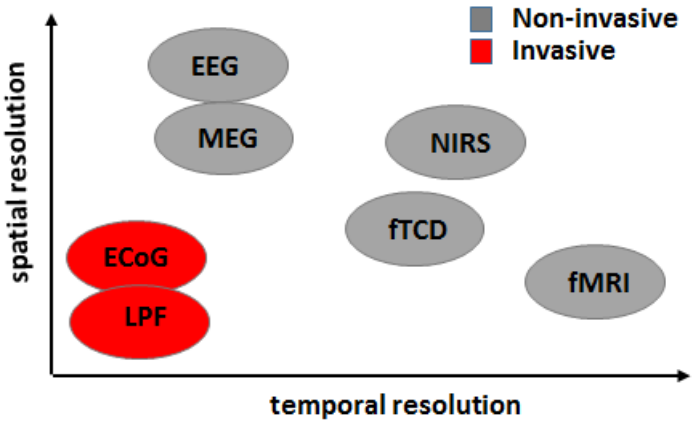

Figure 2.2: **A comparison of the spatial and temporal resolutions in different signal acquisition methods. This figure is reprinted and modified from van Gerven et al. (2009) with permission from the publisher.**

Surface EEG is to date the most favourite non–invasive method to record brain activity, due to its low cost, easy setup, high temporal resolution and its non–invasiveness. Unless specified, this thesis focuses on non–invasive EEG based BCI. EEG–based BCI requires at least one brain signal associated with an effort (i.e.task) exerted by the user as the input in order to interpret the user's intent. Depending on the BCI paradigm, the task which the users perform could be imagery of the hands' movement in what is known as an endogenous BCI or attending to a visual stimulus in the exogenous BCI.

- Signal acquisition: Surface EEG signals are weak signals in the order of micro volts. The recorded brain signal is amplified, digitised and stored ready for preprocessing, processing and analysing.

- Signal pre–processing: Signal pre–processing aims to enhance the signal before the features extraction phase. The signals are enhanced through artefacts removal, applying spectral filter and spatial filter (Al-ani and Trad, 2010; Bashashati et al., 2007; van Gerven et al., 2009):

    1. Artefacts removal: There are two types of EEG artefacts based upon their source: physiological and external artefacts. The physiological artefacts are difficult to avoid as they originate from the activities of the subject such as ocular (EOG), muscles (EMG) cardiac activities (ECG), respiration and sweating. EOG and EMG are the most problematic artefacts which affect EEG based BCI. Muscle activities such as chewing, swallowing produce artefacts in the frequency above 30Hz. On the other hand, ocular activities normally produce artefacts below 4Hz (Winkler et al., 2011; Fatourechi et al., 2007; Jafarifarmand and Badamchizadeh, 2013) External artefacts arise externally from the environment, such as power line interference, electrodes etc. External artefacts are reduced by applying proper spectral filter, for example a notch filter of 50Hz or 60Hz. EEG trials contaminated with the artefacts are either discarded or cleaned by removal of the artefacts (Fatourechi et al., 2007; van Gerven et al., 2009).
    2. Spatial filter: The signal could be optimised by applying spatial filtering and the resultant signal is a linear combination of the multiple electrodes. In a survey study (Bashashati et al., 2007), the following spatial filters were used to optimise EEG signal in BCI designs. These techniques are in two aspects, (1)re–referencing: e.g., common average reference (CAR), Laplacian transform, and (2) spatial filtering: e.g., principle component analysis (PCA), common spatial patterns (CSP), independent component analysis (ICA).

- Feature extraction: There are several properties of EEG signal that has been used as features for BCI classification. These features include the amplitude of the signal (Lee et al., 2008; Wolpaw and McFarland, 2004), the latency of the signal (Lee et al., 2011), band power (Pfurtscheller et al., 2000b; Blankertz et al., 2008a), time–locking to the stimulus property (Luo and Sullivan, 2010), Fast Fourier Transform (FFT) power (Gao et al., 2003), etc.

- Classification: The extracted features are classified by the classification algorithms and translate it to a control signal. (Bashashati et al., 2007). Currently, five different classification algorithms are used in EEG based BCI, (1) linear, (2) neural networks, (3) nonlinear Bayesian, (4) nearest neighbour, (5) a combination of classifiers in (1)–(4) (Lotte et al., 2007).

Lotte et al. (2007) suggested that the classification error could result from three types of errors, (1) system noise, (2) mapping bias and (3) variance caused by the training data. The system noise is unavoidable. To reduce the overall classification error, the mapping bias and variance caused by the training data has to be reduced. The two sources of the errors depend on the complexity and the stability of the classifiers. The classifiers with higher complexity (unstable) tend to have low bias error but high variance error. On the other hand, simple classifiers (stable) tend to have high bias with low variance (Lotte et al., 2007; Al-ani and Trad, 2010). The choice of the classifier is a compromise between the bias and variance.

Some post classification mechanisms can be put in place to reduce the misclassification error. For example, in the BCI proposed by Lee et al. (2008), the classification is made every one second. However, the classification is finalised only when the same classification is made in three successive times. A voting mechanism is employed in a SSVEP based BCI (Luo and Sullivan, 2010). The final classification is based on the voting result of the last few classifications. The feature threshold is also used to reduce the rate of false positives. For example, in an environment control system based on SSVEP BCI, the feature was FFT power at the stimulating frequency and the corresponding 2^{nd} harmonic. The threshold was the double of the mean power between 4 and 35Hz. The corresponding stimulating frequency which resulted in the maximum feature exceeding the threshold is recognised as the attended target. Otherwise the classification is rejected. It is clear that these post processing mechanisms are the trade–off between the false positive rates, system speed and the true positive rates (Bashashati et al., 2007).

- Command translation and execution: The control signal is translated to the physical signal which controls the device. The pre–defined corresponding action is executed and produces the output.

- Output: Depending on the output devices, the output could be a selected letter in a spelling application or a light bulb being switched on or off in an environment control system.

- Feedback: The classification result and the output of BCI show the users how BCI interprets their intention and are used to provide the users the feedback which in general is able to improve BCI performance.

2.2 Visual pathway of the eyes

This study focuses on steady–state visual evoked potential (SSVEP) based BCI. SSVEP response is elicited through the eyes. This section provides a short review on how the eyes work.

The eye consists of three distinct tunics (layers) as seen in Figure 2.3. From the outermost to the innermost, they are:

1. Outer fibrous tunic: this layer consists of the sclera and cornea. This part of the eye offers the support and protection of the eye shape and structure. It also provides an attachment point for the extrinsic muscles.

2. Middle vascular tunic: this layer consists of choroid, ciliary body and the iris. This part provides the routes for the blood vessels and lymphatics for the tissue of the eyes. Iris controls the light entering into the eyes by regulating the size of the pupil. Regulate the shape of the lens and control the aqueous humour circulating in the chambers of the eyes.

3. Inner nervous tunic: this layer consists of the retina. Retina transfers the light into electrical signal and sends the visual information to the brain by optic nerves.

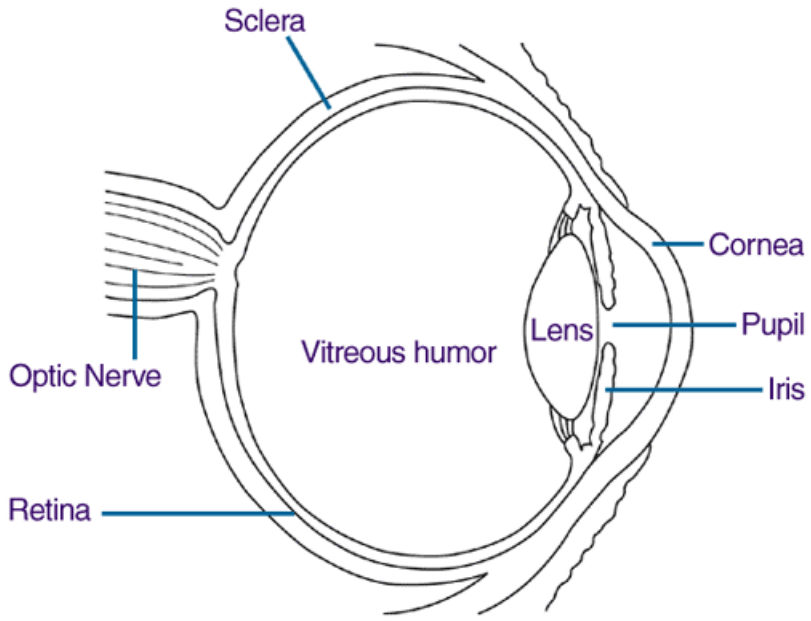

Figure 2.3: **Human eye structure. Courtesy: National Eye Institute, National Institutes of Health (NEI/NIH). Website: https://www.nei.nih.gov.**

The process of the human vision is as following:

1. The lights of the object enter the eyes through the cornea.

2. The lights then go through the pupil. The size of the pupil is controlled by the iris. The amount of the lights enters the eyes is dependent on the pupil size.

3. The lights pass through the lens next and reach the retina.

4. The retina is the tissue at the back of the eye balls with millions of light sensing nerve cells which turn the lights into electrical impulses.

5. The electrical impulses are sent to the brain by the optic nerve and the image is formed.

The retina is the innermost layer of the eye which consists of a pigmented retina and a sensory retina. The pigmented retina is a thin layer which can enhance the visual acuity and prevent the light bouncing back and scattering from the sensory retina. The sensory retina contains three types of the neurons, photoreceptors, bipolar and ganglionic. The visual network in the retinal is complicated. The photoreceptors synapse with the bipolar neurons which then synapse with ganglionic neurons. Between the photoreceptors and bipolar neurons, there exist horizontal cells. Between the bipolar and ganglionic neurons, there exist amacrine cells. Both cells can influence the interactions between photoreceptors, bipolar and ganglionic neurons. Thereby, change the perception of the vision. The axons of the ganglion cells converge at optic disc and leave the retina as the optic nerve. The two optic nerves, one from each eye, partially cross at optic chiasm. At this point, half of the fibres cross over and terminate in the lateral geniculate nucleus of the opposite side of the brain and half process to and terminate in the lateral geniculate nucleus of the same side of the brain. Most of the axons terminate in the lateral geniculate nucleus of the thalamus and some terminate in the superior colliculi. The visual information travels from the lateral geniculate nucleus and reach the visual cortex of the occipital lobe. The cells in different areas of the visual cortex are for different vision features, such as shape, movement and colour. The neurons of the visual cortex transfer the information into an image. The visual pathway starts from the photoreceptors to the visual cortex.

Two types of the photoreceptors which detect the light are called rods and cones. Rods are the photoreceptors which do not involve the discrimination the colours and enable human to see in the reduced light environment. The numbers of the rods are estimated 110–125 millions. On the other hand, cones are the photoreceptors which enable the human to have colour vision. The numbers of the cones are estimated approximately 7 millions. Three types of cones, termed as R–G–B cones, have different sensitivity curves to the wavelength of the light. The peak sensitivity of the curves of three cones do not accurately correspond to the colours of red, green and blue. Therefore, sometimes they are also named to correspond the peak sensitivity at the wavelength, i.e. long (L), medium (M) and short (S) wavelength. The wavelengths of the peak sensitivity of three cones are 564–580nm (L), 534–555nm (M) and 420–440nm (S). The numbers of these three types of the cones are not equal. The ratio of R:G:B cones is 40:20:1. In human eye, the maximum absorptions are 498nm, 440nm, 534nm and 564nm for the rods, B type cone, G type cone and R type cone respectively. The perception of the colour vision is subject to the various extents of the three types of the cones stimulated. For example, the colour of blue stimulates the S type cone more than the L and M type cones

Human visual system consists of three main pathways, the PC (Parvocellular) pathway, the MC (Magnocellular) pathway which process the specific visual information and has specific function (Vialatte et al., 2010; Duszyk et al., 2014; Di Russo et al., 2002). The MC and the PC begin from retina. The PC pathway carries the information of colours (red/blue), spatial contrast and shape. The MC pathway detects the motion and depth (Vialatte et al., 2010; Duszyk et al., 2014). The MC pathway has characteristics of higher conduction velocity, faster adaptation to stationary stimulus, larger receptive field and lower contrast sensitivity compared to the PC pathway. Visual stimuli with higher temporal frequency (5-40Hz) and low spatial frequency can preferentially activate the MC pathway. Visual stimuli with low temporal frequency and high spatial frequency can result in more activation in the PC pathway (Di Russo et al., 2002). Therefore, the contribution of the pathways on SSVEP is highly dependent on the properties of stimuli. For example, black and white checkerboards with high temporal frequency and low spatial frequency can evoke larger SSVEP in the MC pathway than in the PC pathway, while colour checkerboards at low temporal frequency and high spatial frequency can produce stronger SSVEP in the PC pathway than in the MC pathway (Vialatte et al., 2010).

2.3 BCI paradigms

This section starts from the discussion of origin of event–related potential in the views of the traditional evoked model and phas–rest model. Next, it provides an overview on different BCI paradigms based on different brain signals, including Sensor Motor Rhythm (SMR), event–related (de–) synchronisation (ERD/ERS), P300, and Visual Evoked Potential (VEP).

2.3.1 Genesis of event–related potential

The mechanism of the genesis of event related potential is unknown and a debatable matter in the neuroscience study (Barry, 2009; Sauseng et al., 2007; Klimesch et al., 2007). The traditional view of event related potentials (ERP) is that ERP is an additive evoked response to an event/stimulus independent from the ongoing EEG. It is a stimulus (time) locked response with fixed polarity and latency, the so called evoked model. ERP can be extracted by averaging several single trials. The background uncorrelated EEG will be filtered out by averaging. The rival model views ERP as the result of the phase re–organisation of (part of) the ongoing EEG, referred as phase–rest model (Sauseng et al., 2007; Moratti et al., 2007). It is argued that the traditional average method to enhance ERP might mislead the interpretation of ERP. The deflations of ERP components might reflect the instances of the phase–reset of ongoing EEG, instead of the interpretation of the classical evoked model (Jansen et al., 2003).

EEG can be characterised by the frequency, amplitude and phase of the oscillations. Frequency is related to the activation of the neuron region. Amplitude

reflects the level of neurons involvement to the process. Phase reflects the excitability of the neurons (Sauseng et al., 2007). To validate the mechanisms of ERP genesis involves the comparison of these characteristics before and after the event/stimulus. The characteristics of validating phase–rest model include (Barry, 2009; Sauseng et al., 2007; Shah et al., 2004):

1. Ongoing oscillation (frequency): To support phase–reset model, an ongoing EEG oscillation of the dominate frequency is expected to exist in pre–stimulus period to reset the phase.

2. Phase concentration (phase): A phase concentration must be seen in the post–stimulus period in phase–reset model.

3. Power (amplitude): Phase–rest should not induce change (increase) of the power at the dominate frequency.

4. Change of the sources of the neural activities: It is also expected the source of the brain activities overlapping in the pre–stimulus and post–stimulus periods in phase–rest model.

It is worthwhile to be noted that phase–reset model does not decline the evoked response outside the dominate frequencies but the phase–rest mechanism is the main contribution of averaging ERP (Shah et al., 2004).

However, it is argued that these characteristics are not appropriate and none of them provides clear evidence for phase–reset model to dissociate from the evoked model (Sauseng et al., 2007; Hanslmayr et al., 2007). For example, the evoked potential might be too small to be detected or masked by an event de–synchronisation (Sauseng et al., 2007). Another example is that phase concentration can be seen during ERP N1 component window period which a change of EEG amplitude might appear randomly (Hanslmayr et al., 2007). Furthermore, the evoked response of the similar periodicities to ongoing EEG can induce a phase concentration (Risner et al., 2009). Due to the scale of scalp EEG, it is hard to differentiate if the neural sources are exact the same before and after the stimulus onset (Sauseng et al., 2007).

Most of the studies assessing ERP mechanism cannot provide enough evidence to fully support one model and exclude the other. It is difficult to separate phase–reset from the evoked response and vice versa. To improve spatial resolution and temporal resolution in the recording and analysis methods will help to disentangle one from the other. Microelectrode (depth electrode) and intracranial EEG recordings provide higher spatial resolution, which help to understand the mechanisms (Sauseng et al., 2007). Fell et al. (2004) employed depth electrodes to record EEG and confirmed that evoked mechanism dominated in MTL–P300 and AMTL–N400 generation. However, phase rest model was not completely ruled out from the process. For MTL–P300 target response, a clear phase concentration and power increase were seen during the time period from 200ms to 500ms and at time period from 300ms to 1000ms respectively. So both models contributed

to P300. For AMTL–N400, initially, only phase–locked of hit response was observed from 100ms to 400ms without change of power. But at a later time course from 500ms to 800ms, a significant power was seen. But MTL–P300 non–target response is solely contributed by the phase–rest mechanism. Shah et al. (2004) conducted an animal experiment of the odd ball paradigm on a monkey which has multi–electrode arrays implanted. They supplied the evidence that evoked mechanism as the predominate role in the genesis of ERP. Like other studies, phase–rest model was not excluded from ERP generation. By the investigation of Event Related Spectral Perturbation(ERSP) and Inter–trial coherence (ITC) of P300 used in BCI, Ming et al. (2010) also confirmed that both mechanisms contributed to the generation of P300. ERSP and ITC are the measurement of event related power change and the degree of synchronisation between EEG and the event respectively Delorme and Makeig (2004). Moratti et al. (2007) investigated the relationship between spontaneous EEG and SSVEP. It was concluded that the change of SSVEP power during the stimulation was weak while the change of inter–trial phase locking (ITPL) was significant across most of the subjects. Phase–rest of ongoing EEG played a more important role than evoked model in the generation of SSVEP.

While none of the studies can provide exclusive evidence to support only one of the mechanisms, most studies demonstrated the contribution of each model on ERP components at different times (Moratti et al., 2007; Barry, 2009). Barry (2009) indicated that the early exogenous auditory ERP component mainly resulted from the phase–rest of the ongoing EEG. On the contrary, the later endogenous ERP component was mainly induced by evoked response. Another auditory ERP study by (Jansen et al., 2003) indicated that the auditory ERP in time range of 50–250ms was resulted from phase–rest of ongoing EEG. Hanslmayr et al. (2007) demonstrated that the phase–rest of alpha band contributed to VEP early component. Although a significant phase concentrate shown in delta band, the evoked model was not excluded from contributing to the later ERP components of this frequency band. Becker et al. (2008) investigated the impact of the alpha band on visual evoked potential by model simulation and experiment. The results of model simulation and experiment indicated that the early component of ERP was fit to the evoked mechanism and independent of the alpha band rhythm. But phase–rest of the alpha band rhythm contributed to the later ERP component.

The aforementioned studies could not conclude that ERP has solely resulted from either of the two models but the mixture of two. However, these studies did quantify the contribution of each mechanism. Understanding the genesis of ERP can provide a better picture of the cognitive process, neural information process and EEG response to external stimulus. For example, in SSVEP study, phase–rest was regarded to gate frequency tagged information flux and improved the SNR for neural processes (Moratti et al., 2007).

2.3.2 EEG based BCI brain signal

BCI detects the brain activity and translates it to an appropriate command. The change of the electrical oscillation can be induced either by the sensory stimulation or motor activities. Sensory stimulation results in event related potential while the motor behaviour, on the other hand, modulates the rhythms of EEG(Pfurtscheller and Lopes da Silva, 1999; Pfurtscheller and Neuper, 2010). Different EEG based BCI paradigms utilise different phenomena as the system inputs, including (Pfurtscheller and Neuper, 2001; Guger et al., 2011):

1. Sensor Motor Rhythm (SMR), event–related (de–)synchronisation (ERD/ERS)
2. Slow Cortical Potential (SCP)
3. P300
4. Visual Evoked Potential (VEP)

SCP based BCI needs intensive training and is less accurate but more stable and independent on sensory, motor and cognitive functions compared to the other paradigms (Guger et al., 2011). SCP is not a popular paradigm recently(Guger et al., 2011). The rest of this section will provide a brief overview on BCIs based on SMR, P300 and VEP.

2.3.2.1 Motor sensory

There exists a few rhythms in the brain signals which can be recorded in EEG, such as the alpha rhythm in the occipital area, Rolandic mu rhythm and central beta rhythm etc. Execution, imagination or observation of movement of the limbs can modulate the mu and beta rhythms which can be recorded from sensorimotor cortices. The phenomenon of the attenuation of mu rhythm over the contralateral sensorimotor cortex is termed as event–related de–synchronisation (ERD) which is associated to the movement or plan of movement. On the contrary, event–related synchronisation (ERS) is the phenomenon of the increase of mu rhythm which is associated to post–movement and relaxation (Pfurtscheller et al., 2000b; Pfurtscheller and Neuper, 2001, 2010; Blankertz et al., 2008a). The amplitude and the frequency of brain rhythms depend on the number of coherently activated neurons (Pfurtscheller, 2001). The more neurons that are synchronously activated, the larger the amplitude is and the lower the frequency is. The amplitudes of the rhythms are negatively correlated to the frequency and so does ERD/ERS(Pfurtscheller and Lopes da Silva, 1999).

Sensor–motor rhythm (SMR) BCI paradigm is based on the detection of the change of these rhythms to discriminate the subjects intent. SMR BCIs normally provide a cue to guide the users to perform the tasks in a pre–defined time window (Pfurtscheller and Neuper, 2001). As it takes time for the rhythms to change in response to the motor event, it was suggested the interval between two events should be at least 10s to allow ERD/ERS to develop and recover, especially for the alpha band (Pfurtscheller and Lopes da Silva, 1999). It was

also suggested that ERD distribution of imagery of one–side limb was limited to the contralateral sensorimotor cortex to actual movement (Pfurtscheller and Neuper, 2001). Imagery of movement is one of the preferable strategy in this BCI paradigm (Pfurtscheller and Neuper, 2001). Motor imagery tasks, such as imagining the movement of the right hand, left hand, foot and tongue can modulate SMR. ERD induced by hand movement imagery was observed in all subjects but the one by foot was not seen in every subject. (Pfurtscheller and Lopes da Silva, 1999; Pfurtscheller and Neuper, 2010). Therefore, it is crucial to determine the most suitable strategy for each subject.

One EEG feature of this BCI paradigm is the frequency band power of the rhythms. To extract this feature, EEG data were bandpass filtered. The frequency band of the bandpass filter is an important parameter in ERD/ERS analysis. It was suggested that the fixed frequency band might result in incorrect classification. Pfurtscheller and Lopes da Silva (1999) suggested three methods to determine this subject–specific parameter:

1. Reactive frequency: this method compares the power spectrum between the baseline and the active period. Depending on the frequencies of interest, the active period could be the preparation phase, execution phase or recovery phase. By comparison of the powers between baseline and active period, the most significant frequency band was found.

2. Continuous wavelet transform: the frequency band is found by time frequency analysis using the wavelet transform. The peak frequency found in the wavelet transform is more accurate than the method of comparison of power spectra.

3. Peak frequency: Klimesch et al. (1998) suggested to use the mean peak frequency f_a as the anchor for each frequency band of the rhythms. The bandwidth of each frequency band is 2Hz. f_a can be found by the following steps: (1) calculate the power spectrum of the mean EEG of all epoch of each electrode. (2) the peak frequency of each electrode can be found according to individual power spectrum. (3) f_a is obtained by averaging all the peak frequencies. The frequency bands of the band pass filter and band power are subject dependent.

Several groups have demonstrated that SMR BCI can provide a reliable, accurate and robust communication.

One of BCIs developed by Wadsworth BCI research group uses the brain signals of mu (8–12Hz) and beta (18–26Hz) rhythms (Wolpaw et al., 2000). The users learn to modulate mu and beta rhythm by motor imagery via the training sessions. It takes 2–3 weeks to the users to learn to communicate or control via BCI, such as answering a simple question, selecting items from a menu, moving a cursor in one, two or three dimensions and control a hand prostheses etc. Figure 2.4 illustrates an example of modulated mu rhythm corresponding to the top and bottom targets of cursor movement. In controlling the cursor in two

dimensions, each trial starts when the target appears. 1s later, the cursor shows in the centre of the monitor. The cursor begins to move until it hits one of the edges. If it hits the target, the cursor disappears and the target flashes for 1s as the reward. Otherwise, the cursor remains for 1s and the target disappears. The screen becomes blank for 1s and the next trial starts. Graz BCI group

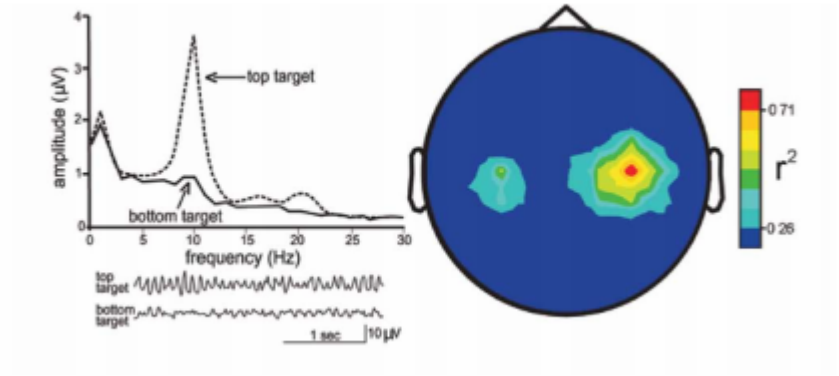

Figure 2.4: **EEG data in frequency domain and r^2 topography.**Users learn to modulate mu and beta rhythms to move the cursor. In this figure, mu rhythm for top target is more prominent than the button target. **This figure is reprinted from (Mak and Wolpaw, 2009) Copyright © 2009 IEEE.**

utilises ERD/ERS associated with motor imagery as the control signal. Graz BCI discriminates EEG patterns associated imagery (Pfurtscheller et al., 2000b). Similar to Wadsworth BCI, the participants of Graz BCI also included patients. Figure 2.5 shows ERD/ERS of C3 and C4 during imagery movement of right and left in Graz BCI experiment(Pfurtscheller et al., 2000b). The experiment starts with a training session without feedback. Each trial begins when a fixation cross is displayed at the centre of the screen. A beep is sounded at 2s after the onset of the cross. At 3s, the cue indicating to the right or left appears for 1.25s. The subject imagines the movement of his/her right or left hand according the direction of cue.

The data from the training session is used to train a subject dependent classifier. The classifier is applied later to an on–line experiment with feedback. There are two types of feedback, the delayed feedback and continuous feedback. In the delayed feedback experiment, the feedback is provided at the end of each trial. In the continuous feedback, the feedback provided to the users lasts for 4s in each trial. The classifier is updated after few feedback sessions.

Berlin Brain–Computer Interface (BBCI) is also based on the modulation of SMR (Blankertz et al., 2008a,b). The core of BBCI is machine learning which aims to transfer the learning/training to machines and reduce the training of the users. There are two phases operated in BBCI machine learning system, the calibration phase and feedback phase. In calibration phase, BCI classifier is trained by EEG data when the users perform the mental tasks without feedback. In feedback

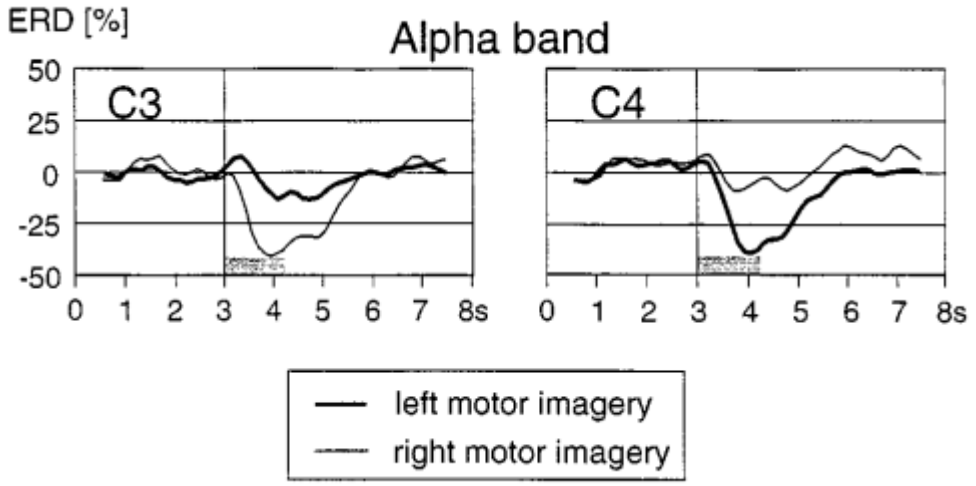

Figure 2.5: **Grand average ERD of C3 and C4 during the imagery movement of right and left.** The baseline is between 0.5s to 2.5s. ERD and ERS are the negative and positive deflections compared to the baseline. The gray bar stands for the time interval when the cue appears. **This figure is reprinted from (Pfurtscheller et al., 2000b) Copyright © 2000 IEEE.**

.

phase, BCI uses the output the classifier trained in calibration phase as the input of BCI application and provides the online feedback to users.

BBCI employs three types of motor imagery movements to modulate SMR, left hand, right hand and right foot. EEG recorded in calibration phase is used to train the classifier. The performances of three classifiers which contain two of the three imaginary movements are assessed. Two imaginary movements of the classifier which results in the best performance are chosen as the mental tasks for feedback phase. In feedback phase, the users move the cursor to one of the vertical bars located at two edges of the screen by performing the motor imagery. A trial starts after 750m after onset of the cue indicating the target to hit. A trial completes when the cursor hits one of the vertical bar. If the bar hit is correct, the bar turns to green. If the bar is hit incorrectly, it turns to red. The next trial starts after 520 ms. In a performance assessment study for fourteen nave to BCI, the mean accuracy of thirteen subjects in feedback session was 82.6% $\pm$ 11.4%. Figure 2.6 depicts the ERD of C3 and C4 and topography of imagery movement of right and left.

The research of SMR BCI is focused on optimisation of EEG features, selection of electrode locations, and frequency band power, choice of motor/imagery movement and spatial filters (Wolpaw et al., 2000; Pfurtscheller et al., 2000b; Blankertz et al., 2008a).

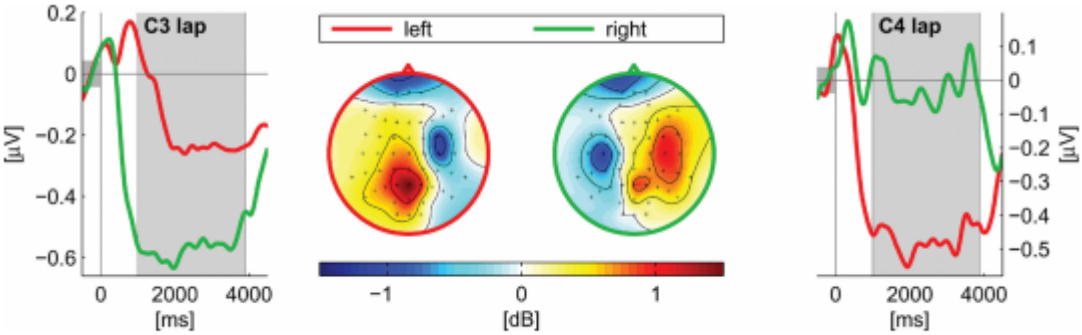

Figure 2.6: **EEG of electrodes C3 and C4 and topography during motor imagery of right and left hand.** ERD is significant at contralateral sensorimotor of the imagery movement. **This figure is reprinted from (Blankertz et al., 2008a) Copyright © 2008 IEEE.**

2.3.2.2 P300

P300 is a component of ERP which can be elicited by the oddball paradigm. In oddball paradigm, two stimuli are presented to the subjects. One of the stimuli is more frequent than the other. The infrequent stimuli are the rare and task–relevant targets (Polich, 2007; Hagen et al., 2006). The rare stimulus elicits ERP with a large positive deflection of a latency approximately 300ms (between 200ms to 700ms) after the stimulus onset and was prominent over parietal–occipital and fronto–central area. P300 can be elicited by many sensory modalities, for example, auditory, visual or tactile. A mental prosthesis speller based on P300 was first proposed by (Farwell and Donchin, 1988). In this P300 speller, a 6×6 matrix of letters and commands was presented to the subjects on a computer screen. In one intensified sequence (a trial), each row or column was intensified once in a random order. Hence each intensified sequence contained 12 flashes and only two of 12 were task–relevant and rare which constituted an oddball paradigm which elicited P300. The subjects were instructed to focus on the selected letter/command, one of 36 cells in the matrix. Subjects were also asked mentally to count the number of the selected target being intensified. P300 was detected by averaging EEG of the same row or the same column. The target was the intersection of the row and column which elicited P300.

P300 could be described by its amplitude and latency. Farwell and Donchin (1988) used the amplitude of P300 as the feature to identify the attended target. P300 has low SNR. This ratio was enhanced by averaging a couple of epochs (Farwell and Donchin, 1988). The amplitude of P300 could be affected by the interval between two targets. As the row and column was intensified randomly, the target to target interval was random too. Therefore, the inter–stimulus interval (ISI) could affect the detection of P300. In Farwell and Donchin (1988) study, the amplitude of averaged P300 elicited by longer ISI (500ms) was larger than but shorter ISI (125ms). ISI is an important parameter which could affect the accuracy and speed in P300 BCI paradigm. P300 can be affected by the

visual stimuli, such as the intensity and target probability (Polich et al., 1996). Sellers and Donchin (2006) investigated the impacts of matrix size (the number of the cells in the matrix), i.e. the probability of the target, and ISI on P300 based BCI. Two matrix sizes, 3×3 and 6×6, and two ISIs, 175ms and 350ms, were evaluated. The results suggested that although 6×6 matrix elicited larger P300, the combined condition of 3×3 and shorter ISI had highest classification accuracy than the other conditions. The impact of ISI was not consistent in the study of Farwell and Donchin (1988).

A speller is the most common application of P300 based BCI. The row–column (R–C) paradigm introduced by Farwell and Donchin (1988) to intensify the stimuli is the most popular paradigm to present the virtual keyboard. Two common errors might be induced by RCP. One of the errors is termed as adjacency distraction error. When the subjects try to focus their attention on the target cell, they might be distracted by the non–target cells at the same row or column and elicit a wrong P300. Another error is termed as double flashes error. This error occurs when the row and the column containing the target cell is intensified in succession. The elicited P300 of two successive flashes are overlapped in time and result in the change of amplitude and morphology (Townsend et al., 2010). Moreover, if the interval between two target flashes is less than 500ms, it may cause the attention blink or repletion blindness (Fazel-Rezai and Abhari, 2009). Recently, there were a few different methods to present the virtual keyboard to enhance the elicited P300 and prevent the perceptual errors to improve the accuracy. These paradigms were:

1. Single Character (S–C) paradigm: Guan et al. (2004) proposed P300 speller which intensified one single character a time. The background theory behind this method was that amplitude of P300 increased as the target probability decreased. As a result, P300 was easier to be detected. In their study, two spellers of the similar keyboard layout, one using R–C paradigm and one using S–C were compared. The results showed that S–C had higher classification accuracy and ITR than R–C paradigm so were the amplitudes of elicited P300. However, the results in the study of Guger et al. (2009) showed that R–C paradigm had better performance although the amplitudes of P300 elicited by S–C were larger. The author suggested that the letter selection time of S–C was longer than R–C paradigm. It might cause the tiredness of the subjects and hence reduced the performance. In the study of Guan et al. (2004), the interval of one intensification sequence of R–C and S–C paradigms were the same. Furthermore, more non–target training sets were used to train the SC paradigm classifier than those used for the R–C paradigm classifier.

2. CheckerBoard (C–B) paradigm: Townsend et al. (2010) proposed a checkerboard paradigm to solve the problems of adjacency distraction and double flashes. In this paradigm, an 8×9 matrix comprising the letters, symbols and commands were presented to the users as shown in Figure 2.7c. To explain how this paradigm worked, the matrix was viewed as a conventional

checkerboard of white and black cells as shown in Figure 2.7a. As a result, the selection was located in either a white or black cell as seen in Figure 2.7a. The selections in the white cells and black cells were further split into a 6×6 white matrix and a 6×6 black matrix in a random manner respectively as shown in Figure 2.7b. The flash sequence started from the rows of two matrices, from the first row to the last row, white matrix first and followed by black one. After all rows of two matrices flashed, the columns were flashed in a similar manner, from the most left column to the right column, white matrix first and followed by the black one. Six elements were presented to the subjects in each flash. After 24 flashes, the elements in both white and black matrices were randomly reallocated. The layout of the matrix remained the same to the subjects all the time as seen in Figure 2.7c. But the flash elements were different in between trials. In this paradigm, for each cell, its adjacent cells were in the opposite colour matrix. The flashing elements were either from the white or black matrix. The adjacent elements could not be included in the same flash. The adjacency distraction error was avoided. Moreover, once a cell flashed, it waits for the opposite colour matrix to flash for 6 rows or 6 columns before it flashed again. It took at least 6 further flashes for one cell to flash again and so the double flashes errors were eliminated. The classification accuracy and ITR of C–B paradigm were better than C–R paradigm (mean accuracy: 92% vs. 77%, ITR 23 bits/min vs. 17 bits/min). The amplitudes of P300 elicited by C–B paradigm were also larger than C–R paradigm. This might be contributed by the reduction of target probability of C–B paradigm.

3. Region based (R–B) paradigm: region based paradigm was proposed by Fazel-Rezai and Abhari (2009) to reduce adjacency distraction error. In R–B paradigm, the characters were grouped in seven different regions on the screen. Each region contained 7 characters as shown in Figure 2.8a. Each region was intensified randomly. The selection of one character in this paradigm required two selections. First selection was to select the region which contained the target. The characters of the selected region of the first selection were split into seven regions as shown in Figure 2.8b. Each character was intensified randomly. In this example, the circled region containing 3, 4, 5, 6, 7, 8 and 9 was selected. The numbers of the selected region were further expanded into 7 regions. The intensification of the target was similar to S–C paradigm but with larger scale in the first selection. Compared to the original C–R paradigm (6×6 matrix), R–B paradigm had higher accuracy than the C–R one. The author showed improvement to the reduction of adjacency distraction error and of the target probability.

These P300 based spellers used visual stimulus to elicit P300. As mentioned in the start of this session, auditory modality can also elicit P300. Furdea et al. (2009) developed an auditory P300 based BCI speller. In this auditory P300 system, a similar virtual keyboard (5×5 matrix, containing 25 alphabets) to Farwell and Donchin (1988) was presented to the subjects. A unique number was assigned to each row (1 to 5) and column (6 to 10). In the visual C–R paradigm P300 speller,

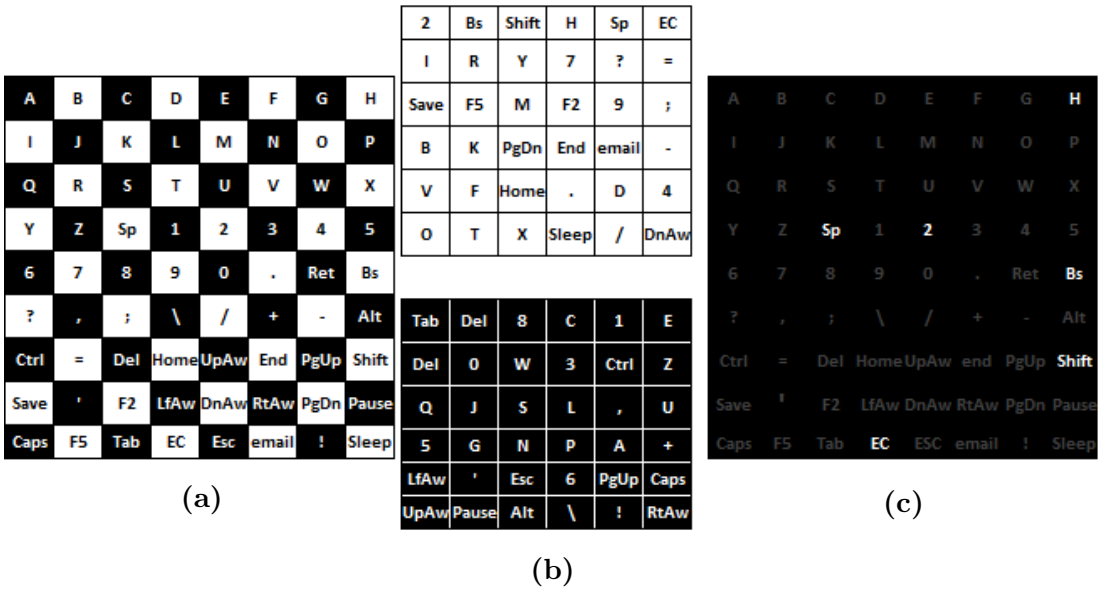

Figure 2.7: **An 8×9 matrix of P300 based BCI in checkerboard paradigm.**(a) A virtual conventional checkerboard divided the selections into white and black cells. The checkerboard was for the explanation purpose and wasnt seen by the subjects. (b) The elements of white cells and black cells were split into one white and one black checkerboard respectively randomly. After a complete flash sequence (24 flashes), these elements were split randomly again. These two matrices were not seen by the subjects. (c) The visual stimulus presented to the subjects during the trials. The locations of the elements were the same. But the intensified elements of each flash differed depending on the matrix shown in (b). The example showed the elements of top row of white matrix were intensified. **This figure is reprinted from (Townsend et al., 2010), page 1111, with permission from Elsevier.**

the target is coded by the intensified row and column. In an auditory P300 system, the stimuli are presented by the voice of a spoken number representing the row and column and the target is coded by the numbers assigned to the rows and columns. The task of the subjects is to focus on the numbers presenting the coordinates of the target and count their occurrence. The amplitudes of P300 elicited by auditory stimulus were not significantly different from the ones elicited by a visual one but had higher latencies. The accuracy and bit rates of auditory were lower than the visual system, mean accuracy 65%. A greater subject variance was seen from the accuracy of auditory system, from 100% to under 15% compared to a more consistent one in the visual stimulus system, 100% to 75%. However, 9 out of 13 subjects achieved over 70% accuracy. This modality of P300 BCI demonstrated its feasibility to most subjects.

Käthner et al. (2013) also employed the auditory modality to elicit P300. In their study, a 5×5 matrix same as Furdea et al. (2009) was presented to the subjects to show the coordinates of the targets. The row and column were coded by the direction and pitch of a tone. Five different combinations of the directions and pitches represented in five columns. The same combinations of the directions and pitches presented in five rows. The tone sequence first presented the columns

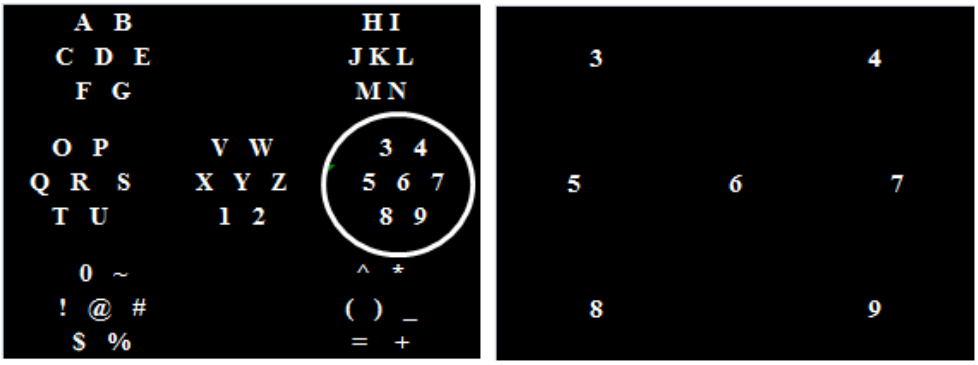

(a) **(b)**

Figure 2.8: **Visual stimulus of P300 based BCI in region based paradigm.** In region based paradigm, the characters were allocated into 7 regions. Each region was intensified in random order. One target required two successive selections. (a) The layout of the regions in the first selection. Each region contained 7 characters. (b) When one of the regions was identified as the selection, the characters of the selected region were further separated into 7 regions. Each region contained only one character as shown in the right of the figure. **This figure is reprinted from (Fazel-Rezai and Abhari, 2009), Copyright © 2009 IEEE.**

followed by the sequence presenting the rows. The subjects selected the target by focusing on the tones for the column and the row of the target. Several ISIs were tested in the experiment to determine the optimal accuracy and speed. Data analysis showed that compared to the visual paradigm, auditory stimulus elicited larger P300 with greater latency at ISI = 560ms. The accuracy and bit rate of the auditory paradigm were lower than the visual. Moreover, the accuracy decreased as ISI decreased. The performance of the accuracy also showed a greater inter–subject variance. For ISI = 400ms, the mean accuracy was 65% ± 31.03%. Sixteen out of twenty subjects achieved ≥ 70% of accuracy at least one of ISIs. The author concluded that auditory P300 BCI was feasible to most healthy subjects. But its performance could not level with the visual one, in terms of the accuracy and bit rate etc.

Brouwer and Van Erp (2010) examined the feasibility of a tactile modality of P300 BCI. The tactile stimuli were implemented by vibrating tactors placed around the waists of the subjects. Three experiments were performed to evaluate the impact of the tactor number, stimulus onset asynchrony (SOA) and the duration of on off on BCI performance. It was found that in tactile modality, the tactor (target) number had no significant impact on the accuracy. However, the fewest tactor number (2) elicited smaller amplitude of P300 response. SOA and the durations of tactor on and off all affected BCI performance. In their experiment, it was found that the medium SOA (=376ms) with same duration of on off (=188ms) yielded the best mean performance with a mean ITR=3.71 bits/min while the highest bit rates were seen in shorter SOA. The study demonstrated the feasibility of tactile P300 BCI. However, the author concluded that it required further improvement before it could be applied to any potential application.

For patients with visual impairment, the auditory and tactile modalities P300 BCI can provide an alternative option other than the visual one. However, these modalities manipulate the level of discrimination task difficulties and workload of the users. As a consequence, it affects the performance. For example, in Brouwer and Van Erp (2010), some subjects reported the difficulties of discriminating the target and the adjacent non–target tactors. The author also suggested that in the visual modality, there was a visual perception difference between target and non–target but not in the tactile modality. In the auditory modality of Käthner et al. (2013), the subject also reported difficulties in ignoring the non–targets. The author had similar comments on the perception of the targets and non–targets in visual modality which could not apply to the auditory modality. The discrimination task of the auditor modality proved more difficult and demanding which might increase the workload of the users and affect the resulting P300. Both studies pointed out that the motivation of the subjects is a factor which affects BCI performance.

2.3.2.3 Visual Evoked Potential (VEP)

VEP based BCI paradigms are based on different types of VEPs as the control signal, mainly flash visual evoked potential (FVEP), SSVEP and code modulated visual evoked potential (c–VEP) (Bin et al., 2009a; Lee et al., 2008). Visual stimuli are required in VEP based BCI to elicit the visual evoked potential. In FVEP paradigm, visual stimuli are modulated by different duration of ON–OFF sequences. FVEP is time–locked and phase–locked to the stimuli onset or offset. EEG is segmented according to the sequences of ON–OFF of stimuli. The sequence of the stimulus results in the largest FVEP is identified as the attended target (Lee et al., 2008). In SSVEP paradigm, each visual stimulus is modulated by a unique flickering frequency. EEG data can be transferred to the frequency domain. Induced SSVEP can be observed prominent at the flickering frequency and/or its harmonics. The attended target can be identified by the frequency with the largest SSVEP. c–VEP can be induced by the visual stimuli modulated by a pseudorandom binary sequence. All stimuli are modulated by the same binary sequence except a fixed time lag between two successive stimuli. This paradigm assumes that the induced VEP is identical from trial to trial, a response which can be predictable. The target can be identified by matching the templates of the stimuli (Bin et al., 2009a, 2011). In short, the visual stimuli of three VEP based BCIs are modulated by the time, the frequency and the code. Both FVEP and c–VEP systems require synchronous signal for the onset of the stimuli (Bin et al., 2009a).

Lee et al. (2008) implemented a FVEP based BCI. The visual stimuli were modulated by the sequences of random duration of ON and OFF. The sequence was mutually independent between the stimuli. EEG data were segmented by the sequences of stimuli onset and offset. FVEP was enhanced by average of a few (10) epochs. FVEP showed clear latencies at valleys N1, N2 and peaks P1, P2. The properties of the latencies and voltages were extracted as the classification

features. These peaks and valleys were found in 200ms after the onset or offset of the stimuli. P2 and N2 were observed more prominent in FVEP induced by onset of the stimulus. P1 and N1, on the contrary, were more robust in FVEP induced by the offset of the stimulus. The difference between P2 and N2 of onset induced FVEP and the difference between P1 and N1 of offset induced FVEP were calculated. The sequence of the stimulus resulting the largest peak–valley of above two differences was identified as the attended target. In this paradigm, one of the key parameters was the number of epochs which were averaged to enhance FVEP. The number of epochs could affect the accuracy and speed. On one hand, increasing this number improved the accuracy. On the other hand, more epochs decreased the processing speed. In their experiment, 10 epochs averaging achieved accuracy higher than 90%.

The latencies of the peaks and valleys VEP affect the performance of ITR. In Lee et al. (2008) experiment, the participated subjects demonstrated the reliability and short latency of two peaks and valleys of both the onset and offset FVEP. These peaks and valleys occurred in 130ms after the onset or offset of the stimulus. To prevent the responses of the consecutive onset–offset (or offset–onset) overlapping, the duration of ON or OFF lasts at least 116.7 ms(10 frame refresh intervals of a 60Hz monitor) in their experiment. (Bin et al., 2011) realised a c–VEP based BCI whose average ITR was over 100bits/min. The visual stimuli were modulated by a pseudo 63 bits binary m–sequence which represents white and black (1 and 0 as binary suggests) series in a stimulating cycle. All stimuli were modulated by the same m–sequence, except a fixed time lag of 2 frame refresh intervals (2 circular shift bits in the sequence) between two adjacent targets. The experiment first obtained VEP referenced template when the subject stared at one of the designate target for 200 stimulation cycles, referred as the referenced target. VEP referenced template was the average result of 200 epochs EEG. The stimuli were modulated by the same m–sequence except a fixed time lag. Therefore, the response of each stimulus was expected the same with the time lag. The expected templates of the other stimuli were obtained by circular shifting the referenced template according to the time lag between the stimuli and the referenced target. The attended target was identified by templates matching, the correlation coefficient of EEG and the stimuli templates. The template of the stimulus resulted in the highest correlation coefficient was identified as the attended target.

It is clear to be seen that in c–VEP paradigm, the stimulating sequence and time lag of adjacent stimuli were two important parameters. First, the length of the sequence affected ITR performance. Second, the time lag and sequence length both determined the maximum number of the targets. In the study of (Bin et al., 2011), 16 and 32 targets were evaluated. The stimuli of both systems were modulated by the same m–sequence. The results showed that 16 targets had higher accuracy than 32 targets but lower ITRs. It was suggested that the higher accuracy of 16 targets was contributed by longer time lag (4 frames vs. 2 frames) which in term affected the autocorrelation functions of the stimulus templates. Three VEP based BCI have distinct properties in terms of visual stimuli mod-

ulation, features of classification, classification methods and performance. Lee et al. (2008) identified the target by averaging the epochs which had lower computation complexities than the classification methods employed by SSVEP and c–VEP paradigms (SSVEP based BCI will be discussed in later session/chapter). The lower computation complexity was at the cost of ITR. FVEP had lowest ITR (<35 bits/min) among three VEP based BCIs. A c–VEP based spelling BCI with online adaptation was able to reach 144bits/min. The speed of spelling was up to 21.3 letters per min which is close to normal keyboard speed (Spüler et al., 2012). Both FVEP and c–VEP based BCIs can have more stimuli (≥ 25) than frequency–coded SSVEP. As a result, frequency–coded SSVEP based BCI is more suitable to a system with fewer options.

The motion visual evoked potential (m–VEP) can also be used as input to a BCI system. Motion visual evoked potential is evoked by brief motion visual stimuli. The advantages of m–VEP include the large amplitude of the response and consistency of the response across the subjects (Hong et al., 2009). (Hong et al., 2009) had a comparison study of m–VEP (N200) based BCI and P300 based BCI. The virtual keyboards of both systems were similar, a 6×6 matrix comprising the letters and numbers. In m–VEP based BCI, a vertical bar, the motion stimulus, appeared in the right edges of the virtual keys of the same row or same column simultaneously at the onset of the stimuli. The bars moved leftward for a brief time and disappeared. The moving bars appeared in the next row or column. The motion stimuli appeared in a random order of the rows and column, but appeared in the rows before in the columns. A stimulating cycle included the motion stimuli appearing in 6 rows and 6 columns. The subject made the selection by starring at the key desired. The target was identified by the detection of attended row and column. The colours of the bars were different at each time they appeared. The subjects were asked to perform the mental tasks of naming the colour of the attended target. The duration of a complete stimulating cycle was 2.4s. This paradigm was able to achieve comparable performance of P300 based BCI with less electrodes. m–VEP was elicited by low luminance and contrast which reduced the fatigue and discomfort of the subjects. However, this paradigm was limited by the duration of a complete stimulating cycle. The average ITR of this speller was less than 20 bits/min.

m–VEP was also applied to an Internet browsing BCI application by Liu et al. (2010). The principle of the browsing system was similar to the one of a m–VEP speller. The major difference was that only 6 targets were in the Internet browsing system. Also, the moving stimulus appears in targets one by one. The duration of a complete stimulating cycle lasted for 1.1s. As a result, ITR was higher than 40 bits/min.

2.3.2.4 Steady–State Visual Evoked Potential (SSVEP)

This section provided an overview of SSVEP. A detailed review on SSVEP based BCI was given in sections 2.5 and 2.6. Visual evoked potentials (VEP) are the brain response to visual stimulation, such as the flash light and reversal graphic

pattern etc. Depending on the stimulating frequency, VEPs can be divided into transient visual evoked potential (tVEP) and SSVEP (Tobimatsu et al., 1996; Tobimatsu and Kato, 1996). When the stimulation rate is low, the sensory pathway has enough time to go back to baseline state before the next stimulation. tVEP is evoked by a low stimulus rate ($< 1Hz$) (Tobimatsu et al., 1996; Tobimatsu and Kato, 1996) and tVEP can be characterised by a few deflations whose amplitude and latency are time–locked to the stimulus. P100 is one of the most important components of tVEP deflations. The amplitude and latency show abnormal values in some clinical conditions/diseases (Tobimatsu et al., 1996).

When the stimulation rate is high, the sensory pathway has not got enough time to reset before the next stimulation. The responses are overlapped and become steady (Di Russo et al., 2007). SSVEP can be elicited by the repetitive presentation of the visual flickering stimuli with the frequency over 6Hz (Di Russo et al., 2007; Wang et al., 2006; Toffanin et al., 2009). SSVEP can be characterised by the amplitude and phase (Tobimatsu and Kato, 1996; Di Russo et al., 2007). SSVEP is a sinusoidal like response with the same fundamental frequency of stimulus and its higher harmonics and/or sub–harmonics frequencies (Herrmann, 2001; Wang et al., 2006; Di Russo et al., 2007). SSVEP becomes prominent after a several hundred milliseconds of the stimulus onset (Moratti et al., 2007; Morgan et al., 1996). It can be observed most significant from the occipital area over the brains visual cortex and can be recorded using EEG (Herrmann, 2001; Pastor et al., 2003; Moratti et al., 2007; Di Russo et al., 2007; Toffanin et al., 2009). SSVEP is often used to study the neural process associated with a frequency–tagged stimulus. SSVEP power and phase can be measured in a narrow band spectrum centred at the stimulating frequency. This property is useful to discriminate SSVEP from ongoing EEG and artefacts which have broadband spectrum. Therefore SSVEP is relatively immune to artefact and has high SNR (Silberstein et al., 2001). Longer stimulation period can increase SNR (Srinivasan et al., 2006). Phase–reset of ongoing EEG is the mechanism of SSVEP. This mechanism may also enhance SNR. SSVEP is stable and is not disturbed by transient disturbance (Moratti et al., 2007) SSVEP is widely used in cognitive studies, such as visual attention, object recognition and working memory. SSVEP is sensitive to the parameters of the visual stimuli, such as flickering frequency, colour, size and intensity (Morgan et al., 1996; Srinivasan et al., 2006).

The visual attention studies (Müller et al., 1998; Toffanin et al., 2009; Ding et al., 2006; Herrmann, 2001; Walter et al., 2012; Morgan et al., 1996) showed that the amplitude of SSVEP can be modulated by the visual spatial attention without shifting the gaze of the eyes termed as covert attention. The amplitude of SSVEP is highly correlated to the level of attention (e.g. attended, divided attention and ignored) (Toffanin et al., 2009). The amplitude of SSVEP induced by shifting the gaze directly on the stimulus by overt attention can be 10 times larger than covert attention. The attention also affected the amplitude and scalp distribution of SSVEP. The analysis of the scalp distribution and source of SSVEP showed that in covert attention, SSVEP was found strongest at contra–lateral

parieto–occipital area. In overt attention, central occipital area was found most prominent (Walter et al., 2012). That fact that SSVEP can be modulated by covert attention is an important fundamental basis for an independent SSVEP BCI. It will be discussed in section 2.5.1. SSVEP is a phase–locked response to visual stimulus. The use phase–tagged technique to discriminate SSVEP will be discussed in section 2.5.2. The modulation effect of attention to SSVEP phase is subject–variant (Morgan et al., 1996; Müller et al., 1998).

The neural process of SSVEP is not completely understood (Vialatte et al., 2010). A cluster of neurons of the cortex synchronised by a flickering stimulus is considered as a SSVEP neural network. SSVEP is a frequency–dependent response to the frequency of the stimuli. It was suggested that there are three SSVEP neural networks corresponding to three different frequency bands, i.e. low band from 5–12Hz, middle band from 12–25Hz and high band from 25–50Hz (Wu, 2014b). SSVEP can be seen more predominate at some particular frequencies, so called resonance frequencies (Herrmann, 2001). For example, SSVEP responses at the frequencies of 10, 20 40 and 80Hz are stronger than at their adjacent frequencies. The frequencies around 15Hz can elicit the strongest SSVEP in human as suggested by Pastor et al. (2003) while Wang et al. (2006) suggested 15Hz, 31Hz and 41Hz of three different bands evoke stronger SSVEP. The amplitude of SSVEP elicited by different frequency bands is different (Pastor et al., 2003; Wang et al., 2006). In general, the low and middle frequency bands can elicit larger SSVEP than high frequency band. However, the background noise at low and middle frequency band is also stronger than the high frequency band. As a result, the SNRs of the three frequency bands are similar (Wang et al., 2006).

The accepted frequency band of SSVEP is limited to 5Hz to 50Hz (Vialatte et al., 2009). However, some studies demonstrated that SSVEP could be elicited between 1 and 100Hz (Herrmann, 2001). Vialatte et al. (2009) recorded SSVEP at the stimulating frequencies between 0.5Hz to 5Hz. The results showed periodicity but less sinusoidal. The author suggested this resulted from the superposition of few harmonics and low SNR at the low frequency in this frequency band. FFT was used to verify if the response was SSVEP or a mere transient VEP. FFT showed peak values of the response occurred at the frequencies around 1, 2.5 and 5Hz which were close to the sub–harmonics of 10Hz, one of the resonance frequencies described in Herrmann (2001).

SSVEP is also used in some clinic diseases studies, such as Parkinson, Alzheimer, and schizophrenia (Vialatte et al., 2010; Silberstein et al., 2001). The patients of these diseases showed abnormalities in their visual pathways. For example, it was reported by Krishnan et al. (2005) that the elicited SSVEP powers at the frequencies of beta and gamma bands by the schizophrenia patients were lower than the normal subjects. On the contrary, the noise at the frequency of beta band was higher.

One of the disadvantages of SSVEP stimulation is the visual stimuli might evoke

visual–evoked seizures. It was estimated that 0.3% to 3% of the population has photosensitivity. Intensity and frequency are two most important factors that induce seizure. Frequencies between 15 and 25Hz are most likely to trigger seizure (Fisher et al., 2005).

2.3.3 Hybrid BCI

The hybrid BCI (hBCI) is defined as a BCI system consisting of at least of one conventional BCI and another system based on a different BCI paradigm, a physiological signal or a signal from external devices. hBCI is able to take advantage of the different systems involved and improve the classification accuracies. hBCI process the inputs in either a sequential or simultaneous manner. In sequential hBCI, the output of one system is used as the input of the other system or as a switch to enable the other system. For simultaneous BCI, the signals from different systems are processed in parallel at the same time. The main issue hBCI facing is the selection of the best possible combination from different BCI paradigms that exist (Pfurtscheller et al., 2010a; Amiri et al., 2013a,b). Theoretically speaking, hBCI could be developed using any combination of different BCI paradigms. This section is focused only on a hBCI which comprises of a SSVEP based BCI and other BCI paradigms.

Pfurtscheller et al. (2010b) demonstrated a sequential hBCI which combined ERD and SSVEP based BCI to open and close a hand orthosis. In the proposed system, ERD BCI was used as a switch to activate SSVEP based BCI to open or close the orthosis and to deactivate SSVEP based BCI during the resting period in a self paced BCI setup. After the training to operate SSVEP and ERD hBCI, the subjects were asked to open and close the hand orthosis using SSVEP based BCI with and without the ERD BCI. The results showed that with the ERD BCI as the brain switch, the overall false positive rates were lower than the ones without it. SSVEP based BCIs were also incorporated with P300 paradigm in a smart home control system (Edlinger et al., 2011). The user used SSVEP to start or stop the operation of P300 BCI system to choose the control commands. With SSVEP as the switch, the user was able to decide when to use the system.

Allison et al. (2010b) proposed a simultaneous hBCI comprising SSVEP and ERD paradigms. The subjects in their experiment performed three different mental tasks, motor imaginary task, visual attention and both. The classification accuracies of the task with both motor imaginary and visual attention combined were higher than the ones of only one of two tasks performed separately. The author suggested that the hybrid BCI might provide more information for the classification. The mental tasks performed in the hBCI might have also made the users more focused and concentrating and as a result, the performance was improved. A 6×6 P300 conventional speller integrated SSVEP was introduced by Panicker et al. (2011). SSVEP was used to control detection. The rows and columns of the matrix were flashed as the same as conventional P300 based BCI. But the elements of the matrix also flickered at the same frequency to elicit SSVEP which

indicated whether the user intended to operate the speller or not. The results showed the feasibility of the hBCI as P300 and SSVEP were able to be elicited at the same time. The off-line experiment classification accuracies with SSVEP were higher than those without SSVEP. Xu et al. (2013) also combined SSVEP into a 3×3 P300 speller. In their paradigm, each item of the matrix had two phases, flicker phase and event phase. Each item of the matrix was intensified in a random order. When the item was flashed, it was in event phase without flickering. On the other hand, the other 8 items were in the flicker phase in which they flickered at 15Hz without being intensified. Therefore, EEG of the attended target exhibited P300 without SSVEP which was termed as SSVEP blocking. The features combined P300 and SSVEP blocking achieved higher classification accuracy.

Yin et al. (2014) also proposed a hybrid BCI comprising P300 and SSVEP paradigms in a speller application. The target was identified by the detection of P300 and SSVEP. In their method, the letters/characters (36 targets, a–z, 1–9 and del) were divided into 6 subgroups. Each subgroup had the same number of targets. The items of the same subgroup flickered at the same frequency. Different subgroups were assigned a different frequency to elicit SSVEP. Each subgroup was a P300 speller and the items were intensified in random order to elicit P300. The detection of SSVEP was to determine which subgroup was attended. P300 was to determine the item in the attended subgroup was focused. Thus the attended target was identified. Compared to the conventional 6×6 matrix, the number of the flashes of the targets was reduced to half. Compared to the speller based on SSVEP alone, the number of the selection increased or it required fewer selections to obtain the letter. As a result, ITR increased.

From the above aforementioned studies, hBCIs could improve the classification accuracies, ITR and reduce false positives. While most of hBCIs employed two BCI paradigms, Choi and Jo (2013) assessed the feasibility of a sequential hBCI consisting of P300, SSVEP and ERD paradigms to control a robot to navigate, explore and recognizse the object in a maze. SSVEP and P300 were used for the control commands and ERD was used to change the states. The significance of the proposed hBCI was that hBCI could be used for complicated tasks.

However, there are some issues related to hBCI that still require investigation. For example, what kind of feedback should be provided and which paradigm the feedback should be based on? Also, the interference of the tasks between two (or more) chosen paradigms is unknown. For example, in a P300/SSVEP study, it was found that P300 response of hBCI was similar to stand alone P300 BCI. But SSVEP was worse in hBCI (Z. Allison et al., 2014). In a hBCI of ERD/SSVEP study, the subjects showed no interference and interference between two tasks were 50:50 (Allison et al., 2012). In the same study, it was also found that ERD activity developed faster than SSVEP but SSVEP was more prominent than ERD in a simultaneous hBCI.

2.4 Target users and the applications

Kübler et al. (2013) suggested that the functionality, independence and ease of use were three important factors to be considered in the design BCIs for the daily use as an assistive technology. A BCI acceptance survey study to target users of ALS patients, revealed that there was a gap between the expectation and reality in terms of accuracy, speed and training at the time of the survey conducted by (Huggins et al., 2011). However, the gap was narrowing. For example, the survey showed the expected word processing speed was 15–19 letters per min compared to the actual speed in reality of 5 letters per min at the time of the survey. The current BCI spelling speed could be over 20 letters per min (Spüler et al., 2012). In this section, an overview of the potential users and applications were provided.

2.4.1 Target and potential users

The primary aim of BCI research is to help the severely disabled and paralysed patients to restore the communication and movement. Wolpaw et al. (2006) suggested that the efficacy which these patients can benefit from BCI depended on the degree of the physical impairment and further divided these potential users into three groups, (1) completely locked–in, (2) only limited neuromuscular activities intact and (3) substantial neuromuscular activities remaining.

The patients in the first group were completely locked–in. Whether they were able to benefit from BCI remained unclear. A few studies have demonstrated that the patients were able to learn to communicate via BCI effectively before they entered the late stages of the diseases in various BCI paradigms. Two nearly completely paralysed patients learnt to regulate their slow cortical potentials after 4 to 6 weeks of training (Kübler et al., 1998). (Kübler et al., 2005; Wolpaw and McFarland, 2004) reported that ALS patients and spinal cord injury patients were able to control cursor movement in two dimensions by the modulation of mu and beta rhythms. P300 based BCI demonstrated its usability as an alternative communication channel for ALS patients in the studies of (Sellers and Donchin, 2006; Nijboer et al., 2008). Birbaumer (2006) showed that the patients who learnt to control BCI before they became completely locked–in were able to maintain the ability of operating BCI when they were completely locked–in. It was suggested that the completely locked–in patients were unable to use BCI if they learnt to control BCI after they were at the late stage of the disease, i.e. becoming completely locked–in (Birbaumer, 2006). Birbaumer and Cohen (2007) hypothesised that the totally locked–in patients might develop the conditions (decline of cognitive function, extinction of thought) which prevented them to learn to control the BCI. Therefore, if the patients could learn to control BCI at an earlier stage of the disease before being totally locked–in, it is more likely they would be able to communicate via a BCI system as the disease progressed (Birbaumer, 2006; Mak and Wolpaw, 2009). The authors suggest that further investigation is required to understand the benefits the first group of totally locked–in patients could get from BCI.

The second group was the primary target users. When the conventional methods could not provide sufficient assistance, BCI could be an option. A few studies to investigate the relationship between the BCI performance and the level of impairment showed that both healthy subjects and patients could operate BCI effectively. For example, a performance comparison study between the healthy subjects and paralysed patients in a four–class P300 based BCI indicated that the overall performance of the healthy subjects was significantly better than the most impaired patients but not the less impaired patients (Piccione et al., 2006). Another similar study based on a six–class P300 BCI also had a similar conclusion that healthy subjects had better performance than patients (Hoffmann et al., 2008). However, both studies showed that even severely disabled patients were able to control a P300 based BCI. Kübler and Birbaumer (2008) also suggested that most of the patients of this group could control BCI. Due to the limitation of current BCI systems, the third group of patients might be better off using the assistance of conventional technology (Wolpaw et al., 2006).

In normal circumstances, BCI might not be considered as a communication method by healthy people due to its low speed, relatively low accuracy, low bandwidth compared to existing interfaces, such as the mouse and the keyboard. However, in some particular situations, which were termed as induced disability or situational disability by Nijholt et al. (2009), healthy subjects might benefit from BCI. Apart from the performance, BCI normally require special dedicated hardware, software and the assistance of set up. As the technology progresses and the hardware and software improve, for example, dry electrode, graphics user interface and advanced signal processing, Allison et al. (2007) suggested that the healthy people might consider BCI as a choice for the following reasons:

1. BCI as an addition to existing interfaces and auxiliary when induced disability occurs.
2. BCI can provide extra information which the existing interfaces cannot.
3. BCI can improve performance.
4. BCI can provide a private and confidential communication channel.
5. BCI can detect the intention earlier than the actual action.
6. BCI is fun and novel.

Nijholt et al. (2009) further pointed out that game players and game developers were the potential users of BCI due to matched characters between them and BCI. For example, the gamers were aware that playing a game was a skill to learn and training/practice was required in order to improve such skill. The gamers adopted the new technology and accepted that the benefits from adopting the new technology might be minimal. However, for this group, BCI might be designed differently for the medical purpose.

2.4.2 Applications

BCI can be used to substitute or restore the impaired motor function of patients. Soekadar et al. (2011) classified BCI systems into (1) assistive BCI and (2) restorative BCI according to the aims of BCI use. The lost motor functions of the patients can be substituted and restored by the aid of the assistive BCI system and the restorative BCI system respectively. The assistive BCI provides the paralysed, disabled patients with an alternative channel to communicate and control the device. The main applications of this aspect include:

1. Communication: Text speller is the major application to restore communication of the patients. Few speller applications of BCI has been developed and tested outside laboratory environments for patients. The evaluation results demonstrated the usability of these systems as a communication channel. These spelling BCI applications included, a motor imagery based speller proposed by Perdikis et al. (2014), the thought–translation device based on slow cortical potential from Birbaumer et al. (2000, 2003), P300 speller from Vaughan et al. (2006); Sellers et al. (2006). SSVEP paradigm was also employed in spelling applications(Hwang et al., 2012; Volosyak et al., 2009).

2. Prosthesis control: Most of the commercial prosthesis control required voluntary motor activities which might not be suitable to the patients with severely neuromuscular impairment (Guger et al., 1999). Guger et al. (1999) used EEG based BCI to open and close hand prosthesis by imagery of right hand or left hand movement. A tetraplegic patient learnt to control the hand prosthesis via motor imagery based BCI and was able to lift light weight objects after a few months of training (Pfurtscheller et al., 2000a). A four–class SSVEP based BCI was able to control an electrical hand prosthesis to open, close, turn the wrist right or left (Muller-Putz and Pfurtscheller, 2008).

3. Environment control: Cincotti et al. (2008) proposed a home environment control system comprised motor imagery (MI) based BCI to improve the quality of life and independence of the patients suffering from neuromuscular disorders. The system allowed the patients to control the light, TV, alarm and door etc. It also included a robotic platform which allowed the patients to virtually move. The result of the pilot study showed that BCI could enable the patients to use the environment control system.

4. Locomotion control: Long et al. (2012) proposed a hybrid BCI consisted of P300 and MI paradigms which could control the directions and speed of a wheelchair. This hybrid wheelchair control system had four commands, turn right, turn left, accelerating and decelerating. The wheelchair was turned right or left by the motor imagery of right and left hand respectively. The wheelchair was accelerated when P300 and the idle state of motor imagery were detected. On contrary, when the imagery of foot movement and the idle state of P300 were detected, the wheelchair was decelerated. It was tested and evaluated in simulated and real wheelchair.

BCI was applied to neurorehabilitation therapy. For example, motor imagery was shown useful on the motor rehabilitation for stroke patients. Current stroke rehabilitation therapy such as active motor training depended on the residual motor function of the patients which might not be suitable for the patients with limited motor function. Motor imagery does not rely on the physical movement but could activate the motor network (Ang and Guan, 2013). Therefore, BCI was an alternative option to current therapy for the patients. Also, current therapy was unable to provide the feedback to the therapists and patients for monitoring and learning. BCI was a solution to provide such feedback (Kaiser et al., 2012). Daly and Wolpaw (2008) suggested two strategies of the restorative BCI in neurorehabilitation. The first strategy was to use BCI to train the patients to produce normal brain activities. In this stage, BCI measured the brain activities of the patients, extracted the features of the signal and used the these features as the feedback to the patients. The second strategy was to use BCI output to activate the device which assisted the patients to move during the motor tasks. Savić et al. (2014) integrated a hybrid BCI of SSVEP and MI to a functional electrical stimulation therapy for stroke patients. The users of the proposed system first used SSVEP to select one electrical stimulation pattern from three grasp patterns, palmar, lateral, or precision. The users imagined the selected grasp to generate ERD. The detection of ERD triggered the functional electrical stimulation of the selected pattern. The concurrence of MI and sensory stimulation of FES facilitated the motor function recovery.

Recently, BCI applications, such as games control, were developed for healthy people. BCI had more to offer to healthy people, not only regarding device control but also BCI was able to monitor the mental state of the users, e.g. the level of arousal, tiredness, drowsiness and workload etc. BCI provided the direct measure and analysis of the mental state. Müller et al. (2008) evaluated the feasibility of EEG based BCI to monitor the mental state in a security surveillance scenario. Lin et al. (2008) developed a BCI based system to monitor the drowsiness of the drivers and provide the warning. A few BCI based smart home control systems were proposed to control the domestic appliances such as TV, phone etc. Edlinger and Guger (2012) used a hybrid BCI comprising of SSVEP and P300 paradigms to control a smart home in a virtual reality environment. SSVEP was used to turn on/off P300 BCI and P300 BCI was used to select the control command. Kanemura et al. (2013) designed a framework which integrated a wheelchair and smart home for older and disabled people to control household equipment.

BCI was also used as a training tool to improve the memory and attention and slow down cognitive decline in older healthy people. Lee et al. (2013) evaluated the feasibility of BCI used as training tool to improve the memory and attention of healthy older people. The participants of the pilot experiment underwent 24 sections of BCI intervention. The participants used BCI to play card–pairing memory games. BCI was used to open or close a card. The experimental results showed a positive impact when using the BCI on improving memory and attention of the healthy older subjects. A research group of the University of Valladolid also

attempted to use BCI as a training tool to offset the ageing effects in cognitive decline.

2.5 Limitations of SSVEP based BCI

SSVEP based BCI is classified as dependent BCI. The selection of stimulating frequencies for visual stimuli is restricted to the availability of the frequency and user comfort. This section first presents how independent SSVEP BCI can be achieved by covert attention. Next, this section reviews studies which increase the number of visual stimuli over the available frequencies and how user fatigue can be reduced.

2.5.1 Dependent BCI

BCI can be divided into dependent and independent BCI. The output of dependant and independent BCIs does not rely on the brain normal output pathway. However, dependent BCIs require the control of peripheral muscles and nerves in order to generate the brains activities as the input of BCIs. On the contrary, independent BCIs do not depend on these activities to modulate the required brain activities. SSVEP based BCI is categorised as a dependent BCI as it needs its users to control their gaze shift to the targets to generate SSVEP response although the output does not depend on the brain normal output pathway (Allison et al., 2008; Kelly et al., 2005b; Zhang et al., 2010a; Lopez-Gordo et al., 2011). However, some studies have demonstrated SSVEP can be modulated by spatial attention without shifting the gaze. It is referred as covert attention which does not need the gaze control and is different from overt. This is an important fundamental basis for SSVEP based BCI towards to an independent BCI.

In the attention studies of SSVEP, at least two different types of the visual presentations were employed to elicit SSVEP response: One presenting two images flickering by two frequencies at two visual fields, one in left and one in right (Morgan et al., 1996; Müller et al., 1998) and the other one presenting two images, which were distinguished by the colours or shapes, superimposed in the same region (Müller and Hübner, 2002; Chen et al., 2003; Müller et al., 2006). During the experiments, the subjects were asked to attend the image in the left or right visual field or one of the superimposed images in the central vision field and ignore the other one. The subjects kept their fixation in the central region in all conditions. The attended image was the target and the unattended one was the ignored one or distracter. Some experiments also asked the subjects to respond when some conditions are met. For example, a particular letter or number in a sequence or image shape changes was detected. A brief overview of the paradigms of SSVEP covert attention experiments will be presented next in this session.

Morgan et al. (1996) displayed two white rectangular stimuli positioned bilateral to the middle of a monitor. The stimuli flickered at 8.6Hz or 12Hz. An alphabet

sequence comprised by letters randomly chosen from A to K and 5 was superimposed with the stimuli. The subjects were asked to respond when the target 5 was detected. The experimental result showed that SSVEP response can be enhanced by the selective attention.

Chen et al. (2003) presented the stimuli by overlapping 7 vertical bars and 7 horizontal bars on a monitor. The bars were red or green and flickered at two frequencies, 7.41Hz or 8.33Hz. During the trial, the width of one vertical and horizontal bar increased or decreased for three times and back to the original. The subjects were asked to respond the width change from any of three central middle bars of the attended image or to the central bar width change in two different experiments (attend–to–all and attend–to–middle). The results also suggested that SSVEP response can be modulated by the increased and decreased attention of the visual stimuli.

Müller et al. (2006) implemented a continual Brownian–motion–like visual stimulator by superimposing blue and red dots, 125 dots for each colour, in a grey circular background. The flickering frequencies were 7Hz and 11.67Hz for red and blue dots respectively. Throughout the trial, the dots kept moving by changing their positions in random directions and time durations. Subjects were asked to respond the detection of the coherent motion of the attended dots (blue or red). The result indicated that SSVEP response can be enchanced by paying attention to one of the colour dots. The visual stimuli of the study by Müller and Hübner (2002) were the superimposition of a large letter and a small letter. The small letter was located in a gray oval in the centre of the large letter. Both letters were alphabet sequence randomly chosen from A to O. The flickering frequency pair of the letters was 7Hz and 11.67Hz. The subjects were asked to attend either the large letter or small letter and ignore the other. The task was to respond whether H appearing in the attended–letter sequence or not. The result also suggested that SSVEP response was more prominent with attention.

Müller et al. (1998) employed two vertical bars embedded 5 bi–colour (red and green) LEDs as the visual stimuli, one in left and one in right of the visual field. The flickering frequencies of the left bar and right bar were 20.8Hz and 27.8Hz correspondingly. LED colour was red most of the time during each trial. Two of the LEDs located in the top, middle and bottom changed to green simultaneously at random during the trial. The task of the subjects was to respond when the top and bottom LEDs of the attended bar changed to green. The above experiments investigated the effect of covert attention on SSVEP. The experimental results demonstrated that SSVEP was able to be modulated by covert attention without shifting the gaze or head movements. These studies showed that SSVEP elicited by the attended stimulus is stronger than the one elicited by the same stimulus when the other field or other image was attended. Most of independent SSVEP BCI studies were based on covert attention.

Kelly et al. (2005a, 2005b, 2005c) had three pioneer studies which applied SSVEP

modulated by covert attention to BCI. The visual stimulation paradigm was similar to what was described in Morgan et al. (1996). The subjects were asked to count and report the number of the target letter encountered during a trial. In their experiments, several stimulating frequency pairs were tested. The classification features included the elicited SSVEP, the alpha band (8–14Hz) power and the ratio of the alpha band powers at contralateral hemispheres. One of the studies also compared the classification accuracy by overt attention which allowed the subjects to shift their gaze. The classification from the study employed the power and ratio of the alpha band activities was slightly higher than 70%, the threshold of a binary BCI. The classification accuracy by SSVEP features and combined features of SSVEP and the alpha band power achieved 70.3% and 79.5% respectively. Although the combined feature improved the classification accuracy, it was much lower than the performance of overt attention which exceeded 90%. A real time online BCI was implemented and tested in one of their studies which provided auditory and visual biofeedback (Kelly et al., 2005c). 11 subjects tested this system. The highest ITR from one of the subject was 3.27 bits/min. Six subjects had at least one session out of 5 with classification accuracy over 75%. Two subjects achieved the accuracies lower than 50% in all sessions. A further investigation suggested that these two subjects constantly distracted by the letters changing from the unattended side. When they performed overt attention, the accuracy rates exceeded 90%. The author suggested that an independent SSVEP based BCI was achievable. However, the subjects might need more training to learn how to control covert attention and the performance could be improved by subject–specific parameters.

Another independent SSVEP BCI system based on covert attention was proposed by Allison et al. (2008). Three different visual stimuli used to elicit SSVEP were similar to the paradigms of Chen et al. (2003) and Morgan et al. (1996). Two of them were similar to Chen et al. (2003) with two colour schemes. The visual stimuli were superimposed images of 6 vertical and 6 horizontal bars (line–boxes). One of the colour schemes was white or dark gray. One of the colour schemes was red or green. The vertical bars flickered at 10Hz and the horizontal bars flickered at 12Hz. The third visual stimuli were two black and white checkerboards situated at left and right side of the monitor. The flickering frequencies for the left and right checkerboards were 6Hz and 15Hz. During the experiments, the subjects were asked to attend the vertical or horizontal bars in the bar stimulation or attend one of the checkerboards in a checkerboard stimulation. The experiment results showed that about half of the subjects were able to product robust SSVEP to control SSVEP BCI. The colours of bars had no significant impact on SSVEP. However, SSVEP response resulting from the checkerboards outperformed the response of the line–boxes. The author suggested that the visual stimuli were the root cause of the different performance. The subjects might shift their gaze in the experiment of checkerboards. Meanwhile, the author also pointed out that the attention strategy which the subjects adapted might also affect their performance. Therefore, providing appropriate training to learn an attention strategy may improve the performance.

Zhang et al. (2010a) adapted a similar visual stimuli described in Müller et al. (2006). The visual stimuli comprised two groups of dots, one red and one blue. Instead of moving, the red dots rotated counter–clockwise and blue rotated in clockwise direction at the same angular speed, 1° per frame. The red dots and blue dots flickered at 12Hz and 10Hz respectively. Three–day training was provided to subjects participating in the experiment. The average classification accuracy was around 71% which again was slightly higher than the threshold 70% in a binary BCI (Kübler et al., 2004). Nearly half of the subjects improved their performance by the training. SSVEP amplitudes of these subjects were increased significantly on the third day compared to the first day. This showed the training could help the performance of covert attention. To avoid the interaction between two stimuli which declined SSVEP, if the dots of different colours overlapped, the blue colour dots were displayed. This was to avoid the interaction between two steady–state stimulation and declined SSVEP response in the experiment.

Lesenfants et al. (2011) compared the classification of SSVEP overtly and covertly induced by three patterns of visual stimuli, block pattern, lines pattern and checker pattern. In block pattern overt stimulation, stimuli were two filled–squares located in the left and right. The stimuli of line pattern or checker pattern were employed in covert attention stimulation. The line pattern stimuli were two images of 7 vertical and 7 horizontal bars which were superimposed at the same location and were similar to the line–boxes stimuli in Allison et al. (2008) study. The checker pattern was the same as the line pattern but the overlapped segments of the vertical and horizontal bars were removed. The stimulus flickered at $^{85}/_{8}$Hz or $^{85}/_{6}$Hz with colour red or yellow on an 85Hz monitor. The classification accuracies showed no surprises. The overt block pattern had the best classification accuracy of 99% across all subjects. For the covert stimulation, the checker pattern had better performance than the line pattern. The average accuracy of checker pattern was over 75% for stimulating duration over 5s. The author suggested that the stimuli without overlapped segment helped the subjects to concentrate. The results also supported that the interaction of two stimuli might result in a weaker SSVEP response (Zhang et al., 2010a). The components of SSVEP harmonics modulated by covert attention did not improve the classification performance and did not show significance.

Most of independent SSVEP BCIs presented the visual stimuli on a monitor. Lim et al. (2013) integrated two LED arrays into the eye pieces of glasses. Unlike the usual SSVEP BCI which presented the same frequencies to both eyes simultaneously, the stimulating frequencies to the left and right eye were different in the proposed SSVEP BCI. The subjects were asked to focus and concentrate their attention on one LED array with their eyes closed. The data analysis showed that the light through the eyelids also elicited SSVEP and resulted in an average classification accuracy of 90% from the on–line experiment with trial duration longer than 3s. A more recent independent SSVEP study evaluated the feasibility of SSVEP independent BCI on the healthy subjects and locked–in syndrome

patient in both offline and online experiments (Lesenfants et al., 2014). The independent SSVEP based BCI also used LEDs as the visual stimuli which was a 7cm $\times$ 7cm square in the form of interlaced pattern composed of red and yellow LEDs flickering at 14Hz and 10Hz respectively. The mean accuracies of the healthy subjects were 85% and 74% in offline and online experiments. For the patients group, only 2 out of 6 patients performed over 63%, which was the chance level in their experiment, accuracy in the offline experiment and one of 4 patients above 70%, which was the lowest accuracy in order to communicate in BCI of two classes, in the online experiment. Their study also investigated SSVEP response elicited by covert attention. It was found that the spectrum power at the stimulating frequency of the target and its corresponding harmonics decreased compared to the overt attention. The frequency components of SSVEP harmonics did not improve the classification accuracies. The spectrum power at non–target stimulating frequency was close to the one of the target stimulating frequency. The author also suggested that the low accuracies of the patients might be due to their clinical conditions.

In these independent SSVEP BCI studies, the subjects attended the target by covert attention without shifting their gaze at the cost of the classification accuracy. Overall speaking, the average accuracy of each study was slightly over 70%, the threshold of effective binary BCI. Lopez-Gordo et al. (2011) proposed a method to customise subject–specific visual stimuli to enhance SNR of SSVEP by covert attention. The method investigated SNR of SSVEP modulated by covert attention at the different combination of spatial frequencies and temporal frequencies. SNR was defined by the following equation:

$$SNR = \frac{|V_{af} - V_{if}|^2 + |V_{a1} - V_{i1}|^2}{N_f + N_1} \tag{2.1}$$

Where V_{af} and V_{a1} were the amplitude and phase of SSVEP at fundamental and 2^{nd} higher harmonics frequency when attending the visual stimuli. V_{if} and V_{i1} were the amplitude and phase of SSVEP at fundamental and 2^{nd} higher harmonic frequencies when ignoring the visual stimuli. N_f and N_1 were the mean power of noise at frequency span [-2 2]Hz central at fundamental and 2^{nd} higher harmonics frequencies but excluding these two frequencies. The analysis results showed that the best configuration might not elicit the strongest SSVEP. This could be explained by the numerator of SNR which was SSVEP power difference between attended condition and ignored condition at the stimulating frequency and its 2^{nd} harmonic. Although the maximum response was expected at 4 cycles per degree (cpd) of the spatial frequency, the optimal SNR was actual occurred at higher spatial frequency. At higher spatial frequency, the power of SSVEP in ignored condition tended to be smaller due to the smaller stimulus. The classification features of most independent SSVEP BCI did not include the response of the ignored one. Optimal SNR study might provide independent SSVEP BCI an feature to classify the subjects selection. For example, the ratio of SSVEP power at stimulating frequencies can be used as a feature for classification. When a selection was made, one of the stimulating frequencies must be attended while

the others are ignored. The attended frequency should have prominent SSVEP compared to the ignored ones. The above studies demonstrated the feasibility of independent SSVEP BCI. However, so far, these independent SSVEP BCI studies only allowed a binary selection. The overall classification accuracy was slightly over 70%. However, it also showed that appropriate training which might help the subjects to learn attention strategy and improve BCI performance. The bilateral visual stimuli might outperform the visual stimuli of two superimposed images in the central region although it requires more evidence to rule out the gaze shifting effect.

2.5.2 Visual stimulator

Frequency is the most important parameter to SSVEP. Frequency can determine SSVEP response and the comfort of users. The range of frequency which can elicit SSVEP is from 6Hz and up to 90Hz. Different frequency bands have different characteristics, in terms of induced SSVEP response, noise, comfort/fatigue of the users, available frequencies which can elicit SSVEP response and induce complications.

Conventional SSVEP BCI assigned each target a different frequency (Gao et al., 2003; Jia et al., 2011; Wong et al., 2010; Zhang et al., 2012; Shyu et al., 2010). However, there were some limitations in frequency selection as follows: (1) Not all frequencies can elicit prominent SSVEP response. (2) Frequencies which have common harmonics or are multiples of each other should be avoided to prevent any confusion. (3) Some frequencies could cause fatigue or induce complications (e.g. seizure). (4) For stimulators presented on a monitor, the stimulating frequencies are restricted by the monitor refresh rate. Only the sub–frequencies of the refresh rate are available for accurate stimulation. These factors limit the number of frequencies available to be selected (Hwang et al., 2013; Jia et al., 2011; Zhang et al., 2012; Shyu et al., 2010). The limited frequency selection is a major challenge to SSVEP based BCI design and attracts a lot of research attention.

Gao et al. (2003) and Hwang et al. (2012) used LEDs as the visual stimuli to implement an environment controller with 48 commands and a QWERT style keyboard with 30 inputs respectively. All LED visual stimuli flickered at distinct frequencies in a frequency band with very narrow frequency resolution, 0.2Hz and 0.1Hz respectively. Both studies demonstrated the feasibility of BCI and delivered high ITR. Both studies employed Fourier Transforms to detect the gazed target. In order to accurately detect SSVEP with high frequency resolution, it requires longer time of data recording (Mukesh et al., 2006; Lee et al., 2010). Five and ten seconds of data acquisition were required to get 0.2 and 0.1Hz resolution without zeros padding. The time required for acquiring data for one selection of the two studies were 3s and at least 4s with zeros–padding. ITR was limited by the data acquisitioned time. The frequency bands of two studies were 6–16Hz and 5–9.9Hz which are close to the spontaneous the alpha band. Such frequency bands could make the subjects uncomfortable and fatigued. Also, some of the

classification methods, e.g. CCA and MEC, might not be suitable to such systems as the volume of algorithms with high computational complexity require shorter recording time, computations is proportional to the number of targets.

There were several methods proposed to create more targets despite the limited available frequencies. These methods encoded SSVEP in different manners, for example, one target presented by more than one frequency, adding phase lags to stimuli etc. Table 2.1 is a list of SSVEP encoding methods. Most of them can be applied to both the monitor and light stimulators.

Table 2.1: **List of SSVEP encoded methods.** Most of these methods can be applied to both monitor and LED.

SSVEP decoded method	No. of Frequencies	No of Stimuli	Proposed By
Convetional	N	N	
Mixing phase and frequency	N	$> N$	(Wong et al., 2010; Lee et al., 2010; Jia et al., 2011)
Dual frequencies stimulation	N	$N + C_2^N$	(Shyu et al., 2010; Hwang et al., 2013)
Multiple Frequencies Sequential Coding (MFSC)	N	$\geq N^2$	(Zhang et al., 2012)
Half filed stimulation pattern	N	N^2	(Materka and Byczuk, 2006; Materka and Poryzala, 2013; Yan et al., 2009)
Presentation approximation	-	-	(Wang et al., 2010b)

Mukesh et al. (2006) recorded SSVEP induced by two overlapping stimuli flickering at two different frequencies (f and $\frac{f}{2}$) on the centre of the monitor. SSVEP spectrum showed prominent not only at f and $\frac{f}{2}$ but also at the combined frequencies of f and $\frac{f}{2}$. As one of the stimulating frequencies is the harmonic of the other, it was hard to associate the response at the higher frequency to the combined frequencies, the harmonics or both effects. Nonetheless, it demonstrated the feasibility of dual frequency stimulation. Shyu et al. (2010) used two LEDs flickering at two different frequencies (f_1 and f_2, $f_1 < f_2$) to present a visual stimulus. Four different frequencies can present six ($= C_2^4$) different targets. The frequencies of the pair to present a target are different. Besides the peaks at stimulating frequencies, the peaks can be also observed at the combined frequencies, $f_{hs} = 2f_1 - f_2$ and $f_{hb} = 2f_2 - f_1$. Where $f_{hs} < f_1$ and $f_{hb} > f_2$. In some trials, SSVEP responses at the stimulating frequencies were not prominent. SSVEP at f_{hs} and f_{hb} can help to discriminate the selection.

The visual stimulus of dual frequency stimulation can be presented in half–field stimulation pattern to encode SSVEP. Half–field stimulation is a phenomenon that the visual stimulus at one of the visual fields fabricates predominant VEP response in the contra–lateral visual cortex (Materka and Byczuk, 2006; Materka and Poryzala, 2013). The visual stimuli of half–field stimulation were presented by two stimuli located bilaterally at left and right visual fields flickering at two

frequencies which can be the same or different. The difference of the signals at the bilateral electrodes enhanced SSVEP signal and suppressed the noise when two flickering frequencies were the same but with opposite phases (Materka and Byczuk, 2006; Materka and Poryzala, 2013). Yan et al. (2009) proposed half field stimulation pattern which could create N^2 targets by N frequencies. In half–field stimulation pattern, the subjects attended the target and remained the fixation in the middle of two stimuli. The frequency pair of the target can be detected at the contra lateral hemispheres (Yan et al., 2009). One downside of the half–field stimulation pattern was that some subjects reported that it was difficult to maintain the fixation at the middle point between the two stimuli. As a consequence, the performance was affected.

In the study of Shyu et al. (2010), some trials did not display strong SSVEP response in a dual frequency stimulation experiment at the stimulating frequencies. In Yan et al. (2009) a half–field stimulation pattern experiment, subjects reported the difficulty to remain the fixation in the middle. In an earlier study, Cheng et al. (2001) observed that if the subjects did not keep the fixation at the centre of the monitor in a dual frequency stimulation, as a consequence, one frequency might be stronger or weaker than the other. To resolve the fixation problem, the visual stimuli were presented by two overlapped blocks of two different colours, red and green, flickering simultaneously at two frequencies (f_1 and f_2, $f_1 < f_2$). The reversal of red–black and green–black were ON and OFF for each frequency. The colour was yellow when both stimuli were ON. This paradigm also successfully elicited SSVEP at both stimulating frequencies and their combined frequencies. For example, at frequencies $f_2 - f_1$, $2f_1 - f_2$ and $2f_2 - f_1$. Teng et al. (2010) drove the LED by summation of two or three sinusoidal waveforms of different frequencies to test the impact of multiple stimulating frequencies on SSVEP response. In a dual frequency stimulation, if the difference of the stimulating frequencies is less than 4Hz, SSVEP was only observed at one of the stimulating frequency (normally at lower of two). Only when the difference of the stimulating frequencies was larger than 4Hz, SSVEP peaks at both stimulating frequencies could be seen. For triple frequencies stimulation, even the difference between the stimulating frequencies was larger than 4Hz, not all SSVEP at stimulating frequencies could be observed (Teng et al., 2010). This was another downside of LED dual frequency stimulation as it limited the frequency selection. This phenomenon was also exhibited in some cases in the study of overlapped dual frequency stimuli of Cheng et al. (2001).

Hwang et al. (2013) proposed a checkerboard dual frequency stimulation which resolved the fixation problem. In conventional graphics reversal stimulation, the checkerboard can be seen as two mutual groups, group 1 and group 2 which have different colours (phases) at any given time. In conventional checkerboard reversal pattern stimulation, group 1 and group 2 flicker at the same frequency (half of the stimulating frequency) so the group colour is different. In the modified checkerboard reversal method proposed by Hwang et al. (2013), the cells of group 1 flickered at one frequency (f_1) and the cells of group 2 flicker at another

f_2. Such flickering mechanism resulted in four different images during the stimulation. Two of them are the conventional checkerboards. Two of them were either all white or black. The resultant SSVEP showed prominent at frequency $f_1 + f_2$. Four frequencies could present 10 different targets, 4 of the targets with $f_1 = f_2$. N frequencies made total $N + C_2^N$ targets in this dual frequency stimulation method.

The dual frequency method modulated the target by two different frequencies simultaneous. Zhang et al. (2012) proposed the method– Multiple Frequencies Sequential Coding (MFSC). MFSC presented the target by a few frequencies in a serial order within a stimulation cycle. One stimulation cycle comprised of a few coding epochs (a fixed number, M) and one resting epoch for the subject to shift the gaze. In each coding epoch, the target was assigned a frequency. The detection of the target is based on the sequential combination of frequency detection of the coding epochs in a stimulation cycle. MFSC procedure added the temporal information as part of the process. The number of the available targets depends on the numbers of the coding epochs (M) within a stimulation cycle and the number of the frequencies used (N). For example, if the numbers of the coding epochs and selected frequencies are both 3 (M=N=3). The total available targets were up to 27 ($N^M = 3^3$). In this example, each stimulation cycle had 3 encoding epochs. Three different frequencies,f_1, f_2 and f_3 were used. This scenario made 27 different frequency combinations (targets). This method required the synchronisation between the stimulator and the data acquisition module in order to form the correct sequential order and operate BCI in asynchronous mode. The synchronisation was achieved by sending an onset signal at the beginning of each coding epoch and the resting epoch. If the users started to make selection after the first coding epoch onset, this caused a cycle lag which was different from conventional self paced BCI. The cycle lag might be one of the drawbacks of this system which only decoded a selection in a cycle starting from the first coding epoch. MFSC increased the number of available targets by increasing the number of the coding epochs in a stimulation cycle at the expense of reducing ITR. More coding epochs in a cycle meant more time required to detect the selection. The classification performance of each coding epoch which was independent to each other was also tested and confirmed in the study.

One of the applications of SSVEP based BCI is spelling. MFSC can create enough targets for a spelling application to allow a single selection for one letter. One of the protocols to select the letter in spelling application is a decision tree (Cecotti, 2010a). On the contrary, in a decision tree protocol, the selection of one letter requires more than one step. In such a protocol, the letters and space, for example, can be divided into 3 groups (hence each groups has 9 letters/selections) at the very beginning of the selection process. After one of the groups is selected, the letters in the selected group are further divided into three groups until each group contained only one letter/selection. In the example, it required three frequencies for letter groups and each letter required three sequential selections (9–3–1). Such system might need two more frequencies as function keys. In the example, a spelling system of decision tree protocol, each letter was encoded by

three frequencies. However, more mental tasks and strategies are required than MFSC. It also creates 27 different selections by 3 different frequencies. From the operation point of view, without taking the cognitive and mental loads into account, it might be more flexible and efficient than MFSC without the cycle lag. The selection of function key such as delete only needed one selection.

(Jia et al., 2011) proposed a method to encode the visual stimuli mixed frequencies with phases. The visual stimulator is a Thin Film Transistor (TFT) monitor of 60Hz refresh rate. The stimulating frequencies were 10Hz, 12Hz and 15Hz, which are all sub–frequencies of 60Hz. Six, five and four visual stimuli flickered at 10, 12 and 15Hz, with different stimuli phases. Three frequencies presented 15 visual stimuli. The flickering sequence of the 15 visual stimuli is illustrated in Figure 2.9. This method encodes SSVEP using both frequency and phase. To understand the underlining classification of this method, three types of the phases are defined. The first is the stimulus phase which is the phase lag of the onset of the stimuli of the same frequency. The second is SSVEP phase which is SSVEP latency, the time between SSVEP peak occurrence and the onset of the stimulus. The third phase is the measured phase which is SSVEP latency to the stimulus phase of 0°. Figure 2.9 illustrates four stimuli flickering at 15Hz, the stimulus phases are 0°, −90°, −180° and −270°.

For classification, it first detected the frequency of the attended target followed by phase detection. To detect the phase, a reference phase has to first be calculated. Reference phase of each target is a subject–specific parameter. It is the average of the measured phases from EEG of the preliminary experiment. FFT amplitude was used to detect the frequency, a conventional SSVEP power spectral density (PSD) classification. To detect the phase, FFT coefficients were projected to the direction of the reference phase plane of the targets flickering at the detected frequency. The largest projection is identified as the attended target. Ideally, the measured phase of the attended target should be the same as the corresponding stimulus phase. However, this is unlikely to be realised in practice, but, it should be close to its corresponding stimulus phase, stimulus phase of the same flickering frequency should divide 360° equally. As the measured phase varies, the reference phases of the same stimulating frequency might not be divisible by 360° and would require calibration. The calibration could be done by adding the differences between the reference and the related stimulus phases, followed by averaging. The average value is then added to the stimulus phases as the calibrated reference phases. It was found that the standard deviation of the differences between the actual reference phase and stimulus phase were 15°, 16° and 16° for 10, 12 and 15Hz respectively. If such difference was normally distributed, for 95% confidence level, the difference would fall within two times of the standard deviations (=30° and 32°) as the phase margin. It was suggested that the stimuli of the same frequency should not exceed 6 whose phase margin is 30°.

The monitor screen is comprised of a matrix of pixels and is refreshed in a row by row fashion. Therefore, a time lag exists in different vertical positions during

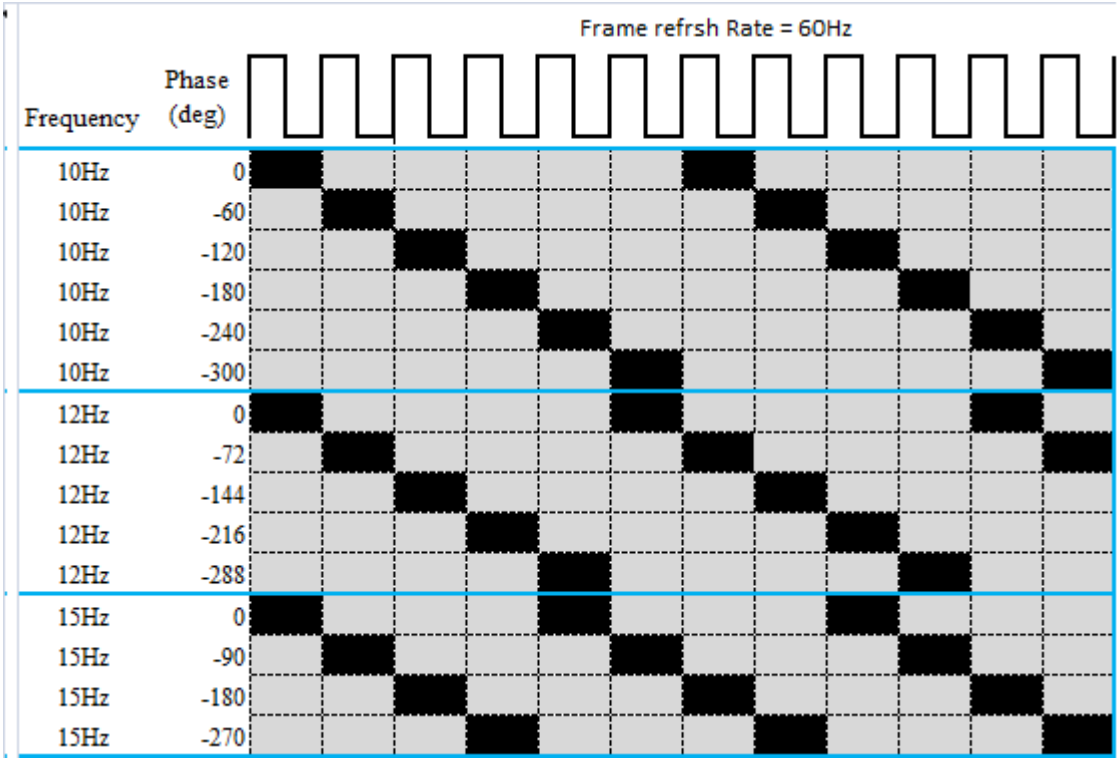

Figure 2.9: **Flickering sequence of 15 targets implemented by 3 different frequencies and different phases.** The refresh rate of the monitor is 60Hz. The phase difference between two adjacent stimuli is 1 refresh interval which results in 60°, 72° and 90° of the phase difference for 10, 12 and 15Hz respectively. **This figure is reprinted from (Jia et al., 2011) Copyright © 2011 IEEE.**

the refresh process. In other words, there is a phase lag between the images of different vertical positions on the screen. Based on the phase lag caused by the vertical positions, (Wong et al., 2010) developed a phase encoding method which took the vertical phase lag into account. In their study, there were two different phases, one was the phase from conventional phase tagged method, referred as predefined phase; one was the phase caused by the vertical positions in the monitor, referred as vertical phase. The stimuli positioned in the same row were given a different predefined phase. These stimuli were duplicated to a different row. Thereby, the stimuli of the same row had different predefined phases but the same vertical phases. The stimuli of the column had different vertical phases but the same predefined phases. The stimulus phase was the sum of the predefined phase and vertical phase. In their study, six visual stimuli of 20Hz were presented in a matrix of 2×3. The predefined phase was $-120°$ and the vertical phase $-60°$. The resultant phases of 6 stimuli were $0°$, $-120°$, $-240°$, $-60°$, $-180°$ and $-300°$ in row order.

The above method created more phase variation by including the phase difference caused by the relative vertical positions. For the six targets, the centre of the rows is at top and bottom quarter of the screen. Under the same condition, if 12 targets are presented in the matrix of 4×3. If the centre of the rows is at

the position of $^1/_8$, $^3/_8$,$^5/_8$ and $^7/_8$ of the screen (from top), the relative vertical phase of two adjacent rows was $-30°$. The resultant phases of this condition are $0°$, $-120°$, $-240°$, $-30°$, $-150°$, $-270°$, $-60°$, $-180°$, $-300°$, $-90°$, $-210°$, and $-330°$. The phase margin was only $\pm 15°$. To create more stimuli and maintain a phase margin, it may require a high resolution screen. When all stimuli flicker at the same frequency, the predefined phase and the vertical phase must be carefully chosen to prevent the duplicated phase.

Lee et al. (2010) implemented a cursor system with 8 LEDs flickering at the same frequency with distinct stimulus phases. The phase delay, referred between two adjacent stimuli was $45°$ which made the phase margin $\pm 22.5°$. The system was synchronised by the onset of the stimulus with no phase lag. To detect the attended target, the time latency from SSVEP peaks to the onset of the stimulus with no phase lag was measured. A control experiment measured this time latency for all targets in a one minute data recording set up. The latency of the stimulus with no phase lag was referred to as t_{ref} which was used as a time reference to detect the attended target and was subject-specific. In an online experiment, t_{peak}, the latency of SSVEP peak occurrence was estimated. The detected time delay, t_d was also calculated as the difference between t_{peak} and t_{ref}. t_d was converted to detected phase. The distances between detected phase and the expected phase delay of each target were calculated. The closest one was the attended target. Ideally, the detected phase should be the same as the phase delay of the detected target. However, there was always a difference between them. The standard deviation of the difference of the detected phases and stimulus phases was around $\pm 11.69°$ across all subjects. For 95% confidence level, the phase margin was around two times of the standard deviation, around $23°$. It was suggested that the stimuli of the same frequency in the phase tagged system should not exceed eight.

SSVEP phase drifts for various reasons, for example, due to the changes of the cognitive condition, the task and the adaptation of the stimuli. As a result, the reference phase and reference time required to be recalibrated or adjusted also changes. Wu et al. (2011) integrated this phase calibration process into a biphasic stimulus method. In the biphasic stimulus method, the stimuli were encoded by the same stimulating frequency but distinct phases. However, each stimulation cycle (1.8s) were divided into two stimulating periods (0.9s each) with two different phases. The phase of first stimulating period (reference phase period) was reference phase which was the same and applied to all stimuli. The phase of the second stimulating period (phase–shift period) was different stimulus–to–stimulus. EEG of a stimulation cycle was segmented into a reference phase epoch and a phase–shift epoch. In their experiment, eight stimuli were created by two stimulating frequencies. Four stimuli flickered at one of the two frequencies and the phase lag of two neighbouring stimuli was $90°$. Fourier transform was applied to EEG. Hotelling t–squared test was used to detect the frequency. The detected phase was the difference between the phase extracted from EEG reference epoch and the phase extract from EEG phase–shifted epoch and the target was iden-

tified. It was found that there was a phase transition period, around 150ms, at the time between two stimulating periods. The EEG of the phase transition period was excluded from both epochs. This method required two different phases stimulation in one cycle. Therefore, ITR might be affected due to the longer stimulation time.

As mentioned earlier, the frequency selection of the visual stimuli based on a monitor is restricted by the monitor refresh rate. Only the sub–frequencies of the refresh rate can be selected. However, a frame–based approximation method proposed by Wang et al. (2010b) resolved this limitation. A sixteen–button virtual telephone keypad on a 60Hz TFT monitor was presented. The selected frequencies of the stimuli ranged from 9 to 12.75Hz with 0.25Hz resolution. The average accuracy rate of this system is over 95% and the average ITR rate is 75.4 bits/min. The sub–frequencies of the 60Hz monitor are 30, 20, 15, 12, 10, 8.57Hz. From the monitor refreshing frames point of view, 10Hz stimulus completes an ON and OFF every 6 frames. For 11Hz stimulus, it takes 5.45 frames which are unlikely to be realised if the time durations of ON and OFF are the same. The approximation presentation method maintained the frequency, 11 of on–off but changed the number of frames for some ON and OFF. In other words, the time durations of ON and OFF in the approximation presentation method in one ON–OFF flash were not always the same. For example, the sequence of frames of 11Hz in one second could be [3 3 3 2 3 3 3 2 3 3 2 3 3 3 2 3 3 2 3 3 2]. The pair of two underlined numbers stands for one ON–OFF flash. The sequence of 11Hz is illustrated in Figure 2.10. The sequence contained 11 ON–OFF flashes. The number of frame intervals was 60. This sequence kept the total frames to 60 and maintained 11 times of flashes in a second. FFT spectrum demonstrated a clear peak at the stimulating frequency and its harmonics. SSVEP elicited by approximation and conventional methods in terms of SSVEP amplitude, SNR and classification accuracy was compared by Nakanishi et al. (2013). The results demonstrated that conventional method elicits better SSVEP response than approximation method but the difference between two methods was not significant. The approximation method can be used in SSVEP BCI systems which require a lot of targets.

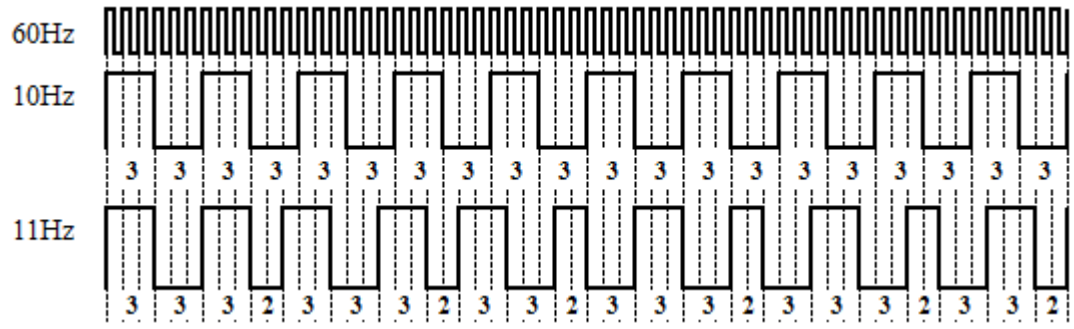

Figure 2.10: **Frame sequence for 10Hz and 11Hz stimuli presented on a monitor with 60Hz refresh rate (Wang et al., 2010b)**

Cecotti (2010b) investigated the feasibility of the duty cycle as a feature in SSVEP classification when the visual stimulator is presented on a monitor. The author defined the duty cycle as the ratio of the black screen to one stimulation cycle. Obviously, the duty cycle was also restricted to the monitor refresh rate. For example, for 10Hz stimulating frequency in a 60Hz refresh rate monitor, the duty cycles can only be 50%, 33.3%, 16.7% with 3, 2 and 1 frame of black frames (3, 4 and 5 frames of graphics), respectively. It was found that different duty cycles can induce different SSVEP distributions, mainly at the fundamental, 2^{nd} and 3^{rd} harmonics. The difference of the spectra could be used as a feature to classify the attended target. In other words, the stimuli flickered at the same frequency with different duty cycles could be discriminated. However, the discrimination was clearer when the difference of the duty cycles was large. A large difference of the duty cycles also limited the frequency selection as only lower frequencies are more likely to have large differences of duty cycles.

The visual stimulators could be presented on monitors (CRT and TFT monitors) or in the form of flickering light (LED). For light stimulation, the waveform driving the stimuli is an important factor which can affect SSVEP response. A square wave is one of the most common waveforms to drive LED visual stimuli in SSVEP based BCI paradigm. The shape of the waveform is an important parameter in addition to the frequency and the duty cycle.

Wu (2009) explored the influence of a square wave duty cycles on SSVEP response from 10% to 90% at stimulating frequency 10Hz. It was found that 40% and 50% duty cycles were the optimal duty cycles to elicit the most prominent SSVEP. Duty cycles 10%, 20%, 80% and 90% on the other hand elicited weaker SSVEP. Overall speaking, duty cycles had similar impact on SSVEP at the fundamental and 2^{nd} harmonics. When the duty cycle was over 50%, some 2^{nd} harmonic responses were larger than the ones of the fundamental. The duty cycle duration of a square wave can offset its DC component (from a Fourier series point of view). The author suggested that the DC component of square wave provided constant luminance stimulation to the eyes and inhibited some cells of eyes to change the polarity caused by stimuli. When the duty cycle was under 50%, DC component was not big enough to induce strong inhibition. When the duty cycle exceeded over 50%, DC value was big enough to lead strong inhibition. As a result, 40% and 50% duty cycle induced prominent SSVEP response.

Optimal duty cycles can enhance SSVEP response. Lee et al. (2011) also examined the influence of duty cycles on SSVEP at the stimulating frequency 13.16Hz, 11 different duty cycles from 10.5% to 89.5%. Before examining SSVEP response, the study conducted a survey about the visual comfort to the visual stimuli with different duty cycles. The results of the visual comfort survey indicated that most subjects felt the higher the duty cycles the more comfortable the visual stimuli. Over 60% of the 30 subjects considered 89.5% duty cycle as comfortable and delightful. Six of the 30 subjects continued the next experiment to evaluate how the duty cycles impacted SSVEP response. SSVEPs elicited by 13.16Hz with

11 different duty cycles from 10.5% to 89.5% were recorded and examined. The results showed that different duty cycles caused different impact on the amplitude of SSVEP at fundamental and 2^{nd} harmonic. As the duty cycle increased, SSVEP amplitudes at the fundamental frequency also increased. On the contrary, those of the 2^{nd} harmonic decreased. As a result, the ratio ($R_f = \frac{Amp_{har}}{Amp_{base}}$) of the amplitude of SSVEP at fundamental (Amp_{base}) and 2^{nd} harmonic (Amp_{har}) decreased as duty cycle increased. With 89.5% duty cycle, SSVEP at 13.16Hz was the most prominent and the one at 26.32Hz was the weakest compared to the other duty cycle values. The authors suggested the longer stimulation period of the high duty cycle contributed to an increased SSVEP response. The 2^{nd} harmonic was highly related to the rise of attention. The authors suggested that due to the discomfort of low duty cycles, the subjects might have paid more attention as a result the 2^{nd} harmonic was stronger than for high duty cycles. The shorter OFF period might contribute to the comfort of the visual stimuli. Based on the results of the visual comfort survey and SSVEP investigation experiment, an SSVEP BCI system consisting of 6 LEDs driven by high duty cycles (89.5%) was implemented. This study showed that carefully chosen duty cycles could not only enhance SSVEP but also improve the comfort of the users to the visual stimuli at a low–middle frequency band. The impact of duty cycles was not consistent with the finding of another study Wu (2009) which showed similar impact on SSVEP of the fundamental and 2^{nd} harmonic.

The impact of the duty cycles on SSVEP responses reported in the studies of Wu (2009) and Lee et al. (2011) did not agree with each other. Both studies investigated only one frequency and the frequencies of the two studies were not the same. Shyu et al. (2013) investigated the impact of the duty cycle on SSVEP response at a wider frequency range from 21Hz to 36Hz (in 3Hz increments) with duty cycles from 10% to 90% (in 10% increments). The results demonstrated that the optimal duty cycles to elicit the biggest SSVEP were subject–dependent and frequency–dependent. The optimal duty cycles found in their experiment varied from 20% to 80% across all subjects and all stimulating frequencies. Therefore, a 50% duty cycle of the square wave might not be the only optimal choice. Instead, a duty cycle should be chosen according to the stimulating frequency and the individual subject in order to boost his/her SSVEP response. The study also demonstrated that duty cycle was time–invariant. Once an optimal duty cycle has been chosen, it required no further calibration.

Beside the square wave, the sinusoidal, and triangle waveforms can also turn LEDs on and off. The driving mechanisms of the three waveforms are different. Square wave has only two states which either turns LED on or off. For sine and triangle waves, as long as the voltage levels of the waves, which are not a constant, exceed the LED threshold, the LED is on. Besides the driving mechanism, from a Fourier series point of view, they also differ in the frequency components content. Teng et al. (2011) investigated SSVEP spectra induced by LED driven by different waveforms: sinusoidal, triangle and square waves. The

impacts on SSVEP responses were examined by comparison of SSVEP at three frequencies, fundamental, 2^{nd} and 3^{rd} harmonics. It was found that a square wave with 50% duty cycle outperformed both the sinusoidal and triangle waves and elicited SSVEP responses at the three frequencies in most trials, especially at the fundamental and 3^{rd} harmonic. Interestingly, apart from the fundamental SSVEP, 2^{nd} harmonic could be seen regardless of the waveform. Theoretically, a sinusoidal wave has no harmonics. A square wave with 50% duty cycle and a triangle waveform had only odd harmonic components. This indicated that SSVEP harmonics might result from the fundamental frequency or the artefacts of the stimuli. It was concluded that a square wave with 50% duty cycle was the preferred waveform to elicit the strongest SSVEP at the fundamental frequency while sinusoidal waveform was the preferred one to minimise the harmonics. In the same study, it was also found that square wave of a 50% duty cycle can elicit stronger and consistent SSVEP than 10% and 25% duty cycles. The study did not investigate duty cycles over 50%.

2.5.3 Fatigue

The selection of the stimulating frequencies of the visual stimuli was a dilemma between the user comfort and the response. The lower frequency band resulted in more prominent response but caused user discomfort and fatigue. It also had the risk to induce epileptic seizures. On the other hand, the higher frequency band can reduce fatigue of the users but produced weaker SSVEP response (Diez et al., 2011).

There were several SSVEP studies attempted to reduce the fatigue and increase the comfort of the users. For example, Diez et al. (2011, 2013) proposed a BCI using high frequencies (37, 38, 39 and 40Hz) to control a mobile object and a robotic wheelchair. Lee et al. (2011) reported that the high duty cycle driven visual stimuli with stimulating frequency 13.16Hz improved the comfort of the user.

Chang et al. (2014) proposed an SSVEP based BCI using amplitude–modulation technique to modulate the visual stimuli to reduce the fatigue of the users. In their approach, the frequencies of the carrier (f_c) was set above 40Hz and the modulating frequency (f_m) was within the alpha band. The actual stimulating frequencies of the proposed system were $f_c \pm f_m$ Hz which were below 55Hz and higher than 28Hz. This frequency range was higher than the critical flicker–fusion frequency (Lee et al., 2011). The frequencies lower than the critical flicker–fusion frequency induced the discomfort of the users. The visual stimulation of the proposed system also elicited other harmonics which belonged to low frequency band, such as $f_c - 3 \times f_m$ and $2 \times f_m$. These harmonics of low frequency band had the larger amplitude of SSVEP response and contributed to improve the classification performance. As a result, the proposed system had the advantages of high and low frequency bands. In their on–line experiment, the subjects were given three types of visual stimuli modulated in low frequency band, high frequency band and amplitude–modulation. The participants evaluated three types stimuli

in terms of eye fatigue, sense of the flickering and daily use. The results showed that the low frequency stimuli induced more eye fatigue and sense of the flickering than the other two types. On the other hand, the participants preferred the high frequency or amplitude modulation stimuli for daily use than the low frequency stimuli. The online experimental results also showed that the mean accuracies of the amplitude modulation stimuli were higher than the other two.

2.6 Challenges of SSVEP based BCI

The design of asynchronous BCI, inter–subject variance, illiteracy and the speed of BCI remain the challenges of BCI. This section provides an overview of these challenges and possible solutions.

2.6.1 Asynchronous BCI

BCI can be categorised as synchronous and asynchronous BCI. The users of the synchronous BCI follow the cue initiated by BCI and perform the tasks to generate the input of BCI in the pre–defined time window. The users can only control synchronous BCI in the time period initiated by the system. A synchronous BCI is also called cue–based BCI. On the contrast, the asynchronous BCI is a self paced BCI. The control is initialised by the users intention. An asynchronous BCI has two states, intentional control state (IC state, or active state) and no control state (NC state, or idle state). In active state, the users perform the tasks to control BCI. In idle state, the user has no intention to control BCI, users either do not to perform any mental tasks or perform a mental task which would not change the BCI output. In idle state, the asynchronous BCIis more natural but the synchronous BCIis easier to be implemented. Asynchronous BCI detects the brain activities of the two states (i.e. active and idle) all the time. To discriminate these two states and reduce the false positive rate during idle state is one of the main challenges in asynchronous BCI design. To differentiate between active and idle state, normally a rejection classifier or a reliability function with a threshold is employed (Lotte et al., 2008). The performance of such classifier or function is assessed by the specificity and sensitivity, where $specificity = \frac{TN}{FP+TN}$ and $sensitivity = \frac{TP}{TP+FN}$ (Xia et al., 2013). TP, FP, TN and FN stand for True Positive, False Positive, True Negative and False Negative respectively. Several asynchronous SSVEP based BCIs adapted such principle.

Wang et al. (2010a) proposed a rejection classifier for SSVEP based BCI. The features of the classifier were obtained by CCA and maximum contrast combination (MCC). The rejection classifier included the first two largest correlation coefficients between EEG signals and the reference signals of the stimulating frequencies. The third element was SNR by MCC. According to their study, the active state had, in general, high correlation coefficients and SNR while the same features of the idle state were lower. The main cause of the misclassification was

due to some stimulating frequencies overlapping with the alpha band. Therefore, an the alpha band detection mechanism was implemented. If the detection of SSVEP overlapped with the alpha band, its 2^{nd} harmonic was used to ensure whether it was SSVEP response in active state or spontaneous alpha wave of the idle state. The classification accuracy of idle state with the alpha band detection exceeded 90%.

(Xia et al., 2013) developed a reliability function with a threshold for a SSVEP based BCI. SSVEP based BCI had four possible selections. The feature vector comprised of the canonical correlation coefficients of four targets. The ratio of the second largest coefficient to the largest coefficient in the feature vector was used to compare the threshold and discriminate between the active and idle states. The threshold was subject–specific and was calculated from a synchronous experiment and applied to the asynchronous operation mode to detect the active and idle states. In the active state, SSVEP was prominent. The correlation coefficient to the target frequency (the largest one) was significantly larger than the other non–target frequencies (second largest one). Therefore, this ratio was smaller than the threshold in the active state. On the other hand, none of the coefficients in the feature vector was significantly large in the idle state. Therefore this ratio was larger or equal to the threshold. The results showed that the average true positive rate was above 75% and the false positive rates were 2.37% and 12.05% for IC and NC states respectively.

Currently, most BCIs are synchronous which is not natural in real world applications (Leeb et al., 2007). Some BCI applications operated in asynchronous mode have been developed. Leeb et al. (2007) used motor imagery BCI to control a wheelchair in a virtual environment. This application used a threshold to detect the active and idle states. The result demonstrated that the subject can control the wheelchair accurately in a virtual environment. Another similar application from Velasco-Álvarez and Ron-Angevin (2009) also demonstrated that subjects were able to control the wheelchair in a virtual reality environment after a few training sessions.

Diez et al. (2011) used high frequency SSVEP based BCI to move a ball on a screen to a target position. The proposed method detected SSVEP response by analysing the normalised power at the stimulating frequencies. The power of a 2s window was calculated 4 times per second. If the maximum power within a time period (time threshold) was the same as the stimulating frequency, the ball was moved in the selected direction. To reduce the false positive rate caused by Midas Touch Effect (Diez et al., 2011), the time threshold was increased. The classification accuracy varied from 65% to 100%.

2.6.2 User acceptance and inter–subject variance

The system reliability and its ease–of–use affect the user acceptance of BCI (Luo and Sullivan, 2010). Subject–specific setup was able improve the reliability and

performance of the system (Scherer et al., 2009; Cecotti, 2010a). Due to the inter–subject variance, a calibration phase was normally required to determine some subject–specific parameters(Cecotti, 2010a). In SSVEP based BCI, for example, the calibration phase is used to calibrate the amplitude–frequency in a frequency–tagged system and the reference phase in a phase–tagged system for different subjects system (Chang et al., 2012).

The use of gel based electrodes and the number of the electrodes employed are the main issues for the ease of use of the system. Currently, there are dry electrodes available as an alternative of the traditional gel based ones. How to reduce the number of the electrodes employed without compromising the performance remains a challenge in BCI studies (Arvaneh et al., 2011).

Several SSVEP BCI studies attempted to reduce the time for the calibration phase. For example, Volosyak et al. (2010) proposed a multi–target amplitude–frequency method which significantly reduced the required time compared to one target in a time method. In the multi–target method, four different frequencies were stimulated at the same time. For each subjects, the top 5 frequencies which elicited the strongest SSVEP were found by both the single target and multi–target calibration methods. For 4 of the 5 subjects, at least 3 of the 5 frequencies for each subject were the same. The multi–target method only required 25% of the time required in the single target method. Chang et al. (2012) proposed a calibration–free SSVEP based BCI by using a stepping delay flickering sequence to drive the visual stimuli. The detection rate of the system from 8 subjects varied between 91% and 100%. Cecotti (2010a) proposed a calibration–less SSVEP based speller which used subject–independent parameters. The classification accuracies of 8 subjects ranged between 84% and 97%.

Multiple–electrodes could improve BCI performance and inter–subject variance (Luo and Sullivan, 2010; Friman et al., 2007). Several classification methods for SSVEP detection based on multiple electrodes had been proposed and outperformed the conventional power spectral density based analysis (PSDA) using bipolar electrodes (Friman et al., 2007; Lin et al., 2006). Although multiple electrodes improved BCI performance and reliability, more electrodes increased the set up and preparation time, computational cost and were more likely to induce user discomfort (Luo and Sullivan, 2010; Tam et al., 2011).

Reducing the number of the electrodes in the system could bring the following benefits, (Arvaneh et al., 2011; Tam et al., 2011; Lan et al., 2007),

1. A smaller electrode number could reduce the time of preparation and discomfort and improve the usability and comfort of BCI.

2. A smaller electrode number could reduce computation load, the cost of the hardware and make the system more affordable.

3. Reducing the number of the electrodes could remove the redundant/irrelevant

electrodes. As a result, it helps to prevent overfitting of the classifier and provide stable features.

Fewer electrode selection procedures had been developed. For example, in the study of Lin et al. (2006), the electrodes were selected by CCA correlation coefficients. In their electrode selection process, one electrode combined with its 5 nearest electrodes to form an electrode set with 6 electrodes. EEG of this electrode set was used to compute CCA correlation coefficient which was assigned to that electrode. CCA correlation coefficients of one electrode to all stimulating frequencies were averaged. The selection was based the averaged coefficients. 8 electrodes with highest coefficients were chosen as the recording electrodes. In another SSVEP BCI study (Bin et al., 2009b), also based on CCA, the electrodes were selected according to the coefficients of CCA spatial filter. The coefficients of CCA spatial filter indicated the contribution of the electrodes to canonical variant. 9 electrodes with the largest absolute values of the coefficients were selected.

Wang et al. (2004) proposed a lead–selection method which selected an optimal pair of bipolar electrodes, one as the signal electrode and one as the reference for SSVEP paradigm BCI. The lead–selection method used independent component analysis (ICA) to separate electrode signal into SSVEP signal and noise. The signal and noise correlations between different electrodes were computed. The optimal electrodes were selected according to the ratio of the signal and noise correlation of different electrodes. The classification accuracy of the selected optimal electrodes reached almost 100% with a time window of 4s. The results showed that the ITRs of 16 subjects ranged from 57 to 29 bits/min (mean ITR= 42 bits/min). Luo and Sullivan (2010) proposed a 4–class SSVEP BCI which used one single dry electrode. The mean classification rate was over 70% but the detection rates also showed great inter–subject variance from 100% to lower than 20%. Chang et al. (2012) also employed one one electrode in a 6–class SSVEP based BCI. The classification accuracies between the subjects were consistently high (over 90%). These studies showed that high classification rates could be achieved with fewer electrodes.

As the process to determine the best electrode is time consuming, is there universal set of the electrodes which could be applied to all the subjects existed? Schröder et al. (2005) argued that a universal optimal electrode subset might not work for all the subjects due to, (1) inter–subject head shape difference. The signal recorded from the electrode positions might be different, (2) the strategies of the mental task between the subjects might be different and (3) the brain areas which reflect the significance of the mental task between the subjects might be different. EEG differed from session to session and depended on the subjects physiological condition at the time, such as tiredness, attention and the strategies employed for each mental tasks (Tam et al., 2011).

2.6.3 Illiteracy

BCI illiteracy is one of the challenges facing BCI research. BCI illiteracy is a phenomenon when BCI cannot detect the users brain activities needed as input. BCI illiteracy varies across different BCI paradigms. Blankertz et al. (2010b) estimated about 15% to 30% of BCI users cannot control motor imagery based BCI effectively. Another estimated illiteracy across different BCI paradigms was between 10% and 25% (Allison et al., 2010a). BCI illiteracy is less noticeable in BCI paradigms based on event related potentials. None of the estimations of BCI illiteracy is negligible. The reason behind BCI illiteracy is unknown. But it is believed that training and feedback could reduce it.

Few BCI studies, as described later, attempted to answer the following questions:

1. How many people can actually use BCI effectively?
2. What factors can affect BCI performance?
3. How BCI illiteracy can be detected/predicted?
4. How can BCI illiteracy be overcome?

Guger and Edlinger (2007); Guger et al. (2009, 2011) conducted three studies on a large number of subjects (>50) to investigate how effectively people operate BCI in three different paradigms including motor imagery, P300 and SSVEP. Bremen BCI research group also had two field studies (Allison et al., 2010a; Volosyak et al., 2011) for SSVEP based BCI. The studies investigated how many un–screened subjects could actually use BCI as a communication channel and what factors such as age, gender, experience and sleep etc., might affect BCI performance. In the studies (Guger and Edlinger, 2007; Guger et al., 2009, 2011), 99, 100 and 53 subjects participated in the experiments of BCIs based on motor imagery, P300 and SSVEP respectively. These studies provided a brief training session to the subjects and the subject–specific classifiers were obtained from the training sessions. The results showed that most of the subjects were able to control BCI in three studies. But BCI performance in terms of the classification accuracies varied in different paradigms. In motor imagery BCI, only 6.2% of the subjects achieved over 90% accuracies and around 51.3% of the subjects achieve the classification accuracy over 70%. In P300 BCI, 67% of the subjects were able to spell the word LUCAS correctly (100%). Only less than 2% of subjects were unable to spell a single letter. 86.7% of the subjects could control SSVEP based BCI with over 90% accuracy after the training session. About 2% had accuracy lower than 70%. In Bremen two field studies (Allison et al., 2010a; Volosyak et al., 2011), 106 and 86 visitors to the expositions at Hannover were recruited. In the study where the subjects performed a spelling task, the range of the mean accuracies among different text spellings was between 66 to 100%. The overall mean accuracy was over 95%. In the study where the subjects performed the navigation of the maze task, two frequency bands, medium and high, were evaluated. In medium frequency band, only two subjects were unable to complete the task and were regarded as BCI–illiterates. Thirty subjects were unable to

complete the task using the high frequency band. For those who succeeded to navigate the maze, the mean accuracies were 92% and 89% for the medium and high frequency bands respectively.

Most of the subjects in the above studies had no prior experience in BCI. The subjects of motor imagery BCI study from Guger and Edlinger (2007) and Allison et al. (2010a); Volosyak et al. (2011) studies were the visitors to the exhibitions. Most of BCI nave people were able to operate BCI. The performance of SSVEP and P300 BCI was better than the motor imagery BCI in these studies. However, it might not be able to conclude that SSVEP and P300 BCI had less illiteracy than motor imagery BCI, because these experiments had different setup, signal processing methods, etc. However, Breman SSVEP BCI studies also showed less BCI illiteracy in SSVEP paradigm. Their result of the maze navigation study suggested that the high frequency band had more BCI illiterates than the medium frequency band.

These studies also used questionnaire to explore the relation between BCI performance and inter–subject factors, such as age, gender, education level, handedness, hours of sleep in the previous night, experience of BCI and computer game, consumption of alcohol, caffeine and cigarette etc. In general, the impacts of these factors on BCI performance were not statistically significant.

In the spelling study of the Bremen group (Allison et al., 2010a), it was found that the text requiring the least number of cursor movements resulted in the highest ITR. Thereby, the author suggested the design of BCI should minimise mental loading. The mental tasks of the motor imagery BCI was more demanding than SSVEP and P300. This might explain why more subjects can control SSVEP better than motor imagery based BCI for all the subjects who were nave to BCI. However, the length of the spelt text did not show significant impact on BCI performance. The authors pointed out that the subjects did not like the long text and the extent of the application complexity could affect BCI performance. Simple tasks, in general, were performed more accurately than complicated tasks (Kübler et al., 2013).

BCI control is a new skill (Wolpaw et al., 2002). BCI is a close loop system with two controllers, the user and the BCI itself (Pfurtscheller and Scherer, 2010). However, the users are often not given proper training and feedback to learn this skill. As the impact of training was seen in a SSVEP BCI study (Guger et al., 2011) when a brief short training session improved the overall performance significantly. The impact of feedback, on one hand, might help the subjects to concentrate but on the other hand, it might distract the subjects on performing the task itself. The performance of motor imagery BCI was similar with or without the feedback. Pfurtscheller and Neuper (2001) reported that BCI performance does not significantly improve by increasing the feedback sessions when the accuracy exceeded over 80%. They termed this as man–machine learning dilemma (MMLD). In a BCI system, the BCI user and the system itself are

highly interdependent and have to adapt to each other. The adaptation starts from training the BCI. In the training phase, no feedback is provided to BCI user. When the feedback session begins, each feedback session is an adaptation from the user to BCI. However, feedback may introduce noise and unfavourably affect BCI performance. A study on the impact of the biased feedback on BCI performance suggested that the design of BCI feedback should take the users present BCI skill into consideration (Barbero and Grosse-Wentrup, 2010). In the study, it is found that an incorrect feedback has negative impact on BCI performance for those who are able to operate BCI efficiently. However, introducing incorrect classification results to feedback when the subject did not make any error (but only perceives that the interface is performing incorrectly) might improve BCI performance for those whose performance was around chance level. The feedback and motivation are important in BCI performance. The author hypothesised that presenting inaccurate classification results through the feedback to motivate subjects may improve BCI performance.

Vidaurre and Blankertz (2010) proposed an approach of machine learning co–adaptive calibration between the classifier and the users. In the study, the users were divided into three groups according to their BCI performance. In the first group, a classifier was obtained in the calibration phase without feedback. The users of this group performed well in the feedback session. In the second group, the user–specific classifier was obtained but the users of this group did not perform well in the feedback phase. The third group was the users whose classifiers were not obtained. The proposed approach aimed to improve the performance of the users in the second and third groups. There were three steps of co–adaptation,

1. Phase I: In this phase, BCI used a subject–independent classifier which allowed fast adaptation to users. The subject–independent classifier was also adapted.

2. Phase II: The data of Phase I was used to select subject–dependent parameters, such as the frequency band and electrodes of the spatial filter. The electrodes were re–selected in the trials of this phase and the classifier was re–trained.

3. Phase III: The data of Phase II was used to calculate the spatial filter and the subject–dependent parameters were optimised in phase II. An unsupervised classifier was re–trained in this phase.

The accuracy of the users of group two and three improved from 50% to over 70% through this proposed adaptation process.

Allison et al. (2010b) suggested that a hybrid BCI could be a cure to BCI illiteracy. In their study, the subjects were asked to perform three types of tasks, motor imagery task only, attending visual stimuli only, and performing both motor imagery and attending visual stimuli simultaneously in a hybrid BCI of motor imagery and SSVEP paradigm. The results showed when the subjects performed only one of the two tasks, 5 of 14 subjects of each task attained the accuracy

below 70%. However, all subjects attained over 70% accuracy when performing both tasks at the same time in the hybrid BCI paradigm. A similar result was achieved with a hybrid BCI developed to control a wheelchair (Li et al., 2013). In a task evaluation session, BCI determined the best subject–dependent mental strategy. For each subject, the best mental strategy could be motor imagery, SSVEP or both. The experimental results showed that subjects could control the wheelchair by one of the paradigms even if they were illiterate with another paradigm. However, the best performance results came from the combination of both strategies. These studies suggested that hybrid BCI offered the users more modalities to operate the system and in turn more information was provided to the BCI (Li et al., 2013). Moreover, improved signal processing algorithms to analyse the data and extract salient features could also improve BCI illiteracy (Brunner et al., 2010).

Blankertz et al. (2010a) suggested that the resting alpha rhythm can be used as a performance predictor of motor imagery BCI. It was found that the strength of the SMR idle rhythm was highly correlated to the performance of the motor imagery BCI. This predictor comprised of two minutes of EEG recording from subjects C3 and C4 while the subjects are relaxed with their eyes opened. The predictor could be used as a screening criteria before the experiment. Ahn et al. (2013) and (Blankertz et al., 2010a) found that a BCI–illiterate group, exhibited weaker alpha rhythm in comparison to a BCI–literate group, and a strong theta rhythm with eyes opened at resting. Theta band was negatively correlated to BCI performance. They also found that gamma rhythm in the prefrontal area was highly related to BCI performance. The baseline resting rhythm and early self–regulated slow cortical potential could be used as BCI performance predictors for SSVEP and SCP BCI respectively (Fernandez-Vargas et al., 2013; Neumann and Birbaumer, 2003).

2.6.4 Speed

BCI performance can be assessed by three aspects, classification output, application output and influence on its users (Vaughan et al., 2003; Thompson et al., 2013). BCI classification output is a performance measurement of its algorithm to convert the brain signal into one of the possible classes. The bit rate and accuracy are most common indicators in this aspect (Vaughan et al., 2003; Thompson et al., 2013; Kronegg et al., 2005). BCI application output is the performance measurement of a valid user communication bandwidth. The impact of BCI on its user is to determine how BCI makes a difference to its users, for example, the quality of their life (Vaughan et al., 2003; Thompson et al., 2013). To compare the performance across different BCI paradigms, the classification accuracy, bit rate per trial and ITR are normally used as a starting point. ITR is a joint result of accuracy and bit rate. Bit rate (bits/trial) (Wolpaw et al., 1998; Kronegg et al., 2005)can be calculated by the following equation (2.2),

$$B(bits/trial) = \log_2 N + P \times \log_2 P + (1-P) \times \log_2 \frac{1-P}{N-1} \qquad (2.2)$$

In equation (2.2), N is the number of BCI classes, P is the classification accuracy. ITR (bits/min) can be obtained as in (Yuan et al., 2013) by equation (2.3).

$$ITR(bits/min) = B \times \frac{60}{T} \tag{2.3}$$

Where T is time interval (in second) required to generate a classification output.

From above two equations (2.2) and (2.3), it is clear that the parameters N, P and T all affect bit rate and ITR. These three parameters are correlated and have different impact on each other. McFarland et al. (2003) studied the correlation between the bit rate and the number of targets. The bits/trial increased as the number of the targets increased and reached to its highest at 4. The bit rate equation (2.2) suggested that increasing the number of targets will increase the bit rate. However, McFarland et al. (2003) pointed out that this is not necessarily the case if the user had poor performance with fewer number of targets. The same study also suggested that classification accuracy could be improved by increasing the trial interval at a possible cost of decreasing the overall ITR. The study also showed that ITR was highest when the trial interval was 3(McFarland et al., 2003).

Although the above equations (2.2) and (2.3) provide an objective view of BCI information output to assess the performance across different BCIs, it has its limitations. Some assumptions are made for the bit rate equation. First of all, it is assumed that BCI is a memory–less and stable system which can only recognise N classes. It is also assumed that the probability of each class being chosen is the same and is equal to $\frac{1}{N}$. The classification accuracy ($=P$) and error ($=\frac{(1-P)}{(N-1)}$) of all classes is also the same (Wolpaw et al., 1998; Kronegg et al., 2005; Yuan et al., 2013). Nevertheless, none of these assumptions are strictly always true. For example, the equation of calculating bit rate might not be applied to an asynchronous BCI which has no–control (NC) state. NC class is not one of the N classes but it is more likely to be selected than any of the N classes of IC state (intentional control state). Similarly, BCI may have different classes in different conditions which would make equation (2.2) not suitable to use. For example, in a menu selection BCI, the number of classes is different at different stages of the process. Furthermore, in a P300 spelling application, the next letter selected sometimes is highly dependent on the letters that were previously selected. Using the equation without making all these aforementioned assumptions might lead to unexpected results (Kronegg et al., 2005; Yuan et al., 2013; Thompson et al., 2013).

The bit rate is an important performance measure for BCI systems. However, for some applications such as a spelling application, bit rate might not provide an objective view of the BCI performance. For example, in a spelling application, if an erroneous selection is made, it will take at least two extra selections to correct the erroneous one; one to delete the error and one to select the correct letter. For an application like spelling, error corrections are not the information which

the users want to deliver. Furdea et al. (2009) defined the written symbol rate (WSR) which takes error corrections into account. Analogous to bit rate, symbol rate (SR) and WSR are defined by equations (2.4) and (2.5)

$$SR = \frac{B}{\log_2 N} \tag{2.4}$$

Where *B, N* are the same as equation (2.2). WSR is defined by

$$WSR = \begin{cases} \dfrac{2SR-1}{T} & \text{if } SR > 0.5 \\ 0 & \text{if } SR \leq 0.5 \end{cases} \tag{2.5}$$

where T is the interval between two trials. WSR excluded the error selection. In a spelling application, the error correction could be done by deleting the wrongly selected letter. When $SR \leq 0.5$ this means that the users are making more errors than correct selections. SWR is assigned to zero in such case. Townsend et al. (2010) defined the practical bit rate by taking the error correction into account. If the error rate is p_{err}, p_{err}= 1-p (accuracy), (M) selections have to be made to deliver information of N_{total} letters. M could be obtained by equation (2.6)

$$M = N_{total} \sum_{i=0}^{\infty} (2p_{err})^i = \frac{N_{total}}{1 - 2 \times p_{err}} \text{ ,when } p_{err} < 0.5 \tag{2.6}$$

The practical bit rate could be obtained from the expected total selections required. From equation (2.6), $\dfrac{1}{1-2\times p_{err}}$ selections are required to make one correct selection. Therefore, in a system of N selections, the practical bits per selection can be experessed as $\dfrac{\log_2 N}{\dfrac{1}{1-2\times p_{err}}}$=$\log_2 N \times (1 - 2 \times p_{err})$.

The practical bit rate (PBR) is obtained by equation (2.7)

$$PBR = \begin{cases} (1 - 2 \times p_{err}) \times \log_2 N & \text{if } p_{err} < 0.5 \\ 0 & \text{if } p_{err} \geq 0.5 \end{cases} \tag{2.7}$$

p_{err} is replaced by *1-p*. Equation (2.7) is re-written as equation (2.8)

$$PBR = \begin{cases} (2 \times p - 1) \times \log_2 N & \text{if } p > 0.5 \\ 0 & \text{if } p \leq 0.5 \end{cases} \tag{2.8}$$

Figure 2.11 plots the theoretical bit rate and practical bit rate vs. accuracy. The theoretical bit rate (TBR) represents the maximum bit rate the system could deliver. The practical bit rate (PBR), on the other hand, illustrates the realistic rates which could be expected. The difference between the TBR and PBR is due to error correction (p_{err}). When p_{err} is close to zero, PBR is almost equal to TBR. PBR is zero when $p \leq 0.5$.

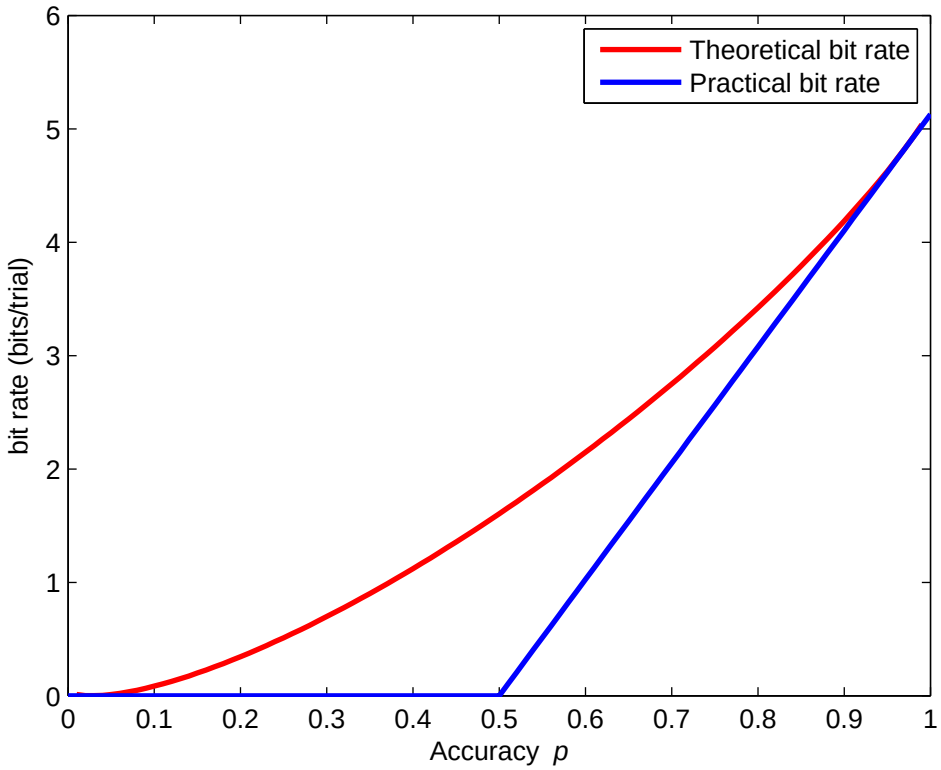

Figure 2.11: **The comparison of the theoretical and practical bit rate.** This plot was based on a BCI with 36 selections, for example a 6×6 P300 speller.

Yuan et al. (2013) supplied a list of guidelines to correctly use these equations to produce an objective measurement of ITR. These guidelines unambiguously defined N, P and T to ensure the ITR provided a true and fair view of BCI performance. For an N class system, N should be based on the total possible selections, instead of the selections at different stages of the process. For the classification accuracy, there should be enough test trials and no error correction mechanism when estimating ITR. A class should be randomly selected with the same probability as other classes. In a synchronous BCI, the time duration between two selections could affect ITR. Therefore, it should be explicitly mentioned if this time duration between two selections was included as part of the time interval when estimating ITR. Finally, ITR should be based on all participants data, not the screened subset of subjects with better performance.

Yuan et al. (2013) also discussed the impact of the number of the classes, the classification accuracy and time interval on ITR. The error of ITR ($\triangle ITR$) can be estimated by the following two equations (2.9) and (2.10) as defined in (Yuan et al., 2013),

$$\triangle ITR = \frac{60}{T} \times \log_2 \frac{P \times (N-1)}{1-P} \times \triangle P \tag{2.9}$$

And

$$\triangle ITR = \frac{-60}{T^2} \times B \times \triangle T \tag{2.10}$$

From equations (2.9) and (2.10) , the parameters T,P and N all affect ITR, especially T.

Without considering the trial interval, the accuracy is often used to measure the performance of BCI classification algorithm. It is very natural and straightforward to compare accuracy with the chance level in the first instance. For example, in a four–class BCI, the result is compared with the chance level 25% ($^1/_4$). An effective BCI should have its accuracy higher than chance level. For example, 70% for a two–class BCI paradigm whose theoretical chance level is 50% (Allison et al., 2010b). Müller-Putz et al. (2008) examined the relationship between the classification accuracy (or chance level) and the number of trials per class and argued that without considering the number of trials, the explanation of the data might be incorrect. It was found that the chance level is affected by the number of trials representing per each class. The larger the number of trials, the closer the chance level is to its theoretical value. For example, a two–class BCI paradigm has a theoretical chance level of 50%, i.e. when the number of trials is close to infinity, however, with 20 trials/class, at a confidence level = 99% , the chance level should be 75% and for a four–class BCI with 100 trials/class, at a confidence level = 99%, the chance level is 35% (Combrisson and Jerbi, 2015). Simply comparing the classification accuracy to the theoretical chance level without considering the number of trials will mislead the interpretation of the results (Müller-Putz et al., 2008).

BCI translates the classification result based on a particular feature vector into a command to the intended application. The extracted features should be modified and optimised according to different conditions to optimise the output and increase the valid bandwidth (Vaughan et al., 2003; Thompson et al., 2013). For example, a built–in word prediction function in a spelling system could increase the valid communication bandwidth. The output of the word is dependent on already selected letters. A simplified error recovering procedure can also improve the efficiency of BCI operation (Yuan et al., 2013). At a BCI application level, the efficiency and utility metrics are used to assess BCI performance. This level is correlated to the computer human interface (HCI).

Bit rate and ITR might not be the only performance indicators (Vaughan et al., 2003; Yuan et al., 2013). However, they are currently the most important and fundamental ones. The enhancement and improvement of a BCI system before and after classification might be considered wasted effort in without a high ITR module.

2.7 Summary

In this chapter, we have presented different BCI paradigms and their advantages and disadvantage. We also focus on SSVEP based BCI and discuss its limitations and challenges. Several studies have proposed different techniques to overcome the limitations and the challenges. These studies have established solid fundamentals and enhanced the feasibility of a SSVEP BCI system.

Chapter 3

Methodology

One of the primary goals of this study is to evaluate the feasibility of a distance adaptable SSVEP based BCI. There are two main experiments in this study. The first experiment, termed as Investigation Experiment, is an initial experiment to explore the impact of the viewing distance on SSVEP response on a limited number of subjects. The second experiment, termed as Feasibility Experiment, is to evaluate the feasibility of a four–class SSVEP based BCI setup. Both experiments are approved by the departmental Ethics Committee.

3.1 Experimental setup

In the Investigation and the Feasibility Experiment, four viewing distances, 60cm, 150cm, 250cm and 350cm, are tested. Four frequencies, 12Hz, 13Hz, 14Hz and 15Hz are chosen as the stimulating frequencies.

3.1.1 Subjects

Subjects were recruited according to the following inclusion/exclusion criteria: age over 18 years old, normal or corrected-to-normal vision, no history of epileptic seizure (in particular, photosensitive epilepsy), no history of any neurological diseases, injuries or trauma, no allergy to conductive gel and English speaking to understand the instruction.

Two subjects (one male and one female, ages 33 and 45) participated in the first experiment, the Investigation Experiment, to examine the impact of the viewing distance on SSVEP. One subject is naïve to BCI and one subject has SSVEP based BCI experience. Consent forms and the experiment information pack are provided to the subjects before the experiment. The experiment procedure is explained briefly. Each subject is seated on a comfortable chair in a dim room. Subjects are instructed to avoid blinking and movement during the experiment, especially during the attending phase. The subjects of the Investigation Experiment are invited to participate the Feasibility Experiment. An additional 8 subjects are recruited for the Feasibility Experiment. A total of 10 subjects

(8 males, 2 females, ages between 21 and 45) participated in the Feasibility Experiment. The procedure and protocol of the Investigation and the Feasibility Experiments are the same.

3.1.2 Data acquisition

Surface EEG is recorded using a 128 channels EEG cap(Montage No. 15, EASYCAP) based on 10–20 international system. SSVEP can be recorded most significantly at the electrodes over the visual cortex (Bin et al., 2009b; Zhang et al., 2011; Lin et al., 2006; Müller-Putz et al., 2005). 11 electrodes over visual cortex are selected as signal electrodes. Cz is chosen as the ground and Fz as the reference electrode. Figure 3.1a shows the electrode montage and channel selection. The subject wears an EEG cap. EEG abrasive skin prepping gel (Nuprep Gel) and EEG conductive gel (Electro–Gel) are applied to the electrode sites to eliminate the dead skin and reduce the impedance between scalp and electrodes. The impedance is kept under 5kΩ throughout the entire experiment. EEG acquisition hardware and software are SynAmps^2 (amplifier) and NeuroScan 4.5 (recording software), both from Compumedics Neuroscan. EEG sampling frequency is 2k Hz. Figure 3.1b shows EEG cap with electrode cables connected in the experiment.

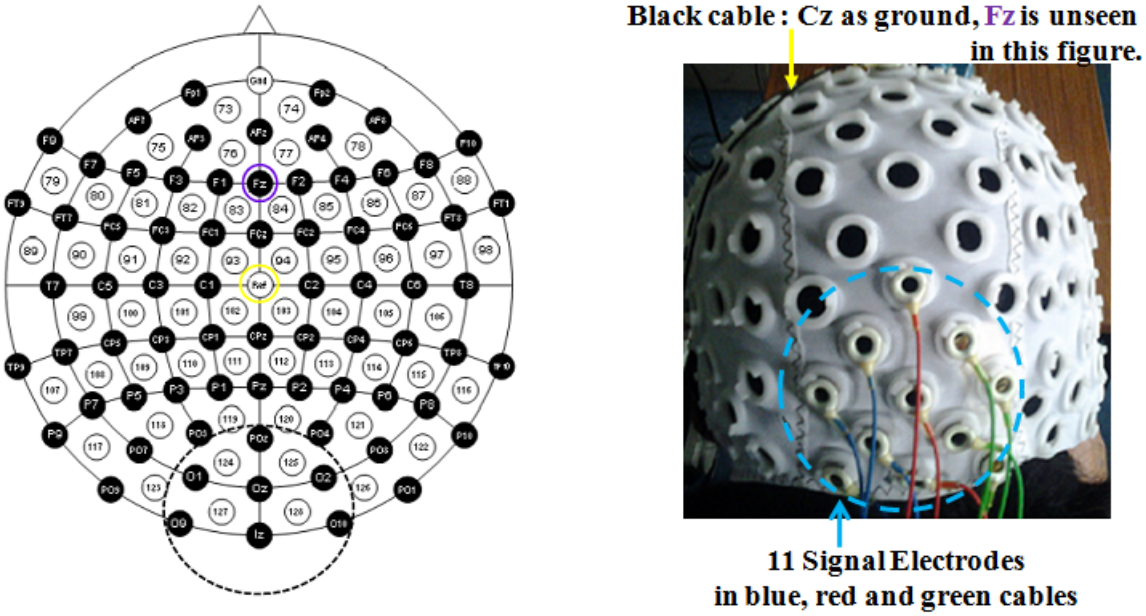

Figure 3.1: **Electrode selection of EEG acquisition.** (a) 11 electrodes (in the black dotted circle) over the visual cortex are selected as EEG recording electrodes. Cz (in the yellow circle) and Fz (in the purple circle) are selected as the ground electrode and the reference electrode respectively. The electrode positions are from http://www.easycap.de. (b) A subject wearing an EEG cap with electrode cables connected in the experiment.

3.1.3 Experiment protocol

The experiment records surface EEG while the subjects are attending the flickering LED. in each experiment, there are 4 blocks, one block for each viewing distance, at most. Each block consists of 4 runs, one run for each class. Each run has twenty trials. Each trial contains two phases, one resting phase and one attending phase. To prevent visual adaptation and habituation, the duration of the resting phase lasts for 5s or 6s at random. The stimulation duration of one attending phase lasts for 5s. The timing scheme of the experiment is shown in Figure 3.2 which is applied to both Investigation and Feasibility Experiment. In the Investigation Experiment, the visual stimulator flickering at one of the stimulating frequencies is presented to the subject at same viewing distance. In the Feasibility Experiment, four LEDs flickering at four different stimulating frequencies are presented to the subject. In the resting phase, the visual stimulator is off. During the attending phase, the LED(s) is/are flickering at the designated frequency. The stimulation duration of each experiment is around 60 minutes. The electrode impedance is checked between two runs. There is a 1–2 minutes break between two runs.

In both experiments, the viewing distances presented to the subjects are in the same fixed order, 60cm-150cm-250cm and 350cm. The attending targets were presented and attended in random order in the Investigation Experiment and in the Feasibility Experiment respectively.

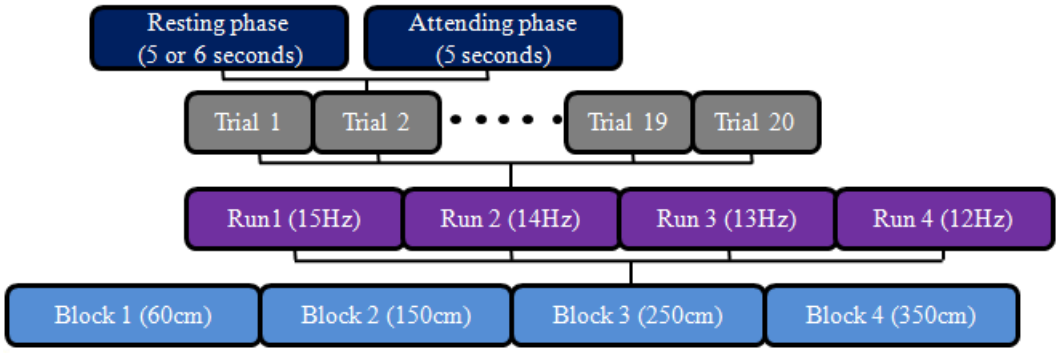

Figure 3.2: **Timing of the Investigation Experiment.** Each experiment has four sessions at most. Each session contains 4 runs. Each run has 20 trials. Each trial includes one resting phase lasting for 5s or 6s randomly and one attending phase lasting for 5s.

In the Investigation Experiment, only one LED flickering at one frequency is presented to the subjects in uncompensated or compensated condition. In uncompensated condition, the intensities of LEDs are the same regardless of the viewing distances. Whereas, in compensated condition, the intensities of LED are increased as the viewing distances increase (compared to the intensities at the viewing distance at 60cm). The intensities of LEDs at the same viewing distance are the same.

In the Feasibility Experiment, four LEDs flickering at different frequencies simultaneously are presented to the subjects. Figure 3.3 shows one of the subjects in the Feasibility Experiment facing 4 LEDs stimuli at the viewing distance 60cm. The intensities at different viewing distances are different. Refer to section 3.3.2 on page 78 for how the intensity of the LED at different viewing distance is adjusted.

Figure 3.3: **One of the subjects in the Feasibility Experiment facing 4 LEDs stimuli at the viewing distance 60cm.** This figure is for illustration purposes only as the room during the experiment is dim.

3.2 Data pre–processing

The recorded EEG data is filtered by a zero shift FIR band pass 1–50Hz filter provided by NeuroScan. EEG was segmented into epochs from 1s before stimulus onset to 5s after stimulus onset. Epoch segmentation was performed by EEGLAB toolbox (Delorme and Makeig, 2004).

3.3 Visual stimuli design and stimulation parameters

In this section, the visual stimulators and the parameters selection used in both experiments are described. This section begins with the selection of the parameters used in the experiments followed by the design of the visual stimulator and the circuit used to drive LED.

3.3.1 Visual stimulus (stimuli)

SSVEP is sensitive to the properties of the visual stimuli, such as flickering frequency, colour, size, duty cycle and intensity of the light (Morgan et al., 1996; Srinivasan et al., 2006). SSVEP′s response is also highly correlated to the level of attention (Morgan et al., 1996; Toffanin et al., 2009). Currently, there is no general agreement on the best configuration of visual stimuli as SSVEP is a confounded response of these parameters which can affect each other. For example, colour of visual stimuli could affect the frequency selection. When using 11Hz of stimulating frequency, red colour of visual stimuli can elicit the strongest SSVEP. At 13Hz of stimulating frequency, blue light can elicit the strongest SSVEP (Zhu et al., 2010a). Duszyk et al. (2014) investigated the effect of visual stimuli colours on SSVEP response. In their experiments, 5 colours, blue, green, white, yellow and red, were tested with different frequencies. Overall speaking, blue colour elicited the weakest SSVEP response regardless of the frequencies used in the experiment. The differences of SSVEP responses elicited by the other four colours were not significant. The mean strength of SSVEP elicited by different colours were in order of white > yellow > red> green. However, the order of SSVEP response elicited by different colours is also dependent on the stimulating frequency. In 14Hz, the order was white > yellow > red > green. In 25Hz, the order was yellow > white > red > green. Gollee et al. (2010) used red light in their SSVEP study to control a functional electrical stimulation system.

SSVEP response is also dependent on the stimulating frequency (Morgan et al., 1996; Herrmann, 2001). The frequency-SSVEP amplitude was normally used to choose the stimulating frequency. However, there was no general rule or guideline to choose the frequencies in terms of frequency band and the frequency resolution. It was highly dependent on the purposes of studies. For example, Gao et al. (2003) and Hwang et al. (2012) implemented environment controller and keyboard by LED visual stimuli. In their studies, they chose low frequency bands with 0.02Hz and 0.01Hz of resolution. In Friman et al. (2007) study, they chose 5, 7, 9, 11, 13, and 15Hz to drive LED visual stimuli which belong to low and medium frequency bands. Bin et al. (2009b) also used the frequencies in low and medium bands, 6.7, 7.5, 8.6, 10, 12 and 15Hz. Volosyak et al. (2011) and Gollee et al. (2010) used medium frequency band (13, 14, 15 and 16 Hz) in their studies. High frequency band (34, 36, 38, 40 Hz) was also used, for example, by Volosyak et al. (2011). Tsoneva et al. (2015) used high frequency band (40 to 60 Hz) in their SSVEP study.

LED is easy to be integrated into most of the environments and its portability fits the aim of the study. In a survey study of visual stimulation methods in SSVEP BCI (Zhu et al., 2010a), it was reported that 24 out of 58 reviewed studies used LED as the visual stimulator. Among those 24 studies using LED, red, white and green colours of LED were used in 8, 4 and 3 studies respectively. 9 out of 24 did not specify the colour. Most of studies used red LED used medium band frequencies (12 to 30 Hz). The classification methods of this study were CCA, MEC and MCC. The frequencies of the studies using these methods were in the

range of 5 to 40Hz. The majority was in the medium band (Bin et al., 2009b; Friman et al., 2007; Gollee et al., 2010; Volosyak et al., 2011). This study chose red LEDs driven by the stimulating frequencies 12, 13, 14 and 15Hz in medium frequency band as the visual stimuli. Changing viewing distance between the visual stimuli and the users could change the perception of the intensity, size of the visual stimuli and the extent of the attention of users.

In the Investigation Experiment, two types of LEDs with different intensities are used as the visual stimuli, OSRAM ™, part no: LR G6SP–CADB–1–1, 7100mcd for higher intensity, and part no: LS E63B–BBCB–1–1, 2525mcd for lower intensity. Both LEDs are red colour and surface mount devices. In the Feasibility Experiment, 4 red colour LEDs of the same type, OSRAM ™, part no: LR CP7P–JSJU–1, are used as the visual stimuli. Each LED is mounted on a small plate. The size of the plate is (L × W: 19.9mm × 19.9mm) for both LR G6SP–CADB–1–1 and LS E63B–BBCB–1–1. The size of the plates is (L × W × H : 20mm × 20mm × 3.85mm) for LR CP7P–JSJU–1.

The plate makes LED easier to be handled during the experiment. LR CP7P–JSJU–1 mounted on a plate is shown in Figure 3.4a. In the Investigation Experiment, one LED plate is attached to the centre of a 60cm (Length)×40cm (Width) board. In the Feasibility Experiment, 4 LED plates are attached to the same board in a rectangular layout symmetric around the centre of the panel. The distance between the centres of two adjacent LED plates is 25cm as seen in Figure 3.4b. Their main characteristics, such as emission angle and spectrum / dominant wavelength are listed in Table 3.1. In the Investigation Experiment, LR G6SP–CADB–1–1 and LS E63–BBCB–1–1 are used to investigate the impact of the viewing distances on SSVEP response. LR CP7–JSJ–1 is used to evaluate the feasibility of proposed SSVEP based BCI.

Table 3.1: **Characteristics of LEDs used in this study.**

LED	Dominant Wavelength (nm)	Viewing Angle (°)	Colour	Class	Experiment
LS E63B-BBCB-1-1	633	30	Red	Exempt group (IEC 62471:2008)	Investigation
LR G6SP-CADB-1-1	625	120	Red	Class 1M (IEC 60825-1)	Investigation
LR CP7P-JSJU-1	623	80	Red	Exempt group (IEC 62471:2008)	Feasibility

LED data sheets and characteristics charts (Tables A-1, A-2,and A-3. Figures A-1, A-2 and A-3) can be seen in Appendix A.

Shyu et al. (2013) demonstrated that the optimal duty cycle was subject and frequency dependent. The aim of this study is not to find the optimal duty cycle for an individual subject and frequency. In this study, LED is driven by a square wave with a 50% duty cycle which has been widely used in other SSVEP studies

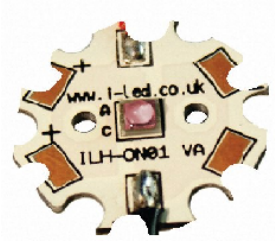

(a) LED plate.

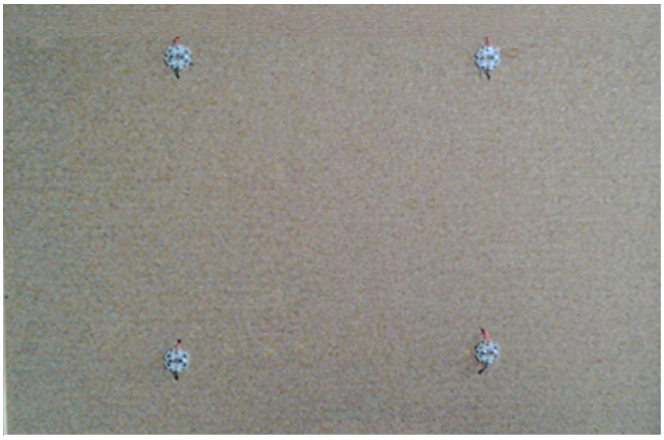

(b) LED panel with four LEDs.

Figure 3.4: **Visual stimulus (stimuli) used in the experiments.** (a) shows one LED stimulus used in the experiment. This image is obtained from RS Components, website: http://uk.rs-online.com. (b) shows the board with 4 LED stimuli.

(Müller et al., 1998; Wu, 2009; Teng et al., 2011).

According to manufacture (OSRAM) data sheets of LEDs, LEDs LS E63B–BBCB–1–1(Version 1.0, 2013)and LR CP7P–JSJU1 (Version 1.2, 2013) fall into the class of Exempt group in Standard IEC 62471:2008. LR G6SP–CADB–11 (Version 2007) falls into CLASS 1M LED PRODUCT according to IEC 60825-1. Safety characterisation of the LEDs was further verified using setup shown in Appendix A, Figure A-4. Power meter (Thorlabs, model no. PM160T) used in setup was to measure the output power of LEDs to ensure that it meets the requirements of Standard EN ISO 15004-2:2007. The power of brightest LED (LR CP7P-JSJU-1 with highest intensity) used in the experiment was tested at 60cm (shortest distance). The result can be found in Appendix A, Figure A-5. The power is under the limitation of Group 1, 5.4.1.3 (limitation is 200 μW) and 5.4.1.6.

3.3.2 LED driver circuit design

The square wave driving LED is generated by a microcontroller (Microchip^{TM}, PIC$^{©}$18F46K20) based circuit. The circuit diagrams are in Figure 3.5 and the actual circuit used in the experiment is depicted in Figure 3.6.

For illustration purposes, only the important modules are shown in Figure 3.5. Each module in Figure 3.6 is matched to a corresponding module in Figure 3.5a. The core of this circuit is the microcontroller which is programmed to perform three main tasks:

1. Control the stimulation timings of the different phases in the experiments.

2. Generate 4 square waves with the frequencies 12, 13, 14 and 15Hz respectively. The duty cycles of 4 square waves are 50%.

3. Send synchronous (event) trigger signal to data acquisition module.

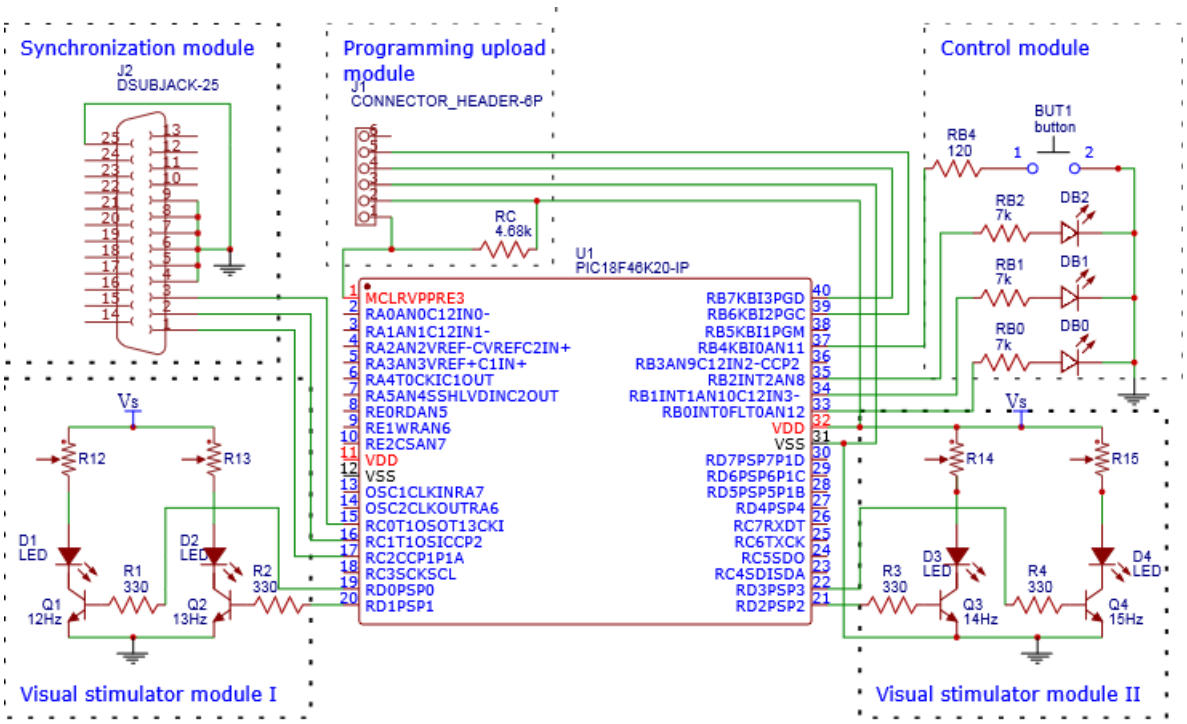

(a)

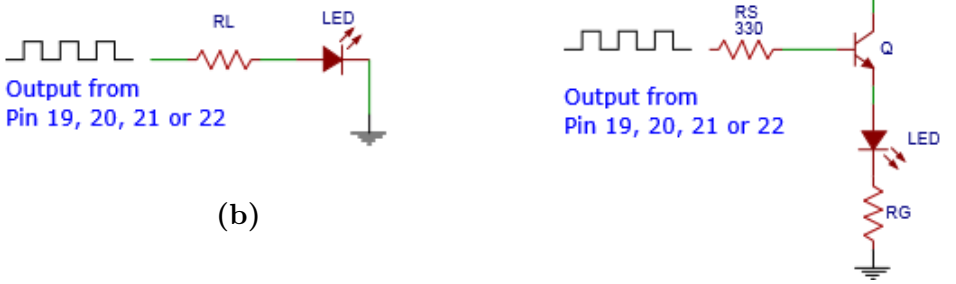

(b)

(c)

Figure 3.5: **LED driving circuits used in the experiment.** (a)The circuit used in the Feasibility Experiment. (b) and (c) only showed the visual stimulator module which is different from (a). The rest of the modules are the same as in (a), (b) and (c). (b) and (c) are used in the Investigation Experiment.

The circuit can be divided into several modules based on their functions:

1. Programming upload module: the microcontroller is programmed through PICKit^{TM}3 (MICROCHIP^{TM}, see Figure 3.6). The program is edited, compiled in C and converted to machine code using MPLAB (MICROCHIP^{TM}).

2. Control module: each run of the experiment starts by push the button switch in this module. Three LEDs in this module are used as the counters.

They flicker before the start and after the completion of one run of the experiment. During the resting phase of each trial in the run, LEDs display the timing progress of the resting phase for every second from 0 to 5 or 6s.

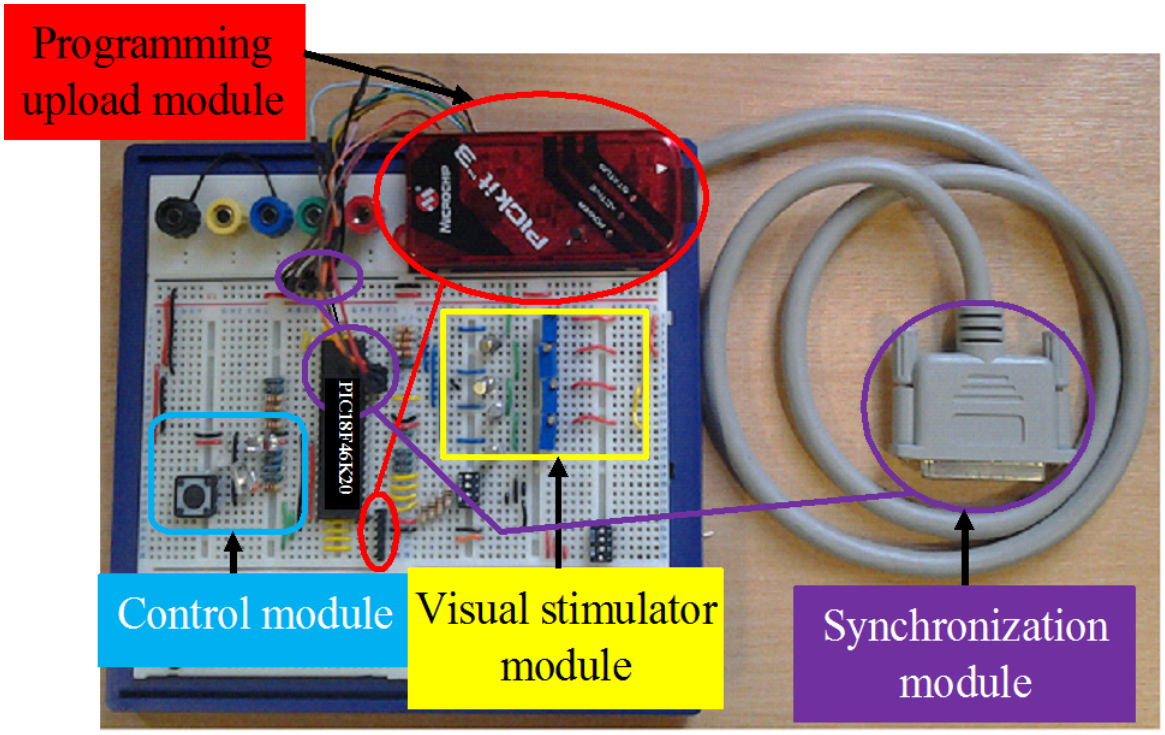

Figure 3.6: **The circuit used in the experiments.** The red box on the top of the circuit is PICKit^{TM}3. The cable on the right of the circuit is connected to the amplifier SynAmps^2 to send the synchronous signal to NeuroScan.

3. Synchronisation module: the circuit sends an 8-pin synchronisation signal to the data acquisition module through a D-25 connector (parallel port). As there are only two events in the experiment, therefore, only three pins which can make up to 7 different events (and one value as the hold-on value) of the microcontroller are used. The other 5 pins out of the 8 are connected to the ground. The circuit sends two synchronisation signals to data acquisition module, the visual stimuli onset (96, the onset of the attending phase) and the visual stimuli offset (64, the onset of the resting phase).

4. Visual stimulator module: the circuit generates 4 square waves of 4 different frequencies with 50% duty cycle to drive the LEDs. The frequencies and duty cycle of the square waves are easily modified when needed by editing the program. The number of the square waves can be increased by employing more pin outputs, for example, pin 23 to pin 26. The intensities of the LEDs are controlled by the serial potentiometers or resistors (R_{12}, R_{13}, R_{14} , R_{15}, R_L, R_G) and the voltage supply V_s illustrated in Figure 3.5. The square waves are used to drive the LED directly or as the switch to turn the transistor on–off.

The circuit was connected to a DC power supply (Digimess Instruments Ltd, model no. HY3003-2, Line regulation: CV≤ 0.01%+2mv, CC≤ 0.2%+2mA, Load regulation: CV≤ 0.01%+3mV (I≤ 3A) CC≤ 0.2%+3mA (I≤ 3A), Ripple and noise: CV≤ 0.5mVr.m.s (I≤ 3A) CC≤ 3mAr.m.s (I≤ 3A)). In the experiment, the square waves driven LEDs were monitored, visualised and assessed by a digital oscilloscope (Tektronix digital oscilloscope TDS 2014). No difference was detected. Figure 3.7a depicted the screen shots of 4 square waves from Tektronix digital oscilloscope. Four waveforms, from the top to the bottom with colours orange, cyan, violet and light green, stand for the square waves of frequency 12, 13, 14 and 15Hz respectively.

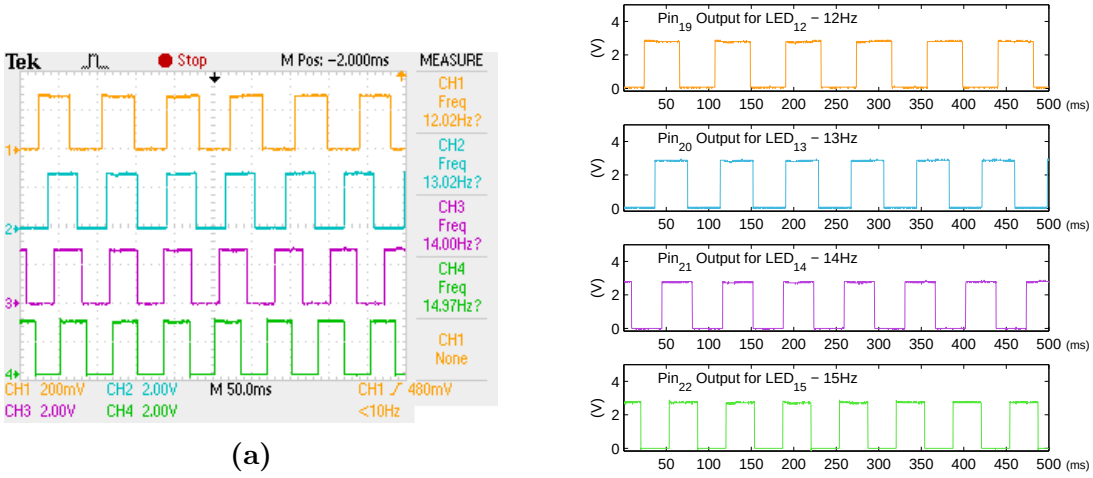

(a) **(b)**

Figure 3.7: **Screen shots of 4 stimulating frequencies from Tektronix digital oscilloscope TDS 2014.** (a) The waveforms presented by the colours of orange, cyan, violet and light green, from top to bottom, are the square waves with frequencies 12, 13, 14 and 15Hz respectively. (b) The sampling data of the screen shots are analysed and re-plotted by Matlab.

The precision and the stability of the square waves are evaluated in terms of their frequencies and duty cycle by analysing the numerical data of the screen shots of Tektronix digital oscilloscope. The waveforms are re–plotted using Matlab using the numerical data of the corresponding screen shots as shown in Figure 3.7b. For explanation purposes, it starts from time 0. The sampling rate of the scope is 5,000Hz. Each square wave contains 2,500 data points, i.e. 0.5 s (500ms). The frequency and duty cycle of each square wave are computed based on two successive ON–OFF (or OFF–ON) intervals. The duty cycle is the ratio between the duration of ON and the duration of ON–OFF (or OFF–ON). The computation result is shown in Table 3.2. The frequency output and duty cycle of each square wave are relatively stable. The circuit design and programming which generate the optimised square waves to drive LEDs are not the primary goals of this study. Overall speaking, the frequency output of each square wave fluctuates within the range of ±0.3Hz around the designed frequency. The output frequency is within

the range of the designated frequency ± 0.25%. The duty cycle fluctuates ±0.3% around 50%. More analysed results can be found from Figure B-1 and Table C-1 in Appendix B and Appendix C.

Table 3.2: **Frequencies and duty cycles of Figure 3.7a.** The results of the frequencies and duty cycle are based on the sampling data of Figure 3.7a and analysed by Matlab. f and D stand for frequency and duty cycle, respectively.

	12Hz		**13Hz**		**14Hz**		**15Hz**	
	f (Hz)	**D (%)**	**f (Hz)**	**D (%)**	**f (Hz)**	**D (%)**	**f (Hz)**	**D (%)**
	12.02	50.00	13.02	50.00	14.01	50.14	14.97	50.00
	12.02	50.00	12.99	49.87	14.01	50.14	14.97	50.00
	12.02	50.00	12.99	49.87	13.97	50.00	14.97	50.00
	12.02	50.00	12.99	49.87	14.01	49.86	14.97	50.00
	12.02	50.00	12.99	49.87	14.01	49.86	15.02	50.15
	12.02	50.00	13.02	50.00	13.97	50.00	15.02	50.15
	12.02	50.00	12.99	50.13	14.01	50.14	14.97	50.00
	12.02	50.00	12.99	50.13	14.01	50.14	14.97	50.00
	11.99	50.12	12.99	50.13	13.97	50.00	14.97	50.00
	11.99	50.12	12.99	50.13	14.01	49.86	14.97	50.00
	-	-	13.02	50.00	14.01	49.86	14.97	50.00
	-	-	-	-	14.01	49.86	14.97	50.00
	-	-	-	-	-	-	15.02	50.15
Mean	**12.01**	**50.02**	**13.00**	**50.00**	**14.00**	**49.99**	**14.98**	**50.03**
SD(%)	**0.08%**	**0.10%**	**0.12%**	**0.23%**	**0.13%**	**0.25%**	**0.13%**	**0.13%**

The voltages of four LEDs in the Feasibility Experiment can be seen in Figure 3.8. The voltage in Figure 3.8 is measured between the anode of LED and the ground when (a) LED is off, (b) the transient period between off and on, (c) LED is on, (d) the transient period between on and off.

The circuit (as shown in Figure 3.5) used in both experiments is the same. The only difference is how the LED is driven. Nonetheless, the intensities of LEDs are altered by changing the serial resistor. The values of R and the corresponding currents and luminance of LEDs at different setup in the experiment are listed in Tables 3.3 and 3.4. The potentiometers (variable resistors) are measured by a multimeter (EUROSONIC ES–214MT). The current is measured in mA using a digital multimeter(MASTECH, MAS830LC). The luminance of LEDs with different serial resistors is measured by a calibrated light meter (ISO-TECH, ILM-01). Table 3.3 lists the values of LED current and the corresponding luminance measured at the distance 60cm for LEDs, LS E63B–BBCB–1–1 and LR G6SP-CADB-1-1 used in the Investigation Experiment. Table 3.4 lists the values of LED current and the corresponding luminance measured at the distance 60cm for LED, LR CP7P–JSJU–1 used in the Feasibility Experiment.

The hypothesis of this study is that the viewing distance will reduce the perception of the intensity. As a result, the stimulation by the light is reduced and in turn affects SSVEP response. The focus of this study is to investigate how the viewing distance of a flickering light stimulus changes SSVEP. However, this

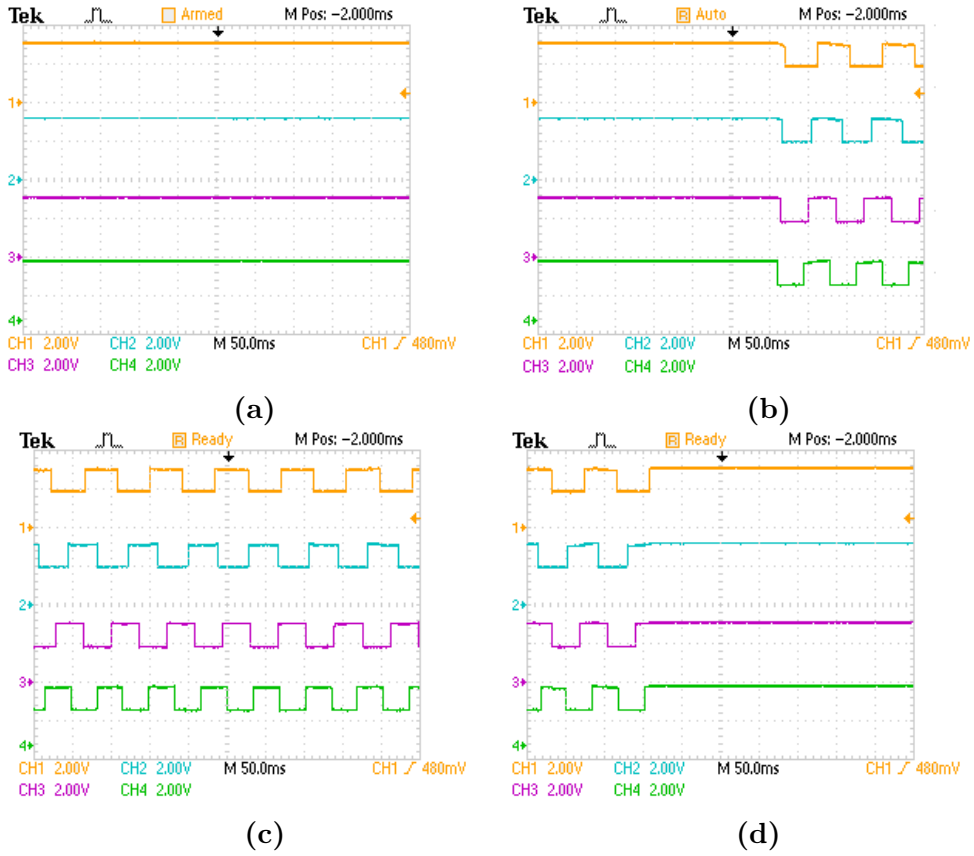

Figure 3.8: **The voltages between LED anodes and the ground.** (a) LED is off, (b) the transient period between off and on, (c) LED is on, (d) the transient period between on and off.

study is not aimed at finding out the optimal intensity corresponding to a viewing distance for each subject. The optimisation of the intensity is important for the user acceptance and comfort but the customising process is time consuming. Therefore, in the experiment, the reduction of LED intensity is done by increasing the value of the resistors, decreasing the voltage and/or changing LED. To increase intensity, it can be done by reducing the value of the resistors. To ensure the safety of the subject's vision, the brightness of the LEDs used in the experiments does not exceed the brightness of the normal light used in the laboratory which is verified by the light meter measurement. The experiment is performed in a dim room. Furthermore, the subjects are advised to stop at any time when they do not feel comfortable.

Before conducting the Feasibility Experiment, an initial resistor/intensity selection experiment is performed to determine the resistor values to be used in the Feasibility Experiment. To the author′s best knowledge, there are no guidelines or rules which describe the relationship between the intensity of the stimulus and the associated SSVEP response. In the Investigation Experiment, it is assumed that the impact of the viewing distance can be compensated by increasing the stimulus intensity. However, it is difficult to know if the compensation is appropriate, i.e. not over or under compensation.

Table 3.3: **Value of the resistor used in the circuit and the corresponding current and luminance of LED, LS E63B–BBCB–1–1 and LR G6SP–CADB–1–1, used in the Investigation Experiment.** Units of current and luminance are in mA and lux. The luminance was measured at the viewing distance 60cm.

LED and circuit	Resistor (Ω)	**150**	**120**	**68**	**50**	**33**	**6.7**
LS E63B–BBCB–1–1	Current	–	1.5	–	–	–	–
Circuit in Figure 3.5b	Luminace	–	0.46	–	–	–	–
LR G6SP–CADB–1–1	Current	1.1	1.3	5.6	9.1	11.2	16.6
Circuit in Figure 3.5c	Luminace	0.34	0.30	0.48	0.69	0.87	2.63

Table 3.4: **Value of the resistor used in the circuit and the corresponding current and luminance of LED, LR CP7P–JSJU–1, used in the Feasibility Experiment.** Units of current and luminance are in mA and lux. The luminance was measured at the viewing distance 60cm.

LED and circuit	Resistor (Ω)	**450**	**300**	**100**	**75**	**30**	**15**	**10**	**5**
LR CP7P–JSJU–1	Current	2.8	3.7	10.5	13.4	27.5	42.0	49.7	61.0
Circuit in Figure 3.5a	Luminace	0.32	0.64	1.85	2.70	5.90	9.65	12.04	21.39

In the initial resistor/intensity selection experiment, the voltage supply and LED are fixed. Changing the value of the resistor is the only way which can change the LED intensity. The purpose of the resistor/intensity selection experiment is to determine the maximum resistor values corresponding to each viewing distance which can elicit a SSVEP response resulting in a 95% classification accuracy. The intensity of the stimulus is not the only factor which can affect SSVEP. Hence, the resistor/intensity selection experiment aims to find an optimal resistor value based on the classification accuracy. In theory, the optimal resistor's value results in 100% classification accuracy. However, this is not always the case. Therefore, we define an optimal resistor′s value as the value which results in at least 95% classification accuracy. The classification rate is computed using CCA with 2s of EEG time window length after the stimulus onset, the number of SSVEP harmonics is 1 and the recorded EEG is down–sampling to 100Hz. All the recorded EEG data of 11 electrodes are used in the analysis.

In resistor/intensity selection experiment, only one visual stimulus (LED part no LR CP7P–JSJU–1) is used. For each viewing distance, one resistor is selected as the starting point. The experiment protocol and setup are similar to that of the Investigation Experiment. The rest of the experiment is described as follows, the flowchart of the procedure can be found in Figure 3.9:

1. one run of 20 trials stimulation is performed by the use of the selected resistor.

2. compute the classification accuracy of 20 trials.

3. if the accuracy is higher than or equal to 95%, the LED is considered too bright and so the resistor's value is increased to reduce the LED brightness. Repeat steps 1 and 2. Otherwise, go to step 4.

4. if the classification rate of the last run is over 95%, it is assumed that the resistor′s value of the last run is the optimal value which results in at least 95% accuracy. The resistor of the last run is chosen as the optimal resistor for the particular viewing distance. Otherwise, it is assumed that a brighter LED will lead to higher classification accuracy. Therefore, the resistor value is reduced and repeats the procedure from step 1.

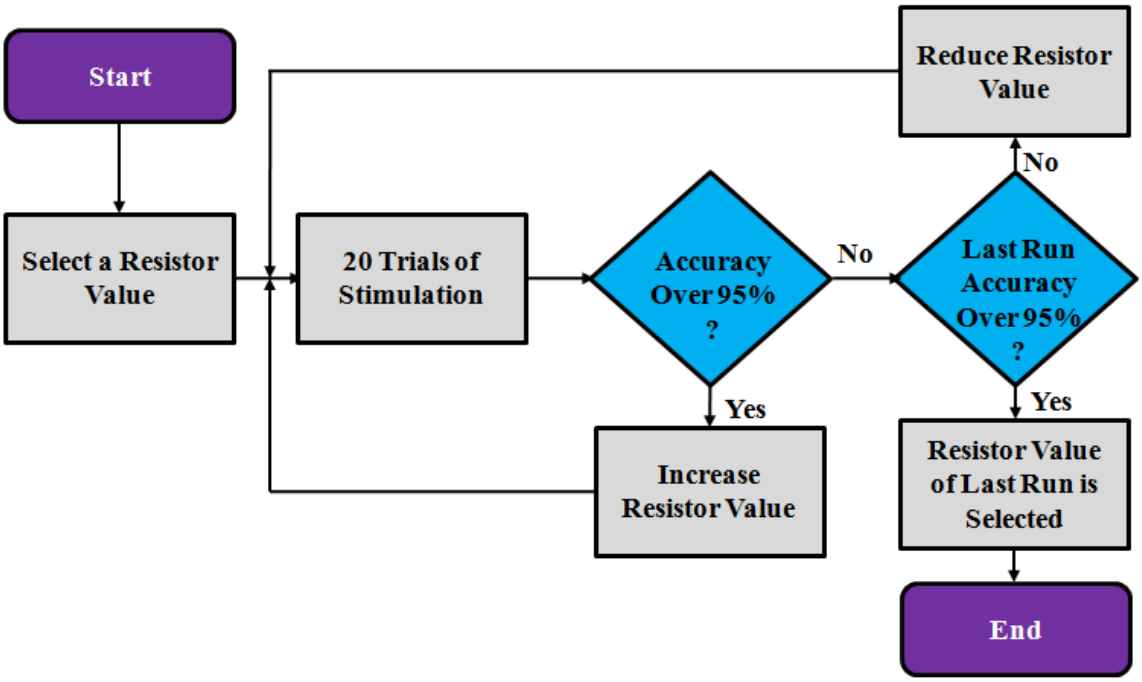

Figure 3.9: **An optimal resistor/intensity selection procedure for one viewing distance.** This procedure aims to find the optimal value of the resistor which can result in 95% classification accuracy.

In resistor/intensity selection procedure shown in Figure 3.9, the change of resistor values depended on the resultant /associated classification accuracy and the viewing distances. If the classification accuracy was low ($\leq 70\%$), a multiple steps of change in the resistor value are examined. The step of change is dependent on the viewing distance. At longer distances, the resultant classification accuracy is more sensitive to resistor value change and hence one step of change was smaller. One step of change is 50 Ω for 60cm and 150cm, and 5 Ω for 250cm and 350cm.

It might be argued that there exists a resistor value between the resistor values of the last two runs which can also result in classification accuracy over 95%. The selected resistor value is not optimal. The resistor/intensity selection experiment is an exhausting, frustrating and time consuming process. Only one subject attends this initial selection experiment. On the completion of the initial

experiment, four resistor values are chosen for four viewing distances. Another resistor set of four resistors of smaller values is estimated according to the resistor set found in the initial experiment. As it is also assumed, the estimated resistor set can make LEDs brighter and thereby elicit stronger SSVEP. This is a precaution and consideration by taking the inter–subject variance into account. For the subjects participating in the Feasibility Experiment, the estimated resistor set is the starting point to adjust the brightness of the LEDs.

It is worth noting that the LED is a directional light source and hence its light intensity varies by the viewing angle. As a result, in the Feasibility Experiment the intensity of the LED varies at different viewing angles which require to be taken into consideration for different viewing distances.

Figures A-1, A-2 and A-3 are the radiation characteristics of the LEDs used in the experiments. These figures which can be found in Appendix A illustrate the relationship between the viewing angles and luminous intensity. The luminous intensity I is a function of the viewing angle (2φ) of LED, $I = f(\varphi)$. The luminous intensity decreases as the viewing angle increases. According to the definition of the viewing angle by the manufacture OSRAM^{TM}, viewing angle of the LED is equal to 2 $\times\varphi$. The viewing angles (2 φ) listed in the data sheets (see Tables A-1, A-2, and A-3 in Appendix A) are 2 times of the angle (φ) where the luminous intensity is equal to 50% of its maximum luminous intensity. The angles subtended between the subjects and a LED of the viewing distances of 60cm, 150cm, 250cm and 350cm are 11.8°, 4.8°, 2.9° and 2.0° respectively and within φ in the Feasibility Experiment.

3.4 Data Analysis

This section covers the scope and techniques of the data analysis in this study. These techniques include FFT, ITC and Stimulus Locked Inter–trace Correlation (SLIC) to visualise SSVEP response, CCA, MEC and MCC to classify EEG data, and Receiver Operating Characteristic (ROC) to assess the performance of classification. The parameters of data analysis, electrode analysis and threshold analysis are also explained in this section.

3.4.1 Analysis of Investigation Experiment

In the Investigation Experiment, the analysis is focused on how the viewing distance affects SSVEP response. The properties of SSVEP elicited at different viewing distances are inspected. These properties include SSVEP power, the phase and time locking to the stimulus. The corresponding classification accuracies of EEG data are also explored. The analysed results in both uncompensated and compensated condition are compared. Fast Fourier transform (FFT) is used to calculate SSVEP power. Inter–trial coherence (ITC) and Stimulus–Locked Inter–trial Correlation (SLIC) analysis are used to examine SSVEP phase– and time–locking to the stimulus properties.

3.4.2 Analysis of Feasibility Experiment

The feasibility of a distance adaptable SSVEP based BCI is assessed based on the classification performance at different viewing distances. Its usability and robustness are further examined by different parameters, such as the EEG recording time after the stimulus onset, the number of SSVEP harmonics and the number of the electrodes used for the classification. This section explains the definition of the terms and the data analysis in the Feasibility Experiment.

3.4.2.1 Experiment condition

The experiment condition is defined by the target stimulus to which the subjects attend and the viewing distance at which the target is placed. There are 16 different *experiment conditions* (4 (targets) $\times$ 4 (viewing distances)) for each subject in the Feasibility Experiment.

3.4.2.2 EEG analysis parameters

The EEG data of each subject at 16 experiment conditions is analysed (classified) using different parameters. These parameters are as follows:

1. EEG time window length (TWL): EEG is epoched 1s before and 5s after the stimulus onset. EEG time window length (TWL) is EEG data window length from the stimulus onset. For the classification, EEG TWL could be up to 5s in this study. For EEG classification in the Feasibility Experiment, EEG TWLs considered are 1.00s, 1.25s, 1.50s, 1.75s, 2.00s, 3.00s, 4.00s and 5.00s.

2. Number of SSVEP harmonics: The number of SSVEP harmonics used in the data analysis varies from 1 to 3. In this study, H1 stands for when only the fundamental frequency of SSVEP is employed for data analysis. H2 and H3 stand for when the 2^{nd} harmonics and 3^{rd} harmonics of SSVEP were added to evaluate the impact of the number of SSVEP harmonics.

3. EEG sampling frequency: EEG is recorded at 2k Hz sampling frequency in the experiment. To reduce the computation time, it is down–sampling to 100Hz.

3.4.2.3 Classification methods

Three classification methods are employed and compared in this study. The three methods are canonical correlation analysis (CCA), minimum energy combination (MEC) and maximum contrast combination (MCC). The output of each classification method for one trial is the feature vector of 4 elements corresponding to 4 classes (stimulating frequencies). The features are the correlation coefficients, SSVEP power and SNR for CCA, MEC and MCC respectively. The stimulating frequency corresponds to the maximum value of the feature vector is regarded as the attended target. All three methods are based on multiple electrodes and are described in detail in section 3.4.5.

3.4.2.4 Number of electrodes (N_y)

This study also inspects the impact of the number of electrodes on the classification performance. 11 electrodes are selected for the EEG acquisition. All electrode subsets from the 11 electrodes are investigated. The number of electrodes (N_y) in one electrode subset varies from 1 to 11. The corresponding electrode subset to the number of electrodes N_y is given by $C_{N_y}^{11}$, $1 \leq N_y \leq 11$. The total electrode subsets are equal to $\sum_{N_y=1}^{11} C_{N_y}^{11} = C_1^{11} + C_2^{11} + C_3^{11} + \cdots + C_{10}^{11} + C_{11}^{11} = 2047$ i.e., for each subject in each experiment condition, 2,047 electrode combination (subsets) are examined and the corresponding classification is estimated. Electrode subsets, total classifications and feature outputs corresponding to the electrode number are listed in Table 3.5. The classifications and feature outputs are based on 20 epochs for one experiment condition.

Table 3.5: **The electrode number and the corresponding number of the electrode set, classification results and feature outputs.**

Electrode No	1	2	3	4	5	6	7	8	9	10	11	Total
Electrode Sets	11	55	165	330	462	462	330	165	55	11	1	2047
Classifications	220	1100	3300	6600	9240	9240	6600	3300	1100	220	20	40940
Features Outputs	220	1100	3300	6600	9240	9240	6600	3300	1100	220	20	40940

The data analysis focuses on the classification accuracy. The recorded EEG in different experiment conditions is classified using the different EEG analysis parameters, classification methods and the number of the electrodes. The classification accuracies are compared.

The results are further analysed by other techniques, such as confusion matrix, ROC to obtain more information about BCI performance. The confusion matrix reveals the recall rate and precision rate. The receiver operating curves provide a different angle on the classification result. When measuring BCI performance, the true positive rate (accuracy) is not the only metric. Confusion matrix and ROC can visualise BCI performance in both true and false positive rates. Furthermore, the analysed results are used to rank the electrodes to select the optimal electrode subsets and the minimal number of the electrodes required without compromising the classification accuracies. Framework of the data analysis in the Feasibility Experiment is shown in Figure 3.10.

3.4.3 SSVEP analysis using FFT

SSVEP is a frequency dependent signal. FFT is one of the most common used techniques to extract SSVEP features in the frequency domain, mainly the power in the stimulating frequency and its harmonics. FFT is used to compute the signal–to–noise ratio (SNR). SNR is an important factor for SSVEP in the clas-

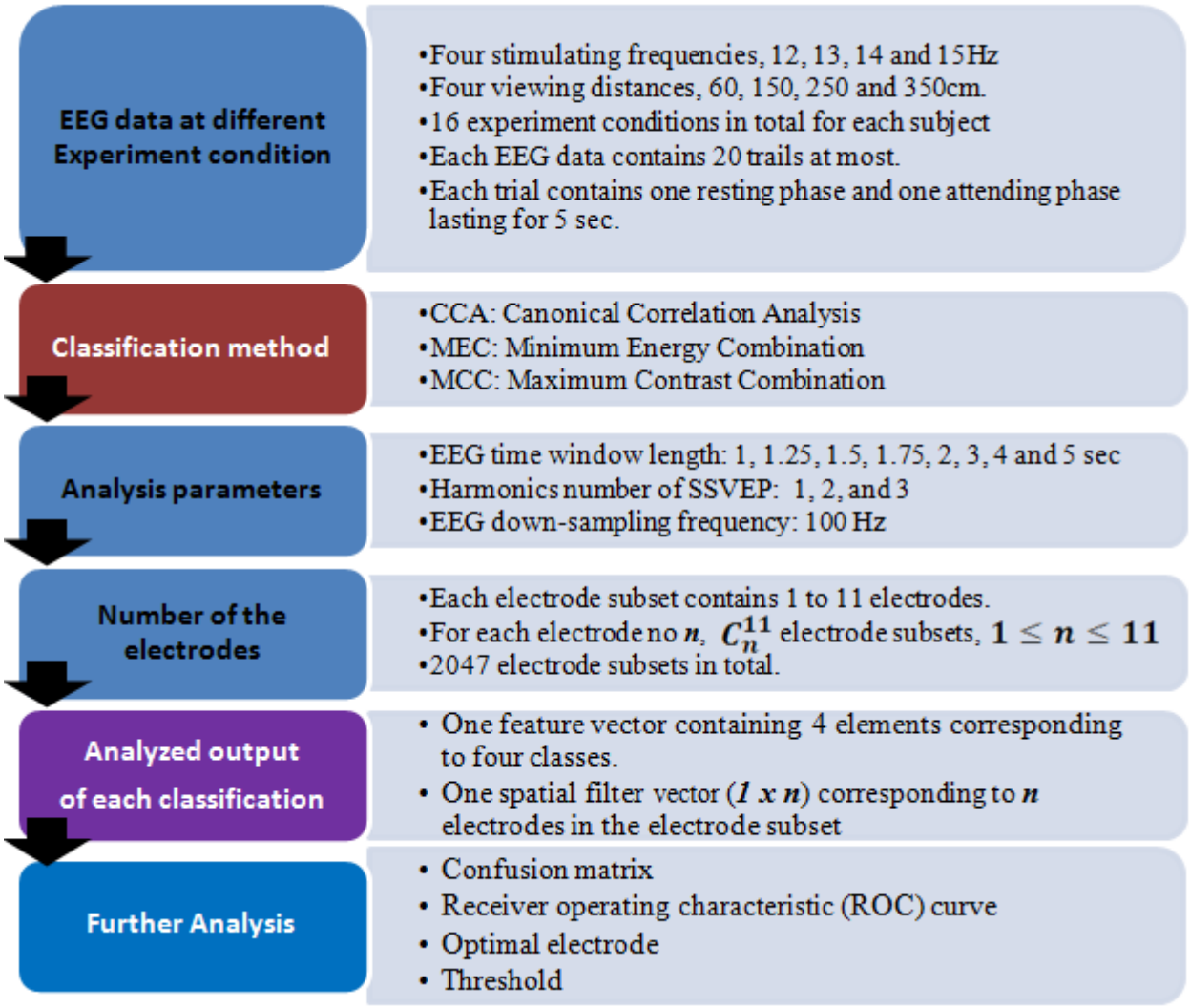

Figure 3.10: **Framework of the data analysis in the Feasibility Experiment.**

sification. SNR at frequency f is defined by equation (3.1) (Wang et al., 2006),

$$SNR_f = \frac{2 \times N \times x(f)}{\sum_{n=1}^{N}[x(f - n \times f_{res}) + x(f + n \times f_{res})]} \tag{3.1}$$

$x(f)$ is FFT power at frequency f. f_{res} in equation (3.1) is the frequency resolution. N is the number of neighbouring frequencies. N is set to 8. SNR analysis is to inspect how the EEG recording time and the viewing distance affect the elicitation of SSVEP. Additionally, the z score of SSVEP is also used to examine SSVEP response. z score is calculated by equation (3.2),

$$z = \frac{x - \mu}{\sigma} \tag{3.2}$$

For each subject for every experiment condition, FFT power before the visual stimulus onset are computed using equation (3.2)where μ is the maximum power among these epochs (20 epochs for most subjects), σ is the standard deviation of the power of these epochs. A z score of 2 is regarded as significant at 95% level.

3.4.4 SSVEP time– and phase–locking properties

SSVEP is phase- and time-locked to the visual stimulus onset (Lee et al., 2010; Luo and Sullivan, 2010; Zhu et al., 2010b). SLIC and ITC will both be used to inspect the impact of the viewing change on these properties.

3.4.4.1 Inter–trial coherence (ITC)

ITC is a time–frequency domain analysis developed by Delorme and Makeig (2004). It is defined by equation (3.3)

$$ITC(f,t) = \frac{1}{n}\sum_{n=1}^{k}\frac{F_k(f,t)}{|F_k(f,t)|} \tag{3.3}$$

Where $F_k(f,t)$ is the spectral estimation of kth trial at frequency f and time t. ITC measures the extent of the synchronisation between EEG and the event. In SSVEP, the event refers to the visual stimulus onset. ITC varies from 0 to 1. A high value of ITC indicates high synchronisation between the recorded EEG data and the event (Delorme and Makeig, 2004).

3.4.4.2 Stimulus locked inte–trace correlation (SLIC)

SLIC is a classification method based on EEG signal in time domain and is proposed by Luo and Sullivan (2010). The process of SLIC is as follows SLIC segments EEG data into traces which starts from the stimulus onset and ends with the stimulus offset according to the flickering sequence of the stimulating frequency. The time interval of each trace is equal to $\frac{1}{f}$, where f is one of the stimulating frequencies. Figure 3.11 illustrates one EEG segment. The first row of Figure 3.11 shows EEG raw data of subject 9 when attending to a 13Hz target at a viewing distance of 60cm. SLIC segments EEG data into the traces between two successive stimulus onsets by LED flickering sequences. The white–black bars at the top of the plots at the second to the fifth row are LED flickering sequences of 12, 13, 14 and 15Hz respectively. The white bar stands LED on and black bar stands LED off. The time span of each trace is between two successive stimulus onsets. Therefore, EEG data were segmented into 12, 13, 14 and 15 traces in one second for 12, 13, 14 and 15Hz respectively as shown in Figure 3.11. The two successive vertical red dash lines is one trace. In this example, the data points of each trace are equal to $\lfloor\frac{f_s}{f}\rfloor$. $\lfloor\frac{f_s}{f}\rfloor$ denoting the largest integer which is smaller or equal to $\frac{f_s}{f}$, f_s is the EEG sampling rate.

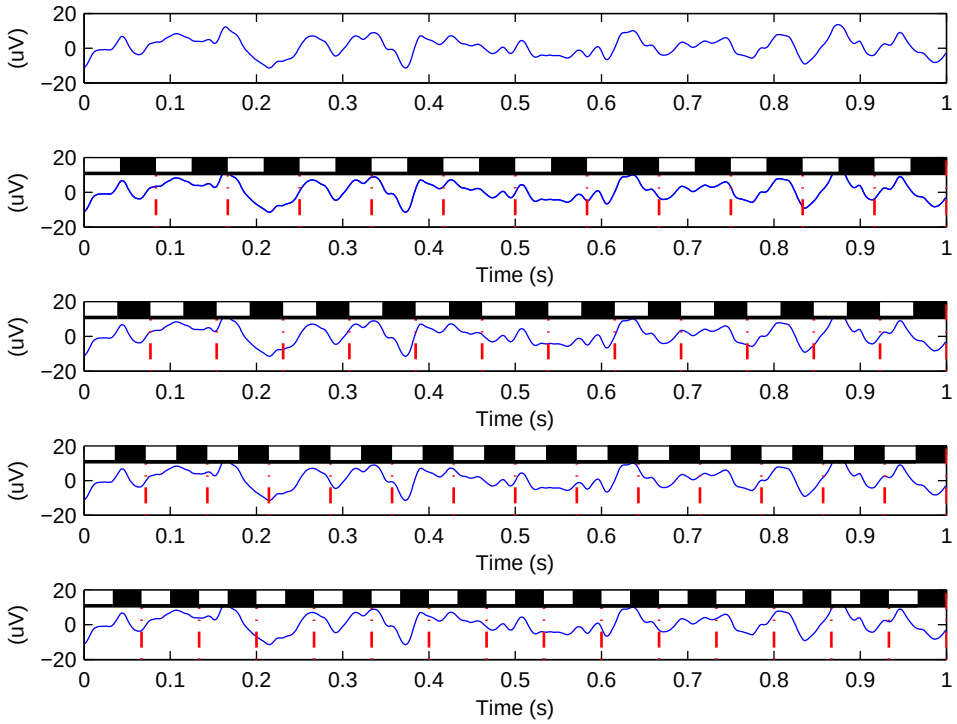

Figure 3.11: **EEG data segmenting of SLIC inter–traces.** EEG raw data of subject 9 is shown in the plot of the first row. The white and black bars shown at the top of the plots from second to fifth plot are LED flickering sequences of 12, 13, 14 and 15Hz respectively. White is on and black is off. The red dash vertical lines are the stimulus onsets of four LEDs. Each trace contains EEG data in two successive stimulus onsets. As a result, 12, 13, 14 and 15 traces are extracted for 12, 13, 14 and 15Hz. The data points of the traces of the same stimulating frequency are the same but different from the traces of other frequencies.

Figure 3.12 shows SLIC inter–traces and pair correlations distribution of Figure 3.11. The thin blue curves in the first row of Figure 3.12 are the traces from EEG data segmentation. For illustration purpose, only part of the traces shown. The red thick curves are the mean of the blue traces of each corresponding stimulating frequency. The mean curve of the attended frequency is sinusoidal like while the ones of the unattended frequencies are flat. This indicated SSVEP response is time locked to the attended–stimulus onset. The second row of Figure 3.12 is the inter–trace correlation distribution. The histogram of the attended frequency has a clear left skew. The histograms of the unattended frequencies are similar to normal distributions with mean value close to 0. Luo and Sullivan (2010) used the medium value of the correlations as the classification feature. The medium value is not affected by the outliers.

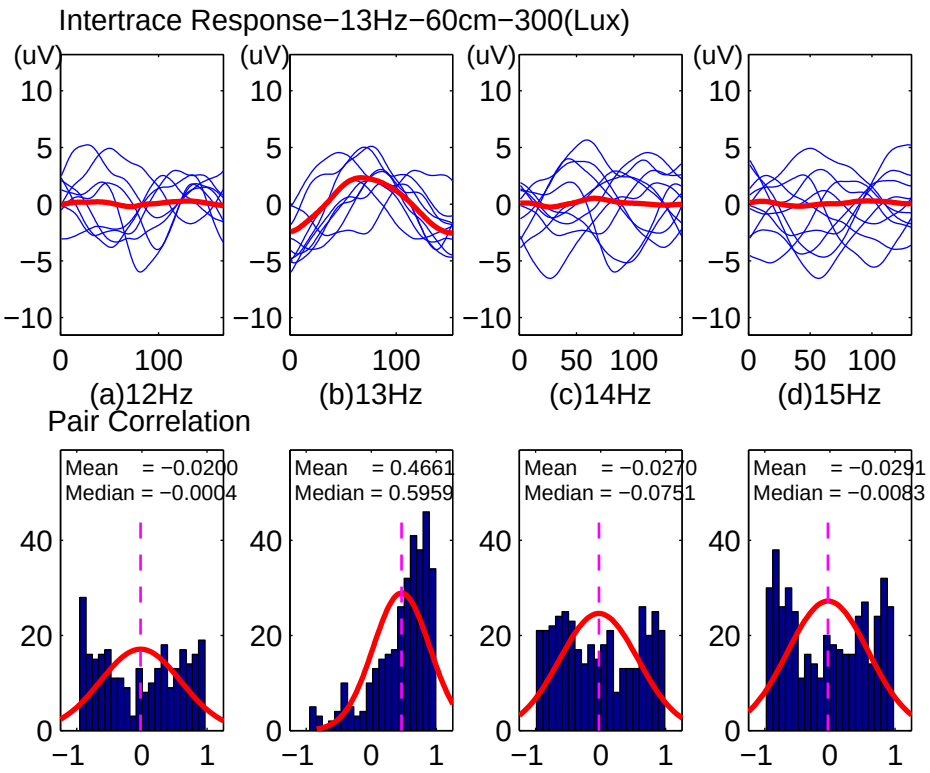

Figure 3.12: **Curves of mean SLIC inter–traces and pair correlation results of Figure 3.11.** The top row of Figure 3.12 shows the mean curves of the inter–trace of different frequencies. y axis is the voltage of unit (V) and x axis is the data point. The EEG sampling rate of this plot is 2k Hz. The second row is the histogram of correlations. Each histogram has 20 bins as shown on x axis. y axis is the number of each bin.

3.4.5 Classification

In this session, three SSVEP recognition methods based on multiple electrodes are discussed, including CCA, MEC and MCC. One of the disadvantages of surface EEG is that the brain signals are weak. Multiple recording electrodes technique could improve the signal recognition (McFarland et al., 1997; Garcia-Molina and Zhu, 2011). Spatial filter technique was normally employed to enhance the signal and suppress the noise in BCI. Spatial filter gives a weight to each electrode according to its importance. The spatial filter results in a new signal which is the linear combination of the multiple electrodes. The new resultant signal (S) can be presented by the original multiple electrode (N_y electrodes) signals (X) and the spatial filter by equation (3.4),

$$S = Xw \tag{3.4}$$

Where X is a matrix with dimension $N_t \times N_y$ and N_t is EEG data points in time and N_y is the number of electrodes. The dimension of the vector w is $N_y \times 1$.

Common average reference (CAR), small Laplacian and large Laplacian are three common spatial filters which had been used in BCI (McFarland et al., 1997). In CAR, the resultant EEG signal of ith electrode is obtained by subtracting the mean of all recording electrodes from EEG signal of ith electrode. EEG signal of the ith electrode was denoted by e_i. X of equaltion (3.4) is $[e_1, e_2, \cdots, e_N]$. The element $w_{n,i}$ in CAR spatial filter matrix is

$$w_{n,i} = \begin{cases} -\frac{1}{N} & \text{when } n \neq i, \\ 1 - \frac{1}{N} & \text{when } n = i. \end{cases} \tag{3.5}$$

In Laplacian, one centre electrode (i) and its 4 surrounding electrodes ($e_{i1}, e_{i2}, e_{i3}, e_{i4}$), nearest neighbouring electrodes for small Laplacian and next nearest-neighbouring for large Laplacian are applied to the spatial filter. The mean of 4 surrounding electrodes is subtracted from the centre electrode. X of equation (3.4) is $[e_i, e_{i1}, e_{i2}, e_{i3}, e_{i4}]$. The element $w_{n,i}$ in Laplacian spatial filter matrix is

$$w_{n,i} = \begin{cases} -\frac{1}{4} & \text{when } n \neq i, \\ 1 & \text{when } n = i. \end{cases} \tag{3.6}$$

In equation (3.6), the distances between the central electrode and each surrounding neighbouring electrodes are the same. The following three SSVEP detection methods also construct a spatial filter based on different principles and extract the features from the constructed signal (Bin et al., 2009b; Friman et al., 2007; Garcia-Molina and Zhu, 2011).

3.4.5.1 Canonical Correlation Analysis (CCA)

Canonical correlation analysis (CCA) is a statistical multi–variant technique which is used to investigate the correlation of two sets of variables. If there are two sets of variable X and Y, CCA finds two vectors $w_x^T = [w_{x1}, w_{x2}, \ldots, w_{xNy}]$ and $w_y^T = [w_{y1}, w_{y2}, \ldots, w_{yNh}]$ which transfer X and Y into two canonical variables $U(= w_x^T \cdot X)$ and $U(= w_y^T \cdot Y)$ such that the correlation coefficient ρ between U and V is maximised. p and q are the number of the variables in variable sets X and Y. CCA can compute more than one pair canonical variables up to $\min(p, q)$ pairs. The correlation between each pair is maximised. The canonical variables of different pairs are uncorrelated. The correlation coefficient ρ of the first pair canonical variable is the largest and the most important.

$$\rho = \max_{w_x, w_y} \frac{E(UV)}{\sqrt{E(U^2)E(V^2)}} = \max_{w_x, w_y} \frac{E(w_x^T X Y^T w_y)}{\sqrt{E(w_x^T X X^T w_x)E(w_y^T Y Y^T w_y)}} \tag{3.7}$$

CCA was first applied to SSVEP recognition by Lin et al. (2006) in an offline analysis. When CCA is applied to an m–class SSVEP based BCI which has N_y electrodes, N points of EEG data in each electrode, EEG sampling rate f_s, the two sets of variables are multiple electrodes EEG signals, X ($N_y \times N$ matrix) and the reference signal, Y of one stimulating frequency f, which contains sine and

cosine components of *f, 2f, ..., N_h* harmonics. The reference signal Y_k ($2N_h \times N$ matrix) of stimulating frequency f_k is expressed by equation (3.8)

$$Y_k = \begin{pmatrix} \sin[2\pi f_k(1/f_s)] & \sin[2\pi f_k(2/f_s)] & \cdots & \sin[2\pi f_k(N/f_s)] \\ \cos[2\pi f_k(1/f_s)] & \cos[2\pi f_k(2/f_s)] & \cdots & \cos[2\pi f_k(N/f_s)] \\ \vdots & \vdots & \ddots & \vdots \\ \sin[2\pi N_h f_k(1/f_s)] & \sin[2\pi N_h f_k(2/f_s)] & \cdots & \sin[2\pi N_h f_k(N/f_s)] \\ \cos[2\pi N_h f_k(1/f_s)] & \cos[2\pi N_h f_k(2/f_s)] & \cdots & \cos[2\pi N_h f_k(N/f_s)] \end{pmatrix} \quad (3.8)$$

In a multiple electrodes BCI system, there are more than one pair of canonical variables can be calculated and thereby more than one correlation coefficient ρ. The correlation coefficients between X and Y_k, denoting by $\rho_{k,1}, \rho_{k,2}, \cdots, \rho_{k,l}$, the maximum number of ρ is l, l=min$(N_y, 2N_h)$. The largest correlation coefficient $\rho_{k,1}$ was found from the first pair canonical variables. $\rho_{k,1}$ is the value used by SSVEP recognition. Correlation coefficient $\rho_{k,1}$ will be referred as ρ_k for each stimulating frequency f_k. CCA finds all maximum correlation coefficients ρ_k between X and Y_k, *k = 1, 2,..., m.* The corresponding stimulating frequency of the reference signal which produces the maximum ρ is identified as the attended target. In a multiple electrodes BCI system, there are more than one pair of canonical variables can be calculated between X and Y_k. However, only the correlation coefficient of the first pair is used for SSVEP detection. CCA finds all maximum correlation coefficients ρ_k between X and Y_k, *k = 1, 2,..., m.* The corresponding stimulating frequency of the reference signal which produces the maximum ρ is identified as the attended target.

Figure 3.13 illustrates CCA process. CCA finds the matrices W_x and W_y and transfers EEG data X and the reference signal of the target k to the canonical variables U and V. The correlation coefficient ρ_k of X and Y_k is found. CCA repeats the same process and finds all the correlation coeifficients $\rho_1, \rho_2, \cdots, \rho_m$, between X and the reference signals of the stimulating frequencies f_k, *k=1, 2,..., m.* The corresponding frequency f_i relating to the maximum of $(\rho_1, \rho_2, \cdots, \rho_m) = \rho_i$, $1 \leq i \leq m$, is identified as the attended target.

(Lin et al., 2006; Bin et al., 2009b). However, some studies argued that the reference signal employed in CCA is not optimal. The reference signal in CCA is applied to all the trials for all subjects which do not take inter–subject and inter–trial variance into consideration. The performance of CCA could be enhanced by estimating a modified reference signal which considers the variance of the subjects and/or the trials. The optimisation of the reference signal not only improves the classification accuracy but also reduces the number of electrodes and the time length of the data required.
The matrix w_x provides a weight factor to each electrode which transfers X to a canonical variable and enhances SNR. Figure 3.14 is the comparison of raw EEG X and the canonical variable $U = w_x^T X$. In this example, Subject 3 attended a 15Hz target at viewing distance 150cm. From this figure, it can be seen that

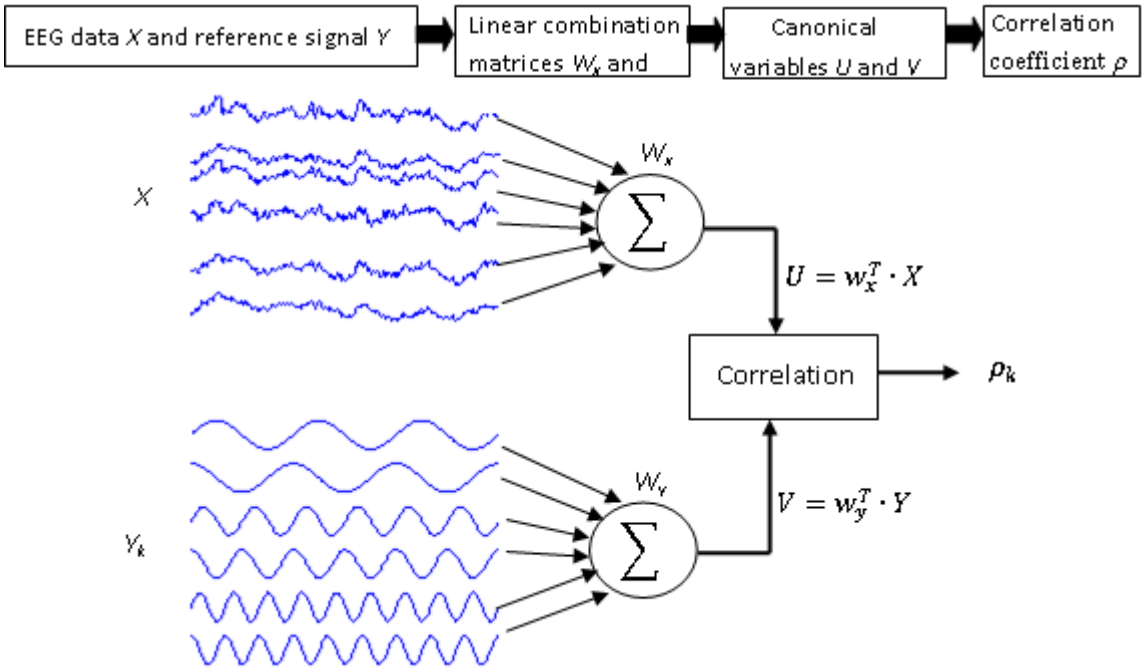

Figure 3.13: **Illustration of CCA process in finding a correlation coefficient ρ between EEG data and one of the reference signals of the target. This figure is reprinted and modified from (Lin et al., 2006) Copyright © 2006 IEEE.**

SSVEP is enhanced and the noise is subpressed. As a result, SNR is enhanced. CCA has been proven as an efficient classification method in SSVEP recognition by a few studies. Modified CCA was also proposed to improve the classification accuracies.

Pan et al. (2011) proposed a modified reference signal by adding SSVEP response phase of the subject to the reference signal used in the original CCA. It is referred to as p–CCA. In p–CCA, SSVEP response phase is estimated by the apparent latency, a time delay of SSVEP response due to the conduction of the visual pathway. It is a subject and stimulating frequency dependent parameter. The results showed that p–CCA outperformed the original CCA by 6.8% in classification accuracy. p–CCA outperformed the original CCA at all stimulation times (EEG data duration) in the experiment. The classification accuracies of both methods improve as the stimulation time increases. It is observed that the classification performance of p–CCA improves more in the shorter time interval than the longer one. The author suggested that it is because SSVEP response is phase–locked to the stimulus and its phase is more concentrated as the stimulation time increases.

3.4.5.2 Minimum Energy Combination (MEC)

Another SSVEP recognition algorithm based on principle component analysis (PCA) in a multiple electrodes BCI system is MEC which is proposed by Friman

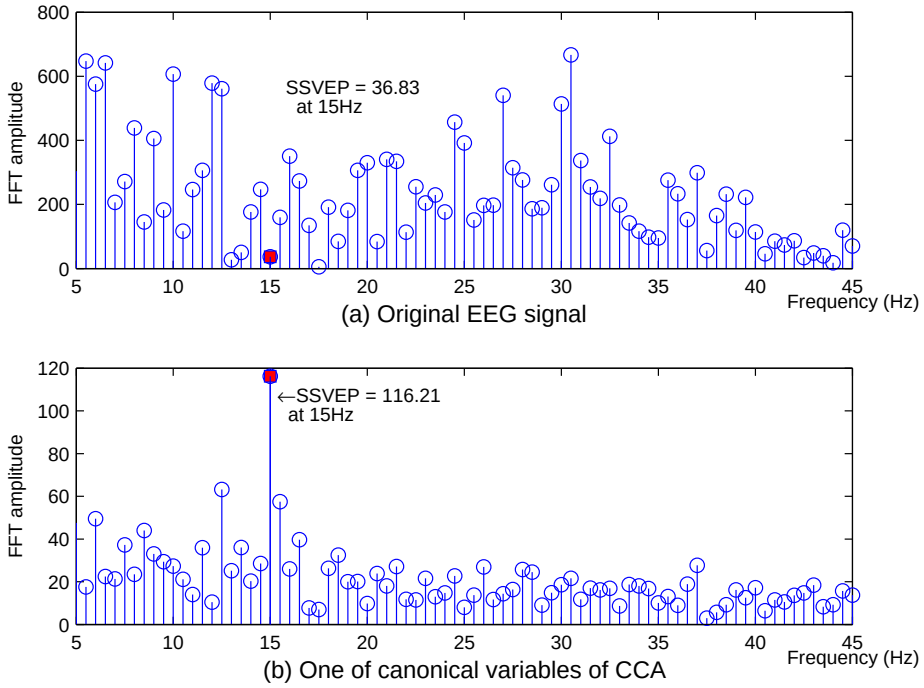

Figure 3.14: **SSVEP spectrum of original EEG X and one canonical variable U. The red squares indicate the response at the stimulating frequency (=15Hz).**

et al. (2007). In MEC algorithm,

1. **EEG signal and SSVEP response mode:** EEG signal y of ith electrode in a multiple electrodes based system can be modelled by equation (3.9),

$$y_i = \sum_{k=1}^{N_h} a_{i,k} \sin(2\pi k f t + \phi_{i,k}) + \sum_j b_{i,j}(t) + e_i(t) \tag{3.9}$$

   $a_{i,k} \sin(2\pi k f t + \phi_{i,k})$ of equation (3.9) is SSVEP response at frequency f and its harmonics. The amplitude and phase of each frequency kf are denoted by $a_{i,k}$ and $\phi_{i,k}$ respectively. The nuisance signal and noise are represented by $b_{i,j}$ and $e_i(t)$.

2. **Subspace of SSVEP:** Let $X = [X_1, X_2, \cdots, X_{Nh}]$, each X_k contains $\sin(2\pi k f t)$ and $\cos(2\pi k f t)$ in the columns. If each y_i has N_t data points, $\mathbf{y_i^T} = [y_i(1), y_i(2), \cdots, y_i(N_t)]$ can be written as $y_i = X\mathbf{a_i} + Z\mathbf{b_i} + e_i$. In a system of N_y electrodes with N_t data points in each electrode, the signals of all electrodes can be expressed by a $N_t \times N_y$ matrix $Y = [y_1, y_2, \cdots, y_{N_y}]$.

3. **Channel signals:** A channel signal is defined as the linear combination of all electrode signals.

$$S = \sum_{i=1}^{N_y} w_i y_i = YW \tag{3.10}$$

If S has N_s channel signals,$N_s \leq N_y$, then S can be expressed as S=YW. Where $W = [w_1, w_2, \cdots, w_{N_s}]_{N_y \times N_s}$ is a matrix of the dimension $N_y \times N_s$.

4. **Remove SSVEP signal from EEG:** To find optimal w which enhances SSVEP and suppresses the noise, MEC first removes SSVEP signal from EEG by projecting electrode signals Y onto a space of base X. As shown in Figure 3.15, $Y_{projection} = X(X^TX)^{-1}X^TY$. $Y_{projection}$ is SSVEP component. MEC removes SSVEP component, $Y_{projection}$ from electrode signal Y. The remaining signal ($\hat{Y} = Y - Y_{projection} = Y - X(X^TX)^{-1}Y$). $\hat{Y}$ should contain the nuisance signal and noise only.

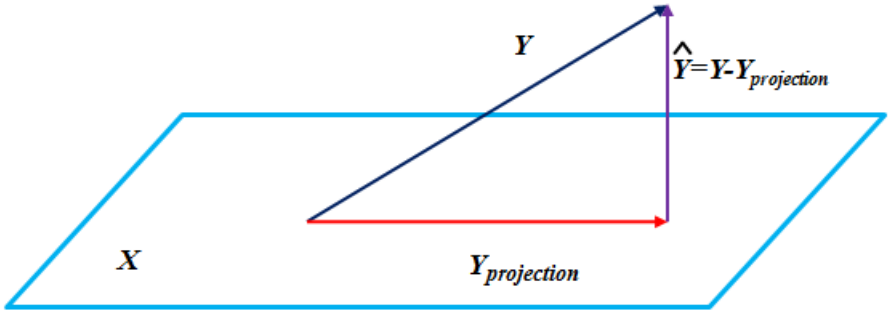

Figure 3.15: **Signal projection on the subspace of SSVEP (X).** The black line denotes the electrode signal containing SSVEP, nuisance signal and noise. The red line denotes SSVEP signal which is the projection of the electrode signal on SSVEP subspace. The purple line denotes the remaining signal of Y after removing the projection.

5. **Select eigenvectors:** MEC aims to find an optimal matrix which minimises $\|\hat{Y}w\| = min(w^T\hat{Y}^T\hat{Y}w)$. $\hat{Y}w$ is the linear combination of the remaining signals of the electrodes. w can be obtained by selecting the eigenvectors of the matrix $\hat{Y}^T\hat{Y}$. The eigenvector corresponding to the smallest eigenvalue is selected first which forms the first channel signal which has the minimum energy of the noise and nuisance signal. To increase the robustness, the eigenvector corresponding to the next largest eigenvalue is also selected until the following criterion (3.11) is met.

$$\frac{\sum_{i=1}^{N_s} \lambda_i}{\sum_{j=1}^{N_y} \lambda_j} > 0.1 \tag{3.11}$$

where N_s represents the minimal number of eigenvectors selected to meet (3.11). Each eigenvector results in one channel signal. i.e. around 90% of the nuisance signal and noise is discarded or 10% of the nuisance signal and noise is kept. Afterwards, N_s channel signals are compiled.

6. **SSVEP detection:** SSVEP power of the channel signal is calculated by

$$P = \frac{1}{N_s N_h} \sum_{j=1}^{N_s} \sum_{i=1}^{N_h} \|X_i^T s_j\|^2 \tag{3.12}$$

The frequency which produces the maximum power is identified as the attended target.

7. **An example of the channel signals:** Figure 3.16 illustrates an example of channel signals when one of the subjects attended 13Hz target at the viewing distance of 250cm.

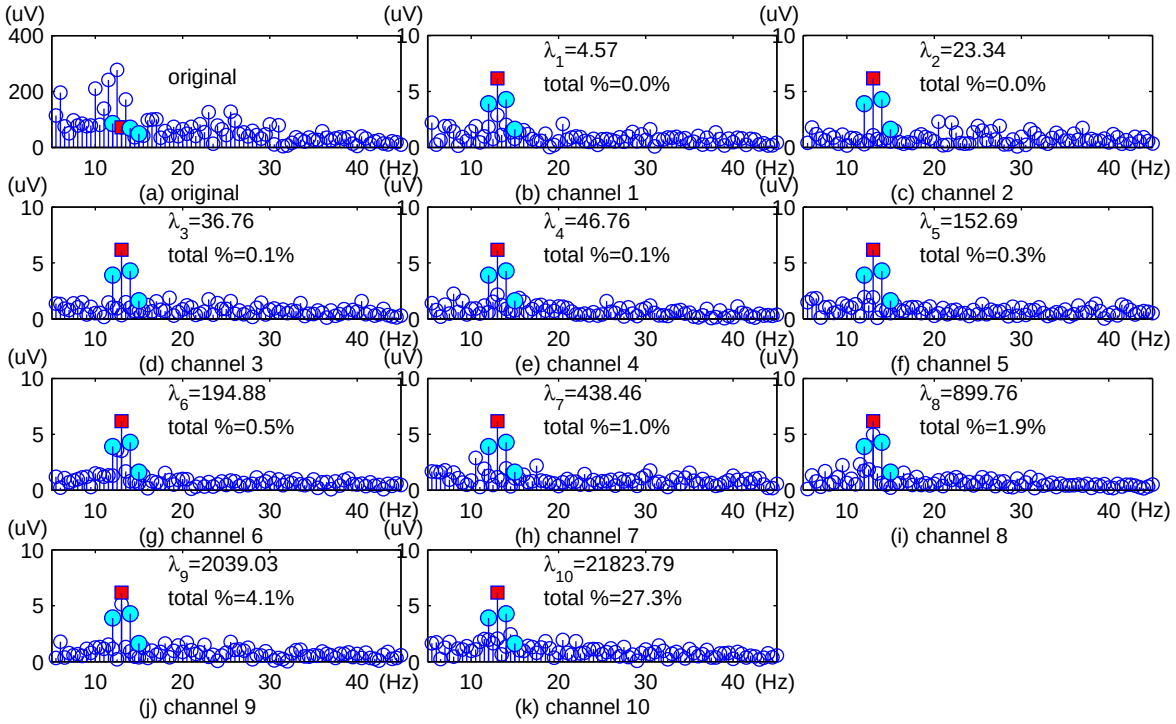

Figure 3.16: **Comparison of FFT of the original EEG and the channel signals of MEC.**(a) The original electrode signal and (b)–(k) 10 channel signals by MEC. The red square is SSVEP response at the attended frequency (13Hz). The cyan circles are signals at unattended frequencies (=12, 14 and 15Hz). 10 selected eigenvalues are shown in the subplots one by one. The total % stands for the sum of selected eigenvalues (from 1 to 10) to the sum of all eigenvalues.

In this example, N_s is equal to 10, i.e. ten out of 11 eigenvalues and the corresponding eigenvectors are selected. In Figure 3.16, the red square denotes SSVEP at the attended frequency. The cyan circles denoted the frequency components of the unattended stimulating frequencies. The corresponding eigenvalue λ_i is shown in each channel signal. The total percentage stands for the accumulated percentage to the sum of all eigenvalues. For example, in the channel signal 5, the total %=$\frac{\sum_{i=1}^{5}\lambda_i}{\sum_{j=1}^{11}\lambda_j}$=0.3%. It is clearly seen in Figure 3.16(a) before applying MEC, SSVEP response at the stimulating frequency is unable to be detected. SSVEP of channel signals (b) to (j), at the attended frequency are easier to be detected. The eigenvalues are selected in an ascending order (from smallest to

largest). The frequency which results in the maximum power is identified as the attended target.

3.4.5.3 Maximum Contrast Combination (MCC)

MCC is another spatial filter which is also proposed by Friman et al. (2007). This method is to enhance the SNR by maximising SSVEP and minimising the nuisance and noise. The maximum SNR is obtained by maximising the following equation (3.13),

$$\max_{w} \frac{\|Yw\|^2}{\|\hat{Y}w\|^2} = \max_{w} \frac{w^T Y^T Y w}{w^T \hat{Y}^T \hat{Y} w} \tag{3.13}$$

Y and $\hat{Y}$ are the same as described in the MEC method. w is found by solving the generalised decomposition of $Y^T Y$ and $\hat{Y}^T \hat{Y}$. The eigenvector corresponding to the largest eigenvalue results in the highest SNR while the eigenvector corresponding to the smallest eigenvalue results in the lowest SNR. Figure 3.17 illustrates an example showing that SNR was enhanced by MCC. The example is when Subject 2 attended 13Hz at the viewing distance of 60cm. The SNR shown in the figure is the ratio of FFT amplitude at the stimulating frequency to the average of the signals between 0 and 45Hz excluding the stimulating frequency.

3.4.6 Confusion matrix

A confusion matrix is a table (*matrix*) that allows the visualisation of the performance of a classifier (Kohavi and Provost, 1988). The confusion matrix of an N-class system is an $N \times N$ square matrix. Table 3.6 shows an example of the confusion matrix for an SSVEP BCI with four classes associated with four the frequencies 12, 13, 14 and 15Hz. Each row represents the classification output of one class. The element $n_{i,j}$ indicates the number of times the class i has been misclassified as class j. When $i = j$, the classification is correct. The diagonal elements of the confusion matrix are the number of times of correct classifications and the other elements denote incorrect classifications. A perfect classifier produces the confusion matrix with only non–zero elements in the diagonal and zeros elements off the diagonal.

Table 3.6: **Confusion matrix of 4 classes.** Each row of the matrix represents the classification output of one class. The element $n_{i,j}$ indicates the number of the class i has been identified as class j.

	12Hz	13Hz	14Hz	15Hz
12Hz	n_{11}	n_{12}	n_{13}	n_{14}
13Hz	n_{21}	n_{22}	n_{23}	n_{24}
14Hz	n_{31}	n_{32}	n_{33}	n_{34}
15Hz	n_{41}	n_{42}	n_{43}	n_{44}

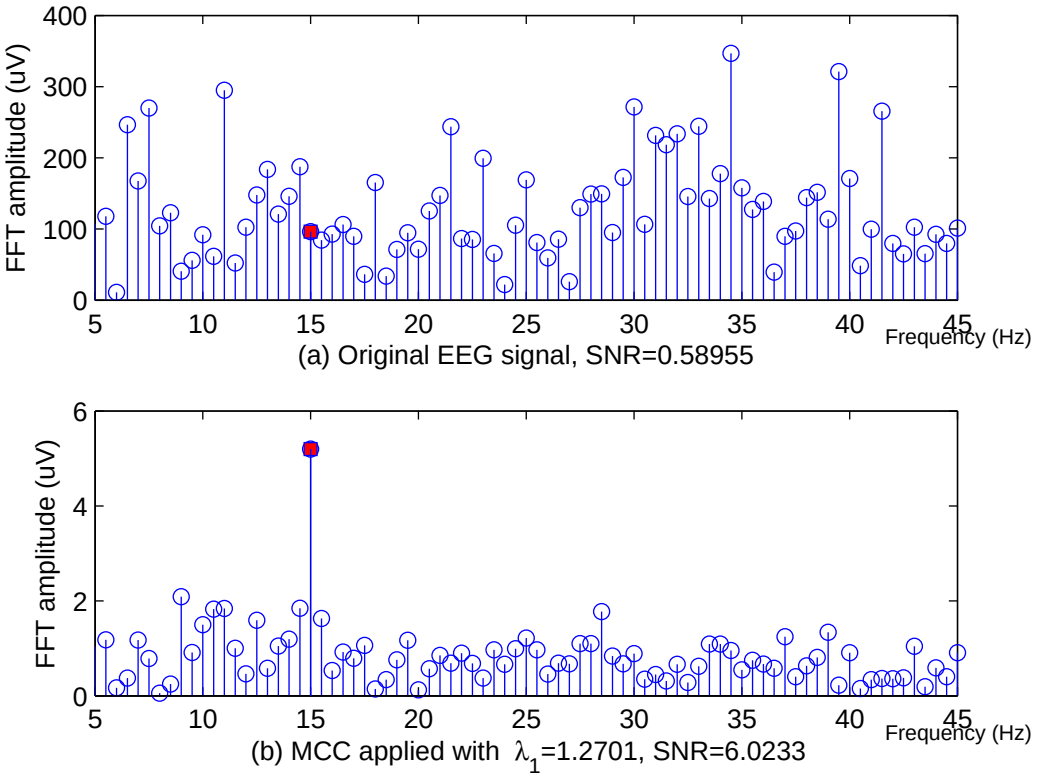

Figure 3.17: **Comparison of the SNRs of original EEG and applied MCC.** MCC enhanced SNR. (a) shows FFT of the original EEG data and the SNR is equal to 0.6.(b) shows FFT of (a) after applying MCC spatial filter. SNR is enhanced to 6.

When using a confusion matrix to evaluate the performance of a classifier, a few performance measurements are computed. These measurements are described as the following using the example of Table 3.6:

- Recall rate or true positive rate (tpr): Recall rate of class i is the percentage of class i being classified correctly as estimated by equation (3.14).

$$recall\ rate\ of\ class\ i = \frac{n_{i,i}}{\sum_{j=1}^{4} n_{i,j}} \tag{3.14}$$

- False positive rate (fpr): False positive rate of class i is the percentage of the classes which are not class i but are identified as class i . fpr is estimated using equation (3.15)

$$false\ positive\ rate\ of\ class\ i = \frac{\sum_{j=1}^{4} n_{j,i}}{\sum_{k=1}^{4}\sum_{l=1}^{4} n_{k,l}} \text{ , where } j \neq i \text{ and } k \neq i. \tag{3.15}$$

- Precision rate: Precision rate of class i is the percentage of classifications identified as class i which are correct.

$$precision\ rate\ of\ class\ i = \frac{n_{i,i}}{\sum_{k=1}^{4} n_{k,i}}. \tag{3.16}$$

- Overall accuracy (acc): Overall accuracy is the percentage of correct classifications and calculated by equation (3.17)

$$acc = \frac{\sum_{i=1}^{4} n_{i,i}}{\sum_{k=1}^{4} \sum_{l=1}^{4} n_{k,l}} \tag{3.17}$$

3.4.7 Receiver Operating Characteristic (ROC)

ROC curve is an efficient technique to assess the performance of a two–class classifier. In ROC plot, the x axis and y axis represent the false positive rate and true positive rate respectively. The true and false positive rates are defined in equations (3.14) and (3.15) in section 3.4.6. Figure 3.18 illustrates an example of ROC plot with a few points denoting the performance of the classifiers.

Figure 3.18 demonstrates a typical ROC curve of a discrete classifier. The diagonal blue line represents the classification result of a random–guess. All points on the line yield the same levels of the true positive rate and false positive rate (50:50). In this example, the classified outputs of the classifier at point A are always recognised as the negative class. As a result, the false and true positive rates at A are 0. On the other hand, the output of the classifier at point G (1,1), are always recognised as the positive class. Therefore, the false and true positive rate is 1. The classifier at point B denotes the perfect classifier with 100% of true positive rate and 0% of the false positive rate. A good classifier should be located in the upper triangle (true positive rate > false positive rate) of the ROC curve as in Figure 3.18 and near the y axis with high true positive rate and low false positive rate. The classifier of point D is considered more conservative than the classifier of point E because the low false positive rate is at the expense of the low true positive rate compared to the one at point E. On the contrary, the classifier of point E is more liberal than point D due to the fact that the high true positive rate comes with the high false positive rate.

The classification output of a discrete classifier, such as SSVEP BCI classifier, is the predicted class label. The output of a discrete classifier is one confusion matrix corresponding to a single pair of false and true positive rates and represents a single point in the ROC curve space. The classification output of the classification algorithms used in this study is based on a 4–element feature vector corresponding to 4 classes. The value of the element stands for the level of the likelihood of the corresponding class. When the threshold is used with the feature vector, the output of the classifier depends on whether the feature is over the threshold or not. One threshold results in one point in ROC space. A continuous ROC curve can be made by changing the threshold from $-\infty$ to $+\infty$. When ROC curve is built, the area under curve (AUC) of ROC is used to evaluate and compare the performance of the classifiers. The value of AUC is between 0 (inclusive) and 1 (inclusive). In general, the larger the AUC is, the better the classifier performance is.

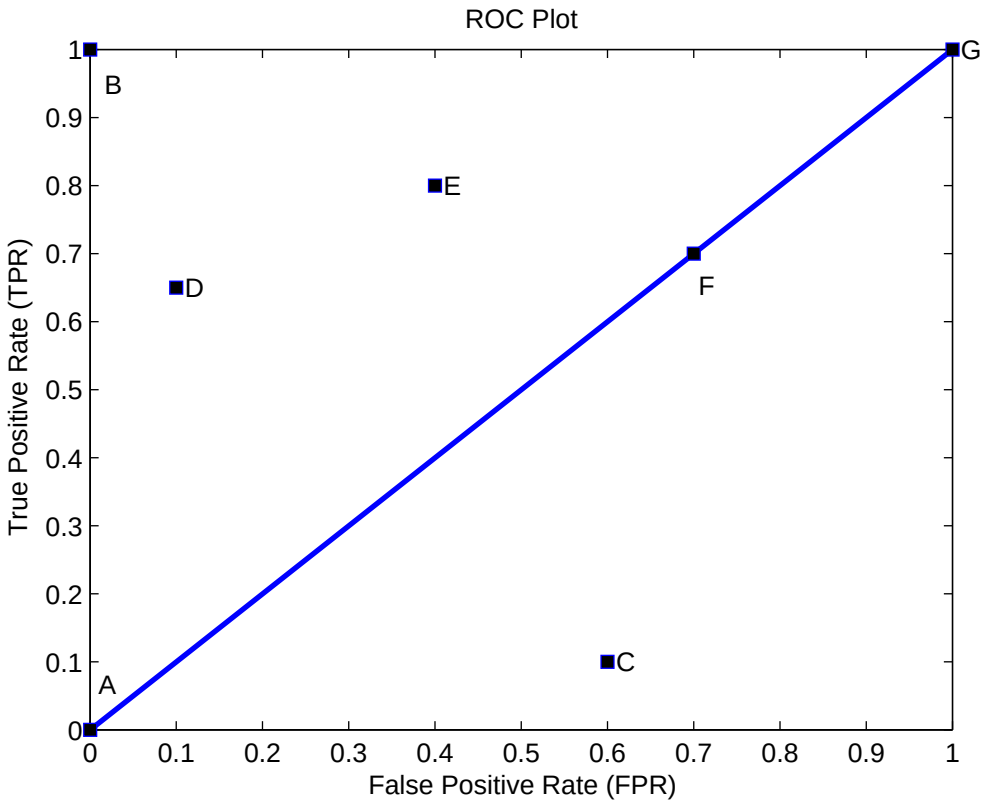

Figure 3.18: **ROC plot example.** Each point shown on the plot illustrates the performance of a discrete classifier. **This figure is reprinted and modified from (Fawcett, 2006), page 862, with permission from Elsevier.**

A single point of the ROC is used with F measurement which combines the recall rate (true positive rate) and precision rate into one metric and is defined by equation (3.18). F measurement and a single ROC point provide a balanced view on the classification performance regarding the true and false positive rates.

$$F = \frac{2 \times (recall\ rate) \times (precision\ rate)}{(recall\ rate) + (precision\ rate)} \tag{3.18}$$

In this study, there are four classes. In order to obtain ROC curve, one class is labelled as the positive class and the other three classes are labelled as the negative class. For example, to obtain the ROC of 12Hz, 12Hz is labelled as the positive class. 13, 14 and 15Hz are labelled as the negative class. The classification results of four classes at the same viewing distance are used to generate ROC.

Each element in the feature vectors is used as the score and is assigned to a label corresponding to one of the four classes. For example, to get ROC of each stimulating frequency at viewing distance 250cm, classification feature vectors of 12Hz, 13Hz, 14Hz and 15Hz at 250cm will be used. To get ROC of 12Hz, the first element of all feature vectors is extracted as score vector. The labels assigned to the elements from 12Hz were 12Hz. Similarly, the labels assigned to 13Hz, 14Hz and 15Hz were 13Hz, 14Hz and 15Hz respectively. The score and label vectors

were used to find ROC of 12Hz. To get ROCs of 13Hz, 14Hz and 15Hz, the score vectors were extracted from second, third and fourth elements from feature vectors for 13Hz, 14Hz and 15Hz respectively. The labels assignment is the same as making ROC of 12Hz.

A true positive is counted if the score of the positive class is larger or equal to the threshold. A false positive is counted in the same manner. By changing the values of the thresholds, a continuous ROC plot and its respective AUC are obtained. Continuous ROC and AUC are used to assess the classification performance of different number of the electrodes employed and the electrodes. The built–in function perfcurve in Matlab is used to plot ROC and compute AUC.

This modified way provides an estimation of the classification performance. For class i, if its corresponding true and false positive rates are *tpr* and *fpr* respectively, then the overall accuracy of the system *acc* could be represented by the following equation (3.19), when the number of the trials of each class are the same.

$$acc = \frac{[tpr + 3 \times (1 - fpr)]}{4} \tag{3.19}$$

In equation (3.19), when the classification output of the negative class is correctly classified as not the positive class, it is counted as one true negative.

3.4.8 Optimal electrodes

This study investigates the minimal number of electrodes required for each subject in order to achieve the highest possible classification rate. The highest classification rate for each subject is defined in each experiment condition as the highest possible classification rate (true positive rate) that could be estimated in that experiment condition regardless of the number of the electrodes. There are more than 2,000 electrode subsets from combining 11 electrodes. For each subject, there might be more than one electrode subset which can result in the highest value for classification accuracy. Those electrode subsets resulting in the highest classification are termed as the *optimal electrode subsets*. The optimal electrode subsets with the least (smallest) number of electrodes are termed as the *minimal optimal electrode subsets*.

3.4.8.1 Optimal electrode sets

By analysing the optimal electrode subsets, the following metrics for each subject are revealed:

1. Minimal optimal number (mon) of the electrode subset: the minimum electrode number of the optimal electrode subsets.

2. Electrode number distribution of optimal electrode subsets: the distribution of the electrode numbers of the optimal electrode subsets. It depicts the optimal electrode subsets by the number of the electrodes.

3. Highest classification accuracy: the highest possible classification rate for one subject in different experiment conditions that can be achieved.

4. Demographics of the electrodes: the demographics of the electrodes illustrating the electrode combinations of the optimal electrode subsets and the minimal electrode subsets. This analysis is to identify which electrodes to include in the minimal optimal electrode and in the optimal electrode subsets for each subject.

3.4.8.2 Electrode rankings

This study also proposes a method to rank the electrodes according to their importance or performance for the electrode selection. The electrode ranking is the order of the electrode being selected. It is flexible as ranking can be applied to any number of the electrode subsets, from 1 to the maximum number of the electrodes (in this study, the maximum number is 11.). It is also adaptable as The electrodes selected can be adjusted according to the classification rate which differs by the subjects and BCI applications. The cross validation demonstrates that the electrodes selected in the order of the electrode ranking outperform over 60% the total electrodes subsets of the same electrode number.

The electrodes are ranked by either the coefficients of the spatial filter or the classification accuracies. When the electrode subset of all electrodes is employed, each coefficient in the spatial filter corresponds to an electrode. When the electrode subsets of one electrode are employed, the classification accuracy corresponds to an electrode too. These two metrics are different in the dependence between the electrodes. In the coefficient method, the coefficients are the results based on the dependence between all electrodes. On the other hand, the electrodes are completely independent in classification accuracy method. The ranking process of each method is described as the following:

- Spatial filter coefficients: For CCA, the spatial filter is for the first canonical variants pair. For MEC and CCA, the spatial filter is the eigenvector of the smallest eigenvalue of the matrix $\hat{Y}^T\hat{Y}$ described in page 91 and the eigenvector of the largest eigenvalue of the generalised decomposition of Y^TY and $\hat{Y}^T\hat{Y}$ matrix described in page 93 respectively. The corresponding electrode with the largest absolute value of the coefficient is ranked first, followed by the second largest until the smallest value.

- Classification accuracy: The classification accuracy of single electrode is the ranking criterion. The corresponding electrode with the highest classification accuracy is ranked first, followed by the second highest until the lowest.

If more than one electrode has the same coefficient or classification accuracy, the electrode of the higher order is ranked first. The order of the electrode is [POz, Oz, Iz, 124, 125, O1, 127, 128, O9, O10, O2]. The efficacy of the electrode ranking are cross validated by the average classification accuracy and highest

classification rate and lowest classification rate of the electrode subsets of the same number of the electrodes. When the electrode ranking is used to select the electrodes, the only parameter required is how many electrodes should be in the electrode subset. If the electrode subset requires N_y electrodes, then the first top N_y electrodes in the ranking are selected. The electrode subset selected by the electrode ranking is termed as ranked electrode subset. The performance of the ranked electrode subset is assessed by performance index (PI). To calculate PI of the ranked electrode subset of N_y, first find the classification accuracy of the ranked electrode subset. Next, count the number of the electrode subsets of N_y electrodes which outperform the ranked electrode subset. This number is denoted as N_{op}. If the total electrode subsets of N_y electrodes is N_{Ny}, then PI is expressed by equation (3.20). The larger PI is the better performance the ranked electrode subset achieves.

$$PI = 1 - \frac{N_{op}}{N_{Ny}} \tag{3.20}$$

3.4.9 Threshold analysis

Threshold is an important parameter in real BCI applications. The value of the threshold will affect the classification results. If the threshold is set too high, the false positives are reduced at the cost of reduced true positives. On the contrary, if the threshold is set too low, the high true positives are at the expense of high false positives. The threshold setting is a compromise between the true positives and false positives.

In a threshold based decision classification system, the class is recognised when the value of the respective feature exceeds the threshold. To inspect the impact of the threshold on the classification performance, a new class termed as UI (Un–Identified) class is created. UI class is recognised when the maximum feature does not exceed the threshold. A conventional confusion matrix of 4 classes is also modified with an extra column named UI to demonstrate the impact of the threshold. The thresholds are found by the following two methods, explained in sections 3.4.9.1 and 3.4.9.2.

3.4.9.1 ROC threshold

As mention earlier in continuous ROC plot, each point on ROC curve corresponded to a threshold. The overall classification accuracy of class i was estimated by equation (3.19). The optimised threshold of class i was the threshold which maximised equation (3.19). The impact of threshold on the classification was evaluated after the threshold for each class was found by applying the threshold to the classification results in the classification profile.

3.4.9.2 Threshold by F measurement

In section 3.4.9.1, the optimised thresholds maximise the overall classification rates. In this section, the optimised threshold of each class is found to maximise F measurement of each class. F measurement is defined in equation (3.18). The process to find the thresholds which maximise F of each class is as following:

1. For each subject, the range of the threshold of each class is found based on four different experiment conditions at the same viewing distance.

2. The threshold range of each class is the minimum and maximum values of the element of the feature vector corresponding to the class. To compute the precision rate of one class, the other three experiment conditions are used to compute the false positives.

3. The applied thresholds start from the minimum value of the range to the maximum value of the range in the steps of $\frac{1}{99}$ of the difference between the maximum and minimum values. The corresponding recall rate, precision rate and F measurement are calculated.

4. The recall rate, precision rate and F measurement resulted from different thresholds are compared. The threshold resulting in the highest F is the optimised threshold.

3.5 Summary

In this chapter, two main experiments, the Investigation Experiment and the Feasibility Experiment, have been presented. The design and the parameters selection of visual stimuli were also explained. Furthermore, the scope and techniques of the data analysis were also explored. The principle, implementation, and evaluation of the proposed electrode ranking method were also described in this chapter.

Chapter 4

Results – data analysis of Investigation Experiment

In this chapter, the impact of the viewing distances on SSVEP response in terms of (1) power spectrum of SSVEP response, (2) the properties of time– and phase–locking to the stimulus and (3) the classification accuracy will be presented and investigated. SSVEP power spectrum is visualised using FFT power spectrum. The time and phase locking to the stimulus properties are examined using SLIC and ITC.

Finally, the classification accuracy is verified by CCA. One of the primary goals of this study is to understand how viewing distances affect SSVEP response and the classification accuracy. In this chapter, 11 electrode signals are applied to CCA. The impact of the numbers and locations of electrodes are investigated in Chapter 5.

4.1 Impact of viewing distances on SSVEP response in uncompensated condition

In uncompensated condition, the intensity of LED visual stimulator is the same at all viewing distances. In this section, SSVEP response and classification accuracy in uncompensated condition at different viewing distance are presented. Table 4.1 showed LED luminance in uncompensated and compensated conditions.

Table 4.1: **Luminance of LEDs at four viewing distances in the Investigation Experiment, one in the uncompensated condition and another in the compensated condition.** Unit of LED luminance is in lux. Intensity of LED at the viewing distance does not require compensation.

LED	60cm	150cm	250cm	350cm
LS E63B-BBCB-1-1 (uncompensated)	0.46	0.17	0.12	0.02
LR G6SP-CADB-1-1 (compensated)	0.30	0.56	0.26	0.18

4.1.1 Power spectrum of SSVEP response

Figure 4.1 depicts FFT power spectrum when the subject attends to a 14Hz target at four viewing distances without LED intensity compensation. The results shown in Figure 4.1 is based on estimating the average power over 11 electrodes and across 20 epochs. EEG sampling frequency was 2k Hz and EEG TWL was 4s which resulted in 0.25Hz frequency resolution in frequency domain. It is clear that the power of SSVEP at the attended frequency14Hz decreases dramatically as the viewing distance increases. The 2^{nd} harmonic (not labelled) also had a similar declining tendency corresponding to the increase of the viewing distance. The results illustrating FFT power spectrum when the subjects attended to 12, 13 and 15Hz can be found in Appendix B. See Figures B-3, B-5 and B-7 on pages 212, 213 and 214 for details.

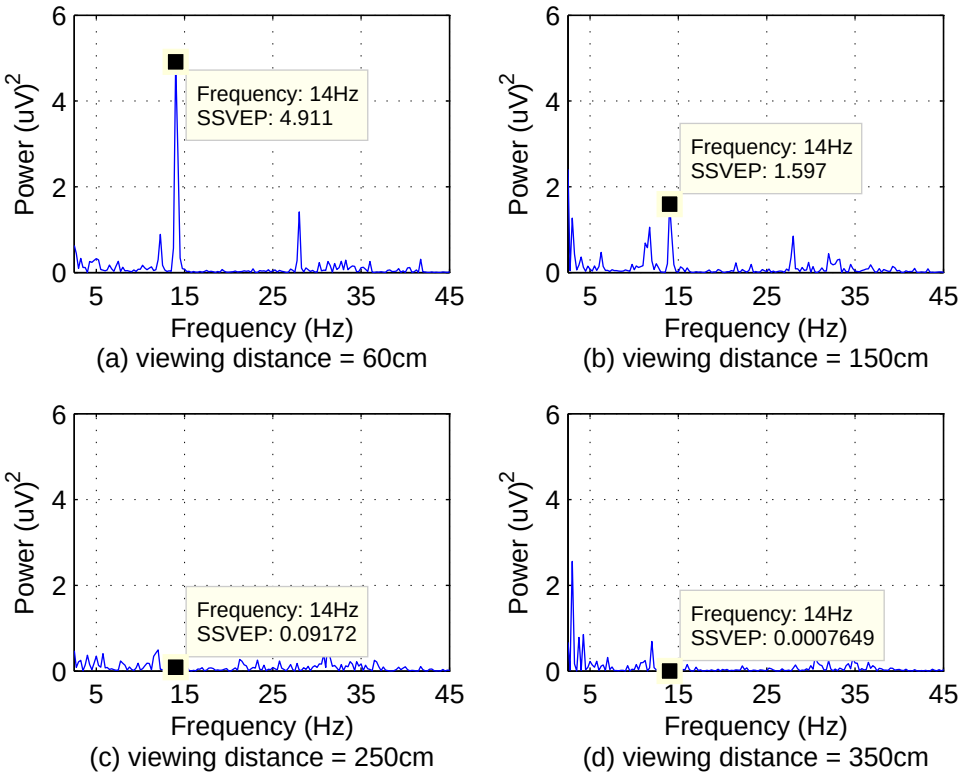

Figure 4.1: **FFT power spectra at four viewing distances without LED intensity compensation.** The attended target of this figure is 14Hz. FFT power spectrum presented is the mean EEG of all epochs and electrodes. It can be observed that SSVEP power at the attended frequency (14Hz) decreases as the viewing distance increases without LED intensity compensation. The power at the 2^{nd} harmonic (not labelled)also decreased as viewing distance increased.

One way Analysis of Variance (ANOVA) was performed to test the significance of the viewing distance on the power of SSVEP. AVONA test of SSVEP power at 14Hz showed a p value < 0.01 and F (3,76)=15.24 (df=3 $\times$ 76). This result indicates that the impact of the viewing distance on SSVEP power is significant.

To examine the differences between the four viewing distances considered in this study, further post hoc test is applied. The results showed that the mean SSVEP power at 60cm viewing was significantly different from the ones at the other three viewing distances. The mean SSVEP power at viewing distance 150cm, 250cm and 350cm were not significantly different. The boxplot of SSVEP power for attending 14Hz and the corresponding ANOVA test result are illustrated in Figure 4.2. The boxplots and corresponding ANOVA tests for attending at 12, 13 and 15Hz can be found in Appendix B. See Figures B-4, B-6 and B-8 on pages 212, 213 and 214. The results all confirm that the significant impact of the viewing distance on SSVEP power apart from 12Hz.

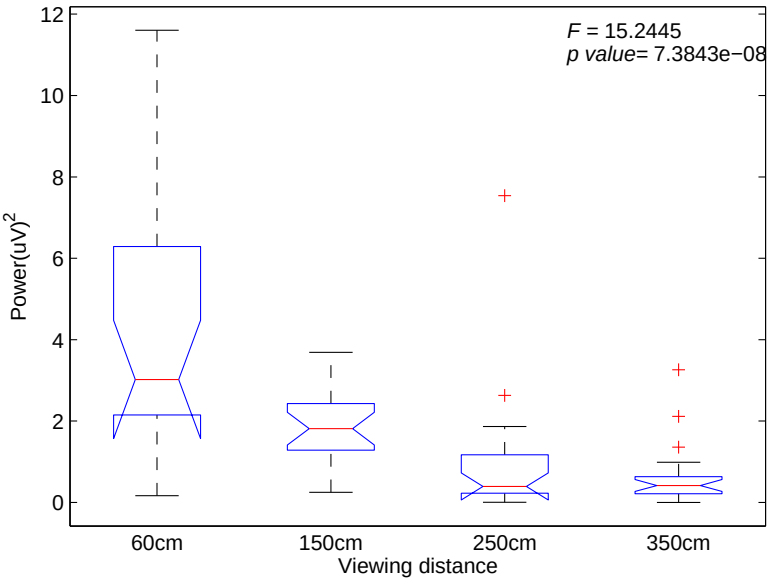

Figure 4.2: **Boxplot of SSVEP power when the subject attended at the target of 14Hz at four viewing distances without LED intensity compensation.** This figure shows that SSVEP response at 14Hz decreases as the viewing distance increases.

4.1.2 Time–locking to the stimulus onset property

SSVEP is time– and phase–locked to the stimulus. SLIC was used to examine the time locked property to stimulus. As explained in Chapter 3, SLIC first divides EEG into segments according to the sequences of the stimulating frequencies. Figure 4.3 demonstrates EEG segmentation by four stimulating frequency sequences. The first row of Figure 4.3 is the original EEG signal when the subject attends at 13Hz target. The second to fifth rows depict the original EEG signal segmented into traces between two stimulus onsets for 12, 13, 14 and 15Hz. The white bar and black bar in the second to fifth rows of the plot indicate LED ON and OFF period. The white and black bars consist a full stimulating periods. In one second, there are 12, 13, 14 and 15 ON–OFF repetitions for 12Hz, 13Hz, 14Hz and 15Hz respectively. As a result, there are 12, 13, 14 and 15 traces for

12, 13, 14 and 15Hz respectively. SLIC computes the correlation coefficients of two different traces within the same frequency.

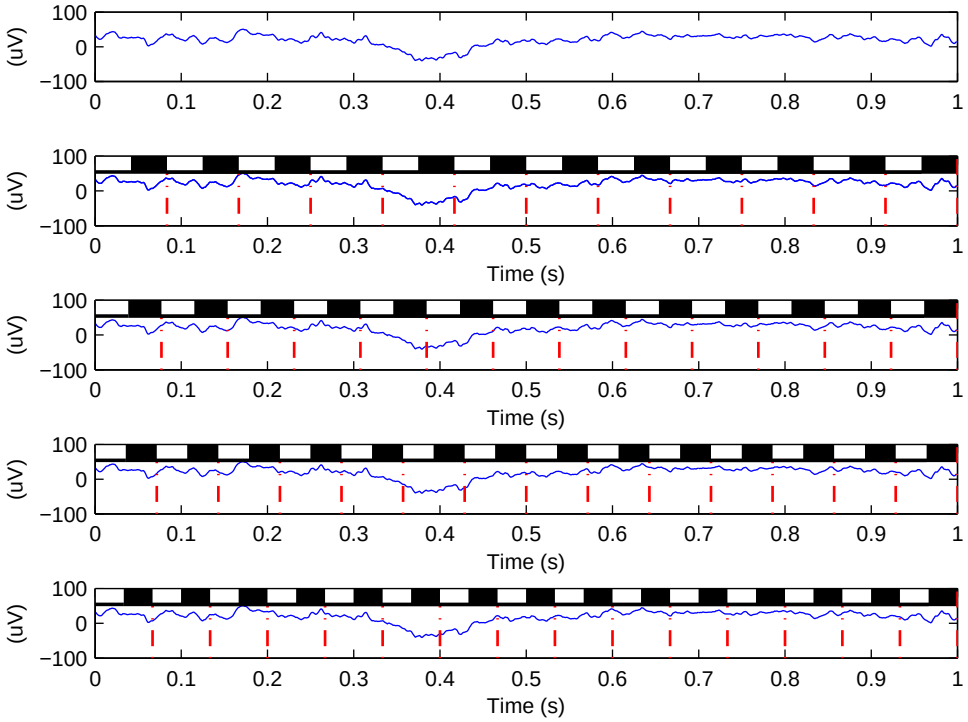

Figure 4.3: **EEG data segmentation by SLIC.** The first row of this figure is the original EEG data. The second to fifth row is the inter–traces of EEG data segmented by 12, 13, 14 and 15Hz respectively. The white–black segments at the top of the second to fifth rows of the sub–figures stand for LED ON–OFF. The attended frequency of this figure is 13Hz.

Figure 4.4 depicts one of SLIC results. In Figure 4.4, the subject attended to 13Hz target at 4 different viewing distances with the same LED intensity. The top row of Figure 4.4 represents EEG inter–traces (the blue thin lines) and the mean curve (the red thick line) of the inter–traces. Figure 4.4 is based on the processing of 2s of EEG data. For illustration purposes, only about one third of the total traces are plotted but the mean curve is the average over all traces (24, 26, 28 and 30 inter–traces corresponding to 12, 13, 14 and 15Hz respectively). The mean curves become flatter as the viewing distance increases and that the mean curve of viewing distance 60cm is a sinusoidal like curve.

The second row of Figure 4.4 shows the histogram depicting the correlation coefficient between two traces. The x axis represents the values of the correlation coefficients which are between -1 and 1 while the y axis stands for the number of occurrence of the correlation coefficients. At the viewing distance of 60cm, a clear left skewed distribution can be seen. As the viewing distance increases, this

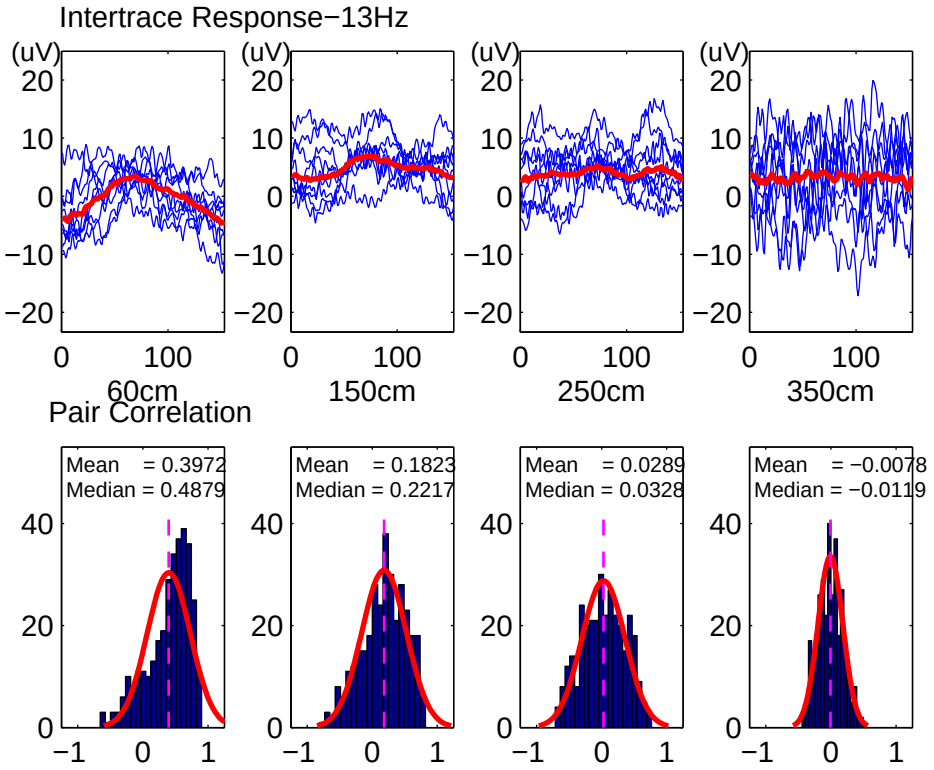

Figure 4.4: **EEG inter–traces and histogram of inter–trace correlation coefficients distribution without LED intensity compensation.** First row is the inter–trace EEG in time domain at different viewing distances. Blue thin line is one single inter–trace and red thick line is the average of all inter–traces. The second row is the histogram of inter–trace correlation coefficients distribution. LED intensity is the same for all viewing distances. This figure demonstrates how the viewing distances affect the time locking property of SSVEP at the attended frequency (13Hz) only.

distribution is more similar to a normal distribution. This can be verified by their median and mean value. At short viewing distances, the median (mean) value of the correlation coefficients is higher than that of the longer viewing distances. At 250cm and 350cm viewing distances, the median (mean) values approached zero. More SLIC results for 12, 14 and 15Hz can be found in Appendix B, see Figures B-15, B-16 and B-17. These results are similar to those exhibited in Figure 4.4. They also demonstrate the impact of changing the viewing distances on the time locking property. That is, this property is clearly seen at 60cm but not equally clear for the longer viewing distance in uncompensated condition.

4.1.3 Phase–locking to the stimulus onset property

Figure 4.5 shows one of ITC results when the subject attends 14Hz target at four viewing distances without LED intensity compensated. From Figure 4.5, ITC at 14Hz drops dramatically at the viewing distances 250 and 350cm compared to the viewing distances 60cm and 150cm. The declined trends can also be

observed at the higher harmonics of 14Hz. EEGLAB is used to calculate ITCs in Figure 4.5. ITC at 14Hz is obtained by linear interpolation of its two neighbouring frequencies, one higher and one lower. The box plots of estimated ITC of 14Hz at four viewing distances can be seen in Figure 4.6.

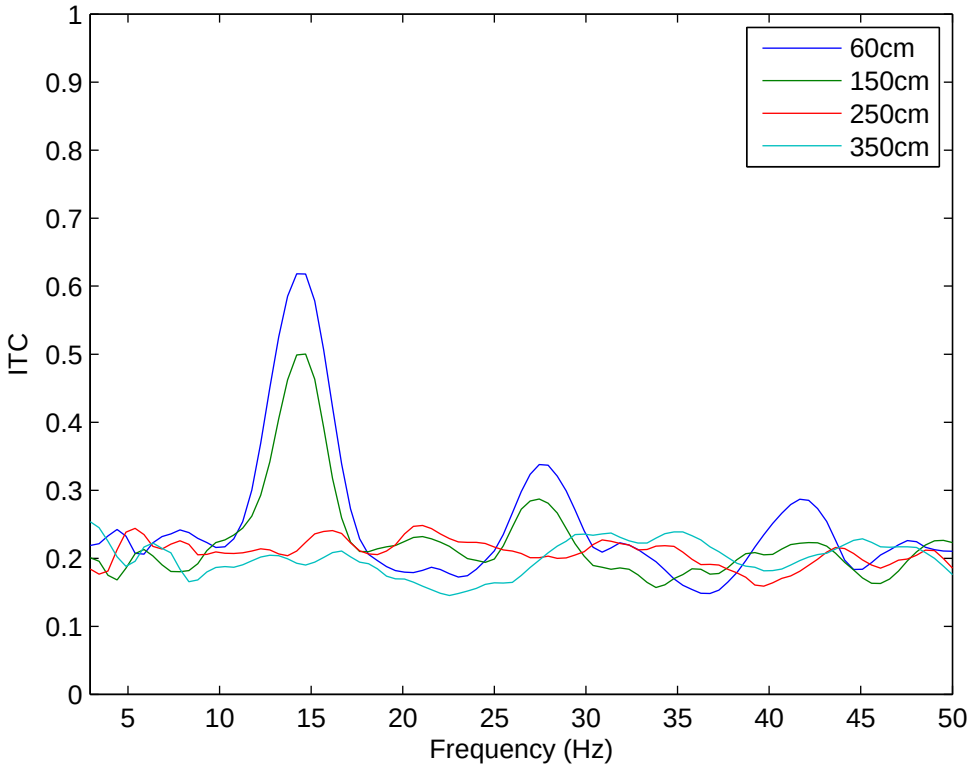

Figure 4.5: **ITC at different viewing distances when the subjects attended at the target of 14Hz without LED intensity compensation.** ITC at the attended frequency (14Hz) decreases as the viewing distance increases. This decrease can also been seen at the higher harmonics of 14Hz.

One way ANOVA is performed to check the significance of the viewing distances. p value < 0.001. The difference of ITC at different viewing distances is significant. In Figure 4.6, the mean ITCs of two closest neighbouring frequencies of the attended frequency are the average across 11 electrodes. More ITC results can be seen in Appendix B. See Figures B-21, B-22, B-23, B-24, B-25 and B-26.

4.1.4 Classification accuracy

In this section, the impact of changing the viewing distance on the classification accuracy in uncompensated condition is inspected. CCA using 11 electrode signals is employed to classify EEG data into one of the 4 possible classes corresponding to the four frequencies. EEG TWL is 2s and EEG was down–sampling by 100Hz. The number of SSVEP harmonics is 1. Table 4.2 lists the classification rates of 4 classes at 4 viewing distances without LED intensity compensation.

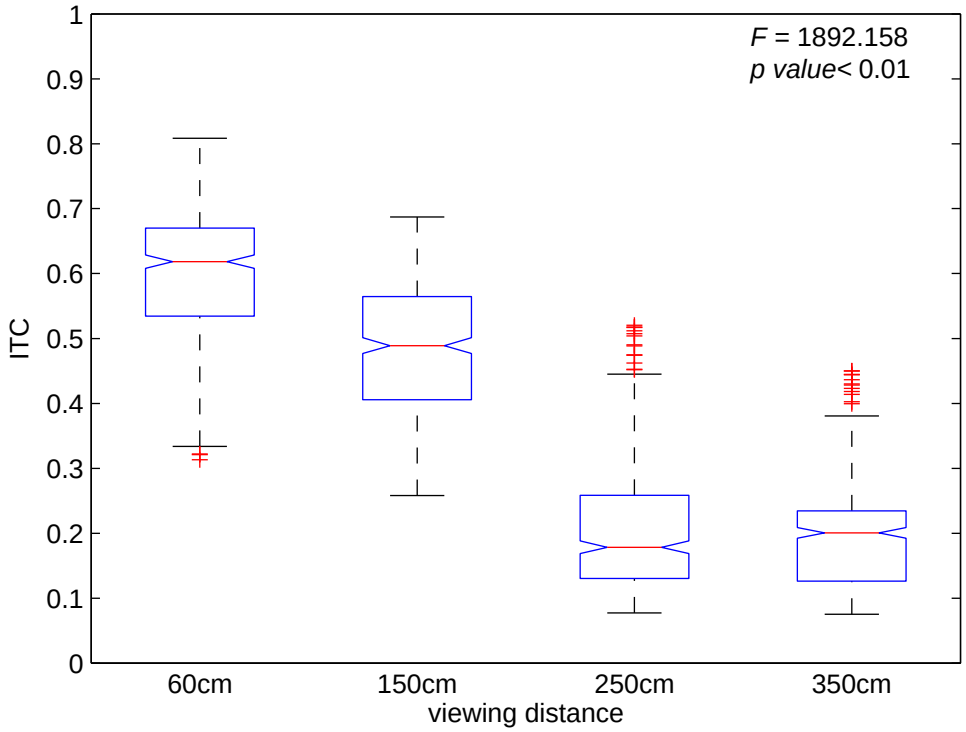

Figure 4.6: **Boxplot of ITC when the subject attended at the target of 14Hz at four viewing distances without LED intensity compensation.** This figure shows that ITC at 14Hz decreases as the viewing distance increases. ITC of 14Hz is obtained by linear interpolation of two neighbouring frequencies of 14Hz.

Table 4.2: **Classification accuracies without LED intensity compensation.** EEG data was classified by CCA using 11 electrode signals.

		12Hz	13Hz	14Hz	15Hz	Accuracy(%)
60cm	12Hz	20	0	0	0	100%
	13Hz	0	20	0	0	100%
	14Hz	6	0	14	0	70%
	15Hz	8	2	0	10	50%
150cm	12Hz	19	1	0	0	95%
	13Hz	14	6	0	0	30%
	14Hz	10	1	9	0	45%
	15Hz	13	2	0	5	25%
250cm	12Hz	18	2	0	0	90%
	13Hz	17	3	0	0	15%
	14Hz	18	2	0	0	0%
	15Hz	18	1	1	0	0%
350cm	12Hz	16	4	0	0	80%
	13Hz	17	2	1	0	10%
	14Hz	17	3	0	0	0%
	15Hz	19	0	0	1	5%

From Table 4.2, apart from 12Hz, the classification accuracies are very low for the rest of the stimulating frequencies apart from the ones at the viewing distance 60cm. At the longer viewing distances, such as 250cm and 350cm, the classification accuracies are lower than the probability of the chance (25%). Overall speaking, 12Hz has the highest classification rate while 15Hz has the lowest. The classification result shows the impact of changing the viewing distance on the classification.

4.2 Impact of viewing distances on SSVEP response in compensated condition

In compensated condition, the intensity of LED is higher at longer viewing distance than at the shorter viewing distance. In this section, SSVEP response and classification accuracy in compensated condition at different viewing distance are assessed in the same manner as in section 4.1.

4.2.1 Power spectrum of SSVEP response

Figure 4.7 depicts FFT power spectra when the subject attends at 15Hz target at four viewing distances with different LED intensities.

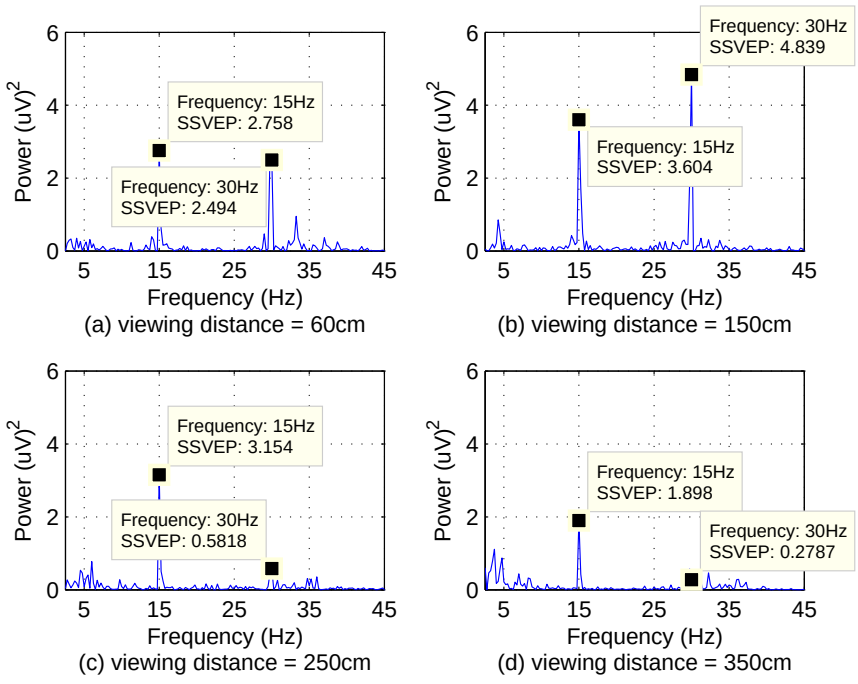

Figure 4.7: **FFT power spectrum at four viewing distances with LED intensity compensation.** The attended target of this figure is 15Hz. FFT power spectrum of this figure is the mean of all epochs and electrodes. SSVEP power at the attended frequency at longer viewing distance can be larger than the one at shorter viewing distance with LED intensity compensation.

With LED intensities compensation, the power of SSVEP at the attended frequency15Hz remains at the similar level at all viewing distances. The power associated with longer viewing distance can be even larger than the one at the shorter viewing distance (compared (a) and (b)). The power of the 2^{nd} harmonic at viewing distance 150cm is stronger than that of the fundamental frequency. One way ANOVA was performed to examine the impact of the viewing distance over the power of SSVEP in compensated condition. The result which can seen in Figure 4.8 shows that p value > 0.01, F (3,76) =2.75 (df=3 $\times$ 76). It shows that the impact of the viewing distance on SSVEP power is not significant with LED intensity compensation. In ANOVA test, for each viewing distance, the test data are SSVEP powers of 20 epochs.

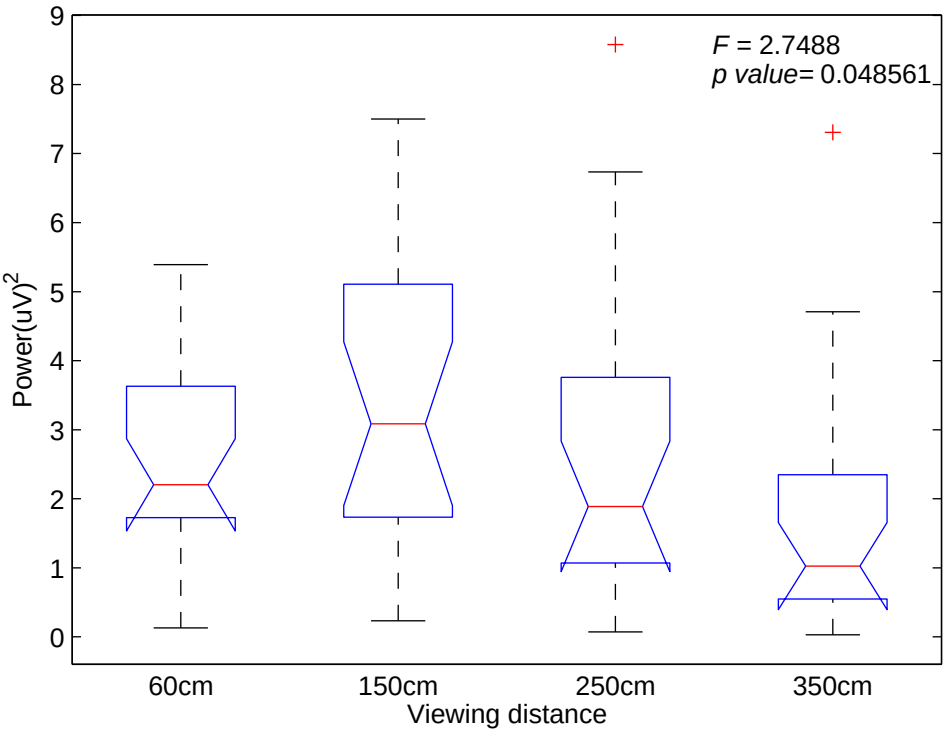

Figure 4.8: **Boxplots of SSVEP powers at four viewing distances with LED intensity compensation.** The attended target of this figure is 15Hz. Each viewing distance has 20 epochs.

Figures illustrating FFT power spectra when the subject attended to 12, 13 and 14Hz can be found in Appendix B. See Figures B-9, B-11 and B-13 on pages 215, 216 and 217 for details. The results indicate that SSVEP response can be prominent at long viewing distance when LED intensities are compensated. These SSVEP power specta are calculated based on mean EEG over 11 electrodes and 20 epochs. EEG sampling rate is 2k Hz and EEG TWL is 4 s. These parameters are the same as the ones used to obtain the results illustrated in section 4.1.

The boxplots and ANOVA test for attending at 12, 13 and 14Hz can be found in Appendix B. See Figures B-10, B-12 and B-14 on pages 215, 216 and 217 for details. As it can been from Figures B-12 and B-14, the p value < 0.01. To understand the difference between different viewing distances, post hoc is applied. Without LED intensity compensated, the powers of the viewing distance 60cm are significantly different from the other three viewing distances. With LED intensity compensation, the significant difference only exists between the longest and shortest viewing distance.

4.2.2 Time–locking to the stimulus onset property

Figure 4.9 shows the individual inter–trace (blue thin line) and the mean intertace (red thick line) in the first row and the histogram of the correlation coefficients between inter–traces in the second row when the subject attends at 13Hz target with LED intensity compensated.

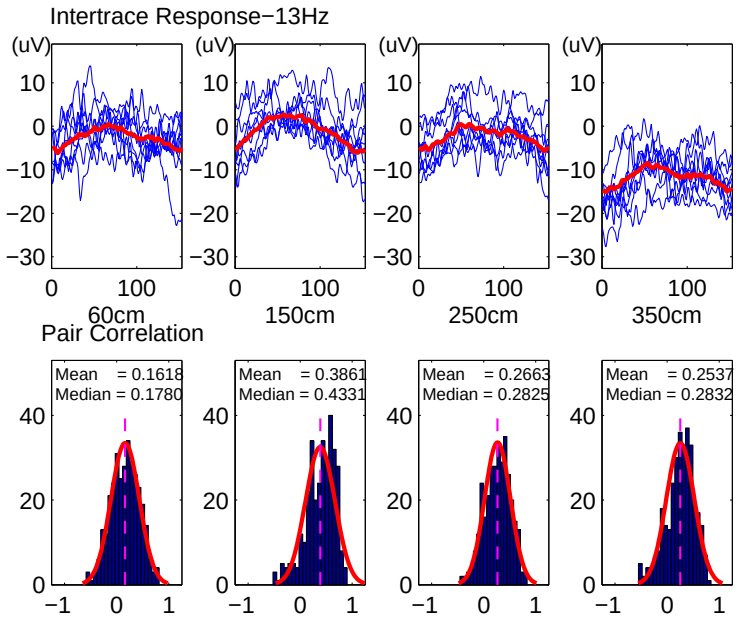

Figure 4.9: **EEG inter–traces and histogram of inter–trace correlation coefficients distribution with LED intensity compensation.** First row is the inter–trace EEG in time domain at different viewing distances. Blue thin line is one single inter–trace and red thick line is the average of all inter–traces. The second row is histogram of inter–trace correlation coefficients distribution. LED intensity is compensated according to the change of the viewing distances. This figure demonstrates that the inter–trace correlation at different view distance remains consistent with LED intensity compensated.

With LED compensation, the mean inter–traces are all in sinusoidal like waveform. The histograms of correlation coefficients at viewing distances 150, 250 and 350cm also show left skewed pattern as seen at the viewing distance 60cm. The mean and median values of the inter–trace correlation coefficients are larger

than the ones shown in Figure 4.4 for all viewing distances. More SLIC results in compensated condition can be found in Appendix B, see Figures B-18, B-19 and B-20 on pages 221 and 223 for details.

4.2.3 Phase–locking to the stimulus onset property

Figures 4.10 and 4.11 show ITC results of different viewing distances and their corresponding boxplots with LED intensity compensation. These two figures provide evidence that ITC are improved in compensated condition. With LED intensity compensated, ITC at the attended frequency and its higher harmonics are significantly increased compared to the ones in uncompensated condition. In Figure 4.10, ITCs of attended frequency, 14Hz at the viewing distances 60 and 150cm are almost overlapped. ITCs of the 2^{nd} harmonic frequency also improved. More ITC results of different stimulating frequencies with LED intensity compensation can be found in Figures B-27, B-29 and B-31 in Appendix B on pages 227, 228 and 229. All these figures demonstrate that ITCs at all viewing distances are increased in compensated condition.

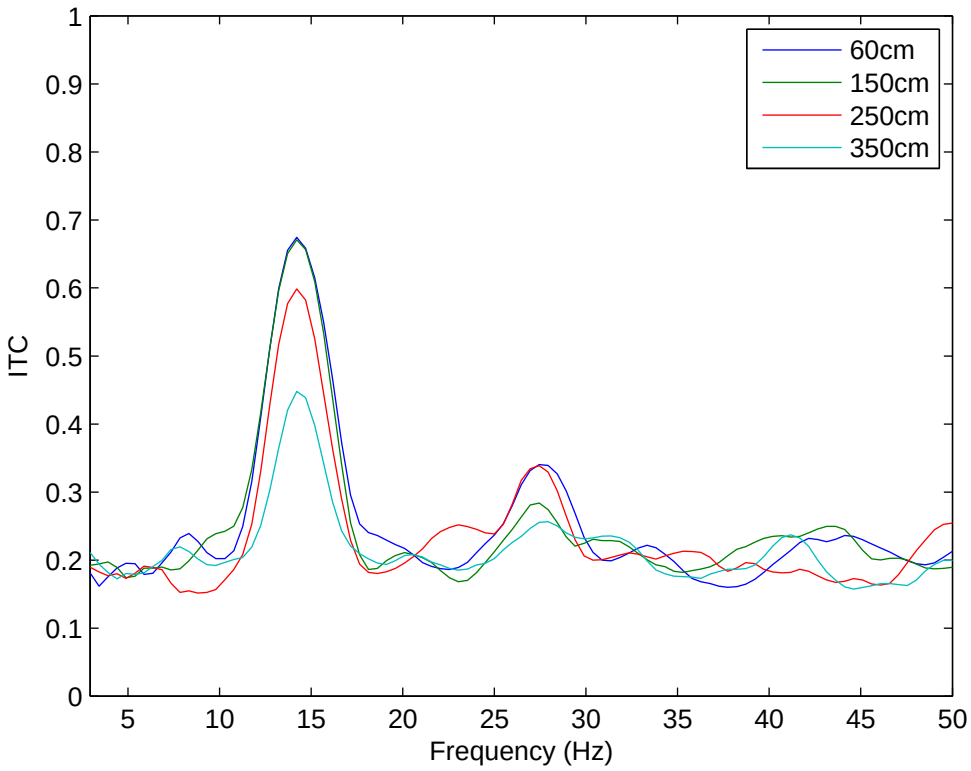

Figure 4.10: **ITC at different viewing distances when the subjects attended at the target of 14Hz with LED intensity compensation.** With LED intensity compensation, ITC values at attended frequency are more stable compared to the ones without LED intensity compensation (see Figure 4.5).

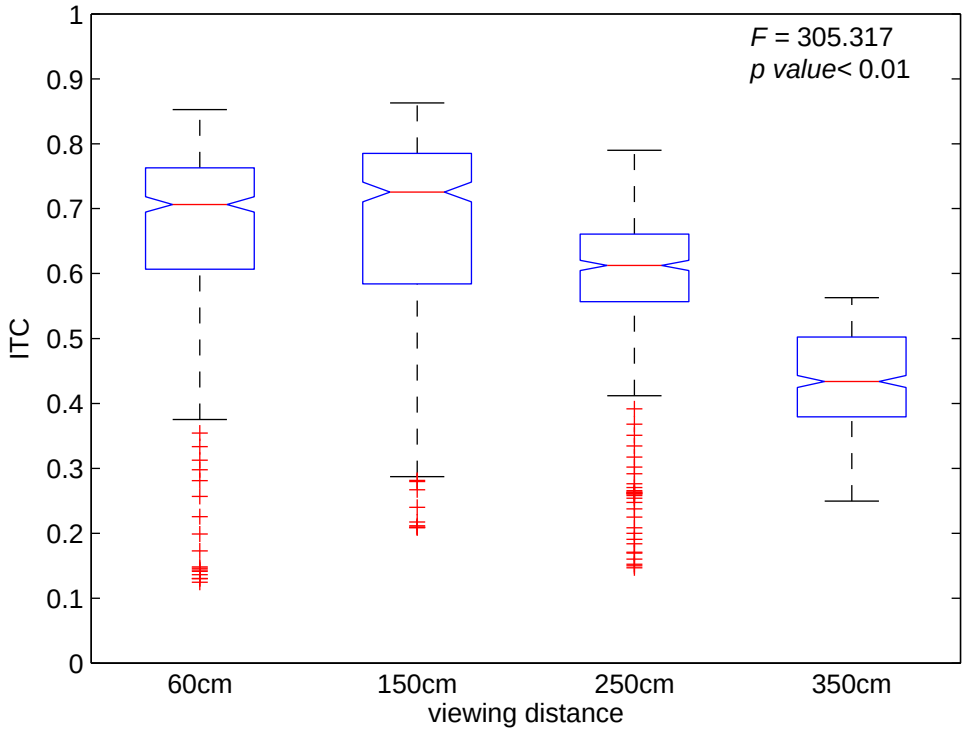

Figure 4.11: **Boxplot of ITC when the subject attended at the target of 14Hz at four viewing distances with LED intensity compensation.** This figure shows that ITC at attended frequency, 14Hz is more consistent than without LED compensation (see Figure 4.6). ITC of 14Hz is obtained by linear interpolation of the two nearest neighbouring frequencies of 14Hz .

4.2.4 Classification accuracy

The same classification approach using the signals of 11 electrode signal is applied to classify EEG data when the subjects attended to one of the targets at different viewing distances in compensated condition. Table 4.3 summaries the classification rates in all experiment conditions. The classification rate of 12Hz remains as high as the one without LED intensity compensation. The classification rates of the other targets improve significantly, although low classification rates can still be observed. The classification rate of 15Hz remains the lowest compared to the other attended frequencies. But none of the classification rates are lower than the probability of the chance (25%).

Table 4.3: **Classification accuracies with LED intensity compensation.** EEG data was classified by CCA using 11 electrodes signal.

		12Hz	13Hz	14Hz	15Hz	Accuracy
60cm	12Hz	20	0	0	0	100%
	13Hz	1	19	0	0	95%
	14Hz	3	0	17	0	85%
	15Hz	6	1	3	10	50%
150cm	12Hz	19	0	1	0	95%
	13Hz	0	20	0	0	100%
	14Hz	2	0	18	0	90%
	15Hz	1	0	0	19	95%
250cm	12Hz	20	0	0	0	100%
	13Hz	4	16	0	0	80%
	14Hz	8	0	12	0	60%
	15Hz	9	1	1	9	45%
350cm	12Hz	18	1	1	0	90%
	13Hz	5	15	0	0	75%
	14Hz	6	1	13	0	65%
	15Hz	13	1	1	5	25%

4.3 Summary

It can be expected that intensity of the visual stimulator decreases as the viewing distance increases. In compensated condition, SSVEP response become more prominent in terms of the power and other related properties. As a result, the classification rates also improve significantly in comparison to uncompensated case. It is difficult to define the optimal response. For BCI, the most important aspect is to convey the subjects intent into a command accurately and speedily. If the classification performance at viewing distance 60cm is used as a benchmark to compare to, the results in Table 4.3 shows that the classification performance at the other distances could outperform or underperform that of the 60cm.

SSVEP response is sensitive to the intensity of the visual stimulus. However, author best knowledge, in most SSVEP studies, the intensity of the visual stimulus is used to explain the modulation depth. In practice, there are a few concerns to increase the intensity of the visual stimulator. On one hand, higher intensity might improve the classification performance. On the other hand, high intensity may potentially induce discomfort of the subject and may become a health and safety issue for the subject's vision. There should be a balance between the performance and the intensity of the visual stimulator. Before Feasibility Experiment, a resistor/intensity selection experiment is performed to find the optimal resistor value (LED intensity) for the subjects. It is seen in this chapter that 15Hz has the lowest classification accuracy. For this reason and also to reduce the time of the experiment, in the resistor/intensity selection experiment, only 15Hz target is used to find the resistor value. It is assumed that the other classes will outperform the class of 15Hz under the same condition.

Chapter 5

Results – data analysis of Feasibility Experiment

In this chapter, the feasibility of a distance adaptable SSVEP based BCI is evaluated. This chapter starts with the resistor/intensity selection experiment as described in Chapter 3. The detailed process, see Figure 3.9. SNRs and z scores across the subjects are examined by different EEG time window lengths (TWLs) at different viewing distances. The confusion matrix and ROC are employed to assess the classification performance by the true and false positives. The impact of the number of the electrodes in the electrode subsets on the classification performance is also investigated. Finally, the electrodes are ranked according to their importance and the classification performance. The efficacy of the ranked electrode subset is cross-validated.

5.1 Initial Resistor/Intensity Selection Experiment

In Chapter 4, it was found that 15Hz had the lowest classification accuracy among all the stimulating frequencies under the same experiment conditions. For this reason and to reduce the time of resistor/intensity selection, only 15Hz stimulating frequency was tested. It was assumed that the other stimulating frequencies should have better classification performance than 15Hz under the same condition. The resistor/intensity selection process was described in Figure 3.9 on page 79 in Chapter 3. The selected resistors based on Figure 3.9 were 450, 100, 30 and 15 Ω for viewing distances 60, 150, 250 and 350cm respectively. Their corresponding luminance at different viewing distances can be found in Table 5.1.

As the resistor/intensity selection experiment is time-consuming and exhausting, only one subject participated in this experiment. The resistors used in the Feasibility Experiment are selected based on the result of one subject. To take the variance of the subjects into account, for each viewing distance, the resistor value used in the Feasibility Experiments slightly lower. The resistors used in the Feasibility Experiment are 300 Ω for 60cm, 75 Ω for 150cm, 15 Ω for 250cm and 5 Ω

for 350cm. This set of the resistors is applied to all the subjects who participated in the Feasibility Experiment. The corresponding luminance at different viewing distances in the Feasibility Experiment can be found in Table 5.1.

Table 5.1: **Luminance of LEDs at four viewing distances in the Feasibility Experiment and Intensities obtained from resistor/intensity experiment.** As it can be seen that LED intensity at viewing distance 350cm is the highest for both experiments.Unit of luminance is in lux.

Resistor (Ω)	**300**	**75**	**15**	**5**	**450**	**100**	**30**	**10**
60cm	0.64	-	-	-	0.32	-	-	-
150cm	-	0.50	-	-	-	0.37	-	-
250cm	-	-	0.70		-	-	0.46	-
350cm	-	-	-	1.03	-	-	-	0.60

5.2 Signal to noise ratio and z scores of SSVEP response

In this section, SNRs and z scores of SSVEP response at different viewing distances are assessed to verify if SSVEP response can be elicited at different viewing distances. SNR is obtained by using equation (3.1) on page 83 and z score is computed by equation (3.2) on page 83. SNR is an important metrics for signal classification. On the other hand, z score is the index of the signal strength.

5.2.1 SNR

Figure 5.1 (a) to (d) represents average SNRs across the subjects of each attended frequency for different viewing distances. Their grand average across the attended frequencies is shown in (e). This figure demonstrates that SNRs increase as EEG TWL increases. It can be seen that, apart from the attended frequency of 13Hz, at the same EEG TWL, SNRs of the viewing distances are in the order of 60cm, 150cm, 250cm and 350cm.

To test the impact of the viewing distance on SNRs of the same attended frequency in the same EEG TWL, one way ANOVA tests are performed on SNRs of ten subjects of the same attended frequency in the same EEG TWL between different viewing distances. p values show that for 12Hz 14Hz, and 15Hz, SNRs of 60cm are significantly different (p <0.01) from the ones of 250cm and 350cm for most of EEG TWLs. However, there is no significant difference in SNRs between viewing distances of 150cm, 250cm and 350cm. For the attended frequency of 13Hz, the impact of the viewing distance is not significant.

The impact of the attended frequency on SNRs is examined by re-organising the data of Figure 5.1. The re-organising data can be seen in Figure 5.2. Apart from

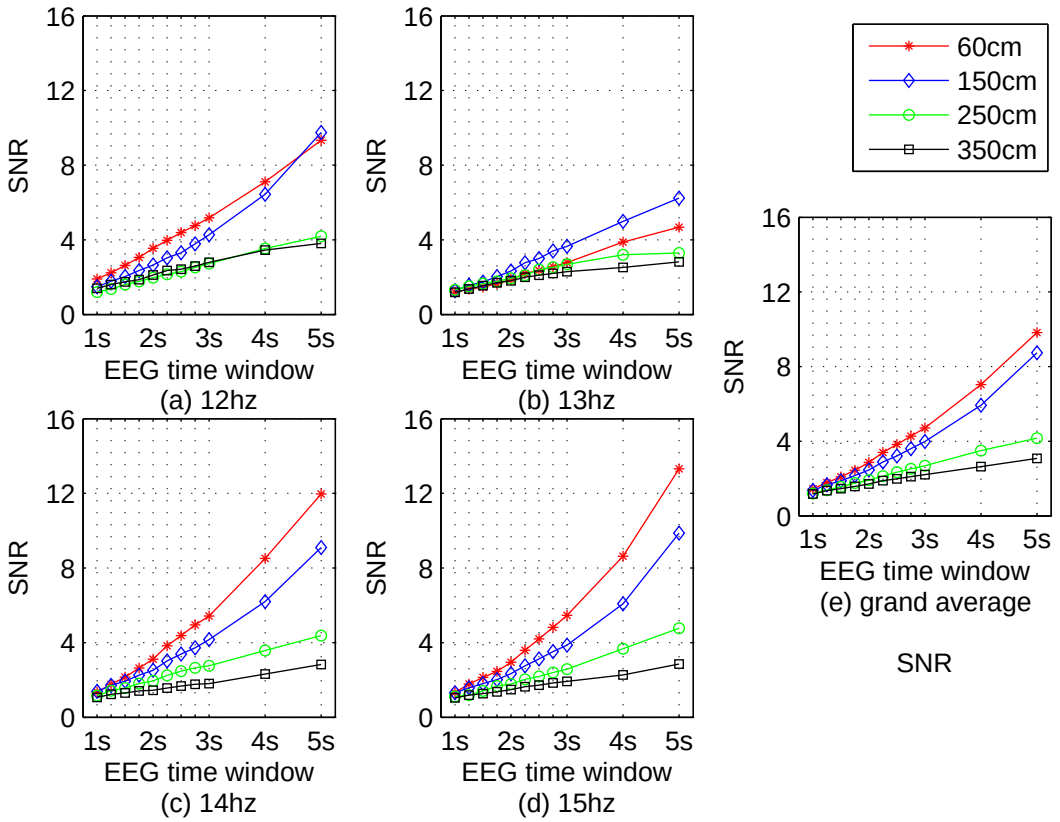

Figure 5.1: **SNRs across the subjects of different viewing distances using different EEG TWL for each attended frequency.** (a) to (d) SNRs across the subjects of different viewing distances using different EEG TWL for each attended frequency. (e) Grand average across the attended frequencies of (a) to (d).

the viewing distance of 60cm, SNRs of all attended frequencies are very close, especially in EEG TWLs between 1s to 3s. One way ANOVA tests are used to test the impact of attended frequency on SNRs of 10 subjects at the same viewing distance in the same EEG TWL. p values show that only SNRs of 12Hz and 13Hz at the viewing distance 60cm between 1s and 3s of EEG TWLs are significantly different (p <0.01).

Figures B-33, B-34, B-35 and B-36 in Appendix B illustrate SNRs of each subject when the subjects attend one of the targets at different viewing distances. They can be found from page 230 to 233 in Appendix B. These figures show great variance among the subjects. Some subjects have significantly higher SNRs than the others. For example, SNRs of the subjects 1, 2, 3, 4 and 6 are higher than the ones of the subjects 5, 7, 8, 9 and 10. For subjects 1, 2, 3, 4 and 6, SNRs are increased relatively stable as EEG TWL increases. However, for subjects 5, 7, 8 and 10, the increase is fluctuated. The orders of SNRs at different view distances are different between the subjects. There is no particular order in common between the subjects. For example, SNRs of 60cm could be largest for one subject but smallest for another subject.

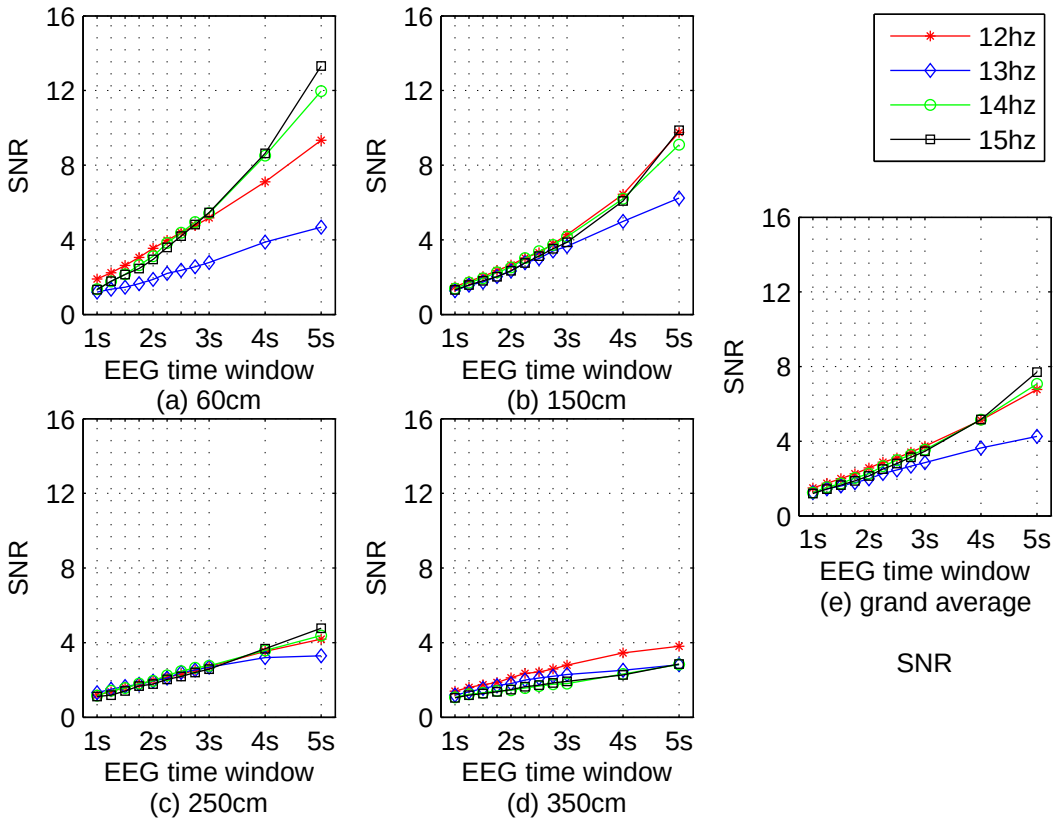

Figure 5.2: **SNRs across the subjects of different attended frequencies using different EEG TWL for each viewing distance.** (a) to (d) SNRs across the subjects of different attended frequencies using different EEG TWL for each viewing distance. (e) Grand average across the viewing distances of (a) to (d).

5.2.2 z scores

Figure 5.3 (a) to (d) represents average z scores across the subjects of each attended frequency for different viewing distances. Their grand average across the attended frequencies is shown in (e). z scores of SSVEP response also increase as EEG TWL increases. Apart from the attended frequency of 12Hz, at the same EEG TWL, z scores of SSVEP response of the viewing distances are in the order of 60cm, 150cm, 250cm and 350cm.

One way ANOVA is performed on z scores of all subjects of the same attended frequency at the same EEG TWL between different viewing distances to inspect the impact of the viewing distance on z scores. The results of p values are similar to the ones found in SNRs. There is no significant difference in z scores between the groups of 150cm, 250cm and 350cm. However, z scores of the group of 60cm is significantly different from the groups of 150cm, 250cm and 350cm in some EEG TWLs. Except viewing distance of 350cm, z scores exceed 2 for all the attended frequencies when EEG TWL is equal to or larger than 2s. For 350cm, z scores exceed 2 between 3s to 4s

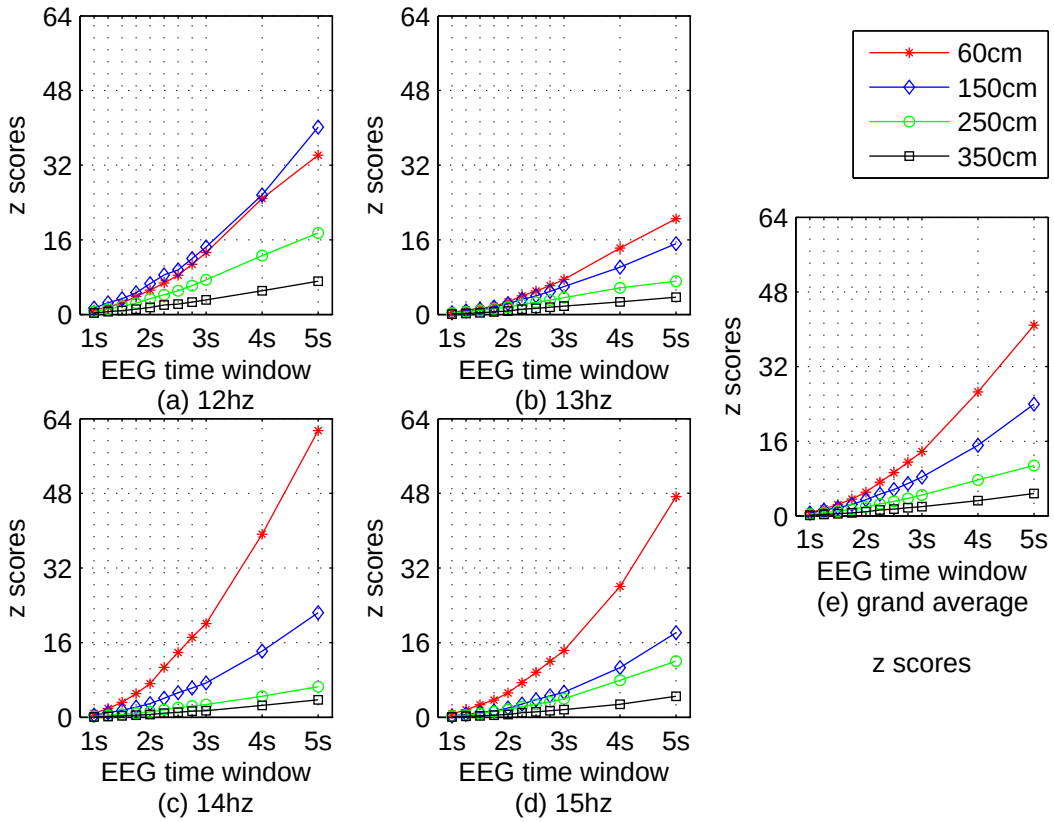

Figure 5.3: **z scores across the subjects of different viewing distances using different EEG TWL for each attended frequency.** (a) to (d) z scores across the subjects of different viewing distances using different EEG TWL for each attended frequency. (e) Grand average across the attended frequencies of (a) to (d).

The impact of the attended frequency on z score is also investigated. Data of Figure 5.3 are rearranged by the viewing distances and the rearranged data are plotted in Figure 5.4. Each subplot of Figure 5.4 shows four attended frequencies. Figure 5.4 clearly shows that z scores of different stimulating frequencies at the same viewing distance are very close between 1s to 3s of EEG TWLs. ANOVA also indicates that the difference of z scores between different stimulating frequencies at the same viewing distance is not significant.

Figures B-37, B-38, B-39 and B-40 are z scores when the subjects attend the target of 12, 13, 14 and 15Hz respectively at 4 viewing distances. They are in the pages 234 and 237 in Appendix B. z scores are similar to SNRs. The subjects with high z scores also have high SNRs. For example, in Figure B-40, z scores of S1, S2, S3, S4 and S6 are prominent compared to the S5, S7, S8 and S10. S5 and S8 have z scores lower than 0. z score is considered as significant when it is equal to or higher than 2.

For both SNRs and z scores, the viewing distance has higher impact than the attended frequency. When EEG TWL is less than 3s, for the same viewing distance, SNRs and z scores of different attended frequencies are very close. SNRs

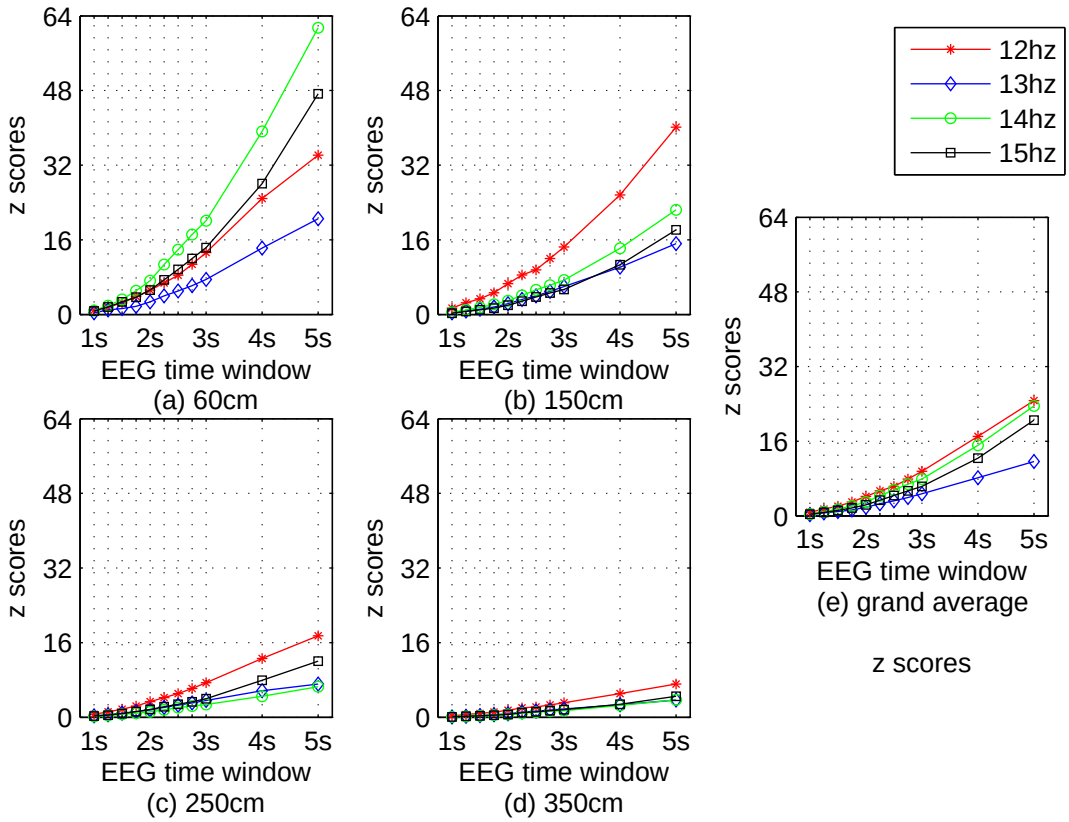

Figure 5.4: **z scores across the subjects of different attended frequencies using different EEG TWL at the same viewing distance.** (a) to (d) across the subjects of different attended frequencies using different EEG TWL at the same viewing distance. (e) Grand average across the viewing distances of (a) to (d).

and z scores of the viewing distance 350cm are lower than the other viewing distances. In section 5.3, the classification performance is evaluated by three classification methods, CCA, MEC and MCC.

5.3 Classification analysis

This section provides an overview of the classification results. Three different classification methods, CCA, MEC and MCC are employed to classify EEG data. To find the suitability of the algorithms, they are compared in the classification accuracies and average time elapsed for one classification. Next, the impacts of several parameters over the classification performance are investigated. These parameters include EEG TWL, the number of SSVEP harmonics, the number of the electrodes etc. Furthermore, based on the results from the aforementioned classification algorithms, confusion matrix and ROC are applied to further assess the classification performance.

5.3.1 Comparison of classification methods

Figure 5.5 shows the classification accuracies from three classification methods, CCA, MEC and MCC. The ratio of $\frac{\#\text{ of epochs being classified correctly}}{\#\text{ of total epochs}} \times 100\%$ is defined as the classification accuracy. In each subplot of Figure 5.5, the classification accuracy is the mean accuracy across 10 subjects and 4 attended frequencies. The number of SSVEP harmonics is 1 (H1) and EEG is down–sampling by 100Hz (termed as fs100Hz). Signal of 11 electrodes is used to classify EEG. The classification results of three classification methods as shown in Figure 5.5 are almost identical. For example, in (a), at EEG TWL 2s, the classification accuracies are 88.25%, 87.63% and 88.13% for CCA, MEC and MCC respectively. In (b), at EEG TWL 3s, the classification accuracies are 88.74%, 88.12% and 88.75% for CCA, MEC and MCC respectively.

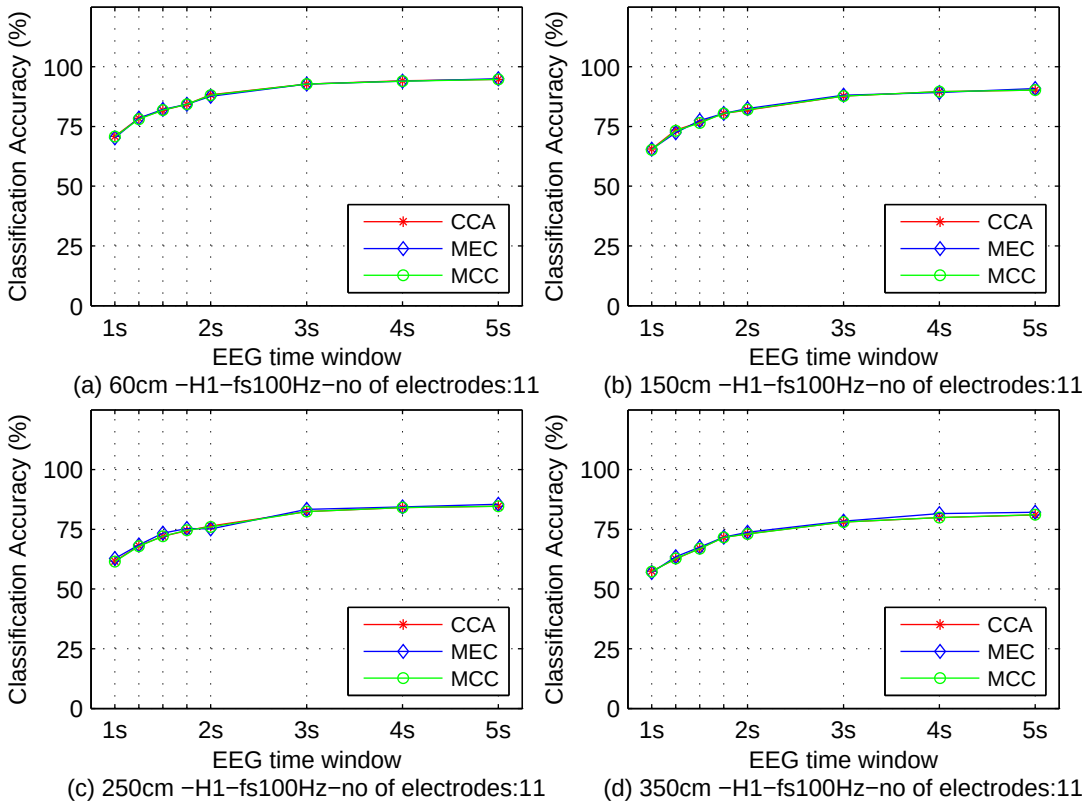

Figure 5.5: **Mean classification accuracies across the subjects and 4 attended frequencies at different EEG TWL for each viewing distance using different classification methods.** (a) to (d) are the mean classification accuracies for the viewing distance 60cm, 150cm, 250cm and 350cm respectively.

The classification accuracies improve as EEG TWL increases for all classification methods. However, the improvement in accuracies becomes saturated after EEG TWL 3s. This can be seen that the curves of the classification accuracies are shaper in EEG TWLs between 1s and 3s than 3s to 5s. Although the classification

accuracies of the different viewing distance vary, the curves of the classification accuracies against EEG TWLs are similar. These methods produce acceptable classification accuracies ($\geq 70\%$) with EEG TWLs equal to 2s or longer.

5.3.2 Number of SSVEP harmonics

In this section, the impact the number of SSVEP harmonics on classification accuracies is investigated. Figure 5.6 represents the comparison of classification results using different number of SSVEP harmonics. In Figure 5.6, the classification method is CCA and the number of the electrodes is 11. The classification accuracies are the mean accuracies across the subjects and the viewing distances. From Figure 5.6, it is clearly seen that the classification accuracies of different number of SSVEP harmonics are almost the same. For example, at EEG TWL 3s, the classification accuracies for attended frequency 15Hz are 74%, 74% and 71% for H1, H2 and H3 respectively. The classification accuracies of H1 are slightly higher than H2 and H3.

The impact of the number of SSVEP harmonics is also inspected on different number of the electrodes. Figure B-41 which can be found in Appendix B presents the same classification accuracies as Figure 5.6. Figure B-41 only uses 7 electrodes. The classification accuracies between H1, H2 and H3 are also almost identical. The impact of the number of SSVEP harmonics is further examined on the other classification methods. The results can be found in Figures B-42 and B-43 in Appendix B. The number of SSVEP harmonics does not show significant impact on the classification accuracies for different classification methods. The classification accuracies between H1, H2 and H3 are very similar.

5.3.3 Classification accuracies of attended frequencies and viewing distances

This section inspects the impacts of the attended frequencies and the viewing distances on the classification accuracies. Figure 5.7 represents the classification accuracies of each attended frequency at different viewing distances. The classification method of this figure is CCA and the numbers of SSVEP harmonics and the electrodes are 1 and 11 respectively. The classification accuracies are the mean accuracies across the subjects. Figure 5.7 shows that for the same attended frequency, its highest classification accuracies can be seen at the viewing distance of 60cm while the lowest appears in the longest viewing distance 350cm. At the same viewing distance, the attended frequency 12Hz has the highest classification accuracies while 15Hz has the lowest ones. The classification accuracies of 12Hz are consistent regardless of the viewing distances. They might be different but very stable. For example, at EEG TWL 2s, the accuracies of 12Hz are 97.5%, 94.5%, 95%, and 94.5% at viewing distance 60cm, 150cm, 250cm and 350cm respectively. On the other hand, the accuracies of 15Hz show great variance between

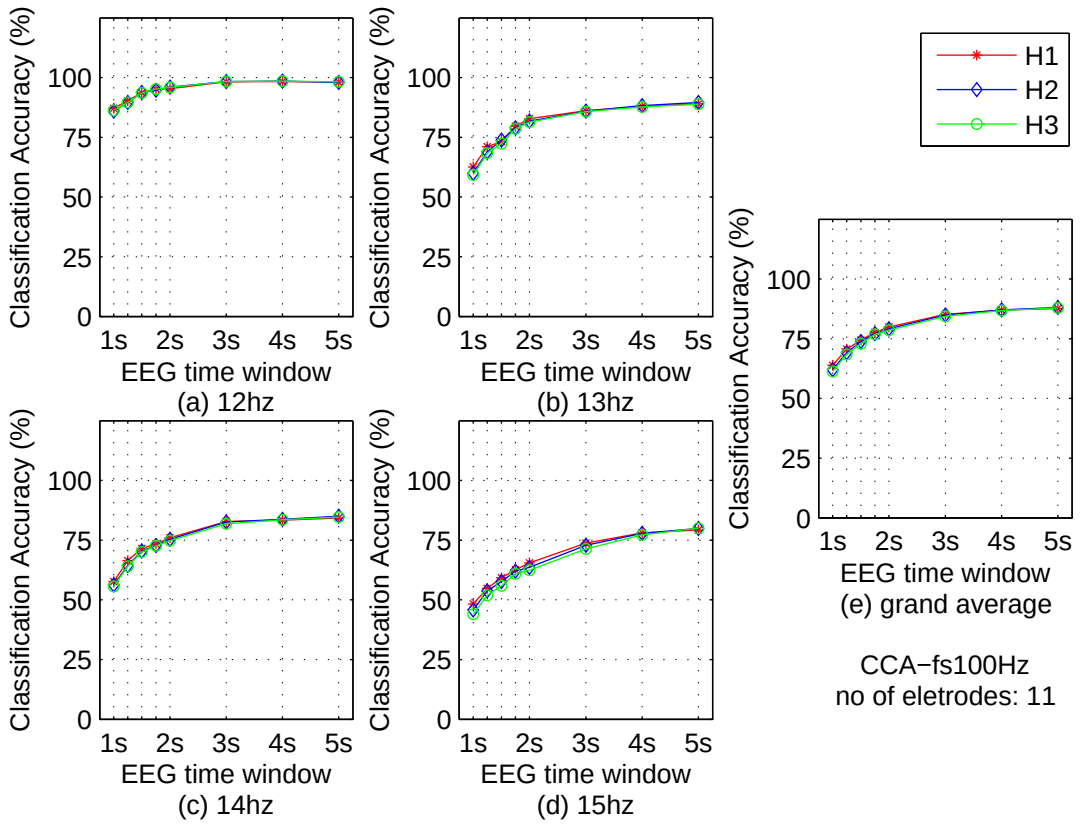

Figure 5.6: **Comparison of classification accuracies using different number of SSVEP harmonics.** In this figure, the classification method is CCA and the number of the electrodes is 11. (a) to (d) are the mean classification accuracies across the subjects and the viewing distances of attended frequency 12Hz, 13Hz, 14Hz and 15Hz respectively. (e) is the mean classification across the subjects, viewing distances and the attended frequencies.

the viewing distances. For example, at EEG TWL 2s, the accuracies of 15Hz are 78%, 68.5%,62.5% and 53% for viewing distances of 60cm, 150cm, 250cm and 350cm. This figure also shows that the classification accuracies of 12Hz is high from 1^{st} second of attending phase compared to the other attended frequencies. At EEG TWL 1s, the accuracies are 81%, 58.5%,54.5% and 36% for 12Hz, 13Hz, 14Hz and 15Hz at 350cm viewing distance. The accuracies of 12Hz are also most reliable. Its accuracies vary from 96% to 100% at EEG TWLs between 3s and 5s. The accuracies of 15Hz vary from 90.5% to 62.5% at EEG TWLs between 3s and 5s.

The classification accuracies obtained by using MEC and MCC classification methods can be found in Figures B-44 and B-45 in Appendix B. The analysis parameters are the same as Figure 5.7. These two figures demonstrate the same outcomes of Figure 5.7. The accuracies improve as EEG TWL increases for all the attended frequencies at all viewing distances. The classification accuracies of 60cm are highest and the ones of 350cm are the lowest among the viewing distances. The classification accuracies of 12Hz are the highest and most

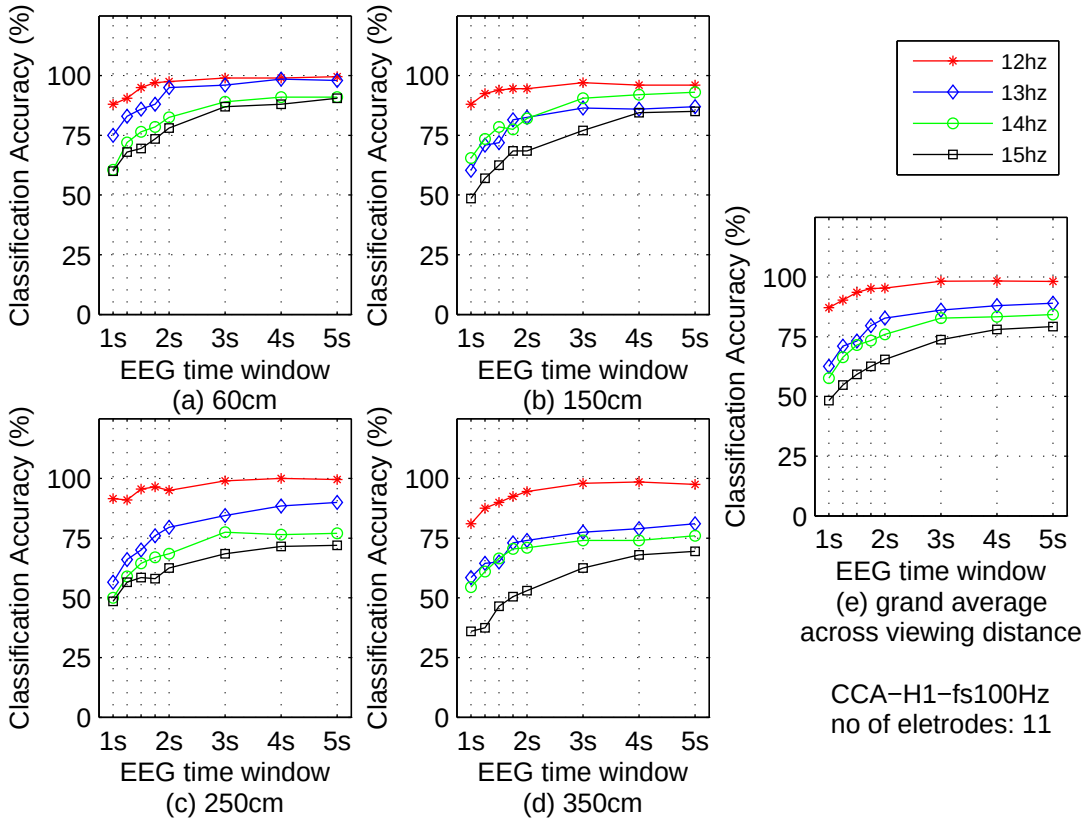

Figure 5.7: **Classification accuracies of 4 attended frequencies at different viewing distances. The classification method of this figure is CCA.** (a) to (d) The classification accuracies of each attended frequency at one of the viewing distances. The accuracies are the mean across the subjects. (e) The grand average across the viewing distances of (a) to (d). The number of SSVEP harmonics and electrodes used in this figure are 1 and 11 respectively.

reliable and the ones of 15Hz are the lowest and most variant across the viewing distances.

5.3.4 Inter–subject variance

Inter–subject variance in the classification accuracies is assessed next. Figure 5.8 shows the mean classification accuracies across the subjects of the attended frequencies at one viewing distance. This figure is the result of CCA using 2s of EEG TWL, H1 and 11 electrodes. The blue vertical bar shows the standard deviations of the accuracies. This figure clearly shows that the accuracies of 12Hz are the highest and the ones of 15Hz are the lowest over the viewing distance. It also shows that the variances of the same attended frequency at different viewing distances are similar. But the variances of different attended frequencies at the same viewing distance are great. In general, inter–subject variance of the classification accuracies of 12Hz is smaller than the others and the variance in 15Hz is the largest. For example, at viewing distance 350cm, the standard deviations of 12Hz and 15Hz are 10% and 36% respectively. The variances of the different

attended frequencies between the viewing distances are similar. For example, at viewing distance 150cm, the standard deviations of 12Hz and 15Hz are 8% and 34% respectively.

One way ANOVA is applied to test the impact of the attended frequency on the classification accuracies at the same viewing distance. In Figure 5.8, the shapes of diamond, circle and square stand for the group of 13Hz, 14Hz and 15Hz. Each column of the dots presents the ANOVA results of the group presented by the dot and the corresponding group in the column. For instance, in column of 12Hz, there are three shapes of dots representing the group of 13Hz, 14Hz and 15Hz. These dots also represent ANOVA results between the groups which the dots present and 12Hz. The black un–filled dot stands for non–significance and the red filled dot stands for the significance. This example shows that the classification accuracies of 12Hz are significantly different from the other attended frequencies. The difference of the classification accuracies of the other attended frequencies is not significant. The similar results can also be observed in the use of different classification methods, MEC and MCC. The results can be found in Figures B-46 and B-47 in Appendix B. The data of Figures 5.8, B-46 and B-47 are used to test the impact of the viewing distances on classification accuracies of the same attended frequency at different viewing distances. ANOVA results show 8 out of 24 tests are significant. The tests shown significance are mainly between the group of 60cm and groups of 150cm and 250cm.

5.3.5 Confusion matrix and ROC

In previous sections 5.3.2, 5.3.3 and 5.3.4, the classification accuracies (true positive rates) have been evaluated. The results demonstrate that in spite of the impact of the viewing distance, the high classification accuracies can be observed at longer viewing distance. In this section, the confusion matrix is used to further inspect the classification performance. The recall rates and precision rates are both explored. The recall rate is the same as the classification accuracy as defined in section 5.3.1. Confusion matrix offers other metrics to evaluate the classifier, for example, precision rate. Figure 5.9 shows the confusion matrix of grand total of all subjects at different viewing distance. The confusion matrix of (a) to (d) is the sum of the individual confusion matrix of each subject. (e) is the grand total of (a) to (d). The columns indicate the classification results of the classifier and rows indicate the actual class. The cell $n_{i,j}$ stands for the number of i class being classified as j class. The classification method of this figure is CCA. The number of SSVEP harmonics and the electrodes are 1 and 11 and EEG TWL is 3s.

Confusion matrix not only reveals the classification accuracies but also the precision rates of different classes. It is known from section 5.3.3 that 12Hz and 15Hz have the highest and lowest accuracies. It is clear shown in Figure 5.9 that 12Hz has highest number of false positives and 15Hz has the lowest number of the false positives at the same viewing distance. In other words, from precision point of

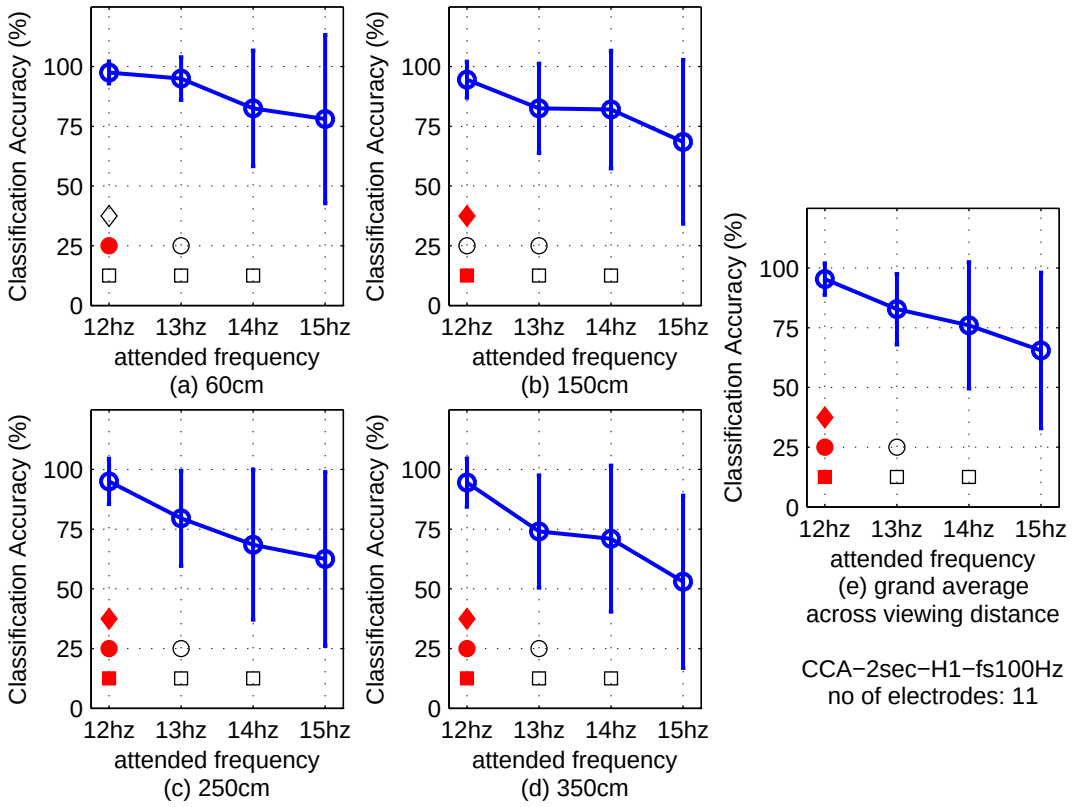

Figure 5.8: **Classification accuracies across the subjects of all attended frequencies at different viewing distance and their grand average. The classification method of this figure is CCA.** (a) to (d) The classification accuracies of each attended frequency at one of the viewing distances. The accuracies are the mean across the subjects. (e) The grand average across the viewing distances of (a) to (d). The number of SSVEP harmonics and electrodes used in this figure are 1 and 11 respectively. EEG TWL is 2s.

view, 15Hz outperforms the other attended frequencies. As the viewing distance increases, the number of false positives of 12Hz increases dramatically. The false positives of 12Hz are 39 at 60cm and increase to 117 at 350cm. The outcome of one misclassification is most likely 12Hz. Confusion matrix using classification methods MEC and MCC with the same parameters can be found in Appendix B, Figures B-48 and B-49. These confusion matrices from different methods are very similar.

Confusion matrix of Figure 5.9 is converted into ROC plots. Each confusion matrix corresponding to 4 points which stand for 4 classes (attended frequencies) in ROC space as shown in Figure 5.10. For a good classifier, ROC point should be as close as to y axis (indicating low false positive rate) and as distant as from x axis (indicating high true positive rate). In Figure 5.10, ROC space is divided/gridded into 25 cells. As it can be seen, the location of the points differs greatly at different viewing distances. For ROC points of 13Hz and 14Hz at each viewing distance, they are either located in the most left–upper area or close to

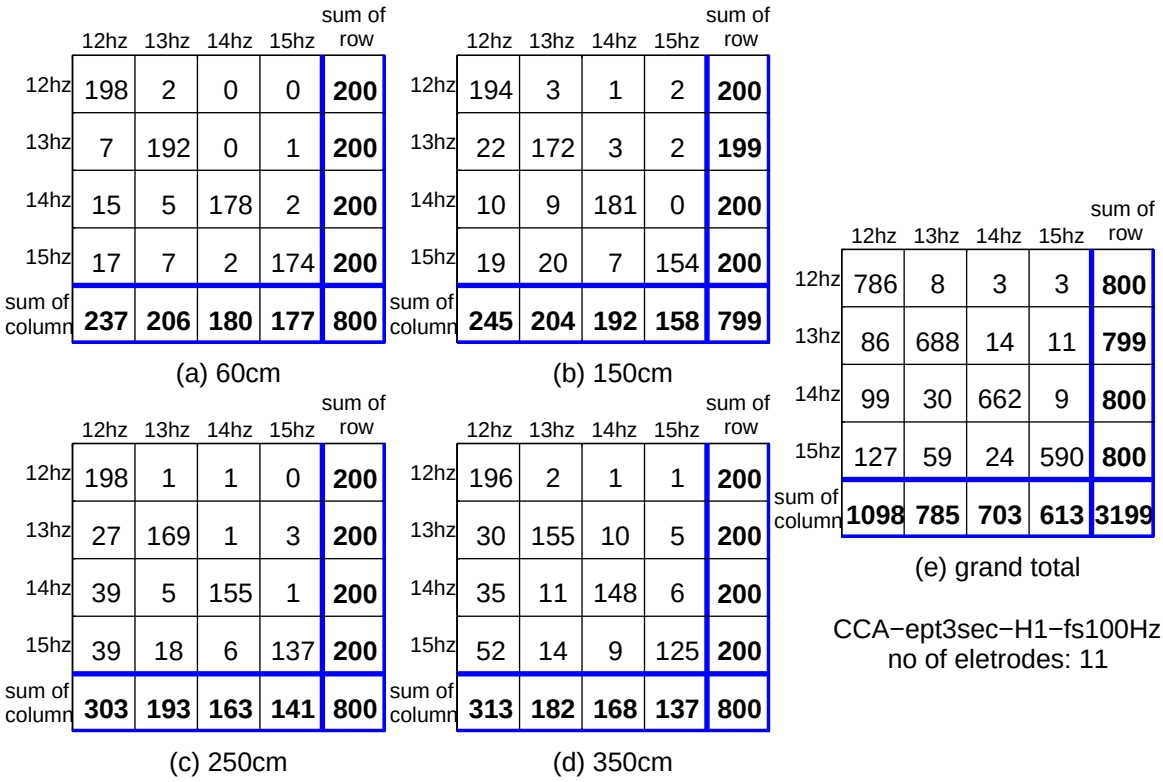

Figure 5.9: **Confusion matrix of grand total of all subjects at different viewing distance using CCA.** The confusion matrix of (a) to (d) is the sum of the individual confusion matrix of each subject. (e) is the grand total of (a) to (d). Each number in the cell is the number of class i being classified as class j. The numbers of SSVEP harmonics and electrodes are 1 and 11 in this figure. The classification method is CCA and EEG TWL is 3s.

this area which indicates that they are superior to 12Hz and 15Hz. The points of 12Hz and 15Hz, they are either distant from both x and y axis or close to x and y axis which indicate that they have either high true and false positive rates or low true and false positive rates at the same time. At the viewing distance of 60cm, all the points are located in the most left–upper area. As the viewing distance increases, the location of the points starts to move away from this area. At the viewing distance of 350cm, none of the points are located in this area. The change of the location is different for each class. The ROC point of 12Hz moves away from y axis as the viewing distance increases but the vertical position does not change much. The ROC point of 15Hz moves towards to x axis while its horizontal position does not change much. The ROC points of 13 and 14Hz change both vertical and horizontal positions with less degree of the change in 12 and 15Hz. In general, 60cm is the best and 350cm is the worst.

For each class, its corresponding F measurement is computed and shown in the right-lower corner of ROC plot. F measurement takes both accuracy and precision rates into consideration and combines them as one metrics. Although 12Hz has the highest accuracies, with the lowest precision rates, F measurements of

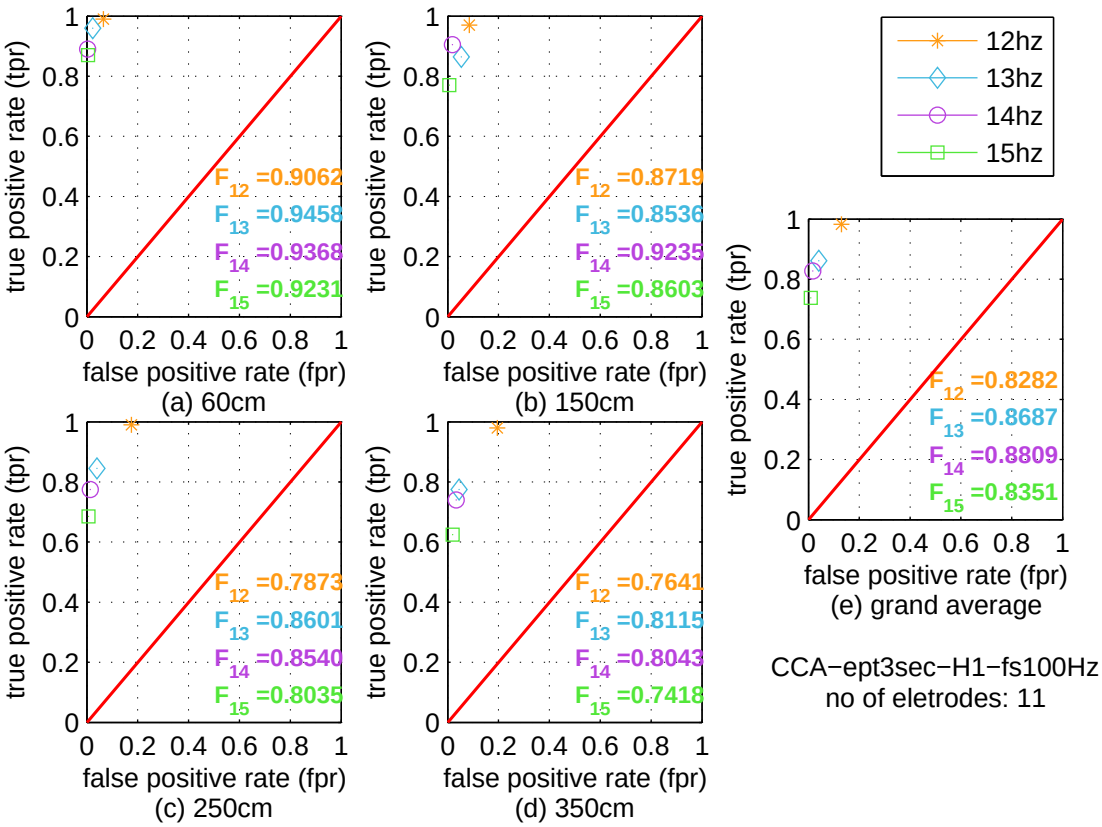

Figure 5.10: **ROC plots corresponding to the confusion matrices of Figure 5.9 and F measurements.** Each ROC plot (a) to (e) is corresponding to one confusion matrix of Figure 5.9 (a) to (e). The classification method and parameters are the same as Figure 5.9.

12Hz are not the highest. On the other hand, F measurements of 15Hz are not the lowest in spite of the lowest accuracies. F measurement confirms that the classification performance of 13Hz and 14Hz are superior to the ones of 12Hz and 15Hz, except at the viewing distance of 150cm.

Confusion matrices of Figures B-48 and B-49 are also converted into ROC plots as shown in Figures B-50 and B-51. These figures are in Appendix B. Their corresponding F measurements are also computed. The results are similar to Figures 5.10. F measurements of the attended frequencies are in the order of 14Hz, 13Hz, 15Hz and 12Hz for three methods. To further evaluate the classification performance, the continuous ROC plots are introduced next.

Figure 5.11 represents the continuous ROC. This figure is based on classification method CCA. The numbers of SSVEP harmonics and the electrodes are 1 and 11. EEG TWL is 3s. For each subplot (a) to (d) in Figure 5.11 , the classification results of each subjects at the same viewing distance are combined together. The classification results using CCA are the canonical correlation coefficients of EEG and the reference signals of four attended frequencies. They are termed as the

scores. Each score is given a label corresponding to the attended frequency. By changing the thresholds, one threshold results in one ROC point and a continuous ROC curve is obtained. In continuous ROC, AUC is used to assess the classification performance. AUC is a value between 0 and 1. The higher value of AUC is, the better classification performance is.

Figure 5.11 shows that in general, the viewing distance of 60cm has higher mean AUC of all attended frequencies compared to the other viewing distances. 350cm has the lowest mean AUC. This result is consistent with F measurements of Figure 5.9. That is F measurements of 60cm are higher than the other viewing distances and the ones of 350cm are the lowest. For individual attended frequency at the same viewing distance, there is no particular order. AUC of 15Hz is normally the lowest. It is not completely same as Figure 5.9. Both results indicate that accuracy and precision should be taken into account to assess classification performance.

Figures B-52 and B-53 in Appendix B are the continuous ROC curves based on classification method MEC and MCC. The numbers of SSVEP harmonics and the electrodes are 1 and 11. EEG TWL is 3s. They can be found in page 244. These two figures are consistent with Figure 5.11.

Next, the impact of the number of the electrodes employed on the classification accuracies are evaluated by the highest, mean and lowest classification accuracies corresponding to the number of the electrodes. The optimal electrode sets and the minimal optimal electrode sets will be discussed in section 5.4 .

5.3.6 Number of the electrodes

Figure 5.12 represents the mean values of the highest, average and lowest accuracies corresponding to the number of the electrodes across the subjects and attended frequencies at different viewing distance. The vertical bar is the standard deviation of the average accuracies of the subjects. This figure is based on classification method CCA. The number of SSVEP harmonics is 1 and EEG TWL is 2s. The number of the electrodes employed in previous classification accuracies analysis is mainly 11. Figure 5.12 shows that different number of the electrodes has the pattern as 11. That is, with the same number of the electrodes, the classification accuracies of the viewing distance 60cm is highest and the one of 350cm is the lowest. This rule is valid to three accuracies, the highest, average and the lowest.

For each viewing distance, the highest accuracies occur at the number of the electrodes between 5 and 7. For example, the highest accuracies are 92%, 88%, 85% and 84% for the viewing distances of 60cm, 150cm, 250cm and 350cm respectively. The corresponding number of the electrodes are (6, 7), (5), (6) and (5, 6). This indicates that more electrodes employed might not result in higher accuracies. However, the average accuracies are linear to the number of the elec-

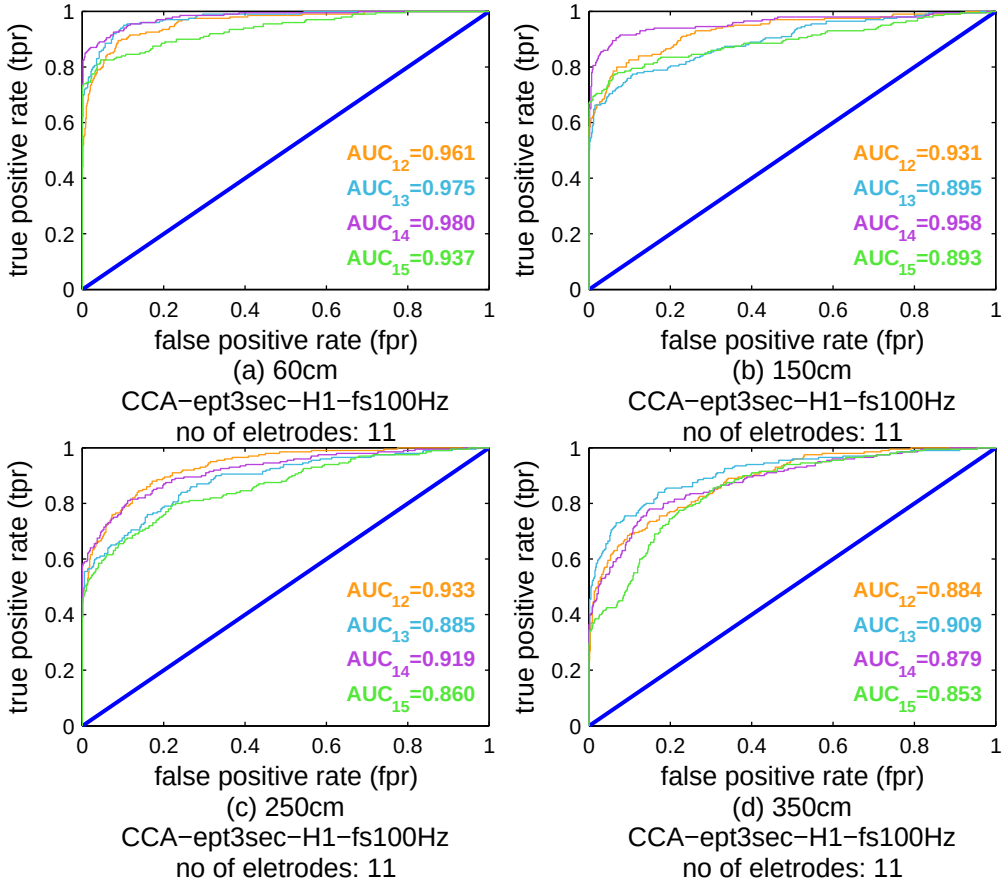

Figure 5.11: **Continuous ROC curves of all attended frequencies at different viewing distances.** The subplots of (a) to (d) are for viewing distances of 60cm, 150cm, 250cm and 350cm respectively. This figure is based on classification method CCA. The numbers of SSVEP harmonics and the electrodes are 1 and 11. EEG TWL is 3s.

trodes. The larger the number of electrodes is, the higher the corresponding average accuracies are. The lowest accuracies do not result from the smallest number of the electrodes. For example, in this figure, the lowest accuracies results from 2 electrodes for all viewing distances. The lowest accuracies are 37%, 30%, 30% and 25% for the viewing distances of 60cm, 150cm, 250cm and 350cm respectively. The inter-subject variances across the number of the electrodes are similar. For example, at the viewing distance 250cm, the standard deviations of the average accuracies are between 25% and 30%. Apart from the viewing distance of 60cm, the smaller number of the electrodes shows less inter–subject variant and the larger number of the electrode shows greater inter–subject variant.

The same analysis is applied to the classifications based on MEC and MCC. Three accuracies corresponding to the number of the electrodes based on MEC and MCC can be found in Figures B-54 and B-55 in page 245 of Appendix B. They are consistent with Figure 5.12.

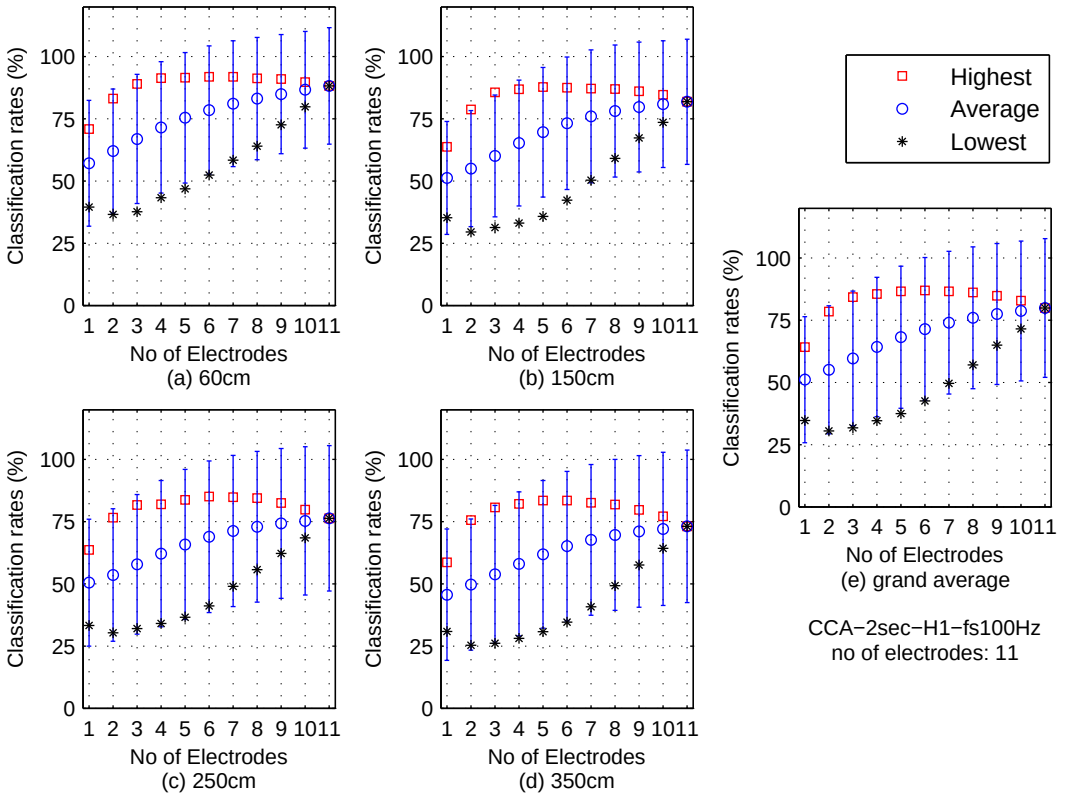

Figure 5.12: **The highest, average and lowest classification accuracies and the standard deviation corresponding to the number of the electrodes across the subject and attended frequencies at different viewing distances.** EEG TWL is 2s and the number of SSVEP harmonics is 1 in this figure. The classification method is CCA.

5.4 Optimal electrode sets

This section is focused on the analysis of the optimal electrode subsets. The optimal electrode subsets of the subject are the electrode subsets which result in the highest classification accuracy in one experiment condition. The optimal electrode subsets with the least electrode number are termed as the minimal optimal electrode subsets. The optimal electrode subsets of the same subject could be experiment-condition and classification method dependent. In this section, the distribution of the optimal electrode subsets over the number of the electrodes is investigated first.

5.4.1 Distribution of optimal electrode subsets

To get the optimal electrode subset distribution, the highest classification accuracy of one subject in one experiment condition is found. For each number of the electrodes (1 to 11), the number of optimal electrode subsets corresponding to one electrode number will be counted and transferred to percentage by dividing the total electrode subsets of the corresponding electrode number n which is equal

to C_n^{11}.

Table 5.2 represents the optimal electrode subsets distribution of 10 subjects over the number of the electrodes and the highest classification rate of each subject across the attended frequencies and the viewing distances. For each subject, the optimal electrode subset distribution of one experiment condition is found. For one subject, there are 16 experiment conditions. Table 5.2 shows the average of 16 experiment conditions for each subject. The columns from 2 to 12 in Table 5.2 represent the ratio between the number of the optimal electrode subsets which result in the highest classification rate and the total electrode subsets of the corresponding electrode number. The column of Highest is the highest classification accuracy in the experiment condition. Table 5.2 is based on CCA with 1^{st} harmonic of SSVEP. EEG TWL is 2s.

Table 5.2: **Optimal electrode subsets distribution over the number of the electrodes and the highest classification rate of each subject across the attended frequencies and the viewing distances. This table is based on CCA.** The percentage (%) in column 2 to 12 represents the ratio between the number of the optimal electrode subsets which result in the highest classification rate and the total electrode subsets of the corresponding electrode number. The column of column head Highest is the highest classification accuracy in the experiment condition. The number of SSVEP harmonics is 1 and EEG TWL is 2s.

ele #	1	2	3	4	5	6	7	8	9	10	11	Highest
S1	7.95%	15.11%	25.95%	41.08%	55.07%	65.38%	71.57%	74.85%	75.57%	75.57%	75.00%	99.38%
S2	0.57%	4.09%	10.45%	19.96%	29.71%	39.88%	50.36%	60.68%	70.57%	79.55%	87.50%	96.88%
S3	10.80%	17.39%	31.02%	46.36%	59.88%	70.71%	78.41%	83.03%	86.25%	88.64%	93.75%	100.00%
S4	10.80%	10.11%	13.83%	19.17%	25.12%	32.49%	40.23%	47.69%	52.73%	57.39%	50.00%	97.19%
S5	1.70%	0.00%	0.27%	0.70%	2.35%	4.96%	8.84%	13.11%	17.39%	22.16%	25.00%	82.50%
S6	2.27%	5.00%	8.83%	13.75%	18.30%	22.56%	26.74%	29.81%	32.16%	34.09%	37.50%	95.63%
S7	0.00%	0.00%	0.27%	0.21%	0.46%	1.06%	1.89%	3.26%	4.09%	5.11%	6.25%	74.38%
S8	0.00%	0.11%	0.34%	1.46%	3.44%	7.13%	11.63%	17.01%	22.73%	28.98%	37.50%	82.50%
S9	0.57%	4.55%	7.05%	10.11%	13.88%	17.09%	19.70%	22.69%	26.36%	32.39%	37.50%	96.56%
S10	3.41%	0.11%	0.57%	0.70%	0.32%	0.20%	0.19%	0.34%	0.91%	1.70%	6.25%	57.19%

Table 5.2 shows that with carefully chosen electrodes, the classification accuracies could be very high. For example, the mean highest accuracies across 16 experiment conditions for subject 3 is 100%. This indicates that for subject 3, in any experiment condition, there is at least one electrode subset results in 100% classification accuracy. Apart from S3, the mean highest accuracies of the subjects 1, 2, 4, 6 and 9 are over 95%. The lowest one is under 60% from S10.

For most of the subjects, the number of optimal electrode subsets could be any number from 1 to 11. Only S5, S7 and S8 do not have optimal electrode subsets in electrode numbers 1 and 2. It is also clearly seen that the ratios between the optimal electrode subsets and the total electrode subsets of the corresponding electrode number increases as the electrode number increases except electrode number 11 and S4, S10. It is monotonically increasing against the electrode number. This might be explained by the followings. First, as the electrode number

increases, it is more likely to include the minimal optimal electrode subset. As long as the extra-added electrodes do not provide irrelevant information, the electrode subsets are very likely to remain the same performance. Moreover, the total number of the electrode subsets become smaller when the electrode number ≥ 7. When the electrode number become 11 which has only one electrode subset, it either results in the same or worse performance. For subject 10, the distribution is not monotonically increasing. It might result from the overall poor performance. The classification accuracies of S10 might be the result of the chance.

Furthermore, for S1, S2, S3, S4, S6 and S9 whose mean highest accuracies are over 95%, their optimal electrode distributions over the number of the electrodes are significantly higher than S5, S7, S8 and S10. The optimal electrode distributions of S5 and S8 whose mean highest accuracies are over 80% are higher than S7 and S10. This might be also explained by the overall poor performance for those subjects with low classification accuracies.

5.4.2 Number of minimal optimal electrode subsets

This section investigates what is the minimal electrode number required in order to result in the highest accuracies for each subject. Figure 5.13 shows the electrode number of minimal optimal electrode subsets of each subject. Each subplot presents one viewing distance. One dot shape presents one attended frequency. The blue bar presents the mean electrode number of 4 attended frequencies at the same viewing distance. Figure 5.13 is based on CCA with 1^{st} harmonic of SSVEP and 2s of EEG TWL.

Figure 5.13 shows that the electrode number of the minimal optimal electrode subset is dependent on the subject and the experiment condition. The range of the electrode number of the minimal optimal electrode subsets across the subjects and the experiment condition is between 1 and 8. The majority is ≤ 4. There is no particular pattern for the electrode number distribution. However, for most of the subjects, the mean values of the different viewing distance are consistent. All of the mean values are less than 6.

5.4.3 Demographics of minimal optimal electrode subsets

This section investigates the demographics of the minimal optimal electrode subsets. It attempt to find which electrodes are in such electrode subset and the subject variance in terms of optimal electrodes. In this section, only the electrodes of the minimal optimal electrode subsets are investigated but not the optimal electrode subsets. As mentioned earlier that the electrodes in the optimal electrode subsets might not be the optimal. The optimal electrode subsets might be optimal because they contain enough electrodes which can result in the highest accuracies. To prevent the bias, only the minimal optimal electrode subsets are inspected.

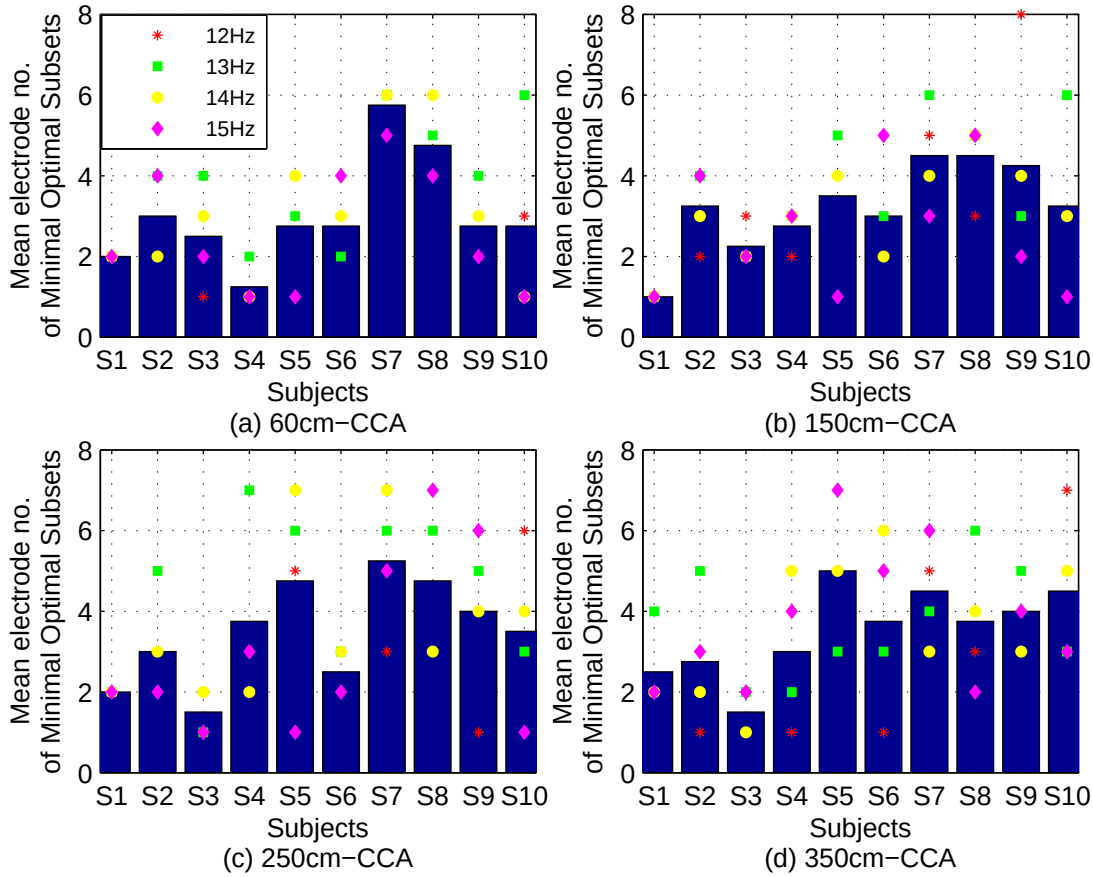

Figure 5.13: **Mean electrode number of the minimal optimal electrode subsets for the subjects at different viewing distances.** The blue bar presents the mean electrode number of the minimal optimal electrode subsets for each subject across the attended frequencies. The dot presents the electrode number of one attended frequency at one viewing distance. This figure is based CCA. EEG TWL is 2s and the number of SSVEP harmonics is 1.

Table 5.3 shows the demographics of the minimal optimal electrodes of the subject across the attended frequencies and the viewing distances. The numbers of this table stand for how many times the corresponding electrodes are in the minimal optimal electrode subset for the corresponding subjects across the attended frequencies and viewing distances. It is obvious to conclude that the electrode Oz is the electrode which is the most common electrode included in the minimal optimal electrode subsets for all subjects. The electrodes O2 and O1 are the next. The higher numbers of the three electrodes indicate that they can work with the many other electrodes to achieve the accuracies. The least common electrode is O10 which is far from Oz.

The same analysis is applied to the classification results based on MEC and MCC. The optimal electrode subsets distributions for MEC and MCC can be found in Tables C-3 and C-4. The optimal electrode subsets distributions of MEC and MCC are similar to the one of CCA. For example, S5, S7 and S8 have no optimal

Table 5.3: **The demographics of the minimal optimal electrodes of the subject across the attended frequencies and the viewing distances. This table is based on CCA with the 1^{st} harmonic of SSVEP and 2s of EEG TWL.** The number shown in the table represents the number of the corresponding electrodes being one of the electrodes in the minimal optimal electrode subset for the corresponding subject across the attended frequencies and viewing distances.

ele	POz	Oz	Iz	124	125	O1	127	128	O9	O10	O2
S1	3	35	18	18	11	26	21	14	20	21	13
S2	10	53	5	18	19	37	25	9	7	5	37
S3	8	56	7	15	10	15	14	14	12	14	17
S4	10	35	13	12	7	8	10	10	10	8	26
S5	8	27	12	8	16	23	26	25	10	3	12
S6	14	48	14	9	14	11	6	10	8	9	15
S7	24	26	5	31	17	11	7	12	8	4	13
S8	15	22	6	15	5	14	5	12	11	4	18
S9	7	13	22	13	23	14	16	19	40	26	15
S10	10	12	12	6	5	13	11	10	9	11	7
Grand Total	109	**327**	114	145	127	**172**	141	135	135	105	**173**

electrode subsets with electrode number 1. Except S4 and S10, the distribution is monotonically increasing against the electrode number without taking electrode number 11 into account. Figures B-56 and B-57 in Appendix B show the electrode number of minimal optimal electrode subsets of each subject across the attended frequencies and viewing distances. Again, they are very similar to the ones of CCA. For example, the ranges of the electrode numbers of the minimal optimal electrode subsets are between 1 and 8. The mean electrode numbers are ≤ 6. Finally, the demographics of the minimal optimal electrode subsets are listed in Tables C-5 and C-6 in Appendix C. Electrode Oz is also the most common electrode found in the minimal optimal electrode subsets, followed by O1 or O2. O10 is the least common electrode found in the minimal optimal electrode subsets.

5.5 Electrode rankings

In section 5.4, it is found that it does not need all the electrode signals to achieve the highest accuracies. In this study, 11 electrodes over the occipital area were pre-selected as EEG acquisition channels. This section proposes an electrode selection algorithm which chooses the electrodes from 11 pre-selected electrodes according to their importance and evaluates the performance of the selected electrodes.

In this proposed electrode ranking method, 11 pre–selected electrodes are ranked according the coefficients of the spatial filters and the classification accuracies. In coefficients of the spatial filters method, the coefficients of the spatial filters are obtained when the signals of 11 electrodes employed for classification. In the classification accuracies method, the classification accuracy of each electrode corresponds to the accuracy resulting from its own. The rankings of the elec-

trodes stand for their relative importance which is measured by the values of the corresponding coefficients or accuracies. After the electrodes are ranked, the electrode with the highest ranking is selected first, followed by the next highest ranked electrode until the lowest ranking of the electrodes is selected. Depending on the number of the electrodes required, this ranking is flexible and suitable for any electrode number. In other words, if the desired electrode number is N_y, $1 \leq N_y \leq 11$, the electrodes of the first N_y rankings are selected to form the electrode set.

The electrode set formed by the electrodes selected by the electrode ranking is termed as the ranked electrode subset. The efficiency of the ranked electrode subset is evaluated by the comparison to the highest, average and lowest accuracies of the electrode subsets of the same electrode numbers N_y varying from 1 to 11. To get an objective view on its performance, a performance index (PI) is introduced. Each electrode number has one corresponding PI. For electrode number N_y, PI is the performance index of the corresponding ranked electrode set in the electrode subsets with N_y electrodes. PI is defined by equation (3.20) and with value between 0 and 1. The higher PI is, the better the ranked electrode set is.

The electrodes are ranked and evaluated by the rule of leave–one–out. In other words, the electrodes are ranked by the data of 9 subjects. The resultant ranking is evaluated by the subject who is excluded from the ranking process. As a result, there will be 10 electrodes rankings.

5.5.1 Ranked by spatial filter coefficients

To use the coefficient of the spatial filters to rank the electrodes, the mean coefficients across the subjects and across the experiment conditions are found. The coefficients of the spatial filters of subjects are either positive or negative. To prevent the cancelling out effect between the subjects, the absolute values of the coefficients are used. For example, one electrode has strongly negative impact on one subject but has the reverse impact on the other subject. If adding these two together directly, the impact of this electrode is cancelled out. The mean coefficients across the subjects and the experiment conditions are divided by the largest coefficient. The final mean coefficients are between 0 and 1 through this division. The electrode with the largest coefficient is ranked the first. The electrode with the second largest coefficient is ranked the second until the electrode with the lowest coefficient is ranked the last (11^{th}).

Figure 5.14 represents the topographies of the mean spatial filter coefficients of 11 electrodes. This figure is based on CCA with the 1^{st} harmonic of SSVEP and EEG TWL 2s. The subplots of (a) to (d) present the mean spatial coefficients of 11 electrode across the subjects and the attended frequencies at different viewing distances. The subplot of (e) is the grand average of (a) to (d). The coefficients of each subject are the coefficients obtained by the rule of leave–one–out.

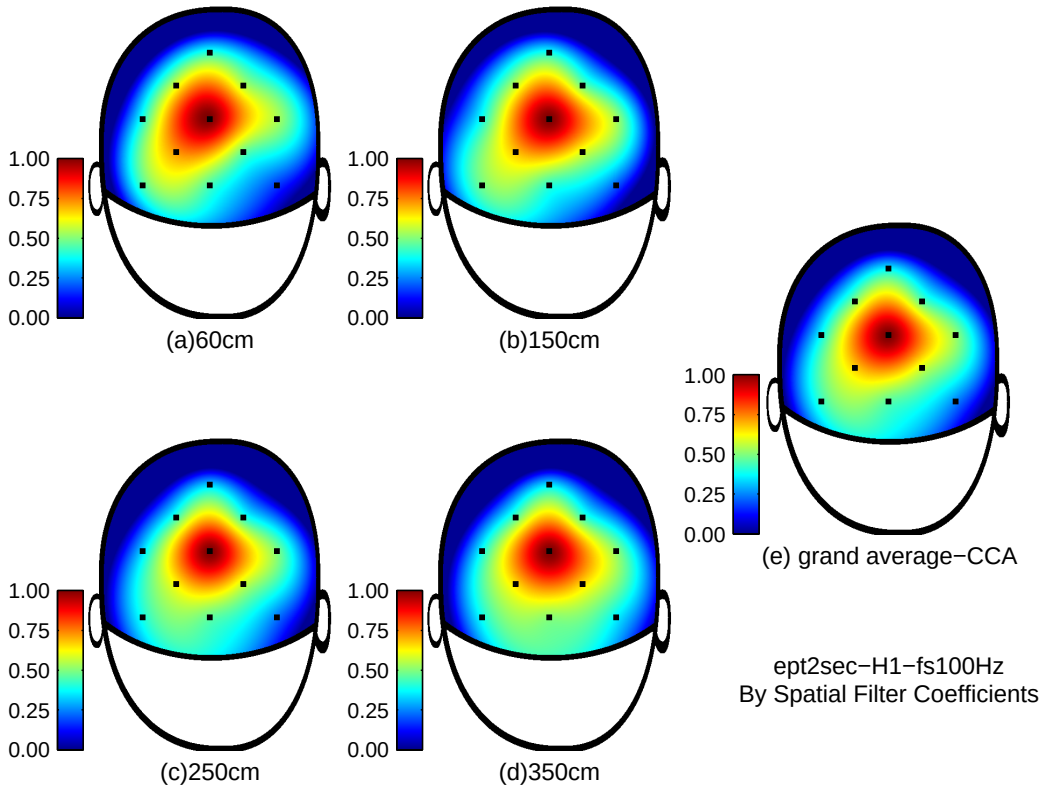

Figure 5.14: **Topographies of mean CCA spatial filter coefficients of the electrodes across the subjects and attended frequencies at different viewing distances.** The spatial filter is obtained using the electrode subsets consisting of 11 electrodes in classification. The classification method of this figure is CCA.

Subplots of (a) to (d) are very similar. The centre of 11 pre–selected electrodes is roughly located in the position of the electrode Oz. The electrode Oz has the highest coefficient. The electrodes surrounding Oz also have higher coefficients, for example, O1, O2, 124, 125, 127 and 128. On the other hand, the coefficients of the electrodes distant from Oz are smaller, for example O10. Compared to Table C-6 which shows the demographics of the minimal optimal electrode sets. They agree to each other. That is, the electrodes with higher spatial coefficients are also more likely found in the minimal optimal electrode sets.

Table 5.4 lists the electrode ranking for each subject by using the rule of leave–one–out across the attended frequencies and the viewing distances. Although the data to construct the rankings are different for each subject, the rankings are very similar as seen from Table 5.4. At least 4 out of 11 electrodes have the same order. They are the first three electrodes, Oz–127–128 and the last one is O10.

Next, the electrode rankings are cross–validated to evaluate its efficiency. The process is as following. For each subject, the electrode rankings are evaluated by

Table 5.4: **Electrode Rankings for each subject by using the rule of leave-one-out across the attended frequencies and the viewing distances. These electrode rankings are based on CCA spatial filter coefficients.** The electrode rankings have at least four electrodes in the same order, Oz, 127 and 128 are the top three rankings and O10 is the last ranking.

ele ranking	1	2	3	4	5	6	7	8	9	10	11
S1	Oz	127	128	O2	124	Iz	125	O9	O1	POz	O10
S2	Oz	127	128	124	O2	Iz	O9	125	O1	POz	O10
S3	Oz	127	128	O2	124	125	Iz	O9	O1	POz	O10
S4	Oz	127	128	O2	124	125	Iz	O9	O1	POz	O10
S5	Oz	127	128	O2	124	Iz	O9	125	O1	POz	O10
S6	Oz	127	128	124	O2	Iz	125	O9	O1	POz	O10
S7	Oz	127	128	124	125	O2	Iz	O1	O9	POz	O10
S8	Oz	127	128	O2	124	Iz	125	O9	O1	POz	O10
S9	Oz	127	128	O2	124	O9	Iz	125	POz	O1	O10
S10	Oz	127	128	124	Iz	125	O2	O9	O1	POz	O10

11 electrode numbers, from 1 to 11. For each electrode number, the classification accuracy of the ranked electrode set and the highest, average and lowest accuracies corresponding to that electrode number in different experiment conditions are found. PI corresponding to that electrode number is calculated. Table 5.5 is the mean results across the subjects and the experiment conditions.

Table 5.5 clearly demonstrates the followings. First of all, the accuracies of ranked electrode sets are monotonically increasing against the electrode number. By using the electrode rankings, increasing the electrode also increase the accuracies. Moreover, the ranked accuracies are much higher than the corresponding lowest accuracies. Except the electrode number 9, the ranked accuracies are also higher than the corresponding average accuracies. However, none of the ranked accuracies are equal to the corresponding highest accuracies. Furthermore, PI indicates that the ranked electrode sets has over 65% to 85% possibility to outperform or have the same performance as the electrode sets of the same electrode number. These all demonstrate that the electrode ranked by the spatial coefficient can be used to select the electrodes.

PIs of Table 5.5 only show an overall view on the performance across the subjects. To further examine the feasibility of the electrode rankings to individual subject, PIs of Table 5.5 are investigated. Table 5.6 lists PIs of the subjects corresponding to the electrode numbers. From this table, it is clearly seen that most of PIs are over 50%. Only 7 out of 110 PIs are lower than 50%. In other words, the ranked electrode sets have more than 50% of the possibility to perform the same or better than the randomly selected. PIs which are over 50% can be observed in any electrode numbers. It not only is seen in the electrodes numbers which have fewer electrode subsets, for example, 1, 2, 9 and 10, but also in the electrode numbers which have more electrode subsets, for example, 4, 5, 6 and 7. This shows that the electrode ranking can be used to select the electrode for the new

Table 5.5: **Electrode rankings evaluation results across the subjects and experiment conditions. The electrode rankings are evaluated by comparing the ranked accuracies resulting from the ranked electrode sets and the corresponding highest, average and lowest accuracies of the same electrode number. PIs are listed in the last row of the table. This table is based on CCA.**

ele #	1	2	3	4	5	6	7	8	9	10	11
Ranking accuracies	57.86%	60.46%	62.93%	68.65%	72.78%	76.72%	76.97%	77.37%	77.40%	79.63%	79.91%
Highest	64.21%	78.53%	84.28%	85.59%	86.63%	87.00%	86.63%	86.16%	84.84%	82.84%	79.91%
Average	51.13%	55.09%	59.68%	64.25%	68.19%	71.46%	74.01%	75.97%	77.52%	78.76%	79.91%
Lowest	34.73%	30.48%	31.77%	34.64%	37.52%	42.62%	49.62%	57.03%	64.96%	71.56%	79.91%
PI	84.49%	69.56%	66.98%	71.87%	76.45%	82.67%	80.61%	78.51%	73.85%	85.06%	100.00%

user of a SSVEP based BCI.

Table 5.6: **PIs of individual subject corresponding to one electrode number when using the leave–one–out electrode rankings. The classification data of this table are based on CCA.** This table expands PIs of Table 5.5 from the mean values to the details of each subject.

ele #	1	2	3	4	5	6	7	8	9	10	11
S1	94.32%	78.75%	89.39%	89.89%	70.08%	81.40%	93.48%	91.89%	92.16%	94.32%	100.00%
S2	88.07%	88.07%	74.28%	87.73%	96.31%	92.11%	87.97%	91.36%	88.30%	95.45%	100.00%
S3	97.73%	97.73%	90.98%	91.78%	99.85%	95.16%	99.51%	87.16%	88.64%	92.05%	100.00%
S4	95.45%	62.95%	81.97%	91.97%	93.97%	94.59%	90.27%	84.24%	75.91%	88.07%	100.00%
S5	80.11%	51.36%	**40.91%**	68.41%	78.61%	83.79%	83.43%	81.48%	84.77%	86.36%	100.00%
S6	98.30%	86.82%	89.32%	86.21%	89.33%	90.83%	80.04%	78.90%	77.39%	83.52%	100.00%
S7	65.91%	**46.59%**	55.19%	78.20%	71.65%	66.48%	64.79%	62.80%	54.20%	80.68%	100.00%
S8	73.86%	76.93%	60.53%	59.72%	90.73%	91.40%	70.97%	72.05%	67.73%	83.52%	100.00%
S9	75.57%	**31.36%**	**27.20%**	**16.23%**	**8.35%**	65.48%	71.10%	76.25%	64.43%	72.73%	100.00%
S10	75.57%	75.00%	60.08%	48.60%	65.64%	65.52%	64.56%	58.94%	**45.00%**	73.86%	100.00%

The electrode rankings derived above are based on 16 experiment conditions which take more than one hour for one subject. In reality, this process needs to be speeded up. The effectiveness of the electrode ranking derived by one experiment condition is evaluated. The process to develop the electrode ranking is the same as described earlier, except that only one experiment condition is considered at one time. The data used to validate the rankings is the same condition of the excluding subject. The mean PIs of each experiment condition are used to evaluate the effectiveness. As a result, there are 16 mean PIs across the subjects over the electrode numbers.

Figure 5.15 illustrates PIs across the subjects at each experiment condition. This Figure is based on CCA classification method. This figure also confirms the usability of the electrode rankings. Only one out of 176 average PIs is lower than 50% (13Hz, 350cm). Quite a few PIs are over 75%.

Electrode rankings are also derived from the classification results using classification methods MEC and MCC. The topographies of the mean spatial filter

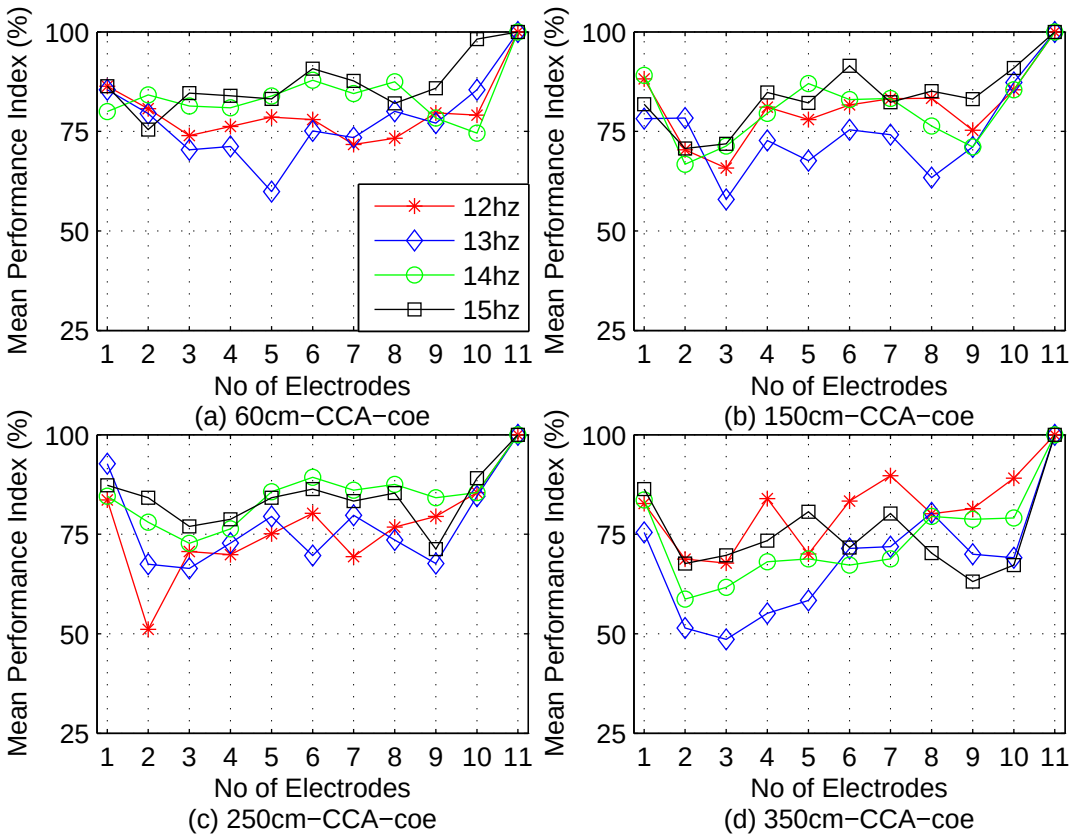

Figure 5.15: **PIs across the subjects for each experiment condition. PIs of this figure are the evaluation metrics of the electrode rankings based on the CCA spatial filter coefficients.** It shows that except one PI is lower than 50%, all PIs are over 50%. It demonstrates the usability of the electrode rankings in selection of the electrodes and the efficiency of the ranked electrode sets.

coefficients of 11 electrodes for MEC and MCC can be found in Figure B-58 and B-59 in Appendix B respectively. The parameters of harmonics and EEG TWL are the same as those of Figure 5.14. Unlike previous analysis, the results of the same analysis of three methods are very similar. The topographies patterns of MEC and MCC are more diversified than CCA, especially MEC. The highest values of the topographies of MEC spatial filter does not always locate in the centre of all electrodes which is Oz. For example, electrodes 127 and 128 at some viewing distances. As a result, the importance of the electrodes in three methods is different. For example, in CCA, the coefficient of the electrode Oz is significantly higher than the others. This is not the case in MEC. It is also different in MCC whose most important electrodes are Oz and O2.

Using MEC and MCC spatial filter coefficients to rank the electrodes, the corresponding leave–one–out electrode rankings are listed in Tables C-7 and C-8. As expected, the corresponding electrode rankings of each subject are also more diversified than CCA. For example, 127 and 128 share the first two top rankings and POz and O10 share the last two using MEC spatial filter coefficients. The electrode ranking using MCC has the Oz as the top ranked electrode which is the

same as CCA. O2 is at the second ranking. The last two ranking positions are mainly shared by O10 and O1. Overall speaking, the electrode rankings using the same spatial filter coefficients for each subject are different but very similar as seen in both MEC and MCC.

The electrode rankings are cross-validated by the highest, average and lowest accuracies of the corresponding electrode number. PIs are also calculated. The results are listed in Tables C-9 and C-10. The raked accuracies are monotonically increasing against the electrode number, same as CCA. The ranked accuracies are much higher than the lowest ones. Majority of them are also higher than the averages. None of PIs in MEC or MCC are lower than 50% which indicates that the ranked electrode has higher opportunity to perform better than the randomly chosen electrode sets.

PIs of the individual subject of Tables C-9 and C-10 are further explored. The results are listed in Tables C-11 and C-12. There are more PIs in MEC and MCC which are lower than 50% than in CCA. See the bold number in both tables. The robustness of the electrode rankings is also examined by using the classification data of one experiment condition. Figures B-60 and B-61 in Appendix B are the PIs across the subjects at each experiment condition. They are based on the classification data of MEC and MCC classification methods. There are more PIs from MEC which are lower than 50%. However, the majority of PIs exceed 50%.

In section 5.5.2, the electrodes will be ranked by the classification accuracy resulting from the corresponding electrode. In this section, the electrodes are ranked by the coefficients of the spatial filter when the 11 electrodes are employed in the classification. The coefficients of the spatial filter are the outcomes of a complete interaction/dependence between all electrodes. The rankings of section 5.5.2 are the results of complete independence between the electrodes. The computations of the coefficients of the spatial filter and the single electrode classification are the lowest compared to the other electrode numbers. It only requires 20 classifications and 220 classifications respectively in one experiment condition.

5.5.2 Ranked by single electrode classification accuracy

In this section, all the procedures for ranking the electrodes are the same as section 5.5.1. The only difference is that this section ranks the electrodes according to classification accuracy of the corresponding electrode not the coefficient of the spatial filter. Therefore, the first thing to know is the single electrode classification accuracy.

Figure 5.16 shows topographies of mean classification accuracies of the corresponding electrodes across the subjects and attended frequencies at different viewing distances. As the classification accuracies between the electrodes are close, therefore the range of the colour-map is roughly between the lowest to highest, instead of 0 to 1 to improve the reading of the topographies. (Other-

wise, the colours of all electrodes are almost the same.) Also, the single electrode accuracies are the same for three different classification methods. Therefore, the electrode rankings by using single electrode accuracies are the same for three methods. In this section, for MEC and MCC, only the evaluation of the electrode rankings and PIs will be presented.

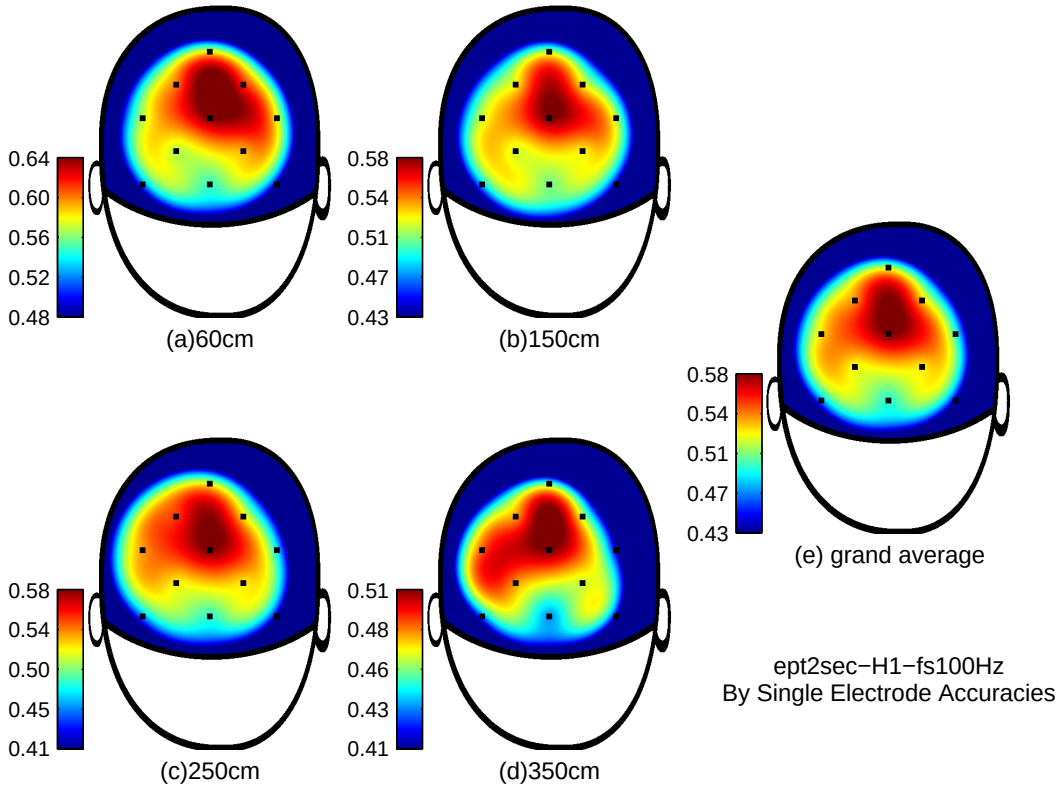

Figure 5.16: **Topographies of mean classification accuracies of the corresponding electrodes across the subjects and attended frequencies at different viewing distances.** The classification accuracy of each electrode is the accuracy results from the corresponding electrode. The classification method of this figure is CCA. In fact, the singles electrode accuracy is the same regardless of the classification method employed. Also, as the accuracies between the electrodes are close, in order to provide a better visualization between the electrodes, the scales of the colour-maps differ. The larger scales of the colour-map will result in the colour un-discriminated between the electrodes. The upper and lower limitation of the colour-map are roughly equal to the lowest and highest single electrode accuracy.

Figure 5.16 shows that the highest single electrode accuracy occurs from the electrode around Oz, or Oz itself. The electrodes surrounding Oz are also exhibiting higher accuracies than the electrode which are distant from Oz, for example O10. Overall speaking, the difference between the electrodes is not significant. The range of the mean accuracies of the electrodes is between 40%-60% .
The efficacy of electrode rankings listed in Table 5.7 is evaluated by comparing the ranking accuracies resulting from the ranked electrode sets and the corresponding

Table 5.7: **Electrode Rankings for each subject by classification accuracies using the rule of leave–one–out across the attended frequencies and the viewing distances.** These electrode rankings are based on single electrode classification accuracy. Electrode Oz is at the first ranking position while O10 is at last for all subjects.

ele ranking	1	2	3	4	5	6	7	8	9	10	11
S1	Oz	124	128	125	127	O1	POz	Iz	O2	O9	O10
S2	Oz	124	O1	128	127	125	POz	Iz	O2	O9	O10
S3	Oz	124	O1	127	128	125	POz	Iz	O2	O9	O10
S4	Oz	125	124	POz	128	O1	127	O2	Iz	O9	O10
S5	Oz	124	125	O1	128	127	POz	O2	Iz	O9	O10
S6	Oz	124	128	O1	125	127	POz	Iz	O2	O9	O10
S7	Oz	124	128	125	O1	127	POz	Iz	O2	O9	O10
S8	Oz	124	O1	125	128	127	POz	Iz	O2	O9	O10
S9	Oz	124	125	128	O1	127	Iz	O9	POz	O2	O10
S10	Oz	124	O1	125	128	127	POz	O2	Iz	O9	O10

highest, average and lowest accuracies. Table 5.8 presents the ranking, highest, average and lowest accuracies and PIs corresponding to the electrode numbers and classification methods. This table also gives an overview on the performance of the classification methods. The number of SSVEP harmonics and EEG TWL used in the analysis of Table 5.8 is 1 and 2s respectively.

The difference of mean highest accuracies across the electrode numbers corresponding to each classification is less than 1%. So are the average and lowest accuracies. This indicates that the performance of three classification methods is almost the same. The mean ranking accuracies across the electrode numbers resulting from the ranked electrode sets are 72%, 70% and 72% for CCA, MEC and MCC respectively. These values are also very close. The corresponding mean PIs are 79%, 73% and 79%. CCA and MCC are slightly better than MEC in the mean ranking accuracies and mean PIs. The lowest PIs occur at the electrode numbers 2 and 3 for three classification methods. For electrode number 5 and 6, PIs of CCA and MCC are also higher than MEC. There are more electrode subsets in these two electrode numbers than the others. The ranking accuracies of three classification methods show the properties of monotonically increasing against the electrode numbers.

PIs of CCA in Table 5.8 are explored for each subject and shown in Table 5.9. Only 8 out of 110 PIs are lower than 50%. The mean PI across the electrode numbers of S3 is highest, which is over 90%. The one of S9 is the lowest which is lower than 60% but exceeds 50%. Only S7, S9 and S10 have mean PIs across the electrode numbers which are lower than 75%. PIs of Table 5.9 shows that electrode rankings by the single electrode accuracy can be used to select the electrodes for each subject.

The same analysis of PIs for each subject is performed on MEC and MCC. The

Table 5.8: **Electrode rankings evaluation results across the subjects and experiment conditions. The electrode rankings are evaluated by comparing the ranking accuracies resulting from the ranked electrode sets and the corresponding highest, average and lowest accuracies of the same electrode number. PIs are also listed.** This table includes the evaluation of three classification methods.

ele #	1	2	3	4	5	6	7	8	9	10	11
CCA Ranking accuracies	57.86%	60.65%	63.31%	68.71%	72.90%	76.53%	76.90%	77.28%	77.47%	79.63%	79.91%
Highest	64.21%	78.53%	84.28%	85.59%	86.63%	87.00%	86.63%	86.16%	84.84%	82.84%	79.91%
Average	51.13%	55.09%	59.68%	64.25%	68.19%	71.46%	74.01%	75.97%	77.52%	78.76%	79.91%
Lowest	34.73%	30.48%	31.77%	34.64%	37.52%	42.62%	49.62%	57.03%	64.96%	71.56%	79.91%
PI	84.49%	69.36%	67.89%	71.72%	77.21%	81.62%	80.04%	77.75%	74.59%	85.06%	100.00%
MEC Ranking accuracies	52.58%	52.93%	57.78%	68.34%	70.56%	73.56%	76.22%	78.15%	77.72%	78.53%	79.75%
Highest	64.28%	78.78%	84.28%	85.97%	86.69%	87.06%	86.78%	86.06%	85.16%	83.25%	79.75%
Average	51.15%	54.84%	59.56%	64.24%	68.28%	71.63%	74.23%	76.17%	77.57%	78.67%	79.75%
Lowest	34.67%	28.02%	30.02%	33.08%	37.05%	42.74%	49.90%	58.00%	65.12%	71.75%	79.75%
PI	68.52%	54.31%	56.39%	70.68%	69.67%	70.68%	75.57%	80.38%	75.86%	79.26%	100.00%
MCC Ranking accuracies	57.89%	60.56%	63.28%	68.62%	72.81%	76.59%	77.06%	77.25%	77.40%	79.59%	79.78%
Highest	64.21%	78.53%	84.25%	85.63%	86.56%	86.97%	86.59%	86.22%	84.94%	82.75%	79.78%
Average	51.14%	55.09%	59.67%	64.24%	68.18%	71.45%	74.01%	75.97%	77.51%	78.73%	79.78%
Lowest	34.73%	30.48%	31.96%	34.61%	37.36%	42.68%	49.59%	57.06%	64.93%	71.50%	79.78%
PI	84.20%	69.16%	67.63%	71.71%	76.04%	81.63%	80.31%	77.66%	74.24%	85.17%	100.00%

results of PIs can be found in Tables C-13 and C-14. There were 13 and 7 out of 110 PIs which are lower than 50% in MEC and MCC respectively. 5 and 3 of 10 subjects have the mean PIs across the electrode numbers lower than 75% in MEC and MCC respectively. One subject has mean PI lower than 50% in MEC. There is no subject with mean PIs over 90% in MEC.

Table 5.9: **PIs of individual subject corresponding to one electrode number using the leave–one–out electrode rankings of Table 5.7. This table shows detail PIs of CCA in Table 5.8 from the mean values to the values of each subject.**

ele #	1	2	3	4	5	6	7	8	9	10	11
S1	94.32%	77.27%	87.88%	86.67%	74.72%	81.40%	93.48%	91.89%	92.16%	94.32%	100.00%
S2	88.07%	88.07%	76.52%	87.73%	96.31%	92.11%	87.97%	91.36%	88.30%	95.45%	100.00%
S3	97.73%	97.73%	90.98%	91.78%	99.85%	95.16%	99.51%	87.16%	88.64%	92.05%	100.00%
S4	95.45%	62.95%	81.97%	91.97%	92.15%	92.55%	87.95%	84.24%	78.75%	88.07%	100.00%
S5	80.11%	**48.18%**	**42.27%**	69.89%	78.61%	80.33%	80.19%	76.55%	84.77%	86.36%	100.00%
S6	98.30%	85.57%	89.32%	84.02%	90.98%	90.83%	84.02%	78.90%	77.39%	83.52%	100.00%
S7	65.91%	50.68%	59.05%	78.09%	71.97%	66.02%	67.50%	63.11%	58.18%	80.68%	100.00%
S8	73.86%	77.84%	62.50%	62.23%	90.73%	91.40%	72.65%	74.73%	71.36%	83.52%	100.00%
S9	75.57%	**30.34%**	**25.68%**	**16.23%**	**8.54%**	59.74%	65.47%	70.57%	61.36%	72.73%	100.00%
S10	75.57%	75.00%	62.73%	**48.60%**	68.22%	66.71%	61.67%	58.94%	**45.00%**	73.86%	100.00%

Finally, the efficacy of the electrode rankings derived by using less classification data is assessed by the corresponding PIs. The electrode rankings are obtained by using the classification data from one experiment condition instead of 16 across the subjects by the rule of leave-out-out. Each subject has 16 electrode rankings corresponding to 16 experiment conditions. Each electrode ranking will be

assessed by comparison the ranking accuracies and the accuracies resulting from the electrode sets with the same electrode number. The corresponding PI is calculated according to the comparison result. The mean PIs across the subjects for each experiment condition are illustrated in Figures 5.17, B-62 and B-63.

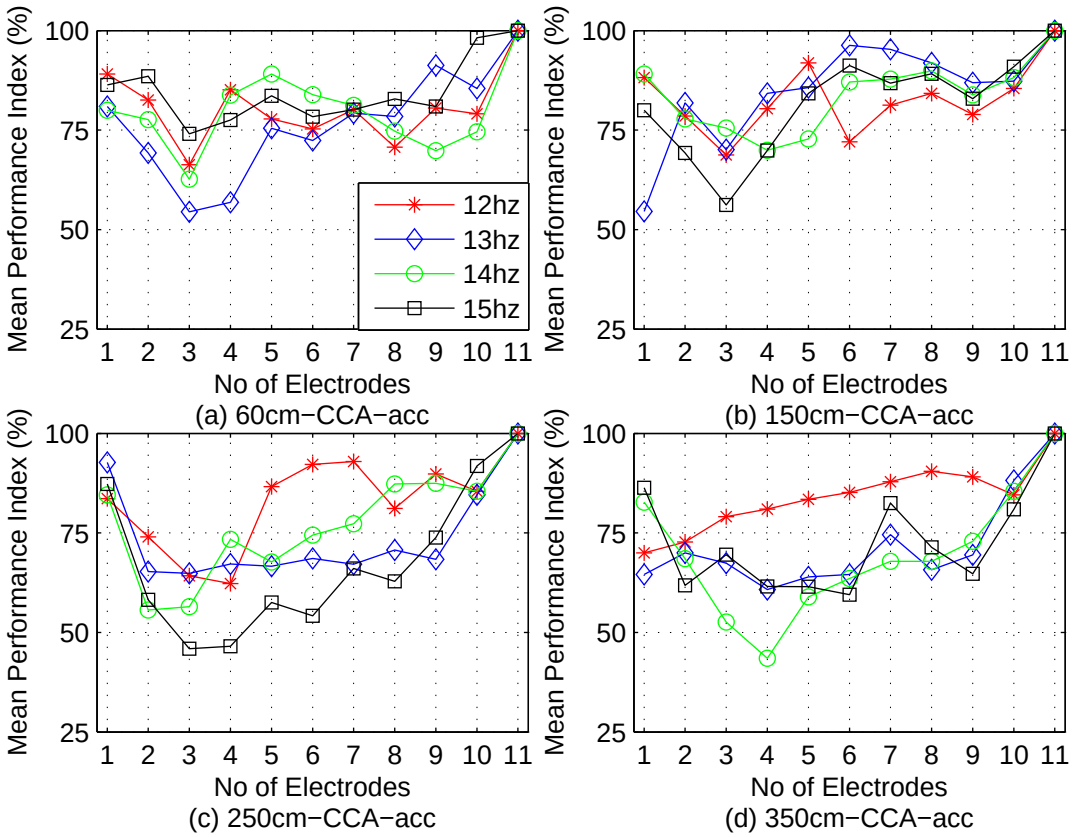

Figure 5.17: **Mean PIs across the subjects for each experiment condition based on CCA. PIs of this figure are used as the evaluation metrics of the electrode rankings based on the single electrode classification accuracy.** It shows that three PIs are lower than 50%, the rest of PIs exceed 50%. It demonstrates the usability of the electrode rankings in selection of the electrodes and the efficiency of the ranked electrode sets.

There are 3 to 4 PIs in each classification method lower than 50%. The electrode numbers are 3 or 4. Compared to the same results of the mean PIs using spatial filter coefficients, the mean PIs of MEC significantly better than the ones using spatial filter coefficients, see Figure B-60 which has more than 10 PIs below 50%. For CCA and MCC, the difference is not significant. However, the majority of PIs exceed 50%. For viewing distances, the mean PIs of the viewing distance 60 cm and 150cm are higher than the other viewing distances. The majority of PIs at 60cm and 150cm are over 75%. Overall speaking, the mean PIs of the electrode number 3 or 4 are the lowest corresponding to the viewing distances. Only 10 out of 528 PIs (across three methods) are lower than 50%. The inter-subject variance is not great as the mean standard deviation across the electrode numbers is around 15% for three methods which is slightly better than the results by the

spatial filter coefficients (between 15% to 17%). PIs demonstrate the electrode ranking works for the individual subject and the efficacy of the ranked electrode sets which have better chance to result in higher accuracies than the randomly selected electrode sets.

So far, there is no threshold applied to the classification. i.e. a classification result is reached without considering if the response is significant enough. In CCA for example, the frequency corresponding to the largest canonical correlation coefficient is regarded as the attended target. In real BCI operation, the threshold is implemented mainly to prevent the false positive, especially for asynchronous BCI which is the nature of SSVEP based BCI. In asynchronous BCI, the user might leave the system in idle state for a long time while BCI keeps producing classification outcomes. The applied threshold will limit the outcomes and reduce the false positives. In this study, there are no idle state recordings in the experiment. The investigation of the threshold in section 5.6 is focused the how threshold can affect the classification results, i.e. true and false positives when BCI is not in the idle state. Next, the impact of threshold on the true and false positive is investigated.

5.6 Threshold analysis

In this section, the thresholds are applied to the classification and the impact of the thresholds over the classification performance is investigated. The threshold analysis also attempts to find the optimised thresholds for each attended frequency so that the overall accuracies are maximised or optimise the metrics of classification measurements, such as F measurement.

5.6.1 Impact of the thresholds on the classification

Equation (3.19) on page 97 is used to find the thresholds which maximise the overall accuracies. Each point in the continuous ROC plot, such as Figure 5.11 corresponds to a false positive rate (x axis) and a true positive rate (y axis) which result from a threshold. The thresholds which maximise equation (3.19) are found in each experiment condition and applied. Before the thresholds applied, the frequency corresponding the maximum value in the feature vector is regarded the attended frequency. When the thresholds applied, the maximum value of feature vector is compared to the corresponding threshold. Only if it exceeds or is equal to the threshold, the corresponding frequency is recognised as the attended target. Otherwise, it is recognised as UI (Un–Identified) class.

Figure 5.18 shows the confusion matrix with thresholds applied. The confusion matrix without applying the thresholds can be found in Figure 5.9. The thresholds applied in this figure are the thresholds which maximise the accuracy of equation (3.19) on page 97. The thresholds are different for different experiment conditions but the same for all subjects in one experiment condition. The thresholds, true positive rates and false positives rates used in equation (3.19) are from

Figure 5.11. For 15Hz, it has no false positives in all viewing distances. The total false positives of 12Hz are 28 (see Figure 5.18 (e)) which are reduced from 312 (see Figure 5.9 (e)). The true positives are also reduced. It indicates that the thresholds have the impact on both false positives and true positives.

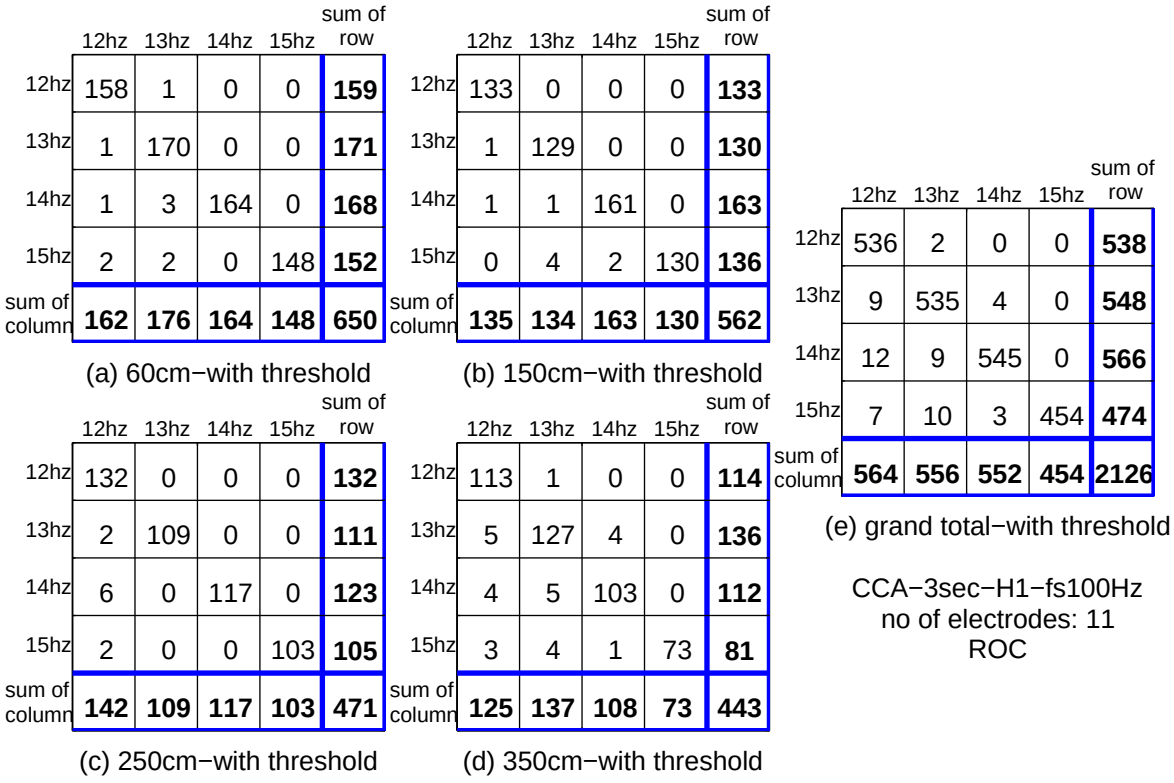

(a) 60cm−with threshold

	12hz	13hz	14hz	15hz	sum of row
12hz	158	1	0	0	**159**
13hz	1	170	0	0	**171**
14hz	1	3	164	0	**168**
15hz	2	2	0	148	**152**
sum of column	**162**	**176**	**164**	**148**	**650**

(b) 150cm−with threshold

	12hz	13hz	14hz	15hz	sum of row
12hz	133	0	0	0	**133**
13hz	1	129	0	0	**130**
14hz	1	1	161	0	**163**
15hz	0	4	2	130	**136**
sum of column	**135**	**134**	**163**	**130**	**562**

(c) 250cm−with threshold

	12hz	13hz	14hz	15hz	sum of row
12hz	132	0	0	0	**132**
13hz	2	109	0	0	**111**
14hz	6	0	117	0	**123**
15hz	2	0	0	103	**105**
sum of column	**142**	**109**	**117**	**103**	**471**

(d) 350cm−with threshold

	12hz	13hz	14hz	15hz	sum of row
12hz	113	1	0	0	**114**
13hz	5	127	4	0	**136**
14hz	4	5	103	0	**112**
15hz	3	4	1	73	**81**
sum of column	**125**	**137**	**108**	**73**	**443**

(e) grand total−with threshold

	12hz	13hz	14hz	15hz	sum of row
12hz	536	2	0	0	**538**
13hz	9	535	4	0	**548**
14hz	12	9	545	0	**566**
15hz	7	10	3	454	**474**
sum of column	**564**	**556**	**552**	**454**	**2126**

CCA−3sec−H1−fs100Hz
no of electrodes: 11
ROC

Figure 5.18: **Confusion matrix of grand total of all subjects at different viewing distance using CCA with the thresholds applied.** The confusion matrix without applying the thresholds can be found in Figure 5.9. The thresholds applied in this figure are the thresholds which maximise the overall accuracy of equation (3.19) on page 97. The thresholds are different among the experiment conditions but the same for all subjects in one experiment condition. The thresholds, true and false positive rates used in equation (3.19) are from Figure 5.11.

Figure 5.18 is based on CCA. The confusion matrices using MEC and MCC with thresholds applied are in Figures B-64 and B-66 in Appendix B. Both demonstrate the similarity as seen in Figure 5.18. Figure 5.19 provides a better view on how the thresholds affect the classification results. Figure 5.19 shows that in order to maximise the accuracy of equation (3.19), for each attended frequency, both false and true positives are reduced. 12Hz is the one affected the most as it has most UIs from both false and true positives. 12Hz is the only frequency which has more reduced number in the false positives than the true positives. The other frequencies have more reduced number in the true positives than the false positives. This can be seen from 4 viewing distances.

UI matrices based on MEC and MCC can be seen from Figure B-65 and B-67 in Appendix B. The more the false positives are reduced, the more the true positives are reduced which is the same as Figure 5.19. The impact on the individual attended frequency is also similar. For example, 12Hz is the only frequency which has more reduced number in the false positives than the true positives. There is no false positives of 15Hz.

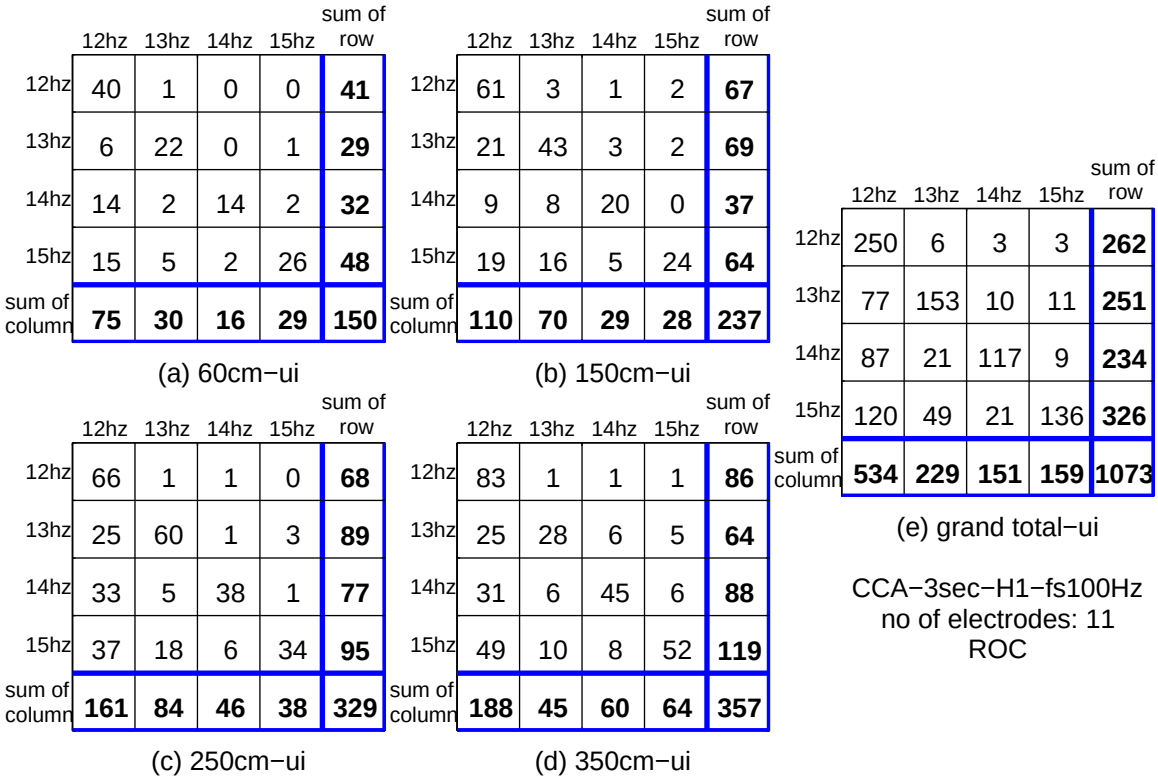

Figure 5.19: **Maxtrix of UI class after applying the thresholds on the classification.** Each UI matrix is the difference between the corresponding confusion matrices of Figures 5.9, and 5.18 in the same subplot. This figure is based on CCA.

The impact of thresholds on the classification is further examined by the use of a modified ROC plot as shown in Figure 5.20. In Figure 5.20, the false positive rate (fpr) is calculated according to the confusion matrix of Figure 5.18. In order to evaluate the impact on the true positive rate (tpr), i.e. the accuracies of the attended frequencies, the corresponding tpr is calculated as the following. The total of classifications is based on the confusion matrix in Figure 5.9 without the thresholds applied, i.e. the total classifications are the same as the original. The number of the true positive, the number of being classified correctly, is based on the confusion matrix in Figure 5.18. As the number of the true positives is reduced, as a result, the modified tpr decreases.

ROC points of all attended frequencies in Figure 5.20 are almost located in line with y axis which indicated that the false positive rates are approaching to ze-

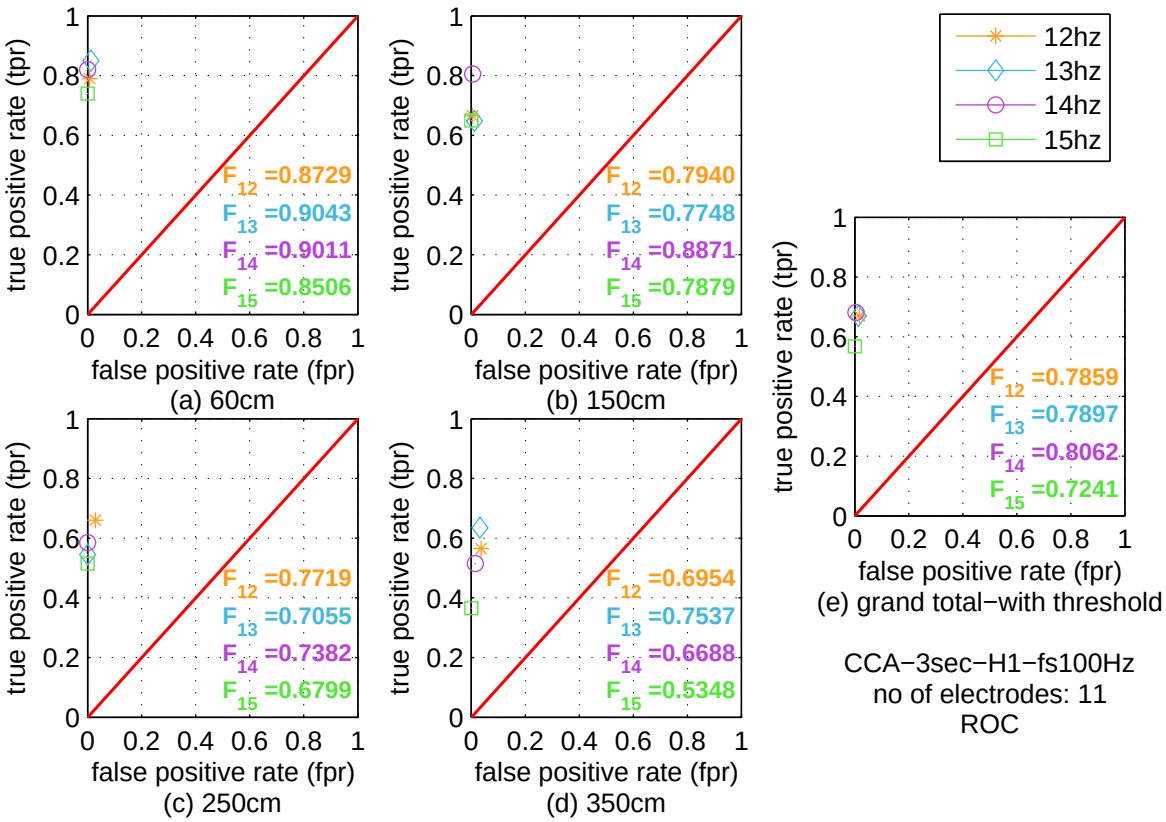

Figure 5.20: **Modified ROC plots corresponding to the confusion matrices of Figure 5.18 and F measurements when the thresholds applied.** The false positive rate (fpr) in this figure is calculated according to the confusion matrix in Figure 5.18. However, to see how the true positive rate (tpr), the accuracies of each frequency, are affected by the thresholds, the total classification number of each row is based on Figure 5.9 and the number of the true positives, the number of being classified correctly, of each frequency is based on Figure 5.18. As a result, the true positive rates decrease.

ros. However, its modified true positive rates also drops significantly compared to Figure 5.10. This means that the applied thresholds will reduce both false and true positives. The number of UIs shown in Figure 5.19 might suggest that the responses of false positives are also strong compared to the ones of the true positives. The total number reduced in the true positives is more than the false positives. The reduction in the false positives is at the expense of reducing the true positive rate.

Modified ROC plots based on MEC and MCC are shown in Figures B-68 and B-69 in Appendix B. As expected, ROC points are in line with y axis but also closer to x axis. It also demonstrates the fact that both false positives and true positives are both affected by applying the thresholds.

In this section, the thresholds on the classification results are evaluated. It is found that the thresholds have the same impact on the false positives and true

positives. The thresholds used in this section are the thresholds which maximise the accuracy in equation (3.19). The thresholds applied in this section are experiment–condition dependent without considering the inter–subject variance. For one experiment condition, it is the same for all the subjects. In next section, the thresholds will take the subjects and experiment conditions into account. The same analysis as this section will be performed.

5.6.2 Thresholds maximising *F* measurement

In this section, thresholds are applied to maximise F measurement which is defined by equation (3.18) on page 96. The thresholds are subject–experiment condition dependent. For each subject, there are four experiment conditions at the same viewing distance. For each attended frequency, the features of 4 experiment conditions are extracted from the classification data which include the features of the true and false positives. For example, for the attended frequency 12Hz, the features of all epochs which are classified as 12Hz are extracted no matter what the actual attended frequency is. The features from the data of the actual attended frequency 12Hz are the true positives. Those from the actual attended frequencies 13, 14 and 15Hz are false positives. For each attended frequency, the minimum and maximum values of the thresholds are the minimum and maximum values of the corresponding features. The maximised F measurement is found by applying different thresholds. The applied thresholds start from the minimum value of the threshold with increment of one tenth of the difference between the maximum and minimum values. The classification is re-evaluated with the applied thresholds. If the attended frequency corresponding to the maximum value of the feature vector is equal or exceeds the threshold, it is classified as the corresponding frequency. Otherwise, it is classified as UI class. The corresponding confusion matrix and the corresponding recall, precision rates and F measurement are compared. The thresholds which result in the highest F values are selected as the optimised thresholds for corresponding subject in the corresponding experiment condition.

Figure 5.21 represents sum of the individual confusion matrix of each subject at one viewing distance obtained with the optimised thresholds found through the above process. The confusion matrix without threshold can be found in Figure 5.9 on page 126. Comparing these two figures, it is clear that for each attended frequency, both the true and false positives are affected. Figures B-71 and B-73 show the confusion matrix with the optimised thresholds applied using MEC and MCC respectively. The impact of the thresholds on the classification is similar to Figure 5.21. The detailed UIs corresponding to Figure 5.21 are shown in Figure 5.22. From Figure 5.22, across the frequencies, only 34 true positives in total are affected by the thresholds. However, total 221 false positives are affected. For each individual frequency, the reduction in false positives is higher than the reduction in true positives. 12Hz is affected most in both true and false positives. On the other hand, 15Hz is the least affected also in both true and false positives. The reduction of the true positives is less than the false positives in all attended

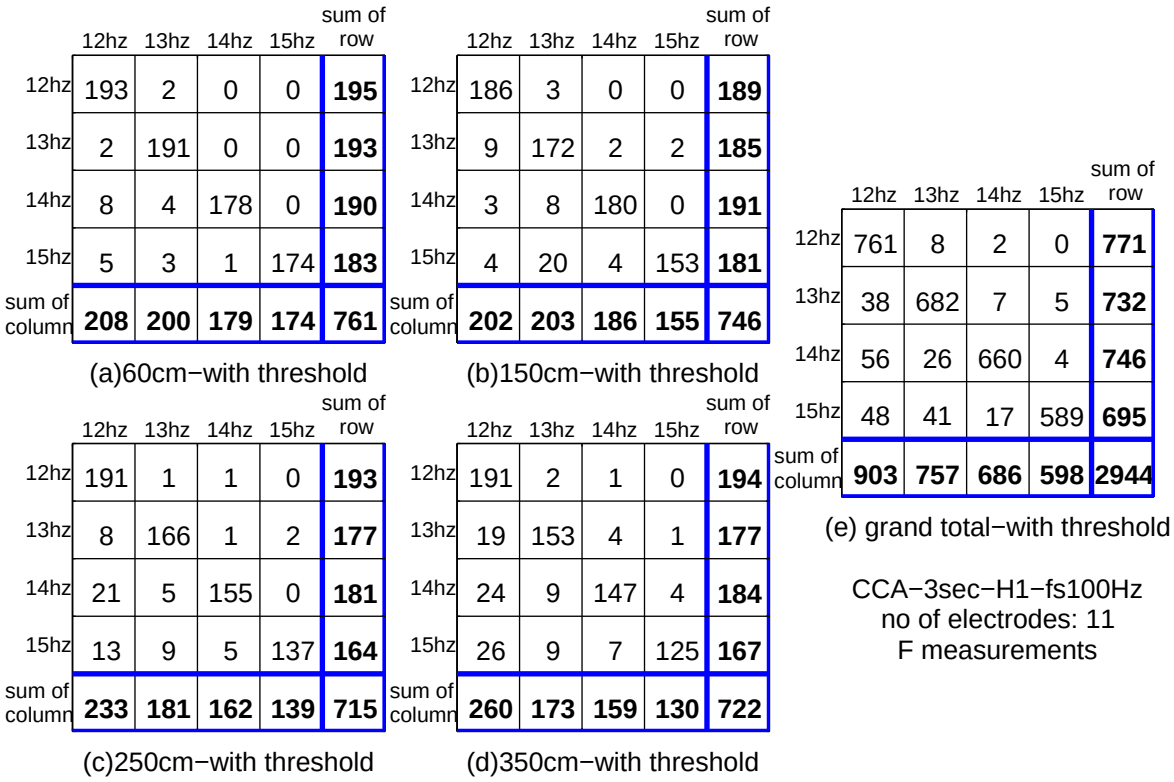

Figure 5.21: **Confusion matrix of grand total of all subjects at different viewing distance using CCA.** This figure is corresponding to Figure 5.9 in which no thresholds are applied. The thresholds of each subject in each experiment condition are different. The thresholds applied to each subject in different experiment condition maximise F measurement of the corresponding experiment condition. If the feature used as the classification criterion is lower than the thresholds, it is classified as UI class. (a) to (d) is the sum of the individual confusion matrix of each subject. (e) is the grand total of (a) to (d). Each number in the cell is the number of class i being classified as class j. The numbers of SSVEP harmonics and electrodes are 1 and 11 in this figure. The classification method is CCA and EEG TWL is 3s.

frequencies. This is different from what has been seen in section 5.6.1. Compared to the other frequencies, 12Hz has more false positives. In order to improve the precision rate, i.e. to reduce the false positives, the thresholds cannot be too low as seen in section 5.6.1. As a consequence, both true and false positives are affected most. 15Hz, on the contrary, has the lowest true and false positives compared to the other frequencies. The gain of the reduction in the number of the false positives might not compensate the loss of the reduction in true positives. Therefore, the optimised thresholds are not too high. It can also be observed that only 4 false positives across the frequencies resulting from attended 12Hz are affected. Without the threshold, the false negatives of 13, 14 and 15Hz when attending frequency 12Hz are 8, 3 and 3 respectively. Each of them is the false positive corresponding to attending 13, 14 and 15Hz. As 12Hz has the most prominent SSVEP response and highest true positives, its corresponding false negatives are low. Also, if the false negatives induce, their corresponding feature

must be very high in order to exceed the ones of 12Hz. Therefore, to reduce these false positives with high values of the features will also reduce more true positives which will decrease F. Only 4 of them are reduced after the thresholds are applied.

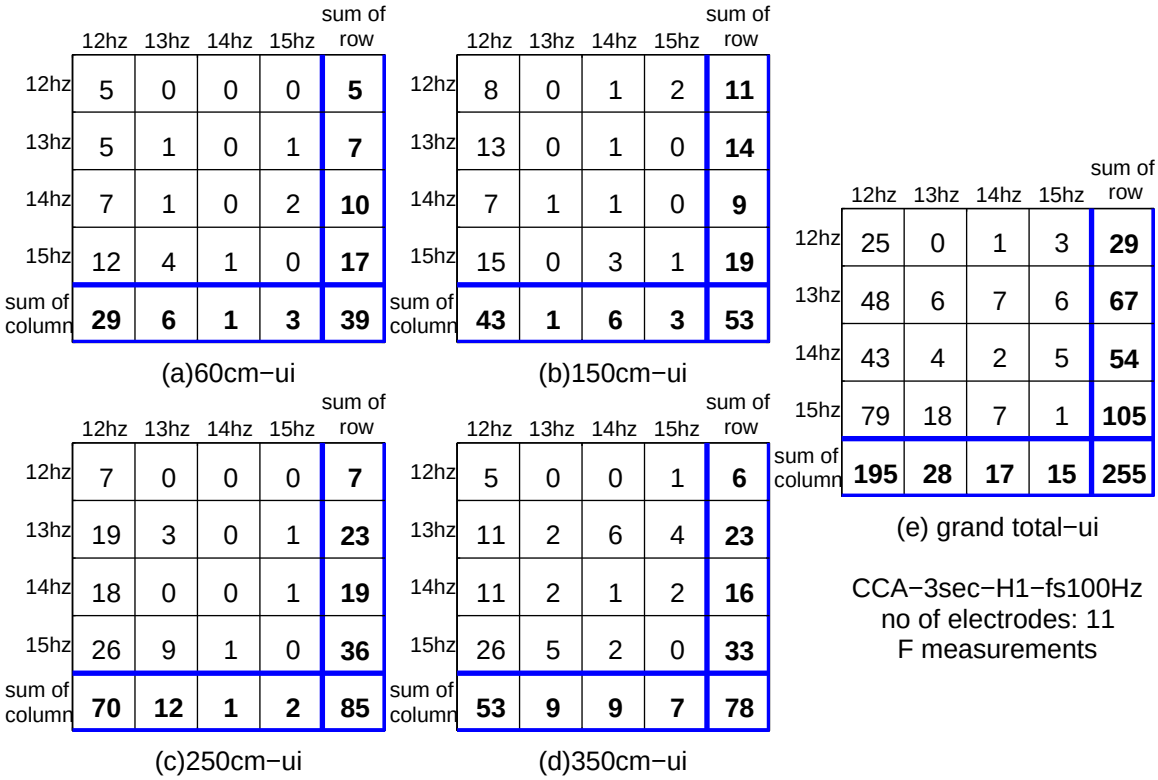

Figure 5.22: **UI number of the confusion matrix in Figure 5.9 with applied thresholds which maximise *F* measurements.** Each matrix of this figure is the difference between two corresponding matrices in Figures 5.9 and Figure 5.21.

Figures B-70 and B-72 illustrate UIs number of Figures B-48 and Figure B-49 when the thresholds are applied. These figures are in Appendix B. These two Figures demonstrate the similarity of Figure 5.22. For example, only 4 and 1 false positives resulting from attending 12Hz are affected by the thresholds for MEC and MCC respectively. They also show that 12Hz has most true and false positives affected. Figure 5.23 shows the revised ROC plot of Figure 5.10 when the thresholds are applied. Each ROC subplot is corresponding to one confusion matrix of Figure 5.21 .

Figure 5.23 represents the modified ROC when the subject-specific thresholds are applied. The false, true positive rate and F are computed by the same way as Figure 5.20. Compared Figure 5.23 and 5.10, the relative positions of ROC points are the same. Compared to Figure 5.10, ROC points in Figure 5.23 move towards to x axis and y axis. This indicates that the thresholds have impact on false and true positives but the change is not significant. Overall speaking, F measurements improve with the thresholds which maximise F for each subject

in all experiment conditions. This suggests that carefully chosen thresholds can improve the classification performance.

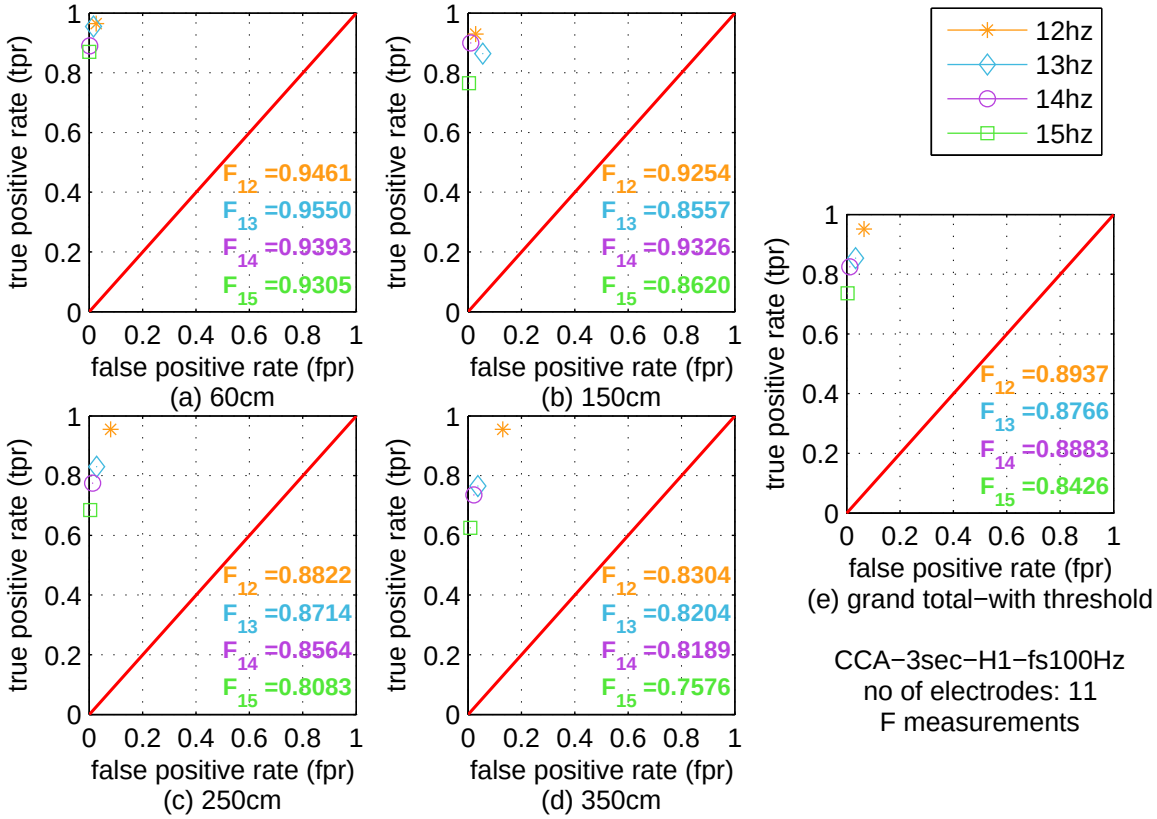

Figure 5.23: **Modified ROC plots corresponding to the confusion matrices of Figure 5.21 and *F* measurements with the thresholds applied.** ROC plots corresponding to the confusion matrices of Figure 5.21 and F measurements. Each ROC plot (a) to (e) is corresponding to one confusion matrix of Figure 5.21 (a) to (e). The classification method and parameters are the same as Figure 5.9. With the thresholds applied, F measurements are higher compared to Figure 5.10.

Figures B-74 and B-75 in Appendix B are modified ROC plots corresponding to the confusion matrix of Figures B-71 and B-73 for MEC and MCC respectively. For MEC and MCC, at least 4 out of 16 F values of Figures B-74 and B-75 are the same as the ones in Figures B-50 without threshold. The other 12 values of F in Figures B-74 and B-75 are higher. For each viewing distance, the improvements of 12Hz are more prominent compared to the other frequencies.

Compared Figures 5.23 and 5.20, ROC points of Figure 5.23 are not as close to y axis as the points in Figure 5.20. However, they are also more distant from x axis than the points of Figure 5.20. This means that the thresholds have the similar impact on both false and true positive in this paradigm. The thresholds can improve the overall the performance. However, the selection of the thresholds is the trad-off between false and true positive rate.

5.7 Interaction between attended and unattended targets

In this section, the interaction between attended and unattended targets was investigated. SSVEP responses of four different stimulating frequencies at different viewing distances were investigated when the subjects attended one of them. SSVEP responses of attended and unattended targets at different time instances in attending phase were also examined.

5.7.1 SSVEP responses of attended and unattended targets

Figure 5.24 illustrates mean FFT responses across the subjects of 4 stimulating frequencies when the subjects attended one of the attended frequencies in the Feasibility Experiment. Figure 5.24 is the mean of 20 epochs from each subject in different experiment conditions. The attended frequency is 12, 13, 14 and 15Hz for the subplots (a), (b), (c) and (d) respectively. It is clearly seen that SSVEP responses of the attended frequencies were elicited at different viewing distances. Moreover, SSVEP response of the unattended frequencies can also be seen. SSVEP of unattended frequencies was more prominent at the longer viewing distance than the shorter one. Figure 5.25 illustrates SSVEPs of one individual subject. SSVEP of unattended frequencies of this subject was more prominent than SSVEPs of unattended frequencies across the subject shown in Figure 5.24.

One way ANOVA test was performed to test the different of SSVEPs of the same attending frequency at different viewing distance. In Figure 5.24, ANOVA results are presented by the dots matrix beside the legend. The shapes of diamond circle and square represent 150cm, 250cm and 350cm respectively. Each row of the dot matrix stands for one viewing distance which is the same as the legend. The shapes of diamond, circle and square stand for the group of 150cm, 250cm and 350cm. Each row of the dots represents the ANOVA results of the group presented by the dot and the corresponding group of the row. The first, second and third row represent the group of 60cm, 150cm and 250cm. For instance, in the first row, three dots represent the ANOVA test results between 60cm and 150cm, 250cm and 350cm (diamond, circle and square). The significance level is 0.01. If p value ≤ 0.01, it is presented by red-filled dot otherwise by black un-filled dot.

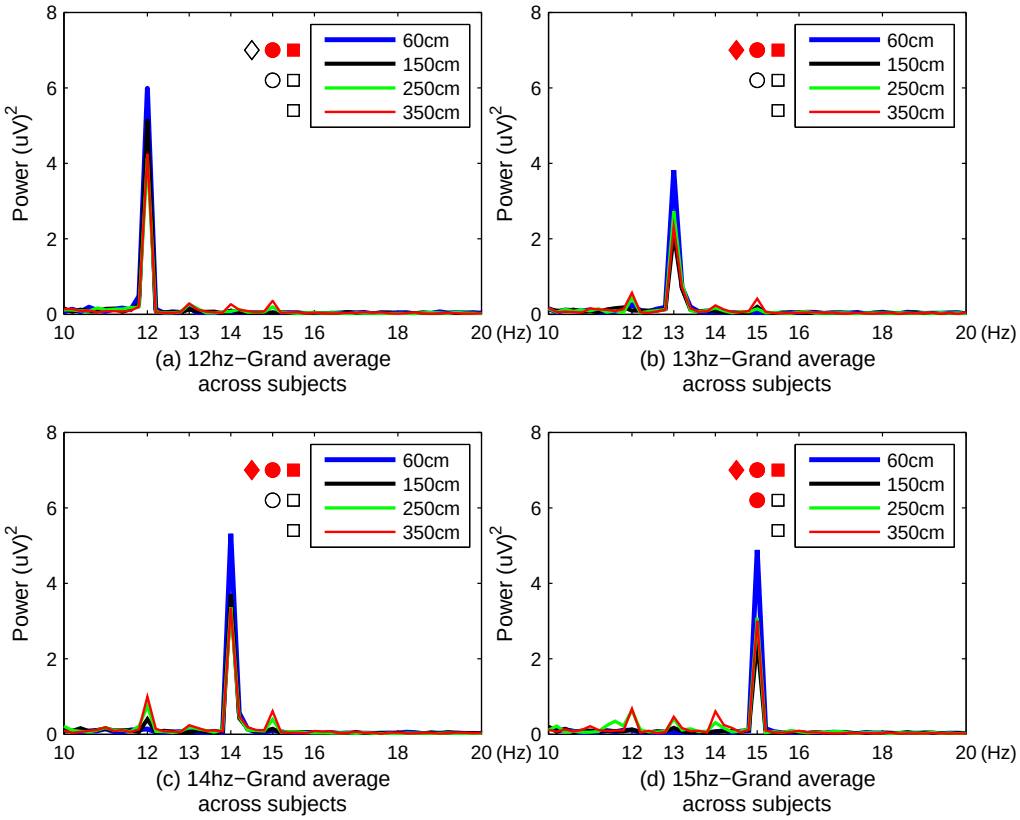

Figure 5.24: **Mean SSVEP response of the same attended frequency across the subjects at different viewing distances and ANOVA test results of SSVEPs of the same attended frequency between different viewing distances.**

For some stimulating frequencies, SSVEP response of the attended frequency is similar to or smaller than the attended one. For example, when this subject attended to 12Hz or 13Hz at the viewing distance of 350cm, SSVEP of unattended 15Hz was higher than attended 12Hz and SSVEP of unattended 14Hz and 15Hz were similar to attended 13Hz.

SSVEP responses of the attended and unattended frequencies were subject dependent. Figures B-76 and B-77 in Appendix B were two examples from two other subjects. One is better and one is worse than the subject of Figures 5.25.

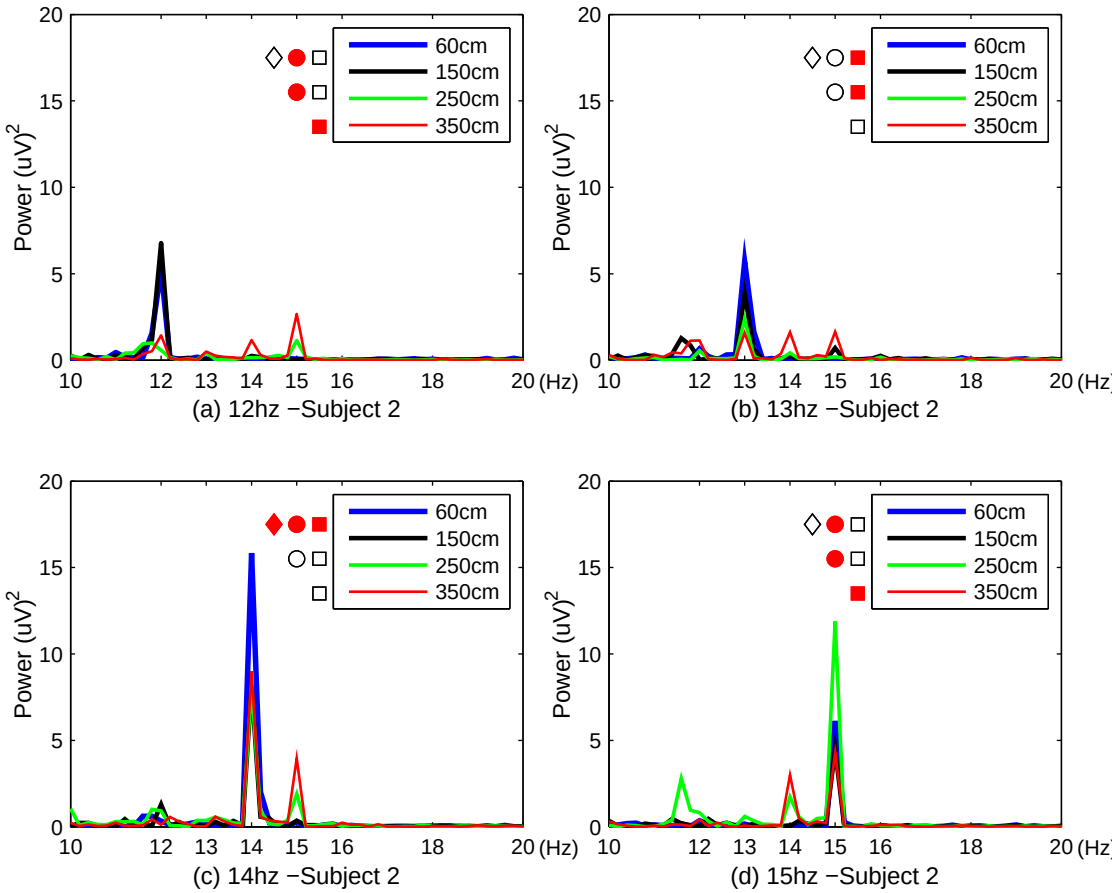

Figure 5.25: **Mean SSVEP response of the same attended frequency of subject 2 at different viewing distances and ANOVA test results of SSVEPs of the same attended frequency between different viewing distances.** The presentation of ANOVA test is the same as described in Figure 5.24.

SSVEP time–locking to the stimulus property of the attended and unattended frequencies were further investigated. Figure 5.26 is the plot of SLIC inter–trace and the corresponding pair correlations of 4 stimulating frequencies when the subject attended to 14Hz at viewing distance 350cm. The time–locking to the stimulus onset is expected to be observed at the attended frequency, 14Hz. Figure 5.26 showed that the inter–trace correlation of 14Hz (attended frequency) was larger than 12 and 13Hz (unattended frequencies). However, the inter–trace correlation of 15Hz was similar to 14Hz and the median value of 15Hz was higher than 14Hz. The mean curves of the inter–traces also demonstrated that the inter–traces of 15Hz were highly correlated although it was unattended. For some subjects, the time–locking property at the attended frequency became less clear, especially at the longer viewing distance.

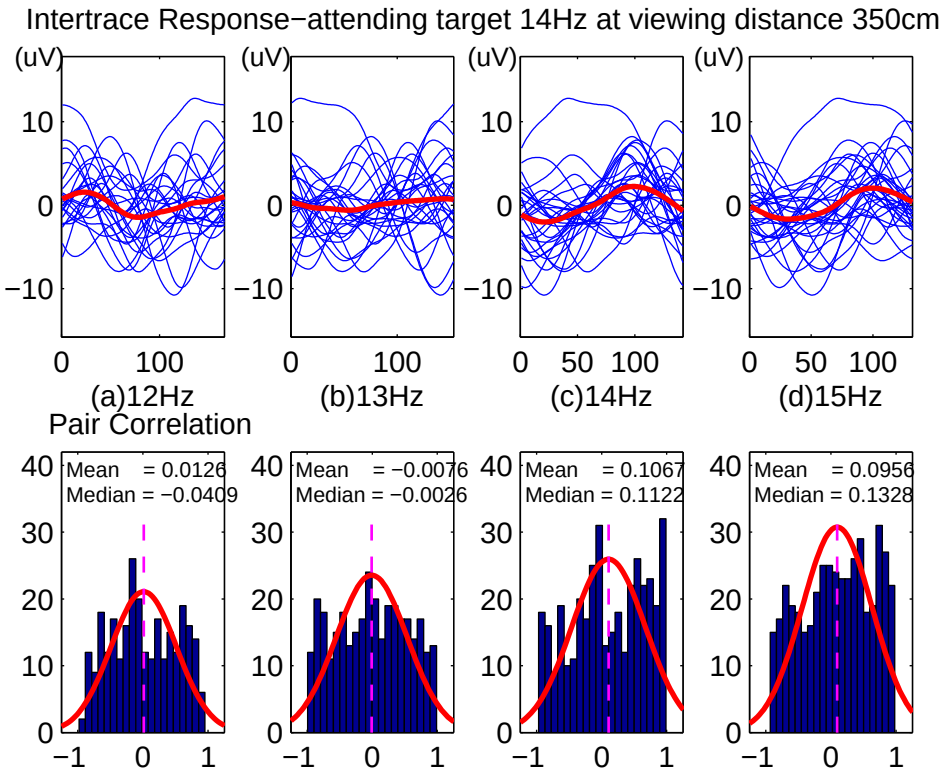

Figure 5.26: **The plot of SLIC inter–traces and the inter–trace pair correlations at four stimulating frequencies when one of the subjects attends at 14Hz target at the viewing distance 350cm.** Both 14Hz and 15Hz show the significance of the time locking property in the mean curve of the inter–traces and correlations when the target 14Hz is attended.

5.7.2 SSVEP response change in attending phase

In this section, the ratios of SSVEP responses between attended frequency and unattended frequencies were investigated. A/U ratio, is defined by the ratio between the power of SSVEP at the attended (A) frequency and the sum of SSVEP powers at three unattended (U) frequencies. A/U ratio is similar to SNR but focused on the signals at the stimulating frequencies which illustrated the ratios of SSVEP at the attended and unattended frequencies.

Figure 5.27 illustrates the mean SSVEP powers across the subjects of all stimulating frequencies when subjects attended 14Hz at 250cm and the corresponding A/U ratios. In this example, SSVEP power of the attended frequency (14Hz) was lower than the powers of unattended frequencies 12Hz and 13Hz in the 1^{st} second of the attending phase. It took more than 2s before the power of 14Hz exceed the one of 12Hz. A/U ratio increases as the time increased. SSVEP of 12Hz remained prominent through the entire attending phase.

Figure 5.28 showed mean SSVEP powers across the subjects of all stimulating

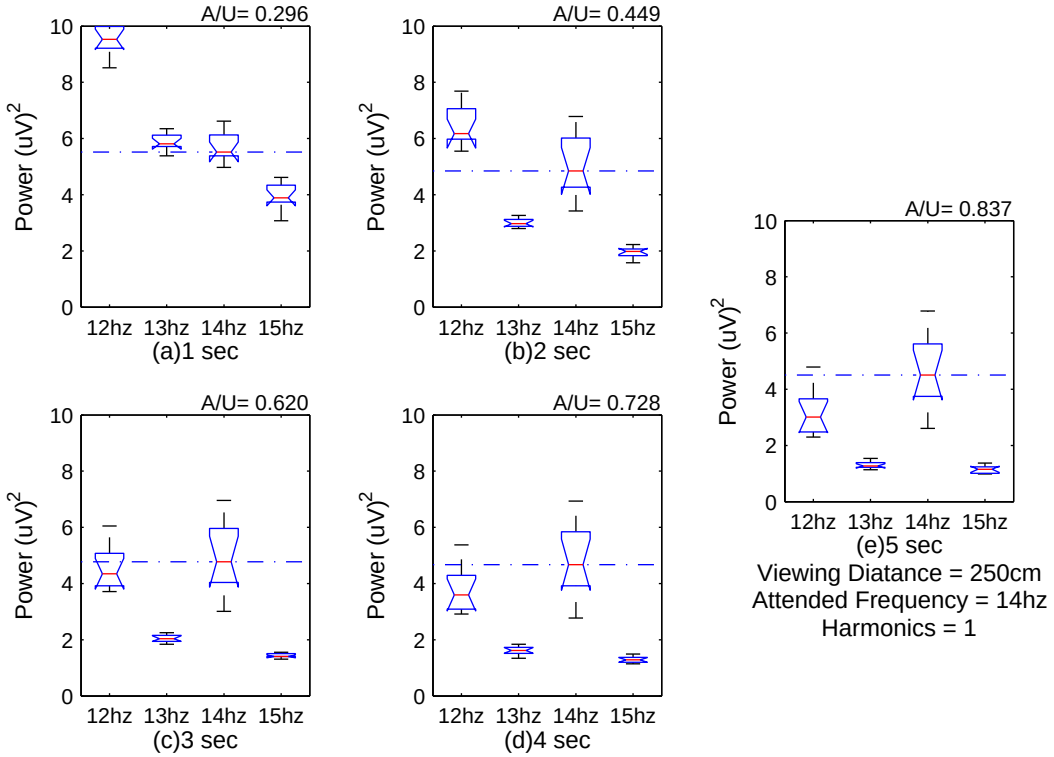

Figure 5.27: **Mean SSVEP powers of SSVEPs of the attended frequency and unattended frequencies and its corresponding A/U ratio through entire attending phase. This figure illustrates SSVEP powers of all stimulating frequencies in (14Hz, 250cm) experiment condition.** This figure illustrates SSVEP powers of all stimulating frequencies in (14Hz, 250cm) experiment condition. A/U ratio increases as the time increases. So do SSVEPs at all stimulating frequencies. It takes more than 2s before the power of attended frequency (14Hz) exceeds the one of 12Hz.

frequencies when the subjects attended the target of 12Hz at the viewing distance 250cm. SSVEP powers of the attended frequency 12Hz were much higher than the unattended ones from the 1^{st} second of the attending phase. A/U ratios were close or exceeded one through entire attending phase.

Figures B-78, B-79 and B-80 in Appendix B depicted mean SSVEP powers across the subjects of all stimulating frequencies in different experiment conditions, (13Hz, 350cm), (15Hz, 150cm) and (14Hz, 60cm). In these examples, SSVEP powers of the attended frequency were lower than the powers of 12Hz in the 1^{st} second of the attending phase.

5.7.3 A/U ratios of different stimulating frequencies

Figure 5.29 illustrates the average A/U ratios across the subjects of each attended frequency at four viewing distances. Each subplot indicates one attended

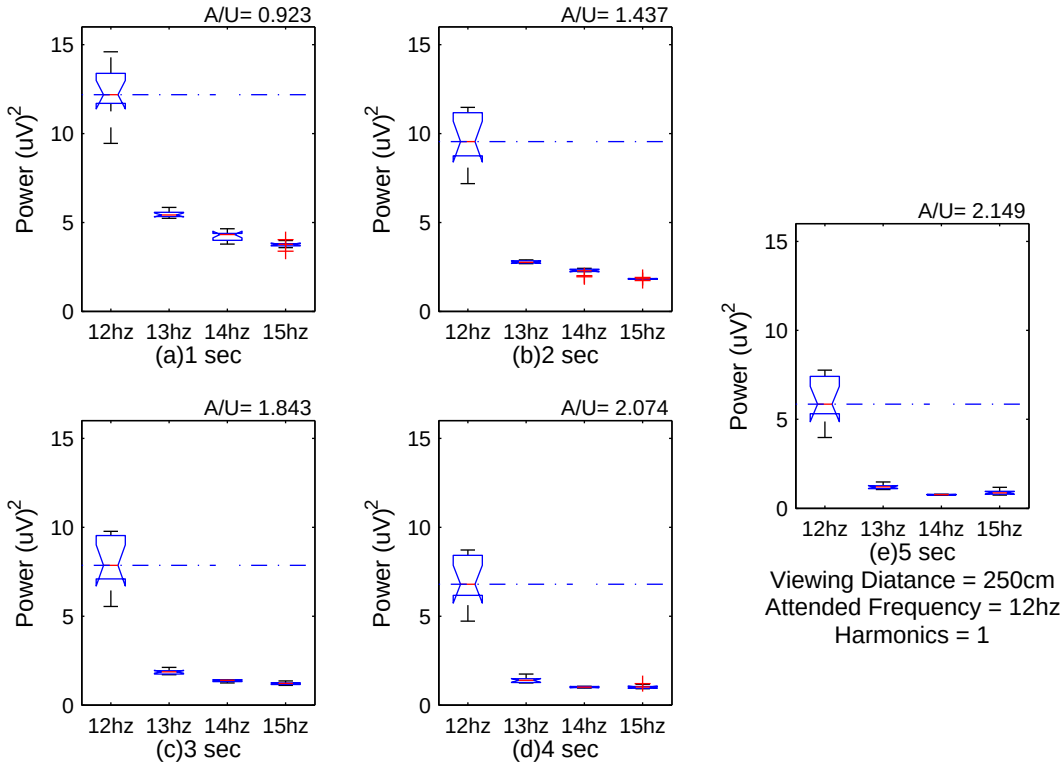

Figure 5.28: **Mean SSVEP powers of SSVEPs of the attended frequency and unattended frequencies and its corresponding A/U ratio through entire attending phase. This figure illustrates SSVEP powers of all stimulating frequencies when the subjects attend the target 12Hz at the viewing distance 250cm** SSVEP powers of attended frequency 12Hz shows prominent from the start (a). A/U ratios through entire attending phase are close or larger than one. Both A/Us and mean SSVEP powers of all attended frequencies increase as the time increases.

frequency and its corresponding A/U ratios at different viewing distances over time. For example, in Figure 5.29 (a), the attended frequency was 12Hz. A/U ratios in Figure 5.29 (a) were the ratios of powers at 12Hz and the sum of the powers of 13Hz, 14Hz and 15Hz over the time at different viewing distances. For each attended frequency, A/U ratios of the same viewing distance increased as EEG TWL increased. In Figure 5.29 (b), at viewing distance 250cm, A/U of 5s was the highest and A/U ratio of 1s was the lowest. The differences of A/U ratios of different TWL at shorter distances (60cm, 150cm) were larger than at longer distances (250cm, 350cm).

The A/U ratios were also used to investigate the false positive rates. Figure 5.30 (a)-(d) represent the false positive rates at different viewing distances for each attended frequency and (e) represents the grand average across the attended frequencies over time. Figure 5.30 shows that the false positive rates decreased as EEG TWL increased. For each attended frequency, A/U ratios increased as EEG TWL increased. The false positive rate of the attended frequency is correlated

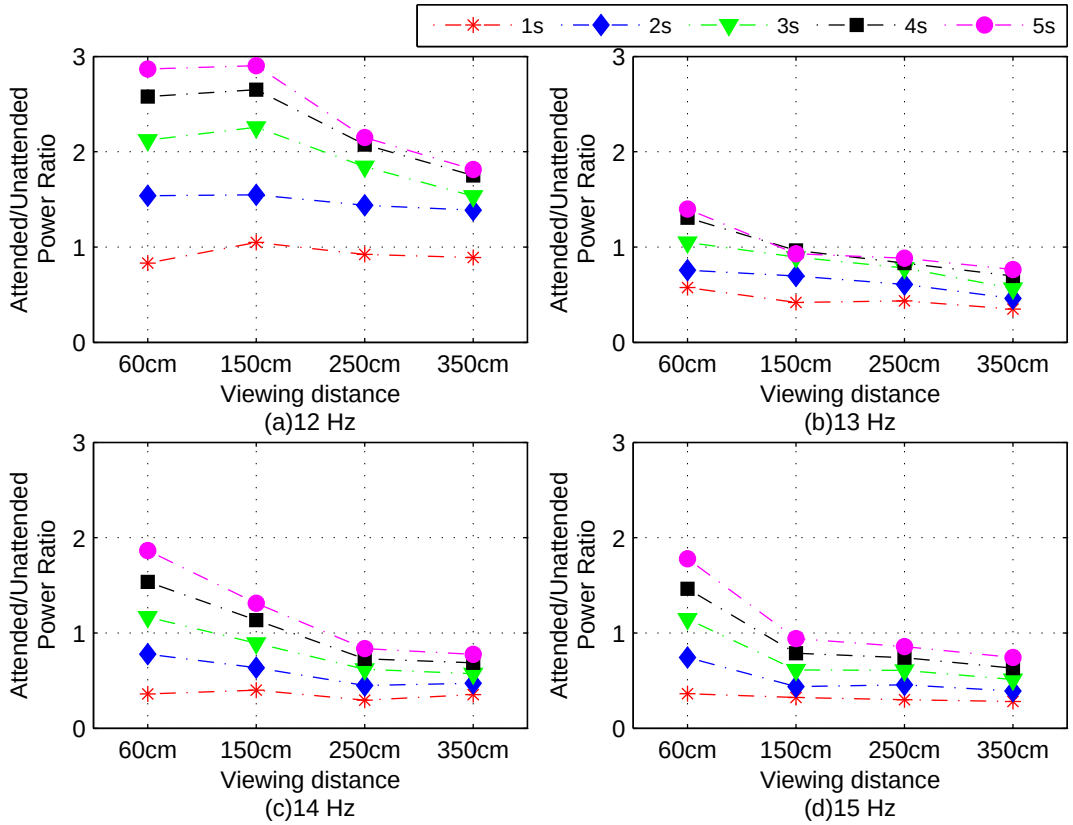

Figure 5.29: **A/U ratios of SSVEP powers between the attended and unattended frequencies across the subjects for one attended frequency at different viewing distances over the time.** Each subplot stands for one attended frequency. Subplots (a) to (d) present the attended frequency 12Hz, 13Hz,14Hz and 15Hz respectively over the time instances from 1s to 5s.

to the A/U ratios of unattended frequencies when they were attended. As a result, the corresponding false positive rates decreased. Figure 5.30 shows the result of CCA. Similar results from MEC and MCC can be found in Figures B-81 and B-82.

5.7.4 A/U ratios of different viewing distances

The data of Figure 5.29 were rearranged according to viewing distances. Figure 5.31 provided another view on how A/U ratios changed over the attended frequencies at the same viewing distance. A/U ratios of 12Hz were always the highest compared to the other frequencies over the time and the viewing distances. Between 1s and 3s, 15Hz had the lowest A/U ratios compared to 13Hz and 14Hz, except 3s at 60cm. This might explain why 15Hz had the lowest classification accuracies.

A/U ratios were used to examine the true and false positive rates. A/U ratios of attended 12Hz were higher than the other attended frequencies. As seen in Figure 5.7, attended 12Hz had higher accuracies than the other attended fre-

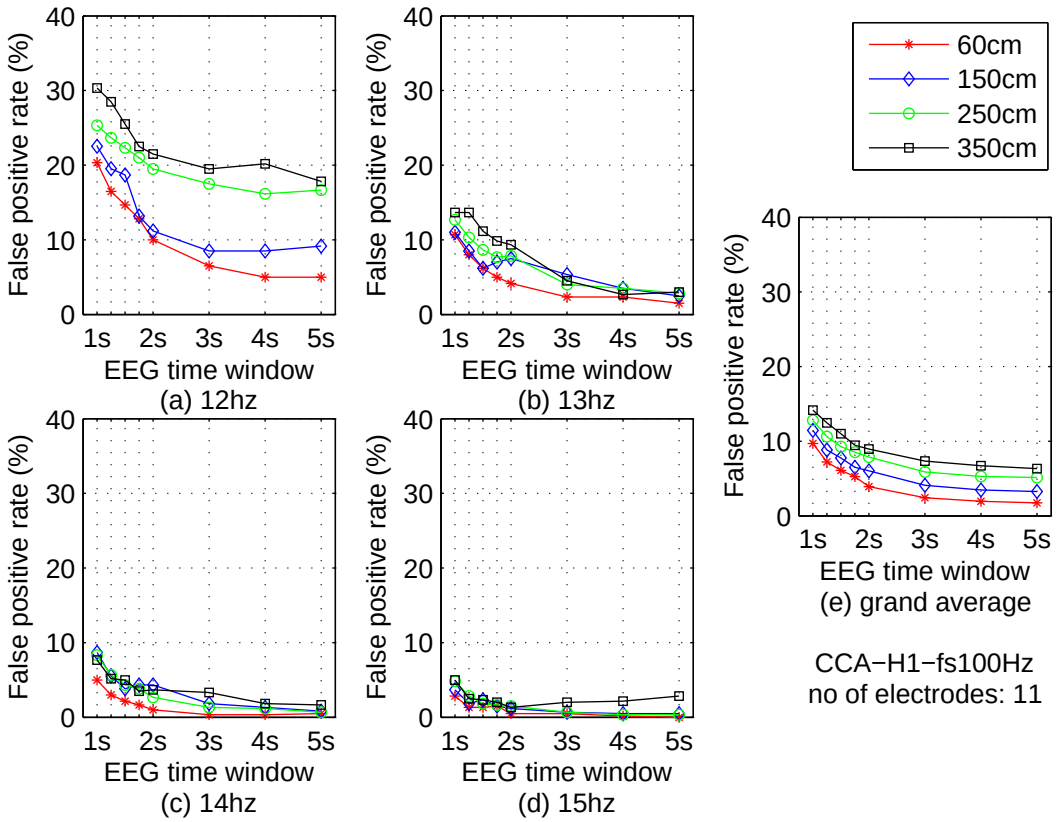

Figure 5.30: **False positive rates of different viewing distances of the same attended frequency and their grand average across the attended frequencies over time. This figure is the result of CCA.** Each subplot stands for one attended frequency. Subplots (a) to (d) present the attended frequency 12Hz, 13Hz,14Hz and 15Hz respectively over the time instances from 1s to 5s.

quencies. Figure 5.32 illustrates the false positives of all attended frequencies for each viewing distance. It is clearly seen that the false positive rates of 12Hz were significantly higher than the other attended frequencies.

The false positive rates of each individual attended frequency were related to the A/U ratios of the corresponding unattended frequencies when they were attended. When 13, 14 and 15 Hz were attended, the powers of unattended 12Hz were high. As a result, the corresponding false positive rates of 12Hz were higher than the other attended frequencies. On the other hand, A/U ratios of 15Hz were the lowest among all frequencies. It explained why the false positive rates of 15Hz were the lowest. The average false positive rates across the viewing distances are 16%, 7%, 3% and 1% for 12Hz, 13Hz, 14Hz and 15Hz respectively at EEG TWL 2s.

The results of the false positive rates by MEC and MCC can be found in Figures B-83 and B-84 in Appendix B. The figures both show that 12Hz had the highest false positive rates and 15Hz had the lowest false positives rates which are the same as Figure 5.32.

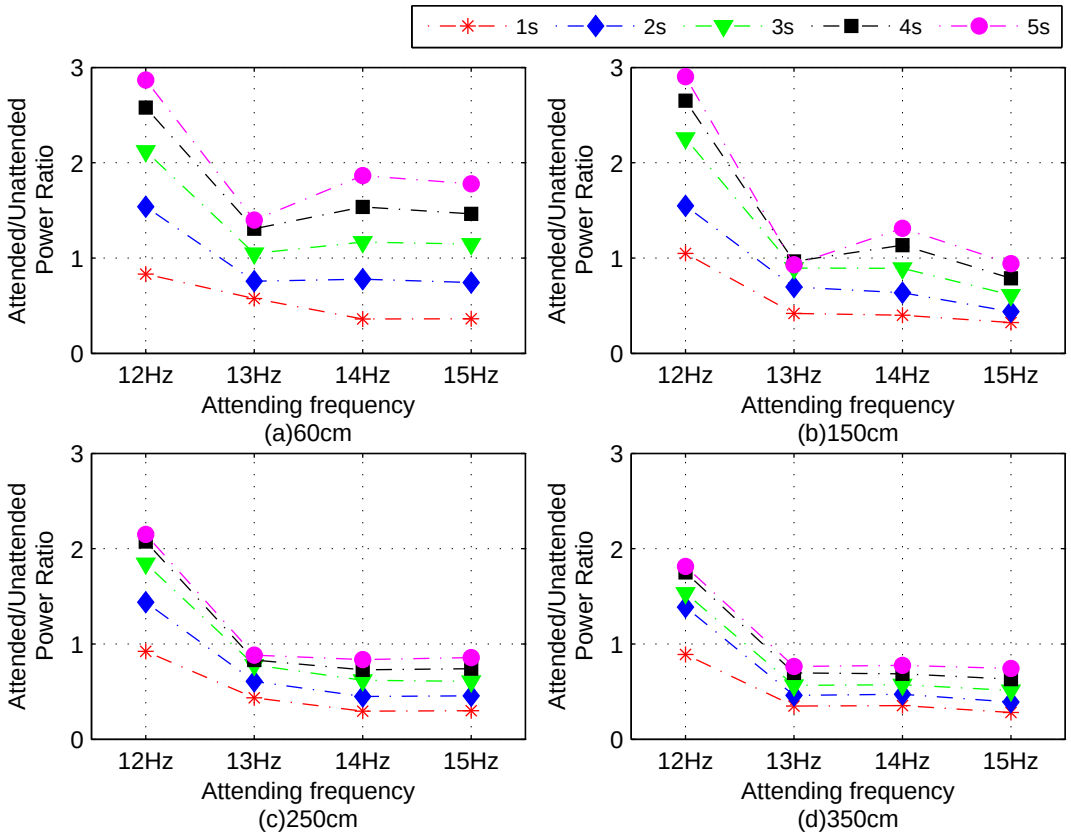

Figure 5.31: **A/U ratios of SSVEP powers between the attended and unattended frequencies across the subjects at one viewing distance for different attended frequencies over the time.** Each subplot stands for viewing distance. Subplots (a) to (d) present the viewing distance 60cm, 150cm,250cm and 350cm respectively over the time instances from 1s to 5s. The data of this figure are the same as Figure 5.29.

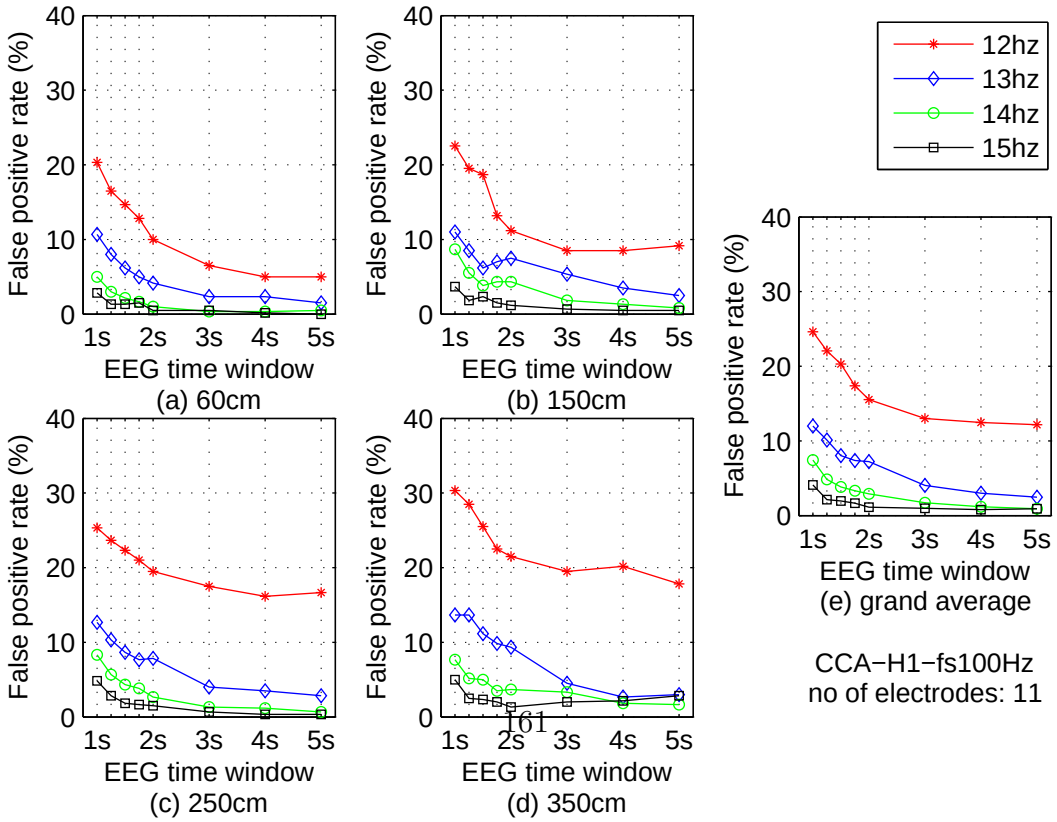

Figure 5.32: **False positives rates of different attended frequencies at the same**

5.8 Summary

It was suggested that a 70% of classification accuracy is the threshold for effective BCI communication (Kübler et al., 2004). Table 5.10 lists the mean classification accuracies across the subjects, the stimulating frequencies of each viewing distance and the corresponding standard deviations. Table 5.11 lists the mean classification accuracies across the subjects and the viewing distances of each stimulating frequency.

From Table 5.10, the mean classification accuracies are over 70% when the EEG TWL exceeded 1.25s. When the EEG TWL exceeded 1.75s, the mean classification accuracies of four viewing distances were over 75%.

Table 5.11 shows that it requires 3s of EEG TWL for mean classification accuracies of all stimulating frequencies to be over 70%. To test the impact of the EEG TWL, ANOVA was applied to the subjects classification accuracies of one viewing distance and one attended frequency of 8 different EEG TWLs seen in Table 5.10. p values ($df = 7\times72$, 8 EEG TWL and 10 subjects in each TWL) showed no significant difference in most of the combinations of viewing distance and stimulating frequency. Only (60cm-12Hz) and (250cm-13Hz) were significance in classification accuracies (p values = 0.002 and 0.003). This result is different from another previous study by Bin et al. (2009b) which showed the significant impact of EEG TWL on classification accuracies.

Table 5.10: Mean classification accuracies across the subjects and stimulating frequencies of each viewing distance and the standard deviations (mean ± std) % using different EEG TWL. This table is the result of CCA.

TWL	**1.00s**	**1.25s**	**1.50s**	**1.75s**	**2.00s**	**3.00s**	**4.00s**	**5.00s**
60cm	(71 ± 13)%	(78 ± 10)%	(82 ± 11)%	(84 ± 10)%	(88 ± 9)%	(93 ± 6)%	(94 ± 5)%	(95 ± 5)%
150cm	(66 ± 17)%	(73 ± 15)%	(77 ± 13)%	(81 ± 11)%	(82 ± 11)%	(88 ± 8)%	(90 ± 5)%	(90 ± 5)%
250cm	(62 ± 20)%	(68 ± 16)%	(72 ± 16)%	(74 ± 16)%	(76 ± 14)%	(82 ± 13)%	(84 ± 13)%	(85 ± 12)%
350cm	(58 ± 18)%	(63 ± 20)%	(67 ± 18)%	(72 ± 17)%	(73 ± 17)%	(78 ± 15)%	(80 ± 13)%	(81 ± 12)%
Mean	(64 ± 17)%	(71 ± 15)%	(74 ± 15)%	(78 ± 14)%	(80 ± 13)%	(85 ± 10)%	(87 ± 9)%	(88 ± 9)%

Table 5.11: Mean classification accuracies across the subjects and viewing distances of each stimulating frequency and the standard deviations (mean ± std) % using different EEG TWL. This table is the result of CCA.

TWL	**1.00s**	**1.25s**	**1.50s**	**1.75s**	**2.00s**	**3.00s**	**4.00s**	**5.00s**
12Hz	(87 ± 4)%	(90 ± 2)%	(94 ± 2)%	(95 ± 2)%	(95 ± 1)%	(98 ± 1)%	(98 ± 2)%	(98 ± 2)%
13Hz	(63 ± 8)%	(71 ± 8)%	(73 ± 9)%	(80 ± 7)%	(83 ± 9)%	(86 ± 8)%	(88 ± 8)%	(89 ± 7)%
14Hz	(58 ± 7)%	(66 ± 7)%	(72 ± 7)%	(73 ± 6)%	(76 ± 7)%	(83 ± 8)%	(83 ± 9)%	(84 ± 9)%
15Hz	(48 ± 10)%	(55 ± 13)%	(59 ± 10)%	(63 ± 10)%	(66 ± 10)%	(74 ± 11)%	(78 ± 10)%	(79 ± 10)%
Mean	(64 ± 7)%	(71 ± 8)%	(74 ± 7)%	(78 ± 6)%	(80 ± 7)%	(85 ± 7)%	(87 ± 7)%	(88 ± 7)%

Chapter 6

Discussion

This chapter discusses the results of the experiments. The primary goal of this study is to evaluate the feasibility of a novel distance adaptable SSVEP based BCI. The impact of the viewing distance on SSVEP response was first investigated in the Investigation Experiment. The intensity/resistor selection experiment attempted to find the minimum intensity which could result in the designated classification accuracy (95%).

The classification performance of a four-class SSVEP based BCI setup at four different viewing distances were further evaluated in the Feasibility Experiment in which the compensated intensities at different viewing distances were based on the results of the intensity/resistor selection experiment. Furthermore, the classification performance using different EEG TWLs, number of SSVEP harmonics and number of the electrodes by three classification methods, CCA, MEC and MCC were inspected and compared.

This study also proposed a procedure for the electrode selection. This electrode selection procedure was based on the electrode rankings. The rankings of the electrodes were obtained according to the spatial filter coefficients of the electrodes and the classification accuracy of single electrode.

6.1 Stimulator selection

Currently, there is no general agreement on the best configuration of visual stimuli in SSVEP in terms of the types, colours of the stimulators. However, LED can elicit stronger SSVEP response compared to the graphics stimuli presented in the monitors (CRT and LCD) (Wu et al., 2008).

The colour of the stimulus has the impact on the performance and comfort (Bieger et al., 2010; Cao et al., 2012; Tello et al., 2015). Bieger et al. (2010) found that the colours of the visual stimulus resulting in better performance in ITR also induced discomfort and vice versa. Cao et al. (2012) showed that the white stimulus has the best performance, followed by colours of gray, red, green and blue. Both studies used LCD monitor to present the stimuli. Tello et al. (2015) examined

the colours of LEDs on the performance and comfort. They tested 4 frequencies (8, 11, 13 and 15Hz) using four colours, blue, green, yellow and red. The results showed that overall speaking, red colour led to the best performance and least comfort across the frequencies. Green and blue were more comfortable with lower ITR. The choice of the colour should balance the comfort and performance.

Visible light (wavelength from 380nm to 780nm) has the thermal and photochemical effects which can cause damage and hazards. Two possible hazards from the light are retinal thermal injuries and blue light hazard which depend on the wavelength of the incident radiation (OSRAM, 2012). OSRAM (2012) suggested that there is no need of specific-safety assessment for OSRAM LED product with the dominant wavelength, λ_{dom}, falling into the range of, (510nm $\leq \lambda_{dom} \leq$ 660nm) On the contrary, the high-power LEDs of blue colour and a small number of green colour with wavelength falling into the range of 450nm $\leq \lambda_{dom} <$ 510nm is likely to induce the risk of the hazard. Typical peak of the white LEDs in the spectrum is 450nm which falls fall into the blue light hazard area.

This study attempts to evaluate the feasibility of the distance adaptable SSVEP BCI. The red LED was chosen due to its high performance and the concern of the safety. After the colour is chosen, the luminance is the most important parameter to choose the LED in this study. The LED was chosen from the low luminance to the high luminance.Three different types LEDs with different maximum luminance and radiation characteristics were chosen in this study.

Three LEDs, all from the same manufacture OSRAM, with different luminance and radiation characteristics were chosen in this study. They are LS E63B-BBCB-1-1(for the Investigation Experiment), LR G6SP-CADB-1-1(for the Investigation Experiment) and LR CP7P-JSJU-1(for the Feasibility Experiment) with λ_{dom} 633nm, 625nm and 623nm respectively. The viewing angle is 30°, 120° and 80° respectively.

The main aim in selecting the most appropriate LED was luminance. The second property was that the LED radiation characteristics are within the field of view of the subjects at any distance. It has been shown that this is satisfied and confirmed by

1. Subjects who participated indicated that they can see the flickering LED during the experiments.

2. EEG recorded in the experiments has exhibited the same flickering frequencies in the associated epochs manifested in SSVEP.

3. Geometrical analysis of the experiment setup described in Figures 6.1 and 6.2. In Figures 6.1 and 6.2, inter-pupillary distance (IPD) is taken into account. Mean IDP of the adult is 63mm. IPD of almost all adults is within the range of 45-80 mm (Dodgson, 2004). In the Investigation experiment, the viewing angles of LEDs are 120 and 30 for LR G6SP-CADB-1-1 and LS

E63B-BBCB-1-1, respectively. In the Investigation experiment, only one visual stimulus was presented to the subjects at the centre of the panel. As it can be seen from the geometry illustrated in Figures 6.1, the subjects were well within the region of LED viewing angle. Figures 6.1 only illustrates the worst scenario when the viewing distance is 60cm as x (distance within viewing angle) is smallest when viewing distance is 60 cm for the same LED.

When there is only one stimulus, the viewing angle of the LED does not play a crucial part. Even the angle is small, the vision of the subjects are still fallen within the viewing angles (for example 30°). However, when there is more than one stimulus, the viewing angle is important as seen in Figure 6.2. If the viewing angle is too narrow, the vision of the subjects might fall outside the viewing angle (for example 30°). However, if it is too wide, it will increase the interference of the neighbour stimulus (for example 120°). To trade off these two, we choose the middle value of two LEDs used in the Feasibility Experiment as the LED used in the Feasibility Experiment.

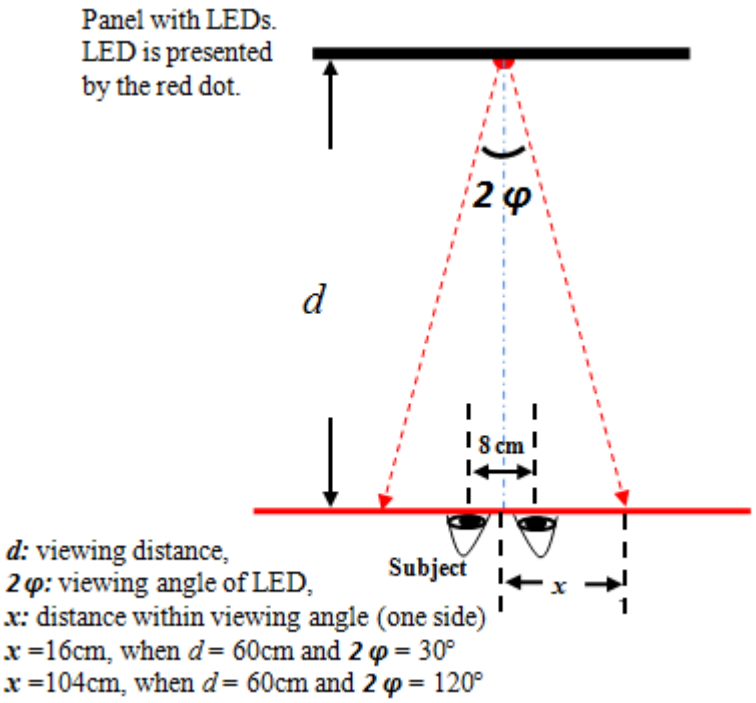

Figure 6.1: **The vision of the subjects was within the viewing angle in the Investigation Experiment.** This figure described the worst case when the viewing distance is 60 cm which has the smallest x.

According to the data sheets of the manufacture, the brightness of LEDs Brightness values are measured during a current pulse of typically 25 ms, with an internal reproducibility of ± 8% and an expanded uncertainty of ± 11% for LS E63B-BBCB-1-1(Version 1.0, 2013), and LR CP7P-JSJU-1 (Version 1.2, 2013).

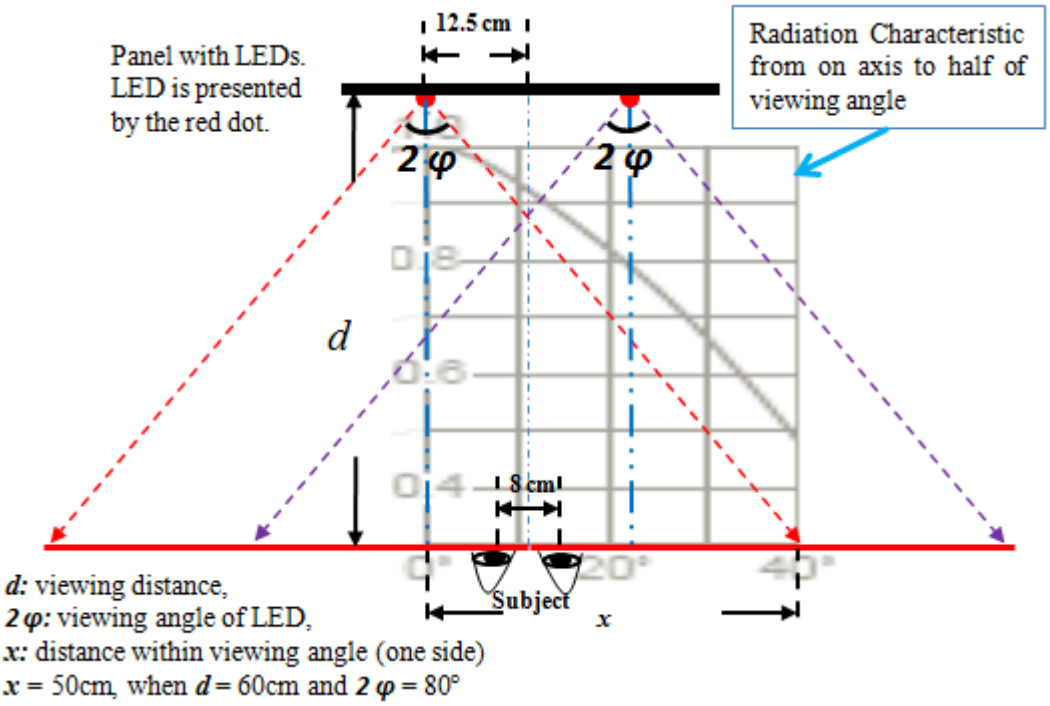

Figure 6.2: **The vision of the subjects was within the viewing angle in the Feasibility Experiment.** This figure described the worst case when the viewing distance is 60 cm which has the smallest x. The radiation characteristic of LED between 0° (optical axis) to 40° (half of the viewing angle) is shown in the background. The radiation characteristic of LED is from OSRAM Opto Semiconductors GmbH.

Brightness groups are tested at a current pulse duration of 25 ms and a tolerance of ± 11% LR G6SP-CADB-1-1 (Version 2007).

6.2 Impact of viewing distance

This section will discuss the impact of the viewing distance on the luminance of the visual stimuli in the Investigation Experiment, the results of the intensity/resistor selection experiment and the compensated intensities applied in the Feasibility Experiment.

6.2.1 Investigation Experiment

SSVEP response was highly dependent on the intensity of the visual stimulus. In the Investigation Experiment, the intensities of visual stimuli decreased as the viewing distance increased in the uncompensated condition as shown in Table 4.1. As a result, SSVEP response was severely deteriorated and the classification accuracies were low in uncompensated condition as seen in Figure 4.1 and Table 4.2. On the other hand, when the intensities of the visual stimuli were compensated, the corresponding SSVEP response became stronger and the classification accuracies were also improved compared to uncompensated condition as seen in

Figure 4.7 and Table 4.3.

This result is consistent with other studies which investigated the luminance effect on SSVEP response and classification accuracies. Mouli and Palaniappan (2016) investigated the effect of the luminance of the visual stimuli on SSVEP response. In their study, the visual stimulus was presented in 4 different luminance levels, 25%, 50%, 75% and 100% of the maximum luminance. They found that as the luminance level increased the amplitudes of SSVEP response also increased, up to the luminance level 75%. The luminance of 75% resulted in the strongest SSVEP. Bieger et al. (2010) examined the influences of stimulation properties on SSVEP based BCI also suggested that the luminance and contrast have the positive impacts on the performance of SSVEP BCI. Moreover, Punsawad and Wongsawat (2014) evaluated how the luminance of the visual stimulator induced the user fatigue in SSVEP BCI. Their results also showed that the higher luminance of the visual stimulator outperformed the lower luminance in terms of the classification accuracy.

6.2.2 Intensity/Resistor Selection Experiment

The intensity/resistor selection experiment attempted to find the optimal intensity at different viewing distance for each subject. The selection criterion was based on the procedure as described in Figure 3.9. As shown in Table 5.1, to achieve the same classification accuracy, the longer viewing distance required higher intensity than the shorter distance. If the intensity of LED at the viewing distance 60cm is normalised as 1, then the intensities to achieve the same classification accuracy were 1.16, 1.44 and 1.88 for the viewing distances 150cm, 250cm and 350cm respectively based on the intensities listed in Table 5.1. The greater the viewing distance is, the higher corresponding intensity is.

Based on the one subject experiment, the experimental result suggested in order to achieve the same classification accuracies the greater viewing distances require higher intensities. This might suggest that changing the viewing distance not only changed the intensity of the visual stimulus but also change other parameters which can affect SSVEP response and the performance of BCI. The higher intensity at greater viewing distance compensated the intensity as well as the other parameters.

6.2.3 Feasibility Experiment

In the Feasibility Experiment, four LEDs flickering at different frequencies were presented to the subjects simultaneously. Also seen in Table 5.1, in the Feasibility Experiment, the intensities of LEDs at different viewing distances were higher than the corresponding intensities found in the intensity/resistor selection experiment. The corresponding ratios of the intensities used in the Feasibility Experiment and found in intensity/resistor selection experiment at each viewing distance were 2.00, 1.35, 1.52 and 1.72 for 60cm, 150cm, 250cm and 350cm re-

spectively.

However, the results showed that

1. there exists a great inter—viewing distance variance in classification performance,

2. there also exists a great inter–frequency variance in classification performance and

3. there exists a great inter–subject variance in classification performance and

4. the classification accuracies were not as high as 95% as expected.

The inter-subject variance is a common problem in BCI research. For example, different subjects induced different SSVEP response with the same visual stimulator with the same luminance (Mouli and Palaniappan, 2016). The Investigation Experiment demonstrated the importance of intensities of the visual stimuli on SSVEP response. Intensity/Resistor Experiment and the Feasibility Experiment suggested that the intensity of the visual stimuli was not the only parameter which affects SSVEP response. There were other parameters which are also important and could be potentially affected by the changing the viewing distance. These parameters will be discussed in the section (6.3).

6.3 Other parameters

The experimental results in the Investigation Experiment demonstrated that the intensity of the visual stimulus could severely affect SSVEP response. However, in the Feasibility Experiment, the higher intensity at greater viewing distance could not produce better classification performance. This suggested that there were other parameters which are also important to SSVEP response and could be influenced by the viewing distance.

Table 6.1 lists the parameters which could affect SSVEP response (Zhu et al., 2010a; Fernandez-Vargas et al., 2013; Wu, 2014a; Duszyk et al., 2014). Some of the parameters are subject-specific, such as their levels of the attention, age and visual acuity. Some of the parameters of visual stimuli are fixed upon the choice, such as stimulating frequency, colour, type, duty cycle and number of the visual stimuli.

Some of the parameters are environment control variables, such as intensity, viewing distance, size and spatial proximity between stimuli. These parameters interact with each other. For example, changing the viewing distance of the visual stimuli could change the perception of intensity, size and the visual angle of the visual stimuli. The viewing distance could also affect the perception of spatial proximity between stimuli. As a result, changing the competition between the stimuli and disturb SSVEP response of attended stimulus.

Table 6.1: **Parameters affecting SSVEP response (Zhu et al., 2010a; Fernandez-Vargas et al., 2013; Wu, 2014a; Duszyk et al., 2014).**

	Parameters	
Subject	Attention span	
	Age	
	Visual acuity	
Visual Stimuli	Stimulating frequency	Intensity/luminance
	Colour	Modulation depth
	Viewing Distance	Size
	Types of visual stimuli	Duty cycle
	Number of stimuli	Spatial proximity between stimuli

6.3.1 Human visual system

In human vision system, the density of the receptors in fovea is much higher than the periphery (Treder and Blankertz, 2010; Larson and Loschky, 2009). The fovea is a small region which subtends about 2° of visual angle in the central of the visual field (Treder and Blankertz, 2010). It has been well documented that the visual stimulus fallen into the central vision can induce stronger SSVEP than in the peripheral vision (Lopez-Gordo et al., 2011).

At shorter viewing distance, the SSVEP of attended target is induced in the central vision while the SSVEP of unattended targets were induced in the peripheral vision which was weaker. As the viewing distance increased, both attended and unattended targets were within the central vision. As a result, SSVEPs of attended and unattended targets were both induced in central vision. That is, as the viewing distance increased, SSVEP response of unattended targets was also increased.

The SSVEP in central vision was time locked to the stimulus while SSVEP induced in peripheral is not. Therefore, averaging epochs should be able to enhance the SSVEP in central vision and suppress the response in peripheral vision (Lee et al., 2010). Figure 5.24 was obtained by averaging epochs across the subject and showed the SSVEP responses of all stimulating frequencies, attended or unattended. It was clearly seen that the SSVEP responses of the unattended targets increased as the viewing distance increased. When the viewing distance was 350cm, SSVEP responses of 4 stimulation frequencies were seen in the spectra. The result provided the evidence that at the greater viewing distance, both the attended and unattended targets were in the central vision.

6.3.2 Proximity between the stimuli

When the viewing distance changed, the perception of the proximity between the stimuli also changed. Reduced proximity between the stimuli could increase the competition between attended and unattended targets which affected SSVEP response of attended target and the classification accuracies. Several studies have investigated this effect (Fuchs et al., 2008; Ng et al., 2011, 2012; Resalat and Setarehdan, 2012; Duszyk et al., 2014). The layout of multiple choices of SSVEP based BCI should ensure the unattended stimuli to fall into peripheral vision and avoid to fall into foveal vision with attended target to reduce the competition between the stimuli and the distraction of the subjects (Kuś et al., 2013). For example, competition of un–attended targets in peripheral vision was also reported by Hwang et al. (2012) in a LED keyboard based on SSVEP study. It was found that the classification accuracies could be improved by increasing the distances between the adjacent keys in vertical and horizontal from 1cm to 2cm. No optimal distance was investigated in their study.

The co-amplification effect can be observed from the experimental result of this study. Figures 5.27 , B-78, B-79 and B-80 illustrate the changes of the SSVEP responses at different time during the attending phase. Apart from the attended target 12Hz, the SSVEP responses of the attended targets were at the similar level to the other unattended targets at the first second. It took 2-3 seconds before the A/U ratios exceeded 0.5. At greater viewing distances, as seen in Figures 5.27 (250cm) and B-78 (350cm), the SSVEP of the attended target did not actually become dominant (A/U ratios were less than 0.9) through the entire attending phase.

Ng et al. (2011, 2012) investigated the impact of the unattended targets in terms of the number, proximity, size and stimulating frequency of visual stimuli. In their experiments, they tested the proximity between attended and unattended targets of 2°, 3°, 5° and 7°. They found that proximity of 5° and 7° performed better than 2° and 3°. They suggested that the visual competition between attended and unattended was most severe when the unattended targets were within 5° of the fovea. To reduce the competition between targets, the proximity between the stimuli should be greater than 5°.

Resalat and Setarehdan (2012) examined the influence of the proximity (termed as inter source distance in their study) of 2 LEDs on SSVEP. The inter source distances used in their experiments were 4, 14, 24, 44 and 64 cm. LEDs in white were placed 60cm in front of the subjects and resulted in horizontal visual angles of 3.8°, 13.4°, 22.6°, 40.2° and 56°. They found that inter source distance of 44 cm could produce the highest classification accuracy while 4 cm produced the lowest.

The result of our study was in line with the aforementioned visual competition studies. In the Feasibility Experiment setup, when the viewing distance was 350cm, the perceptive proximity between the attended and unattended targets

are less than 4.5° both in the horizontal and vertical directions. As a result, SSVEP of attended and un–attended targets were enhanced at viewing distances 350cm. The classification accuracies of 350cm and the false positive rates of 350cm were the worst among the four different viewing distances. In other words, the greater viewing distance could increase the competition between the attended and unattended targets. The layout design of the multiple visual stimuli should take this into consideration.

6.3.3 Perception of LED spatial radiation

The perception of the LED spatial radiation (intensity) is also changed by the viewing distance. In Figure 6.2, the vision of the subjects is within the angle ranges of (8.06°, 15.38°), (3.24°, 6.27°), (1.95°, 3.78°) and (1.39°, 2.70°) from the optical axis of LED for 60, 150, 250 and 350 cm of the viewing distance. These ranges are well within the half of the viewing angle 80°. This is applied to the attended and unattended LEDs. Therefore, although at shorter viewing distance, the percentage of perception of the light is less than the greater viewing distance. The perception of the unattended LEDs is also weaker. This might be able to explain that shorter viewing distance outperformed the greater viewing distance.

6.3.4 User attention and fatigue

SSVEP response is highly dependent on the levels of attention of the subjects. As the viewing distance increased, the visual span also increased. This might make the subject more difficult to focus their attention. Some subjects reported that it became more difficult to focus on the attended target as viewing distance increased. During the attending phase, if the subjects divert their attention to the unattended visual stimuli, it is likely that the SSVEP response of the attended is reduced. Some SSVEP studies also observed that loss of attention and focus could cause the deterioration of SSVEP′s response (Wu, 2014a; Lin et al., 2014).

As mentioned earlier, the intensity of the visual stimuli at the viewing distance of 350cm is the highest among four viewing distances. However, it produced the lowest classification accuracies in average. Mouli and Palaniappan (2016)reported that the maximum luminance induced the weakest SSVEP response of all subjects and also increased the eye fatigue in their experiment. The participants of their study also indicated that the 75% of the maximum luminance was the most comfortable luminance to focus. Bieger et al. (2010) and Wang et al. (2013) also suggested that although the higher intensity could induce stronger response, it also increased the discomfort.

Another possible reason why the greater viewing distances have lower classification accuracies is due to fatigue caused by the experiment protocol. Due to the experiment setup, the order of presenting the visual stimuli to the subjects in the Feasibility Experiment is fixed, in the order of 60cm–150cm–50cm–350cm. The

greater the viewing distance is, the later the experiment is. This order might induce the fatigue of the subjects at the greater viewing distance.

6.4 Impact of spontaneous EEG on SSVEP

In the Investigation Experiment, only one flickering LED was presented to the subjects. The flickering frequency was one of the four stimulating frequencies. The classification results shown in Tables 4.2 and 4.3 on pages 107 and 113 clearly provide evidence that spontaneous EEG could affect classification accuracies of SSVEP. If the flickering frequency was not 12Hz, there should be no SSVEP response at 12Hz. However, as seen in both Tables 4.2 and 4.3, the majority of misclassified outcomes was 12Hz. 12Hz is within the alpha band which might explain the classification accuracies of 12Hz were high in uncompensated condition.

Other evidences also suggested the contribution of the spontaneous EEG. Firstly, the classification accuracies of 12Hz were high from the 1^{st} second of the attending phase. The mean accuracies of 12Hz across the viewing distance at the 1^{st} second of the attending phase were over 85%, compared to 63%, 58%, 48% of 13Hz, 14Hz and 15Hz. Secondly, during the attending phase, attention seemed to have less impact on 12Hz than the other frequencies. The mean increased accuracies across the viewing distances from 1s to 2s were 9%, 32%, 32% and 36% for 12Hz, 13Hz, 14Hz and 15Hz. The mean increased accuracies across the viewing distances from 2s to 4s are 3%, 6%, 10% and 19% for 12Hz, 13Hz, 14Hz and 15Hz. The variance of classification accuracies at 12Hz across the subjects was smallest compared to other frequencies. Also, subjects all showed good classification performance at 12Hz.

Wang et al. (2010a) proposed to use the 2^{nd} harmonic to discriminate the source of the signal, from spontaneous EEG or SSVEP. The assumption of this method was that if the source of signal was from SSVEP, the 2^{nd} harmonic should be prominent. In this study, the higher harmonics were not prominent enough to discriminate the source.

6.5 Impact of competing frequencies

Keitel et al. (2010) investigated the competition between the attended frequencies (10Hz or 15Hz) and the un-attended frequencies (12Hz or 60Hz). They found that the amplitudes of SSVEP of attended frequencies were decreased with the unattended frequencies present. The results showed that 12Hz and 60Hz unattended frequencies had similar impact on SSVEP of attended frequency of 10Hz. However, 12Hz had a higher impact on SSVEP of 15Hz than 60Hz. The amplitude of SSVEP of the attended frequency was suppressed the most when the combination of attended unattended frequencies were 15Hz and 12Hz. It was

suggested that unattended frequency within alpha band had higher impact than outside alpha band on SSVEP of attended frequency. Attended frequency within alpha band was less affected by the unattended frequency.

Keitel et al. (2010) supported the results of this study that the 12Hz had the best performance and 15Hz has the worst performance in terms of the classification accuracy. 12Hz is within alpha band and less affected by un–attended frequencies. It also explains why 12Hz had highest false positive rate. When 12Hz was unattended, it had the higher impact on the others.

6.6 Optimal electrode sets

The classification methods using multiple electrodes can reduce the inter-subject variability by extracting more information from multiple electrode signals. Consequently, it can reduce the calibration phase required from the subjects. However, more electrodes might reduce the inter-variance but it can also bring the irrelevant, redundant information, increase the preparation time and computation cost (Lan et al., 2006). The results of the analysis of the optimal electrode sets show:

- Highest classification: The possible highest classification accuracy of individual subject is different. From Table 5.2, it varies from 100% down to 57%.

- Minimal optimal electrode subset: The minimal electrode numbers required in order to achieve the highest rate for most of the subjects are either 1, 2 or 3 electrodes as seen from Table 5.2. This indicates that high accuracies can be achieved by carefully chosen electrodes with fewer electrodes. The demographics of the minimal optimal electrode subsets can be seen from Table 5.3. All of the electrodes are included in the minimal optimal electrode subsets at least once. However, electrode Oz is the electrode which is most found in the minimal optimal electrode set for all the subjects.

- Optimal electrode subsets: The distribution of the optimal electrode subsets over the electrode number is different between subjects. In Table 5.2, only three subjects (S5, S7 and S8) have no optimal electrode subsets for all electrode numbers. For example, S7 has no optimal electrode subsets for electrode number 1 and 2. For the subjects who have high classification accuracies, there are more optimal electrode subsets than the subjects who have lower classification accuracies. In general, the electrode subsets with more electrodes are more likely to become optimal than fewer electrodes. The classification accuracies are based on the signals of the electrodes. Therefore, more electrodes mean more information and result in higher accuracies. However, it is also possible that the additions of more electrodes are redundant and have no actual impact on the classification performance. For example, in CCA classification, if the additional electrode is the linear combination of the existing electrodes, the addition of this electrode might not have any impact on the result. In other words, if

the subset of the optimal electrode set is already an optimal electrode set, it is likely that the additional electrode(s) might not have real impact. It might require more to fully understand the interaction of the electrodes and give a better definition of the optimal electrode sets but only dependent on the classification accuracies.

Lin et al. (2006) also proposed a channel selection based on CCA. Several electrodes were selected by prior knowledge. For each electrode, its nearest M electrodes were further selected to combine a patch. The patch containing (M+1) electrodes was used to compute CCA coefficient which was assigned to this channel. The channel was selected based on the average of CCA coefficients corresponding to the stimulating frequencies used in BCI system. The results showed the inter-subject variance. However, most of the selected electrodes across subjects were located in occipital area. In their study, M was equal to 5 and the 8 best electrodes were selected for each subject.

Friman et al. (2007) also inspected the impact of electrode number used on the classification. In their study, only the best classification accuracy corresponding to one electrode number was recorded. Their result showed that the higher the electrode number was, the higher the best classification accuracy is using MEC and MCC classification methods.

6.7 Electrode rankings and selection

This study proposes a method to rank the electrodes using the coefficients of the spatial filter or single electrode classification accuracy. The electrode rankings are used to select the electrodes according to the number of the electrodes required. When the electrodes are ranked by the coefficients of the spatial filter, the rankings are based on the importance of the electrode which is the absolute value of its coefficient in transfer matrix. On the other hand, when the electrodes are ranked by the single electrode accuracies, the rankings are based on individual electrode independent of the other electrodes. The importance of the electrode purely depends on the classification accuracy resulting from the corresponding electrode alone. These two methods of rankings require the least computation loads, 20 and 220 classifications for the coefficient method and the accuracy method respectively.

Electrodes are ranked by using the leave–one–out rule. The validation results of PIs are encouraging and promising. The majority PIs are higher than 50% for all subjects, the mean PI across the electrode numbers (1 to 10) over the subjects are 77% $\pm$ 13% and 78% $\pm$ 13% for the coefficients and accuracies, respectively. PIs indicates the ranked electrode subsets are more likely to have at least same performance as the randomly chosen electrode subsets across all the electrode numbers. PIs also demonstrate the proposed electrode rankings an efficient and reliable way in selecting electrodes.

6.8 Summary

As seen in Table 6.1, there are many factors which can affect SSVEP response. Changing the viewing distance also change several parameters. The intensity of visual stimulus decreased as the viewing distance increased. To achieve the same accuracy in one stimulus experiment, the greater distance requires higher intensity. However, in a four-class BCI setup, the classification accuracies decreased at the greater viewing distance even the intensity is highest. There are several explanations. The greater viewing distances make it difficult for the subjects to attend and focus. The high intensity compensation could induce the subject visual fatigue. The greater viewing distances also increase the competition between attended and unattended targets. As a consequence, the SSVEP response of the unattended targets increased.

This chapter also analyzes the electrode ranking algorithm. Optimal electrode subsets show great inter-subject variance in terms of the classification accuracies and electrode locations. PI demonstrates the usefulness of the proposed electrode ranking method.

Chapter 7

Conclusions and future work

This study investigates the feasibility of developing a novel distance adaptable SSVEP based BCI. The results obtained have demonstrated the feasibility of the proposed BCI paradigm. This final chapter concludes the thesis by presenting a summarised critique of the study conducted. The critique will give an account of contributions, limitations and main conclusions of this study. Finally, the chapter presents possible directions of the future work.

7.1 Contributions

The following are the main contributions of this study:

1. **Proposition and demonstration of the feasibility of a novel distance adaptable SSVEP based BCI.** The implementation of the proposed SSVEP BCI is described in Chapter 3. The design, experiment protocol and data analysis can also be found in Chapter 3. Its feasibility can be found in the data analysis of Chapter 5.

2. **Provide the evidence of how viewing distance affects SSVEP response in terms of power strength and other properties and how to compensate it.** In this study it was found that SSVEP response and several SSVEP signal properties become weaker as viewing distance increases. This impact can be compensated by changing the intensities of the visual stimuli. The impact of viewing distance on SSVEP response and the classification accuracies in uncompensated and compensated conditions can be seen in Chapter 4.

3. **Demonstrate the relationship between SSVEP response and the intensity of the visual stimulus.** The intensity compensation corresponding to the change in viewing distance is evaluated by the initial resistor/intensity selection experiment. The resistor/intensity selection experiment design and results can be found in Chapters 3, 5 and 6.

4. **Perform comprehensive analysis to investigate the impact of the number of electrodes over BCI classification accuracies.** In this

study, 11 EEG recording electrodes over the visual cortex are chosen using prior knowledge. Based on the pre–selected electrodes, the classification accuracies of all possible combinations (more than 2000 combinations) of the electrodes with different electrode numbers are evaluated. See Chapters 3 and 5.

5. **Propose and implement a simple, effective and flexible electrode selection method.** An electrodes selection method based on the rankings of the electrodes is proposed. 11 pre–selected electrodes are ranked according to the coefficients of the filters or the classification accuracies. The rankings of the electrodes are used as the order to select the electrodes. The results show that the electrodes selected based on this ranking method outperform the random selection. See Chapter 5.

6. **Investigate and identify the source of deterioration of SSVEP classification accuracies in BCI setup.** Based on the data of this study, the sources of deterioration of SSVEP classification accuracies are spontaneous EEG and unattended targets. The impact of the unattended targets is highly related to the viewing distance. The impact of unattended targets is more prominent as the viewing distance increases. See Chapters 4, 5 and 6.

7.2 Limitations

The limitations of the current study are mainly bound to the constraints of time and resources. We acknowledge the following limitations:

1. Subjects: Due to the time length of the experiment, and subsequent recorded data size analysis, only 10 subjects in total were recruited in the study. Several SSVEP studies (Friman et al., 2007; Lin et al., 2006; Bin et al., 2009b) also recruited a similar number of subjects, 10, 11 and 12 respectively. The participants of this study are younger than 50 years old. However, the potential target users of the intended system might be older than 50 years old. To recruit more subjects in different ages is one of the directions of future work.

2. Experimental setup: There are a few limitations of the experimental setup,

   (a) Viewing distance: Only four fixed viewing distances were tested, 60cm, 150cm, 250cm and 350cm. Viewing distance of 60cm between the visual stimulators and the subjects has been used in a few SSVEP studies (Kelly et al., 2005a,c; Zhang et al., 2010a; Jia et al., 2011; Zhang et al., 2012; Hwang et al., 2012). In this study, longer viewing distances of 150cm, 250cm and 350cm are also evaluated.

   (b) The experiment setup is restricted to the data recording system which connected the electrodes to the amplifier. When changing the viewing distance, the visual stimuli also need to be moved to a different

distance. As a result, (1) the subjects were confined to a particular area, (2) the change of the viewing distances is in a fixed order which is 60cm-150cm-250cm-350cm. It cannot be ruled out that subject fatigue may contribute to the performance at 350cm.

Most BCI studies use the conventional EEG recording system. The subjects wear an EEG cap with electrode cables connected to EEG acquisition equipments(Kelly et al., 2005a; Lin et al., 2006; Friman et al., 2007; Bin et al., 2009b; Hwang et al., 2012; Zhang et al., 2012). However, with advances in wearable and wireless technologies, there are more SSVEP studies employing wearable wireless EEG recording devices (Piccini et al., 2005; Wang et al., 2011; Liao et al., 2012; Lin et al., 2014). This would be one of the directions of future work.

Furthermore, the experiment protocol is not always random in SSVEP BCI study. For example, Lin et al. (2014) evaluated the feasibility of a commercial EEG recording device used in SSVEP BCI during walking. In their study, treadmill was used to imitate walking. The speeds in their study were also in a fixed order, 0m/s–0.45m/s–0.89m/s–1.34 m/s.

(c) Visual stimuli: Intensities of the stimuli are fixed based on the results of the experiment from one subject. Other parameters of the visual stimuli were also fixed such as colours, stimulating frequencies, and the duty cycle of the waveform. Several SSVEP BCI studies also fixed the intensities, colours, stimulating frequencies and the duty cycle of the visual stimuli (Gao et al., 2003; Zhu et al., 2010a; Hwang et al., 2012).

(d) Position of the visual stimuli: The subjects were instructed to fixate their gaze at the centre of the board during the experiment. The position of the board was kept at the same height regardless of the height of the subjects. However, this position could affect the visual angle subtended between LEDs and subjects.

3. SSVEP modulation methods: In this study, SSVEP was frequency modulated. There are other methods which can modulate visual stimuli, such as mixing phase and frequency, dual frequencies stimulation and half filed stimulation pattern (Lee et al., 2010; Shyu et al., 2010; Materka and Byczuk, 2006; Materka and Poryzala, 2013). More information on these methods can be found in Table 2.1 on page 43.

4. Data analysis methods: There were several other methods which can extract the features of SSVEP. However, due to the length of time, only CCA, MEC and MCC were used. Other classification methods include conventional FFT, SLIC in time domain and continuous wavelet transform (Gao et al., 2003; Hwang et al., 2012; Luo and Sullivan, 2010; Zhang et al., 2010b). In this study, FFT and SLIC were used to visualise SSVEP.

5. Performance measurement: Due to the restriction of time, this study evaluates the feasibility of the proposed system by using classification accuracy. This study did not evaluate other performance measurements, such as comfort and speed (Lee et al., 2011; Gao et al., 2003; Hwang et al., 2012).

7.3 Conclusions

A novel distance adaptable SSVEP based BCI is proposed in this study. This study first investigates the impact of viewing distance on SSVEP response and the classification accuracies. It is found that the impact of the viewing distance on SSVEP response can be compensated by changing the visual stimuli. Next, its feasibility is evaluated by presenting four red LEDs flickering at 12, 13, 14 and 15Hz at four viewing distances of 60cm, 150cm, 250cm and 350cm to subjects. EEG data are analysed in terms of its power, time– and phase– locking to the stimulus properties and classification accuracies. The impact of the number and location of the electrodes is also investigated. Moreover, the sources of deterioration of SSVEP detection in BCI setup are also inspected and identified. The main conclusions of this study are summarised as follows:

1. The classification accuracies demonstrate the feasibility of the proposed distance adaptable SSVEP BCI.

2. There is a great inter-subject variance in classification accuracies.

3. SSVEP response can be affected by the change of the viewing distance between the users and the visual stimulators. The change of the viewing distance also changes other parameters which are related to the SSVEP response. The compensation of the intensity of visual stimuli can improve the SSVEP response and classification accuracies significantly. However, intensity is not the only one parameter affected by the viewing distance. The change of the viewing distance also affect the attention, increase the competition between targets and the corresponding high intensity induce the visual fatigue. They all have impact on the performance.

4. The number of the recording electrodes has no direct impact on the classification accuracy, i.e. more recording electrodes do not always result in a higher classification rate. The location of the recording electrodes is more important.

5. The true positive rate and false positive rate of the stimulating frequencies are highly correlated, i.e. the stimulating frequency resulting in high true positives also results in high false positives.

6. The spontaneous EEG is one of the sources causing deterioration of SSVEP classification accuracies. The other source of deterioration of SSVEP classification accuracies is the unattended targets. The impact of the unattended targets is related to the viewing distance and the stimulating frequencies.

7.4 Future work

This study has demonstrated the feasibility of the proposed SSVEP BCI paradigm. However, there are many potential perspectives related to this study, both in academia research and commercial application developments. The future work includes:

1. Subjects: Further study is required to investigate the root causes of the inter-subject variance. As there are many parameters which can affect SSVEP response, one of the direction of inter-subject study might focus on the sensitivities and priorities of different parameters to the subjects.

   The subjects with age within the target population should be included.

2. Optimal intensities of the visual stimuli: Further study is required to investigate the optimal intensities of the visual stimuli corresponding to viewing distance. The higher intensities not only enhance the SSVEP response but also induce the visual fatigue and discomfort which also affect the performance. In a multiple choice SSVEP BCI, higher intensities also increase the inference from the unattended targets. The optimal intensities should trade off BCI performance against the comfort of the users.

3. Visual stimuli: SSVEP responses are highly related to the colours, sizes, stimulating frequencies, duty cycles and driving waveforms of the visual stimuli. Some of the parameters are correlated to each other, for example colours and frequencies. Present study is focused on the evaluation of the feasibility of the distance adaptable SSVEP BCI. Future work should also take the user comfort into account by different choice of the colour and stimulating frequencies. In the practical system, these parameters should be able to change and adapt according to the comfort, preference and performance of the individuals.

4. Viewing angle of the visual stimuli(LEDs): In an ideal scenario, the vision of the subjects is expected to be within the extended viewing angle of attended LEDs and fall out the ones of the unattended. A narrow viewing angle can reduce the interference of the unattended but also make it easier to fall out the viewing angle of the attended target. On the other hand, a wide viewing angle can increase interference of the unattended but easier to fall within the viewing angle region of the attended. The future work should investigate this effect and find the optimal trade off.

5. Interference between stimulating frequencies: It has been well known that the stimulating frequency plays an important part in SSVEP based BCI. However, the interference caused by different combinations of stimulating frequencies in the BCI application is not clear or understood.

6. Experiment setup: The experiment setup should be close to realistic environment. The visual stimuli should be located in a fixed position. The

users should be able to move around and attend the stimulus in any positions within the limitations. The intensities of the visual stimulus should response to the attending position as well as the background intensity where BCI is operated.

The practical BCI should have more than one selection. Therefore the layout and design of the visual stimuli are important. The layout of the visual stimuli should reduce the level of competition of the stimuli, especially at greater viewing distance. The layout of the stimuli also affects the choice of LED, especially the viewing angle of LED. With the advance of the display technology, the visual stimuli are not limited to LEDs. The design of the visual stimuli should improve the performance of BCI and the attention of the users but reduce the visual fatigue and tiredness.

7. Performance measurement: There are other metrics which are worth investigating, such as the comfort of the subjects in terms of the user interface, the colour, the stimulating frequencies and layout of the stimuli.

8. Stimulation methods: This study uses the conventional SSVEP stimulation method, i.e. one target is assigned a distinct frequency. It would be worthy investigating if other different stimulation methods can also achieve the results similar to or better than the results of this study, for example, mixing same frequency with different phases.

9. Evaluation of the effectiveness and usefulness of the proposed BCI in different applications: With the flexible viewing distance, the proposed SSVEP based BCI can be applied to control applications which require flexible space, for example serious games in rehabilitation therapy for patients of stroke and Parkinson′s disease and the intelligent care environment for the older population to help and improve their independence. BCI control can be an option for induced disability in the applications of entertainment game and smart home control for healthy population.

10. Investigation of distractors and intensity in real environment: These distractors include sound, other objects or subjects present and walking in the trial. The distractors can affect the attention of the users and affect SSVEP response. The intensity of the background could affect modulation depth and SSVEP response. These factors need to be taken into account when applying the proposed BCI into practice.

11. Investigate and compare the effectiveness of classification methods using native programming language, such as C/C++.

12. Investigate the effect of LED colour to the subjects with eyesight problem.

References

Ahn, M., Ahn, S., Hong, J. H., Cho, H., Kim, K., Kim, B. S., Chang, J. W., and Jun, S. C. (2013). Gamma band activity associated with BCI performance: simultaneous MEG/EEG study. *Frontiers in human neuroscience*, 7.

Al-ani, T. and Trad, D. (2010). Signal Processing and Classification Approaches for Brain-computer Interface. *Intelligent and Biosensors, Edited by Vernon S. Somerset*, pages 25–66.

Allison, B., Graimann, B., and Gräser, A. (2007). Why use a BCI if you are healthy. In *ACE Workshop-Brain-Computer Interfaces and Games*, pages 7–11.

Allison, B., Luth, T., Valbuena, D., Teymourian, A., Volosyak, I., and Graser, A. (2010a). BCI demographics: How many (and what kinds of) people can use an SSVEP BCI? *Neural Systems and Rehabilitation Engineering, IEEE Transactions on*, 18(2):107–116.

Allison, B. Z., Brunner, C., Altstätter, C., Wagner, I. C., Grissmann, S., and Neuper, C. (2012). A hybrid ERD/SSVEP BCI for continuous simultaneous two dimensional cursor control. *Journal of neuroscience methods*, 209(2):299–307.

Allison, B. Z., Brunner, C., Kaiser, V., Müller-Putz, G. R., Neuper, C., and Pfurtscheller, G. (2010b). Toward a hybrid brain–computer interface based on imagined movement and visual attention. *Journal of neural engineering*, 7(2):026007.

Allison, B. Z., McFarland, D. J., Schalk, G., Zheng, S. D., Jackson, M. M., and Wolpaw, J. R. (2008). Towards an independent brain–computer interface using steady state visual evoked potentials. *Clinical Neurophysiology*, 119(2):399–408.

Amiri, S., Fazel-Rezai, R., and Asadpour, V. (2013a). A review of hybrid brain-computer interface systems. *Advances in Human-Computer Interaction*, 2013:1.

Amiri, S., Rabbi, A., Azinfar, L., and Fazel-Rezai, R. (2013b). A Review of P300, SSVEP, and Hybrid P300/SSVEP Brain-Computer Interface Systems.

Ang, K. K. and Guan, C. (2013). Brain-computer interface in stroke rehabilitation. *Journal of Computing Science and Engineering*, 7(2):139–146.

Arvaneh, M., Guan, C., Ang, K. K., and Quek, C. (2011). Optimizing the channel selection and classification accuracy in EEG-based BCI. *Biomedical Engineering, IEEE Transactions on*, 58(6):1865–1873.

Barbero, Á. and Grosse-Wentrup, M. (2010). Biased feedback in brain-computer interfaces. *Journal of neuroengineering and rehabilitation*, 7(1):34.

Barry, R. J. (2009). Evoked activity and EEG phase resetting in the genesis of auditory Go/NoGo ERPs. *Biological psychology*, 80(3):292–299.

Bashashati, A., Fatourechi, M., Ward, R. K., and Birch, G. E. (2007). A survey of signal processing algorithms in brain–computer interfaces based on electrical brain signals. *Journal of Neural engineering*, 4(2):R32.

Becker, R., Ritter, P., and Villringer, A. (2008). Influence of ongoing alpha rhythm on the visual evoked potential. *Neuroimage*, 39(2):707–716.

Bieger, J., Molina, G. G., and Zhu, D. (2010). Effects of stimulation properties in steady-state visual evoked potential based brain-computer interfaces. In *Proceedings of 32nd Annual International Conference of the IEEE Engineering in Medicine and Biology Society*, pages 3345–8.

Bin, G., Gao, X., Wang, Y., Hong, B., and Gao, S. (2009a). VEP-based brain-computer interfaces: time, frequency, and code modulations [Research Frontier]. *Computational Intelligence Magazine, IEEE*, 4(4):22–26.

Bin, G., Gao, X., Wang, Y., Li, Y., Hong, B., and Gao, S. (2011). A high-speed BCI based on code modulation VEP. *Journal of neural engineering*, 8(2):025015.

Bin, G., Gao, X., Yan, Z., Hong, B., and Gao, S. (2009b). An online multi-channel SSVEP-based brain–computer interface using a canonical correlation analysis method. *Journal of neural engineering*, 6(4):046002.

Birbaumer, N. (2006). Breaking the silence: brain–computer interfaces (BCI) for communication and motor control. *Psychophysiology*, 43(6):517–532.

Birbaumer, N. and Cohen, L. G. (2007). Brain–computer interfaces: communication and restoration of movement in paralysis. *The Journal of physiology*, 579(3):621–636.

Birbaumer, N., Ghanayim, N., Hinterberger, T., Iversen, I., Kotchoubey, B., Kübler, A., Perelmouter, J., Taub, E., and Flor, H. (1999). A spelling device for the paralysed. *Nature*, 398(6725):297–298.

Birbaumer, N., Hinterberger, T., Kubler, A., and Neumann, N. (2003). The thought-translation device (TTD): neurobehavioral mechanisms and clinical outcome. *Neural Systems and Rehabilitation Engineering, IEEE Transactions on*, 11(2):120–123.

Birbaumer, N., Kübler, A., Ghanayim, N., Hinterberger, T., Perelmouter, J., Kaiser, J., Iversen, I., Kotchoubey, B., Neumann, N., and Flor, H. (2000). The thought translation device (TTD) for completely paralyzed patients. *IEEE Transactions on rehabilitation Engineering*, 8(2):191.

Blankertz, B., Losch, F., Krauledat, M., Dornhege, G., Curio, G., and Muller, K.-R. (2008a). The Berlin Brain–Computer Interface: accurate performance from first-session in BCI-naive subjects. *Biomedical Engineering, IEEE Transactions on*, 55(10):2452–2462.

Blankertz, B., Sannelli, C., Halder, S., Hammer, E. M., Kübler, A., Müller, K.-R., Curio, G., and Dickhaus, T. (2010a). Neurophysiological predictor of SMR-based BCI performance. *Neuroimage*, 51(4):1303–1309.

Blankertz, B., Tangermann, M., Vidaurre, C., Fazli, S., Sannelli, C., Haufe, S., Maeder, C., Ramsey, L., Sturm, I., Curio, G., et al. (2010b). The Berlin brain–computer interface: non-medical uses of BCI technology. *Frontiers in neuroscience*, 4.

Blankertz, B., Tomioka, R., Lemm, S., Kawanabe, M., and Muller, K.-R. (2008b). Optimizing spatial filters for robust EEG single-trial analysis. *Signal Processing Magazine, IEEE*, 25(1):41–56.

Brouwer, A.-M. and Van Erp, J. B. (2010). A tactile P300 brain-computer interface. *Frontiers in neuroscience*, 4.

Brunner, C., Allison, B. Z., Krusienski, D. J., Kaiser, V., Müller-Putz, G. R., Pfurtscheller, G., and Neuper, C. (2010). Improved signal processing approaches in an offline simulation of a hybrid brain–computer interface. *Journal of neuroscience methods*, 188(1):165–173.

Cao, T., Wan, F., Mak, P. U., Mak, P.-I., Vai, M. I., and Hu, Y. (2012). Flashing color on the performance of ssvep-based brain-computer interfaces. In *Engineering in Medicine and Biology Society (EMBC), 2012 Annual International Conference of the IEEE*, pages 1819–1822. IEEE.

Cecotti, H. (2010a). A self-paced and calibration-less SSVEP-based brain–computer interface speller. *Neural Systems and Rehabilitation Engineering, IEEE Transactions on*, 18(2):127–133.

Cecotti, H. (2010b). Classification of Steady-State Visual Evoked Potentials based on the visual stimuli duty cycle. In *Applied Sciences in Biomedical and Communication Technologies (ISABEL), 2010 3rd International Symposium on*, pages 1–5. IEEE.

Chang, H.-C., Lee, P.-L., Lo, M.-T., Lee, I.-H., Yeh, T.-K., and Chang, C.-Y. (2012). Independence of amplitude-frequency and phase calibrations in an SSVEP-based BCI using stepping delay flickering sequences. *Neural Systems and Rehabilitation Engineering, IEEE Transactions on*, 20(3):305–312.

Chang, M. H., Baek, H. J., Lee, S. M., and Park, K. S. (2014). An amplitude-modulated visual stimulation for reducing eye fatigue in SSVEP-based brain–computer interfaces. *Clinical Neurophysiology*, 125(7):1380–1391.

Chen, Y., Seth, A. K., Gally, J. A., and Edelman, G. M. (2003). The power of human brain magnetoencephalographic signals can be modulated up or down by changes in an attentive visual task. *Proceedings of the National Academy of Sciences*, 100(6):3501–3506.

Cheng, M., Gao, X., Gao, S., and Xu, D. (2001). Multiple color stimulus induced steady state visual evoked potentials. In *Engineering in Medicine and Biology Society, 2001. Proceedings of the 23rd Annual International Conference of the IEEE*, volume 2, pages 1012–1014. IEEE.

Choi, B. and Jo, S. (2013). A Low-Cost EEG System-Based Hybrid Brain-Computer Interface for Humanoid Robot Navigation and Recognition. *PloS one*, 8(9):e74583.

Cincotti, F., Mattia, D., Aloise, F., Bufalari, S., Schalk, G., Oriolo, G., Cherubini, A., Marciani, M. G., and Babiloni, F. (2008). Non-invasive brain–computer interface system: towards its application as assistive technology. *Brain research bulletin*, 75(6):796–803.

Combrisson, E. and Jerbi, K. (2015). Exceeding chance level by chance: The caveat of theoretical chance levels in brain signal classification and statistical assessment of decoding accuracy. *Journal of neuroscience methods*, 250:126–136.

Daly, J. J. and Wolpaw, J. R. (2008). Brain–computer interfaces in neurological rehabilitation. *The Lancet Neurology*, 7(11):1032–1043.

Delorme, A. and Makeig, S. (2004). EEGLAB: an open source toolbox for analysis of single-trial EEG dynamics including independent component analysis. *Journal of neuroscience methods*, 134(1):9–21.

Di Russo, F., Pitzalis, S., Aprile, T., Spitoni, G., Patria, F., Stella, A., Spinelli, D., and Hillyard, S. A. (2007). Spatiotemporal analysis of the cortical sources of the steady-state visual evoked potential. *Human brain mapping*, 28(4):323–334.

Di Russo, F., Teder-Sälejärvi, W. A., and Hillyard, S. A. (2002). Steady-state VEP and attentional visual processing. *The cognitive electrophysiology of mind and brain (Zani A, Proverbio AM, eds)*, pages 259–274.

Diez, P. F., Mut, V. A., Perona, E. M. A., and Leber, E. L. (2011). Asynchronous BCI control using high-frequency SSVEP. *Journal of neuroengineering and rehabilitation*, 8(1):39.

Diez, P. F., Torres Müller, S. M., Mut, V. A., Laciar, E., Avila, E., Bastos-Filho, T. F., and Sarcinelli-Filho, M. (2013). Commanding a robotic wheelchair with a high-frequency steady-state visual evoked potential based brain–computer interface. *Medical engineering & physics*, 35(8):1155–1164.

Ding, J., Sperling, G., and Srinivasan, R. (2006). Attentional modulation of SSVEP power depends on the network tagged by the flicker frequency. *Cerebral cortex*, 16(7):1016–1029.

Dodgson, N. A. (2004). Variation and extrema of human interpupillary distance. In *Electronic imaging 2004*, pages 36–46. International Society for Optics and Photonics.

Duszyk, A., Bierzyńska, M., Radzikowska, Z., Milanowski, P., Kuś, R., Suffczyński, P., Michalska, M., Łabecki, M., Zwoliński, P., and Durka, P. (2014). Towards an optimization of stimulus parameters for brain-computer interfaces based on steady state visual evoked potentials. *PloS one*, 9(11):e112099.

Edlinger, G. and Guger, C. (2012). A hybrid brain-computer interface for improving the usability of a smart home control. In *Complex Medical Engineering (CME), 2012 ICME International Conference on*, pages 182–185. IEEE.

Edlinger, G., Holzner, C., and Guger, C. (2011). A hybrid brain-computer interface for smart home control. In *Human-Computer Interaction. Interaction Techniques and Environments*, pages 417–426. Springer.

Farwell, L. A. and Donchin, E. (1988). Talking off the top of your head: toward a mental prosthesis utilizing event-related brain potentials. *Electroencephalography and clinical Neurophysiology*, 70(6):510–523.

Fatourechi, M., Bashashati, A., Ward, R. K., and Birch, G. E. (2007). EMG and EOG artifacts in brain computer interface systems: A survey. *Clinical neurophysiology*, 118(3):480–494.

Fawcett, T. (2006). An introduction to ROC analysis. *Pattern recognition letters*, 27(8):861–874.

Fazel-Rezai, R. and Abhari, K. (2009). A region-based P300 speller for brain-computer interface. *Electrical and Computer Engineering, Canadian Journal of*, 34(3):81–85.

Fell, J., Dietl, T., Grunwald, T., Kurthen, M., Klaver, P., Trautner, P., Schaller, C., Elger, C. E., and Fernández, G. (2004). Neural bases of cognitive ERPs: more than phase reset. *Journal of cognitive neuroscience*, 16(9):1595–1604.

Fernandez-Vargas, J., Pfaff, H. U., Rodríguez, F. B., and Varona, P. (2013). Assisted closed-loop optimization of SSVEP-BCI efficiency. *Frontiers in neural circuits*, 7.

Fisher, R. S., Harding, G., Erba, G., Barkley, G. L., and Wilkins, A. (2005). Photic-and Pattern-induced Seizures: A Review for the Epilepsy Foundation of America Working Group. *Epilepsia*, 46(9):1426–1441.

Friman, O., Volosyak, I., and Graser, A. (2007). Multiple channel detection of steady-state visual evoked potentials for brain-computer interfaces. *Biomedical Engineering, IEEE Transactions on*, 54(4):742–750.

Fuchs, S., Andersen, S. K., Gruber, T., and Müller, M. M. (2008). Attentional bias of competitive interactions in neuronal networks of early visual processing in the human brain. *NeuroImage*, 41(3):1086–1101.

Furdea, A., Halder, S., Krusienski, D., Bross, D., Nijboer, F., Birbaumer, N., and Kübler, A. (2009). An auditory oddball (P300) spelling system for brain-computer interfaces. *Psychophysiology*, 46(3):617–625.

Gao, X., Xu, D., Cheng, M., and Gao, S. (2003). A BCI-based environmental controller for the motion-disabled. *Neural Systems and Rehabilitation Engineering, IEEE Transactions on*, 11(2):137–140.

Garcia-Molina, G. and Zhu, D. (2011). Optimal spatial filtering for the steady state visual evoked potential: BCI application. In *Neural Engineering (NER), 2011 5th International IEEE/EMBS Conference on*, pages 156–160. IEEE.

Gollee, H., Volosyak, I., McLachlan, A. J., Hunt, K. J., and Gräser, A. (2010). An SSVEP-based brain–computer interface for the control of functional electrical stimulation. *IEEE Transactions on Biomedical Engineering*, 57(8):1847–1855.

Guan, C., Thulasidas, M., and Wu, J. (2004). High performance P300 speller for brain-computer interface. In *Biomedical Circuits and Systems, 2004 IEEE International Workshop on*, pages S3–5. IEEE.

Guger, C., Allison, B. Z., Großwindhager, B., Prückl, R., Hintermüller, C., Kapeller, C., Bruckner, M., Krausz, G., Edlinger, G., et al. (2011). How many people could use an SSVEP BCI? *Frontiers in neuroscience*, 6:169–169.

Guger, C., Daban, S., Sellers, E., Holzner, C., Krausz, G., Carabalona, R., Gramatica, F., and Edlinger, G. (2009). How many people are able to control a P300-based brain–computer interface (BCI)? *Neuroscience letters*, 462(1):94–98.

Guger, C. and Edlinger, G. (2007). How many people can control a brain-computer interface (BCI). *Proc. BrainPlay*, pages 29–32.

Guger, C., Harkam, W., Hertnaes, C., and Pfurtscheller, G. (1999). Prosthetic control by an EEG-based brain-computer interface (BCI). In *Proc. aaate 5th european conference for the advancement of assistive technology*, pages 3–6.

Hagen, G. F., Gatherwright, J. R., Lopez, B. A., and Polich, J. (2006). P3a from visual stimuli: task difficulty effects. *International journal of psychophysiology*, 59(1):8–14.

Hanslmayr, S., Klimesch, W., Sauseng, P., Gruber, W., Doppelmayr, M., Freunberger, R., Pecherstorfer, T., and Birbaumer, N. (2007). Alpha phase reset contributes to the generation of ERPs. *Cerebral Cortex*, 17(1):1–8.

Herrmann, C. S. (2001). Human EEG responses to 1–100 Hz flicker: resonance phenomena in visual cortex and their potential correlation to cognitive phenomena. *Experimental brain research*, 137(3-4):346–353.

Hoffmann, U., Vesin, J.-M., Ebrahimi, T., and Diserens, K. (2008). An efficient P300-based brain–computer interface for disabled subjects. *Journal of Neuroscience methods*, 167(1):115–125.

Hong, B., Guo, F., Liu, T., Gao, X., and Gao, S. (2009). N200-speller using motion-onset visual response. *Clinical neurophysiology*, 120(9):1658–1666.

Huggins, J. E., Wren, P. A., and Gruis, K. L. (2011). What would brain-computer interface users want? Opinions and priorities of potential users with amyotrophic lateral sclerosis. *Amyotrophic Lateral Sclerosis*, 12(5):318–324.

Hwang, H.-J., Hwan Kim, D., Han, C.-H., and Im, C.-H. (2013). A new dual-frequency stimulation method to increase the number of visual stimuli for multi-class SSVEP-based brain–computer interface (BCI). *brain research*, 1515:66–77.

Hwang, H.-J., Lim, J.-H., Jung, Y.-J., Choi, H., Lee, S. W., and Im, C.-H. (2012). Development of an SSVEP-based BCI spelling system adopting a QWERTY-style LED keyboard. *Journal of neuroscience methods*, 208(1):59–65.

Jafarifarmand, A. and Badamchizadeh, M. A. (2013). Artifacts removal in EEG signal using a new neural network enhanced adaptive filter. *Neurocomputing*, 103:222–231.

Jansen, B. H., Agarwal, G., Hegde, A., and Boutros, N. N. (2003). Phase synchronization of the ongoing EEG and auditory EP generation. *Clinical Neurophysiology*, 114(1):79–85.

Jia, C., Gao, X., Hong, B., and Gao, S. (2011). Frequency and phase mixed coding in SSVEP-based brain–computer interface. *Biomedical Engineering, IEEE Transactions on*, 58(1):200–206.

Kaiser, V., Daly, I., Pichiorri, F., Mattia, D., Müller-Putz, G. R., and Neuper, C. (2012). Relationship between electrical brain responses to motor imagery and motor impairment in stroke. *Stroke*, 43(10):2735–2740.

Kanemura, A., Morales, Y., Kawanabe, M., Morioka, H., Kallakuri, N., Ikeda, T., Miyashita, T., Hagita, N., and Ishii, S. (2013). A waypoint-based framework in brain-controlled smart home environments: Brain interfaces, domotics, and robotics integration. In *Intelligent Robots and Systems (IROS), 2013 IEEE/RSJ International Conference on*, pages 865–870. IEEE.

Käthner, I., Ruf, C. A., Pasqualotto, E., Braun, C., Birbaumer, N., and Halder, S. (2013). A portable auditory P300 brain–computer interface with directional cues. *Clinical neurophysiology*, 124(2):327–338.

Keitel, C., Andersen, S. K., and Müller, M. M. (2010). Competitive effects on steady-state visual evoked potentials with frequencies in-and outside the alpha band. *Experimental brain research*, 205(4):489–495.

Kelly, S., Lalor, E., Reilly, R., and Foxe, J. (2005a). Independent brain computer interface control using visual spatial attention-dependent modulations of parieto-occipital alpha. In *Neural Engineering, 2005. Conference Proceedings. 2nd International IEEE EMBS Conference on*, pages 667–670. IEEE.

Kelly, S. P., Lalor, E. C., Reilly, R. B., and Foxe, J. J. (2005b). Visual spatial attention tracking using high-density SSVEP data for independent brain-computer communication. *Neural Systems and Rehabilitation Engineering, IEEE Transactions on*, 13(2):172–178.

Kelly, S. P., Lalor, E. C., Finucane, C., McDarby, G., and Reilly, R. B. (2005c). Visual spatial attention control in an independent brain-computer interface. *Biomedical Engineering, IEEE Transactions on*, 52(9):1588–1596.

Kelly, S. P., Lalor, E. C., Reilly, R. B., and Foxe, J. J. (2005d). Visual spatial attention tracking using high-density SSVEP data for independent brain-computer communication. *Neural Systems and Rehabilitation Engineering, IEEE Transactions on*, 13(2):172–178.

Klimesch, W., Russegger, H., Doppelmayr, M., and Pachinger, T. (1998). A method for the calculation of induced band power: implications for the significance of brain oscillations. *Electroencephalography and Clinical Neurophysiology/Evoked Potentials Section*, 108(2):123–130.

Klimesch, W., Sauseng, P., Hanslmayr, S., Gruber, W., and Freunberger, R. (2007). Event-related phase reorganization may explain evoked neural dynamics. *Neuroscience & Biobehavioral Reviews*, 31(7):1003–1016.

Krishnan, G. P., Vohs, J. L., Hetrick, W. P., Carroll, C. A., Shekhar, A., Bockbrader, M. A., and O'Donnell, B. F. (2005). Steady state visual evoked potential abnormalities in schizophrenia. *Clinical neurophysiology*, 116(3):614–624.

Kronegg, J., Voloshynovskiy, S., and Pun, T. (2005). Analysis of bit-rate definitions for Brain-Computer Interfaces. In *Csrea hci*, pages 40–46.

Kübler, A. and Birbaumer, N. (2008). Brain–computer interfaces and communication in paralysis: extinction of goal directed thinking in completely paralysed patients? *Clinical neurophysiology*, 119(11):2658–2666.

Kübler, A., Holz, E., Kaufmann, T., and Zickler, C. (2013). A user centred approach for bringing BCI controlled applications to end-users. *Brain Computer Interfaces*.

Kübler, A., Kotchoubey, B., Salzmann, H.-P., Ghanayim, N., Perelmouter, J., Hömberg, V., and Birbaumer, N. (1998). Self-regulation of slow cortical potentials in completely paralyzed human patients. *Neuroscience letters*, 252(3):171–174.

Kübler, A., Neumann, N., Wilhelm, B., Hinterberger, T., and Birbaumer, N. (2004). Predictability of brain-computer communication. *Journal of Psychophysiology*, 18(2/3):121–129.

Kübler, A., Nijboer, F., Mellinger, J., Vaughan, T. M., Pawelzik, H., Schalk, G., McFarland, D., Birbaumer, N., and Wolpaw, J. R. (2005). Patients with ALS can use sensorimotor rhythms to operate a brain-computer interface. *Neurology*, 64(10):1775–1777.

Kuś, R., Duszyk, A., Milanowski, P., Łabecki, M., Bierzyńska, M., Radzikowska, Z., Michalska, M., Żygierewicz, J., Suffczyński, P., and Durka, P. J. (2013). On the quantification of SSVEP frequency responses in human EEG in realistic BCI conditions. *PloS one*, 8(10):e77536.

Lan, T., Erdogmus, D., Adami, A., Mathan, S., and Pavel, M. (2007). Channel selection and feature projection for cognitive load estimation using ambulatory EEG. *Computational intelligence and neuroscience*, 2007:8–8.

Lan, T., Erdogmus, D., Adami, A., Pavel, M., and Mathan, S. (2006). Salient EEG channel selection in brain computer interfaces by mutual information maximization. In *Engineering in Medicine and Biology Society, 2005. IEEE-EMBS 2005. 27th Annual International Conference of the*, pages 7064–7067. IEEE.

Larson, A. M. and Loschky, L. C. (2009). The contributions of central versus peripheral vision to scene gist recognition. *Journal of Vision*, 9(10):6–6.

Lebedev, M. A. and Nicolelis, M. A. (2006). Brain–machine interfaces: past, present and future. *TRENDS in Neurosciences*, 29(9):536–546.

Lee, P.-L., Hsieh, J.-C., Wu, C.-H., Shyu, K.-K., and Wu, Y.-T. (2008). Brain computer interface using flash onset and offset visual evoked potentials. *Clinical Neurophysiology*, 119(3):605–616.

Lee, P.-L., Sie, J.-J., Liu, Y.-J., Wu, C.-H., Lee, M.-H., Shu, C.-H., Li, P.-H., Sun, C.-W., and Shyu, K.-K. (2010). An SSVEP-actuated brain computer interface using phase-tagged flickering sequences: a cursor system. *Annals of biomedical engineering*, 38(7):2383–2397.

Lee, P.-L., Yeh, C.-L., Cheng, J.-S., Yang, C.-Y., and Lan, G.-Y. (2011). An SSVEP-based BCI using high duty-cycle visual flicker. *Biomedical Engineering, IEEE Transactions on*, 58(12):3350–3359.

Lee, T.-S., Goh, S. J. A., Quek, S. Y., Phillips, R., Guan, C., Cheung, Y. B., Feng, L., Teng, S. S. W., Wang, C. C., Chin, Z. Y., et al. (2013). A Brain-Computer Interface Based Cognitive Training System for Healthy Elderly: A Randomized Control Pilot Study for Usability and Preliminary Efficacy. *PloS one*, 8(11):e79419.

Leeb, R., Friedman, D., Müller-Putz, G. R., Scherer, R., Slater, M., and Pfurtscheller, G. (2007). Self-paced (asynchronous) BCI control of a wheelchair in virtual environments: a case study with a tetraplegic. *Computational intelligence and neuroscience*, 2007.

Lesenfants, D., Habbal, D., Lugo, Z., Lebeau, M., Horki, P., Amico, E., Pokorny, C., Gómez, F., Soddu, A., Müller-Putz, G., et al. (2014). An independent SSVEP-based brain–computer interface in locked-in syndrome. *Journal of neural engineering*, 11(3):035002.

Lesenfants, D., Partoune, N., Soddu, A., Lehembre, R., Müller-Putz, G., Laureys, S., and Noirhomme, Q. (2011). Design of a novel covert SSVEP-based BCI. In *Proceedings of the 5th International Brain-Computer Interface Conference 2011*. University of Technology Publishing House.

Li, J., Ji, H., Cao, L., Gu, R., Xia, B., and Huang, Y. (2013). Wheelchair Control Based on Multimodal Brain-Computer Interfaces. In *Neural Information Processing*, pages 434–441. Springer.

Liao, L.-D., Chen, C.-Y., Wang, I.-J., Chen, S.-F., Li, S.-Y., Chen, B.-W., Chang, J.-Y., and Lin, C.-T. (2012). Gaming control using a wearable and wireless EEG-based brain-computer interface device with novel dry foam-based sensors. *Journal of neuroengineering and rehabilitation*, 9(1):1.

Lim, J.-H., Hwang, H.-J., Han, C.-H., Jung, K.-Y., and Im, C.-H. (2013). Classification of binary intentions for individuals with impaired oculomotor function:eyes-closedSSVEP-based brain–computer interface (BCI). *Journal of neural engineering*, 10(2):026021.

Lin, C.-T., Chen, Y.-C., Huang, T.-Y., Chiu, T.-T., Ko, L.-W., Liang, S.-F., Hsieh, H.-Y., Hsu, S.-H., and Duann, J.-R. (2008). Development of wireless brain computer interface with embedded multitask scheduling and its application on real-time driver's drowsiness detection and warning. *Biomedical Engineering, IEEE Transactions on*, 55(5):1582–1591.

Lin, Y.-P., Wang, Y., and Jung, T.-P. (2014). Assessing the feasibility of online SSVEP decoding in human walking using a consumer EEG headset. *Journal of neuroengineering and rehabilitation*, 11(1):119.

Lin, Z., Zhang, C., Wu, W., and Gao, X. (2006). Frequency recognition based on canonical correlation analysis for SSVEP-based BCIs. *Biomedical Engineering, IEEE Transactions on*, 53(12):2610–2614.

Liu, T., Goldberg, L., Gao, S., and Hong, B. (2010). An online brain–computer interface using non-flashing visual evoked potentials. *Journal of neural engineering*, 7(3):036003.

Long, J., Li, Y., Wang, H., Yu, T., Pan, J., and Li, F. (2012). A hybrid brain computer interface to control the direction and speed of a simulated or real wheelchair. *Neural Systems and Rehabilitation Engineering, IEEE Transactions on*, 20(5):720–729.

Lopez-Gordo, M., Prieto, A., Pelayo, F., and Morillas, C. (2011). Customized stimulation enhances performance of independent binary SSVEP-BCIs. *Clinical Neurophysiology*, 122(1):128–133.

Lotte, F., Congedo, M., Lécuyer, A., Lamarche, F., Arnaldi, B., et al. (2007). A review of classification algorithms for EEG-based brain–computer interfaces. *Journal of neural engineering*, 4.

Lotte, F., Mouchere, H., and Lécuyer, A. (2008). Pattern rejection strategies for the design of self-paced eeg-based brain-computer interfaces. In *Pattern Recognition, 2008. ICPR 2008. 19th International Conference on*, pages 1–5. IEEE.

Luo, A. and Sullivan, T. J. (2010). A user-friendly SSVEP-based brain–computer interface using a time-domain classifier. *Journal of neural engineering*, 7(2):026010.

Mak, J. N. and Wolpaw, J. R. (2009). Clinical applications of brain-computer interfaces: current state and future prospects. *Biomedical Engineering, IEEE Reviews in*, 2:187–199.

Martinez, P., Bakardjian, H., and Cichocki, A. (2007). Fully online multicommand brain-computer interface with visual neurofeedback using SSVEP paradigm. *Computational intelligence and neuroscience*, 2007:13–13.

Materka, A. and Byczuk, M. (2006). Alternate half-field stimulation technique for SSVEP-based brain–computer interfaces. *Electronics Letters*, 42(6):321–322.

Materka, A. and Poryzala, P. (2013). High-speed noninvasive brain-computer interfaces. In *Human System Interaction (HSI), 2013 The 6th International Conference on*, pages 7–12. IEEE.

McFarland, D. J., McCane, L. M., David, S. V., and Wolpaw, J. R. (1997). Spatial filter selection for EEG-based communication. *Electroencephalography and clinical Neurophysiology*, 103(3):386–394.

McFarland, D. J., Sarnacki, W. A., and Wolpaw, J. R. (2003). Brain–computer interface (BCI) operation: optimizing information transfer rates. *Biological psychology*, 63(3):237–251.

Min, B.-K., Marzelli, M. J., and Yoo, S.-S. (2010). Neuroimaging-based approaches in the brain–computer interface. *Trends in biotechnology*, 28(11):552–560.

Ming, D., An, X., Xi, Y., Hu, Y., Wan, B., Qi, H., Cheng, L., and Xue, Z. (2010). Time-locked and phase-locked features of P300 event-related potentials (ERPs) for brain–computer interface speller. *Biomedical Signal Processing and Control*, 5(4):243–251.

Moratti, S., Clementz, B. A., Gao, Y., Ortiz, T., and Keil, A. (2007). Neural mechanisms of evoked oscillations: Stability and interaction with transient events. *Human brain mapping*, 28(12):1318–1333.

Morgan, S., Hansen, J., and Hillyard, S. (1996). Selective attention to stimulus location modulates the steady-state visual evoked potential. *Proceedings of the National Academy of Sciences*, 93(10):4770–4774.

Mouli, S. and Palaniappan, R. (2016). Eliciting higher ssvep response from led visual stimulus with varying luminosity levels. In *Students on Applied Engineering (ISCAE), International Conference for*, pages 201–206. IEEE.

Mukesh, T. S., Jaganathan, V., and Reddy, M. R. (2006). A novel multiple frequency stimulation method for steady state VEP based brain computer interfaces. *Physiological Measurement*, 27(1):61.

Müller, K.-R., Tangermann, M., Dornhege, G., Krauledat, M., Curio, G., and Blankertz, B. (2008). Machine learning for real-time single-trial EEG-analysis: from brain–computer interfacing to mental state monitoring. *Journal of neuroscience methods*, 167(1):82–90.

Müller, M., Andersen, S., Trujillo, N., Valdes-Sosa, P., Malinowski, P., and Hillyard, S. (2006). Feature-selective attention enhances color signals in early visual areas of the human brain. *Proceedings of the National Academy of Sciences*, 103(38):14250–14254.

Müller, M. M. and Hübner, R. (2002). Can the spotlight of attention be shaped like a doughnut? Evidence from steady-state visual evoked potentials. *Psychological Science*, 13(2):119–124.

Müller, M. M., Picton, T. W., Valdes-Sosa, P., Riera, J., Teder-Sälejärvi, W. A., and Hillyard, S. A. (1998). Effects of spatial selective attention on the steady-state visual evoked potential in the 20–28 Hz range. *Cognitive Brain Research*, 6(4):249–261.

Muller-Putz, G. R. and Pfurtscheller, G. (2008). Control of an electrical prosthesis with an SSVEP-based BCI. *Biomedical Engineering, IEEE Transactions on*, 55(1):361–364.

Müller-Putz, G. R., Scherer, R., Brauneis, C., and Pfurtscheller, G. (2005). Steady-state visual evoked potential (SSVEP)-based communication: impact of harmonic frequency components. *Journal of neural engineering*, 2(4):123.

Müller-Putz, G. R., Scherer, R., Brunner, C., Leeb, R., and Pfurtscheller, G. (2008). Better than random? A closer look on BCI results. *International Journal of Bioelectromagnetism*, 10(1):52–55.

Nakanishi, M., Wang, Y., Wang, Y.-T., Mitsukura, Y., and Jung, T.-P. (2013). An approximation approach for rendering visual flickers in SSVEP-based BCI using monitor refresh rate. In *Engineering in Medicine and Biology Society (EMBC), 2013 35th Annual International Conference of the IEEE*, pages 2176–2179. IEEE.

Neumann, N. and Birbaumer, N. (2003). Predictors of successful self control during brain-computer communication. *Journal of Neurology, Neurosurgery & Psychiatry*, 74(8):1117–1121.

Ng, K. B., Bradley, A. P., and Cunnington, R. (2011). Effect of competing stimuli on SSVEP-based BCI. In *Engineering in Medicine and Biology Society, EMBC, 2011 Annual International Conference of the IEEE*, pages 6307–6310. IEEE.

Ng, K. B., Bradley, A. P., and Cunnington, R. (2012). Stimulus specificity of a steady-state visual-evoked potential-based brain–computer interface. *Journal of Neural engineering*, 9(3):036008.

Nijboer, F., Sellers, E., Mellinger, J., Jordan, M., Matuz, T., Furdea, A., Halder, S., Mochty, U., Krusienski, D., Vaughan, T., et al. (2008). A P300-based brain–computer interface for people with amyotrophic lateral sclerosis. *Clinical neurophysiology*, 119(8):1909–1916.

Nijholt, A., Bos, D. P.-O., and Reuderink, B. (2009). Turning shortcomings into challenges: Brain–computer interfaces for games. *Entertainment Computing*, 1(2):85–94.

OSRAM, O. S. (September, 2012). Details on photobiological safety of led light sources. *Application Note*, pages 1–11.

Pan, J., Gao, X., Duan, F., Yan, Z., and Gao, S. (2011). Enhancing the classification accuracy of steady-state visual evoked potential-based brain–computer interfaces using phase constrained canonical correlation analysis. *Journal of neural engineering*, 8(3):036027.

Panicker, R. C., Puthusserypady, S., and Sun, Y. (2011). An asynchronous P300 BCI with SSVEP-based control state detection. *Biomedical Engineering, IEEE Transactions on*, 58(6):1781–1788.

Pastor, M. A., Artieda, J., Arbizu, J., Valencia, M., and Masdeu, J. C. (2003). Human cerebral activation during steady-state visual-evoked responses. *The journal of neuroscience*, 23(37):11621–11627.

Perdikis, S., Leeb, R., Williamson, J., Ramsay, A., Tavella, M., Desideri, L., Hoogerwerf, E.-J., Al-Khodairy, A., Murray-Smith, R., and d R Millán, J. (2014). Clinical evaluation of BrainTree, a motor imagery hybrid BCI speller. *Journal of neural engineering*, 11(3):036003.

Pfurtscheller, G. (2001). Functional brain imaging based on ERD/ERS. *Vision research*, 41(10):1257–1260.

Pfurtscheller, G., Allison, B. Z., Brunner, C., Bauernfeind, G., Solis-Escalante, T., Scherer, R., Zander, T. O., Mueller-Putz, G., Neuper, C., and Birbaumer, N. (2010a). The hybrid BCI. *Frontiers in neuroscience*, 4.

Pfurtscheller, G., Guger, C., Müller, G., Krausz, G., and Neuper, C. (2000a). Brain oscillations control hand orthosis in a tetraplegic. *Neuroscience letters*, 292(3):211–214.

Pfurtscheller, G. and Lopes da Silva, F. H. (1999). Event-related EEG/MEG synchronization and desynchronization: basic principles. *Clinical neurophysiology*, 110(11):1842–1857.

Pfurtscheller, G. and Neuper, C. (2001). Motor imagery and direct brain-computer communication. *Proceedings of the IEEE*, 89(7):1123–1134.

Pfurtscheller, G. and Neuper, C. (2010). Dynamics of sensorimotor oscillations in a motor task. In *Brain-Computer Interfaces*, pages 47–64. Springer.

Pfurtscheller, G., Neuper, C., Guger, C., Harkam, W., Ramoser, H., Schlogl, A., Obermaier, B., Pregenzer, M., et al. (2000b). Current trends in Graz brain-computer interface (BCI) research. *IEEE Transactions on Rehabilitation Engineering*, 8(2):216–219.

Pfurtscheller, G. and Scherer, R. (2010). Brain-computer interfaces used for virtual reality control. *Proc. ICABB*.

Pfurtscheller, G., Solis-Escalante, T., Ortner, R., Linortner, P., and Muller-Putz, G. R. (2010b). Self-paced operation of an SSVEP-Based orthosis with and without an imagery-based brain switch: a feasibility study towards a hybrid BCI. *Neural Systems and Rehabilitation Engineering, IEEE Transactions on*, 18(4):409–414.

Piccini, L., Parini, S., Maggi, L., and Andreoni, G. (2005). A wearable home BCI system: preliminary results with SSVEP protocol. In *Engineering in Medicine and Biology Society, 2005. IEEE-EMBS 2005. 27th Annual International Conference of the*, pages 5384–5387. IEEE.

Piccione, F., Giorgi, F., Tonin, P., Priftis, K., Giove, S., Silvoni, S., Palmas, G., and Beverina, F. (2006). P300-based brain computer interface: reliability and performance in healthy and paralysed participants. *Clinical neurophysiology*, 117(3):531–537.

Polich, J. (2007). Updating P300: an integrative theory of P3a and P3b. *Clinical neurophysiology*, 118(10):2128–2148.

Polich, J., Ellerson, P. C., and Cohen, J. (1996). P300, stimulus intensity, modality, and probability. *International Journal of Psychophysiology*, 23(1):55–62.

Punsawad, Y. and Wongsawat, Y. (2014). User performance evaluation with visual stimulator regulation of ssvep-based bci system. In *Asia-Pacific Signal and Information Processing Association, 2014 Annual Summit and Conference (APSIPA)*, pages 1–4. IEEE.

Resalat, S. N. and Setarehdan, S. K. (2012). A study on the effect of the inter-sources distance on the performance of the SSVEP-based BCI systems. *American Journal of Biomedical Engineering*, 2(1):24–31.

Risner, M. L., Aura, C. J., Black, J. E., and Gawne, T. J. (2009). The Visual Evoked Potential is independent of surface alpha rhythm phase. *Neuroimage*, 45(2):463–469.

Sauseng, P., Klimesch, W., Gruber, W., Hanslmayr, S., Freunberger, R., and Doppelmayr, M. (2007). Are event-related potential components generated by phase resetting of brain oscillations? A critical discussion. *Neuroscience*, 146(4):1435–1444.

Savić, A. M., Malešević, N. M., and Popović, M. B. (2014). Feasibility of a Hybrid Brain-Computer Interface for Advanced Functional Electrical Therapy. *The Scientific World Journal*, 2014.

Scherer, R., Müller-Putz, G. R., and Pfurtscheller, G. (2009). Flexibility and practicality: Graz brain–computer interface approach. *International review of neurobiology*, 86:119–131.

Schröder, M., Lal, T. N., Hinterberger, T., Bogdan, M., Hill, N. J., Birbaumer, N., Rosenstiel, W., and Schölkopf, B. (2005). Robust EEG channel selection across subjects for brain-computer interfaces. *EURASIP Journal on Applied Signal Processing*, 2005:3103–3112.

Sellers, E. W. and Donchin, E. (2006). A P300-based brain–computer interface: initial tests by ALS patients. *Clinical neurophysiology*, 117(3):538–548.

Sellers, E. W., Kubler, A., and Donchin, E. (2006). Brain-computer interface research at the University of South Florida Cognitive Psychophysiology Laboratory: the P300 speller. *Neural Systems and Rehabilitation Engineering, IEEE Transactions on*, 14(2):221–224.

Shah, A. S., Bressler, S. L., Knuth, K. H., Ding, M., Mehta, A. D., Ulbert, I., and Schroeder, C. E. (2004). Neural dynamics and the fundamental mechanisms of event-related brain potentials. *Cerebral Cortex*, 14(5):476–483.

Shih, J. J., Krusienski, D. J., and Wolpaw, J. R. (2012). Brain-computer interfaces in medicine. In *Mayo Clinic Proceedings*, volume 87, pages 268–279. Elsevier.

Shyu, K., Chiu, Y., Lee, P., Liang, J., and Peng, S. (2013). Adaptive SSVEP-Based BCI System With Frequency and Pulse Duty-Cycle Stimuli Tuning Design.

Shyu, K.-K., Lee, P.-L., Liu, Y.-J., and Sie, J.-J. (2010). Dual-frequency steady-state visual evoked potential for brain computer interface. *Neuroscience letters*, 483(1):28–31.

Silberstein, R. B., Nunez, P. L., Pipingas, A., Harris, P., and Danieli, F. (2001). Steady state visually evoked potential (SSVEP) topography in a graded working memory task. *International Journal of Psychophysiology*, 42(2):219–232.

Soekadar, S. R., Birbaumer, N., and Cohen, L. G. (2011). Brain–computer interfaces in the rehabilitation of stroke and neurotrauma. *Systems neuroscience and rehabilitation*, pages 3–18.

Spüler, M., Rosenstiel, W., and Bogdan, M. (2012). Online adaptation of a c-VEP Brain-Computer Interface (BCI) based on Error-related potentials and unsupervised learning. *PloS one*, 7(12):e51077.

Srinivasan, R., Bibi, F. A., and Nunez, P. L. (2006). Steady-state visual evoked potentials: distributed local sources and wave-like dynamics are sensitive to flicker frequency. *Brain topography*, 18(3):167–187.

Tam, W.-K., Tong, K.-y., Meng, F., and Gao, S. (2011). A minimal set of electrodes for motor imagery BCI to control an assistive device in chronic stroke subjects: a multi-session study. *Neural Systems and Rehabilitation Engineering, IEEE Transactions on*, 19(6):617–627.

Tello, R. J. M. G., Müller, S. M. T., Ferreira, A., and Bastos, T. F. (2015). Comparison of the influence of stimuli color on steady-state visual evoked potentials. *Research on Biomedical Engineering*, 31(3):218–231.

Teng, F., Chen, Y., Choong, A. M., Gustafson, S., Reichley, C., Lawhead, P., and Waddell, D. (2011). Square or sine: Finding a waveform with high success rate of eliciting SSVEP. *Computational intelligence and neuroscience*, 2011:2.

Teng, F., Choong, A. M., Gustafson, S., Waddell, D., Lawhead, P., and Chen, Y. (2010). Steady state visual evoked potentials by dual sine waves. In *Proceedings of the 48th Annual Southeast Regional Conference*, page 50. ACM.

Thompson, D. E., Blain-Moraes, S., and Huggins, J. E. (2013). Performance assessment in brain-computer interface-based augmentative and alternative communication. *Biomedical engineering online*, 12(1):43.

Tobimatsu, S. and Kato, M. (1996). The effect of binocular stimulation on each component of transient and steady-state VEPs. *Electroencephalography and Clinical Neurophysiology/Evoked Potentials Section*, 100(3):177–183.

Tobimatsu, S., Tomoda, H., and Kato, M. (1996). Normal variability of the amplitude and phase of steady-state VEPs. *Electroencephalography and Clinical Neurophysiology/Evoked Potentials Section*, 100(3):171–176.

Toffanin, P., de Jong, R., Johnson, A., and Martens, S. (2009). Using frequency tagging to quantify attentional deployment in a visual divided attention task. *International Journal of Psychophysiology*, 72(3):289–298.

Townsend, G., LaPallo, B., Boulay, C., Krusienski, D., Frye, G., Hauser, C., Schwartz, N., Vaughan, T., Wolpaw, J., and Sellers, E. (2010). A novel P300-based brain–computer interface stimulus presentation paradigm: moving beyond rows and columns. *Clinical Neurophysiology*, 121(7):1109–1120.

Treder, M. S. and Blankertz, B. (2010). (c) overt attention and visual speller design in an erp-based brain-computer interface. *Behavioral and brain functions*, 6(1):28.

Tsoneva, T., Garcia-Molina, G., and Desain, P. (2015). Neural dynamics during repetitive visual stimulation. *Journal of neural engineering*, 12(6):066017.

Vallabhaneni, A., Wang, T., and He, B. (2005). Braincomputer interface. In *Neural Engineering*, pages 85–121. Springer.

van Gerven, M., Farquhar, J., Schaefer, R., Vlek, R., Geuze, J., Nijholt, A., Ramsey, N., Haselager, P., Vuurpijl, L., Gielen, S., et al. (2009). The brain–computer interface cycle. *Journal of Neural Engineering*, 6(4):041001.

Vaughan, T. M., Heetderks, W. J., Trejo, L. J., Rymer, W. Z., Weinrich, W. Z., Moore, M. M., Kubler, A., Dobkin, B. H., Birbaumer, N., Donchin, E., Wolpaw, E. W., and Wolpaw, J. R. (2003). Brain-computer interface technology: a review of the Second International Meeting . *Transactions on Neural Systems and Rehabilitation Engineering*, 11(2):94–109.

Vaughan, T. M., McFarland, D. J., Schalk, G., Sarnacki, W. A., Krusienski, D. J., Sellers, E. W., and Wolpaw, J. R. (2006). The Wadsworth BCI research and development program: at home with BCI. *Neural Systems and Rehabilitation Engineering, IEEE Transactions on*, 14(2):229–233.

Velasco-Álvarez, F. and Ron-Angevin, R. (2009). Asynchronous brain-computer interface to navigate in virtual environments using one motor imagery. In *Bio-Inspired Systems: Computational and Ambient Intelligence*, pages 698–705. Springer.

Vialatte, F.-B., Maurice, M., Dauwels, J., and Cichocki, A. (2009). Steady state visual evoked potentials in the delta range (0.5-5 Hz). In *Advances in Neuro-Information Processing*, pages 400–407. Springer.

Vialatte, F.-B., Maurice, M., Dauwels, J., and Cichocki, A. (2010). Steady-state visually evoked potentials: focus on essential paradigms and future perspectives. *Progress in neurobiology*, 90(4):418–438.

Vidal, J.-J. (1973). Toward direct brain-computer communication. *Annual review of Biophysics and Bioengineering*, 2(1):157–180.

Vidaurre, C. and Blankertz, B. (2010). Towards a cure for BCI illiteracy. *Brain topography*, 23(2):194–198.

Volosyak, I. (2011). SSVEP-based Bremen–BCI interfaceboosting information transfer rates. *Journal of neural engineering*, 8(3):036020.

Volosyak, I., Cecotti, H., Valbuena, D., and Graser, A. (2009). Evaluation of the Bremen SSVEP based BCI in real world conditions. In *Rehabilitation Robotics, 2009. ICORR 2009. IEEE International Conference on*, pages 322–331. IEEE.

Volosyak, I., Malechka, T., Valbuena, D., and Gräser, A. (2010). A novel calibration method for SSVEP based brain-computer interfaces. In *European Signal Proc. Conf*, pages 939–943.

Volosyak, I., Valbuena, D., Luth, T., Malechka, T., and Graser, A. (2011). BCI demographics II: how many (and what kinds of) people can use a high-frequency SSVEP BCI? *Neural Systems and Rehabilitation Engineering, IEEE Transactions on*, 19(3):232–239.

Walter, S., Quigley, C., Andersen, S. K., and Mueller, M. M. (2012). Effects of overt and covert attention on the steady-state visual evoked potential. *Neuroscience letters*, 519(1):37–41.

Wang, N., Qian, T., Zhuo, Q., and Gao, X. (2010a). Discrimination between idle and work states in BCI based on SSVEP. In *Advanced computer control (ICACC), 2010 2nd international conference on*, volume 4, pages 355–358. IEEE.

Wang, Y., Wang, R., Gao, X., Hong, B., and Gao, S. (2006). A practical VEP-based brain-computer interface. *Neural Systems and Rehabilitation Engineering, IEEE Transactions on*, 14(2):234–240.

Wang, Y., Wang, Y.-T., and Jung, T.-P. (2010b). Visual stimulus design for high-rate SSVEP BCI. *Electronics letters*, 46(15):1057–1058.

Wang, Y., Wong, N., Wang, Y.-T., Wang, Y., Huang, X., Huang, L., Jung, T.-P., Mandell, A. J., and Cheng, C.-K. (2013). Study of visual stimulus waveforms via forced van der pol oscillator model for ssvep-based brain-computer interfaces. In *Communications, Circuits and Systems (ICCCAS), 2013 International Conference on*, volume 2, pages 475–479. IEEE.

Wang, Y., Zhang, Z., Gao, X., and Gao, S. (2004). Lead selection for SSVEP-based brain-computer interface. In *Engineering in Medicine and Biology Society, 2004. IEMBS'04. 26th Annual International Conference of the IEEE*, volume 2, pages 4507–4510. IEEE.

Wang, Y.-T., Wang, Y., and Jung, T.-P. (2011). A cell-phone-based brain–computer interface for communication in daily life. *Journal of neural engineering*, 8(2):025018.

Winkler, I., Haufe, S., and Tangermann, M. (2011). Automatic classification of artifactual ICA-components for artifact removal in EEG signals. *Behavioral and Brain Functions*, 7(1):30.

Wolpaw, J. R., Birbaumer, N., McFarland, D. J., Pfurtscheller, G., and Vaughan, T. M. (2002). Brain–computer interfaces for communication and control. *Clinical neurophysiology*, 113(6):767–791.

Wolpaw, J. R., Loeb, G. E., Allison, B. Z., Donchin, E., do Nascimento, O. F., Heetderks, W. J., Nijboer, F., Shain, W. G., and Turner, J. N. (2006). BCI meeting 2005-workshop on signals and recording methods. *Neural Systems and Rehabilitation Engineering, IEEE Transactions on*, 14(2):138–141.

Wolpaw, J. R. and McFarland, D. J. (2004). Control of a two-dimensional movement signal by a noninvasive brain-computer interface in humans. *Proceedings of the National Academy of Sciences of the United States of America*, 101(51):17849–17854.

Wolpaw, J. R., McFarland, D. J., and Vaughan, T. M. (2000). Brain-computer interface research at the Wadsworth Center. *Rehabilitation Engineering, IEEE Transactions on*, 8(2):222–226.

Wolpaw, J. R., Ramoser, H., McFarland, D. J., and Pfurtscheller, G. (1998). EEG-based communication: improved accuracy by response verification. *Rehabilitation Engineering, IEEE Transactions on*, 6(3):326–333.

Wong, C. M., Wang, B., Wan, F., Mak, P. U., Mak, P. I., and Vai, M. I. (2010). An improved phase-tagged stimuli generation method in steady-state visual evoked potential based brain-computer interface. In *Biomedical Engineering and Informatics (BMEI), 2010 3rd International Conference on*, volume 2, pages 745–749. IEEE.

Wu, H.-Y., Lee, P.-L., Chang, H.-C., and Hsieh, J.-C. (2011). Accounting for phase drifts in SSVEP-based BCIs by means of biphasic stimulation. *Biomedical Engineering, IEEE Transactions on*, 58(5):1394–1402.

Wu, Z. (2009). The difference of SSVEP resulted by different pulse duty-cycle. In *Communications, Circuits and Systems, 2009. ICCCAS 2009. International Conference on*, pages 605–607. IEEE.

Wu, Z. (2014a). SSVEP extraction based on the similarity of background EEG. *PloS one*, 9(4):e93884.

Wu, Z. (2014b). Studying modulation on simultaneously activated SSVEP neural networks by a cognitive task. *Journal of biological physics*, 40(1):55–70.

Wu, Z., Lai, Y., Xia, Y., Wu, D., and Yao, D. (2008). Stimulator selection in ssvep-based bci. *Medical engineering & physics*, 30(8):1079–1088.

Xia, B., Li, X., Xie, H., Yang, W., Li, J., and He, L. (2013). Asynchronous Brain–Computer Interface Based on Steady-State Visual-Evoked Potential. *Cognitive Computation*, 5(2):243–251.

Xu, M., Qi, H., Wan, B., Yin, T., Liu, Z., and Ming, D. (2013). A hybrid BCI speller paradigm combining P300 potential and the SSVEP blocking feature. *Journal of neural engineering*, 10(2):026001.

Yan, Z., Gao, X., Bin, G., Hong, B., and Gao, S. (2009). A half-field stimulation pattern for SSVEP-based brain-computer interface. In *Engineering in Medicine and Biology Society, 2009. EMBC 2009. Annual International Conference of the IEEE*, pages 6461–6464. IEEE.

Yin, E., Zhou, Z., Jiang, J., Chen, F., Liu, Y., and Hu, D. (2014). A speedy hybrid BCI spelling approach combining P300 and SSVEP.

Yuan, P., Gao, X., Allison, B., Wang, Y., Bin, G., and Gao, S. (2013). A study of the existing problems of estimating the information transfer rate in online brain–computer interfaces. *Journal of neural engineering*, 10(2):026014.

Z. Allison, B., Jin, J., Zhang, Y., and Wang, X. (2014). A four-choice hybrid P300/SSVEP BCI for improved accuracy. *Brain-Computer Interfaces*, 1(1):17–26.

Zhang, D., Maye, A., Gao, X., Hong, B., Engel, A. K., and Gao, S. (2010a). An independent brain–computer interface using covert non-spatial visual selective attention. *Journal of neural engineering*, 7(1):016010.

Zhang, Y., Xu, P., Liu, T., Hu, J., Zhang, R., and Yao, D. (2012). Multiple frequencies sequential coding for SSVEP-based brain-computer interface. *PloS one*, 7(3):e29519.

Zhang, Y., Zhou, G., Zhao, Q., Onishi, A., Jin, J., Wang, X., and Cichocki, A. (2011). Multiway canonical correlation analysis for frequency components recognition in SSVEP-based BCIs. In *Neural Information Processing*, pages 287–295. Springer.

Zhang, Z., Li, X., and Deng, Z. (2010b). A CWT-based SSVEP classification method for brain-computer interface system. In *Intelligent Control and Information Processing (ICICIP), 2010 International Conference on*, pages 43–48. IEEE.

Zhu, D., Bieger, J., Molina, G. G., and Aarts, R. M. (2010a). A survey of stimulation methods used in SSVEP-based BCIs. *Computational intelligence and neuroscience*, 2010:1.

Zhu, D., Molina, G. G., Mihajlovic, V., and Aarts, R. M. (2010b). Phase synchrony analysis for SSVEP-based BCIs. In *Computer Engineering and Technology (ICCET), 2010 2nd International Conference on*, volume 2, pages V2–329. IEEE.

Appendices

.

Appendix A

Data Sheets

Table A-1: Data sheet of LED LR G6SP-CADB-1-1(7100mcd). This table is from OSRAM Opto Semiconductors GmbH.

Vorläufige Daten / Preliminary Data **LR G6SP, LA G6SP, LY G6SP**

Kennwerte
Characteristics
(T_A = 25 °C)

Bezeichnung Parameter		Symbol Symbol	Werte Values			Einheit Unit
			red	amber	yellow	
Wellenlänge des emittierten Lichtes Wavelength at peak emission I_F = 140 mA	(typ.)	λ_{peak}	632	624	594	nm
Dominantwellenlänge[5) Seite 16] Dominant wavelength[5) page 16] I_F = 140 mA	(min.) (typ.) (max.)	λ_{dom} λ_{dom} λ_{dom}	620 625* 629	612 617* 624	583 590* 595	nm nm nm
Spektrale Bandbreite bei 50 % $\Phi_{rel\ max}$ Spectral bandwidth at 50 % $\Phi_{rel\ max}$ I_F = 140 mA	(typ.)	$\Delta\lambda$	18	18	18	nm
Abstrahlwinkel bei 50 % Φ_V (Vollwinkel) Viewing angle at 50 % Φ_V	(typ.)	2φ	120	120	120	Grad deg.
Durchlassspannung[6) Seite 16] Forward voltage[6) page 16] I_F = 140 mA	(min.) (typ.) (max.)	V_F V_F V_F	1.90* 2.1 2.65	1.90* 2.1 2.65	2.05* 2.2 2.65	V V V
Sperrstrom Reverse current	(max.)	I_R I_R	not designed for reverse operation			
Temperaturkoeffizient von λ_{peak} Temperature coefficient of λ_{peak} I_F = 140 mA; −10°C ≤ T ≤ 100°C	(typ.)	$TC_{\lambda peak}$	0.15	0.15	0.13	nm/K
Temperaturkoeffizient von λ_{dom} Temperature coefficient of λ_{dom} I_F = 140 mA; −10°C ≤ T ≤ 100°C	(typ.)	$TC_{\lambda dom}$	0.07	0.08	0.10	nm/K
Temperaturkoeffizient von V_F Temperature coefficient of V_F I_F = 140 mA; −10°C ≤ T ≤ 100°C	(typ.)	TC_V	-2.5	-2.5	-2.5	mV/K
Optischer Wirkungsgrad Optical efficiency I_F = 140 mA	(typ.)	η_{opt}	50	62	32	lm/W

* Einzelgruppen siehe Seite 5
Individual groups on page 5

Opto Semiconductors OSRAM

Table A-2: Data sheet of LED LS E63B-BBCB-1-1(2525mcd). This table is from OSRAM Opto Semiconductors GmbH.

LS E63B, LA E63B, LO E63B, LY E63B

Kennwerte
Characteristics
(T_A = 25 °C)

Bezeichnung Parameter		Symbol Symbol	Werte Values				Einheit Unit
			LS	LA	LO	LY	
Wellenlänge des emittierten Lichtes Wavelength at peak emission I_F = 50 mA	(typ.)	λ_{peak}	645	624	610	594	nm
Dominantwellenlänge[5] *Seite 16* Dominant wavelength[5] *page 16* I_F = 50 mA		λ_{dom}	633* ± 6	617* –5/+7	606* –6/+3	587* –7/+8	nm
Spektrale Bandbreite bei 50 % $E_{rel\,max}$ Spectral bandwidth at 50 % $E_{rel\,max}$ I_F = 50 mA	(typ.)	$\Delta\lambda$	15	18	16	15	nm
Abstrahlwinkel bei 50 % E_V (Vollwinkel) Viewing angle at 50 % E_V	(typ.)	2φ	30	30	30	30	Grad deg.
Durchlassspannung[6] *Seite 16* Forward voltage[6] *page 16* I_F = 50 mA	(min.) (typ.) (max.)	V_F V_F V_F	1.9* 2.2 2.5	1.9* 2.2 2.5	1.9* 2.2 2.5	1.9* 2.2 2.5	V V V
Sperrstrom Reverse current V_R = 12 V	(typ.) (max.)	I_R I_R	0.01 10	0.01 10	0.01 10	0.01 10	µA µA
Temperaturkoeffizient von λ_{peak} Temperature coefficient of λ_{peak} I_F = 50 mA; –10°C ≤ T ≤ 100°C	(typ.)	$TC_{\lambda peak}$	0.15	0.15	0.14	0.13	nm/K
Temperaturkoeffizient von λ_{dom} Temperature coefficient of λ_{dom} I_F = 50 mA; –10°C ≤ T ≤ 100°C	(typ.)	$TC_{\lambda dom}$	0.05	0.07	0.08	0.10	nm/K
Temperaturkoeffizient von V_F Temperature coefficient of V_F I_F = 50 mA; –10°C ≤ T ≤ 100°C	(typ.)	TC_V	– 3.4	– 3.7	– 3.7	– 3.7	mV/K
Optischer Wirkungsgrad Optical efficiency I_F = 50 mA	(typ.)	η_{opt}	18	24	24	24	lm/W

* Einzelgruppen siehe Seite 5
Individual groups on page 5

OSRAM
Opto Semiconductors

Table A-3: Data sheet of LED LR CP7P-JSJU-1. This table is from OSRAM Opto Semiconductors GmbH.

Kennwerte
Characteristics
(T_S = 25 °C)

Bezeichnung **Parameter**		**Symbol** **Symbol**	**Werte** **Values**			**Einheit** **Unit**
			red	**amber**	**yellow**	
Wellenlänge des emittierten Lichtes Wavelength at peak emission I_F = 400 mA	(typ.)	λ_{peak}	632	624	597	nm
Dominantwellenlänge[5) Seite 15] Dominant wavelength[5) page 15] I_F = 400 mA		λ_{dom}	620 625 632	612 617* 624	583 590* 595	nm
Spektrale Bandbreite bei 50 % $I_{rel\ max}$ Spectral bandwidth at 50 % $I_{rel\ max}$ I_F = 400 mA	(typ.)	$\Delta\lambda$	18	18	18	nm
Abstrahlwinkel bei 50 % I_V (Vollwinkel) Viewing angle at 50 % I_V	(typ.)	2φ	80	80	80	Grad deg.
Durchlassspannung [4) Seite 20] Forward voltage[4) page 20] I_F = 400 mA	(min.) (typ.) (max.)	V_F V_F V_F	2.0 2.2 2.6	2.0 2.25 2.6	2.0 2.3 2.6	V V V
Sperrstrom Reverse current			not designed for reverse operation			
Wärmewiderstand Thermal resistance Sperrschicht/Lötpad Junction/solder point	 (typ.) (max.)	 $R_{th\ JS}$ $R_{th\ JS}$	 7 9.4**	 7 9.4**	 7 9.4**	 K/W K/W

* Einzelgruppen siehe Seite 5
Individual groups on page 5

**R_{th}(max) basiert auf statistischen Werten
R_{th}(max) is based on statistic values

OSRAM
Opto Semiconductors

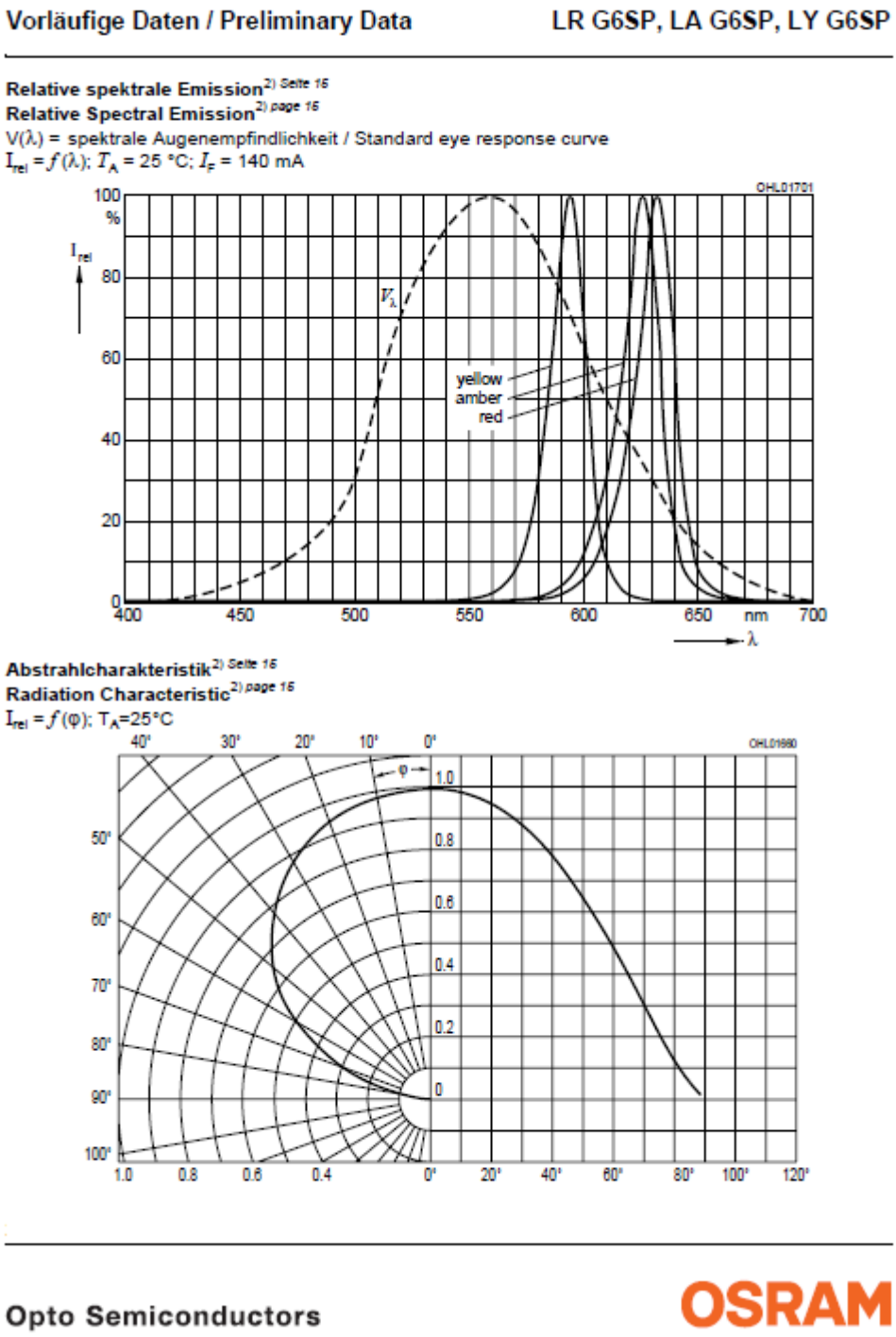

Figure A-1: Spectrum and Radiation Characteristics of LR G6SP-CADB-1-1(7100mcd). This figure is from OSRAM Opto Semiconductors GmbH.

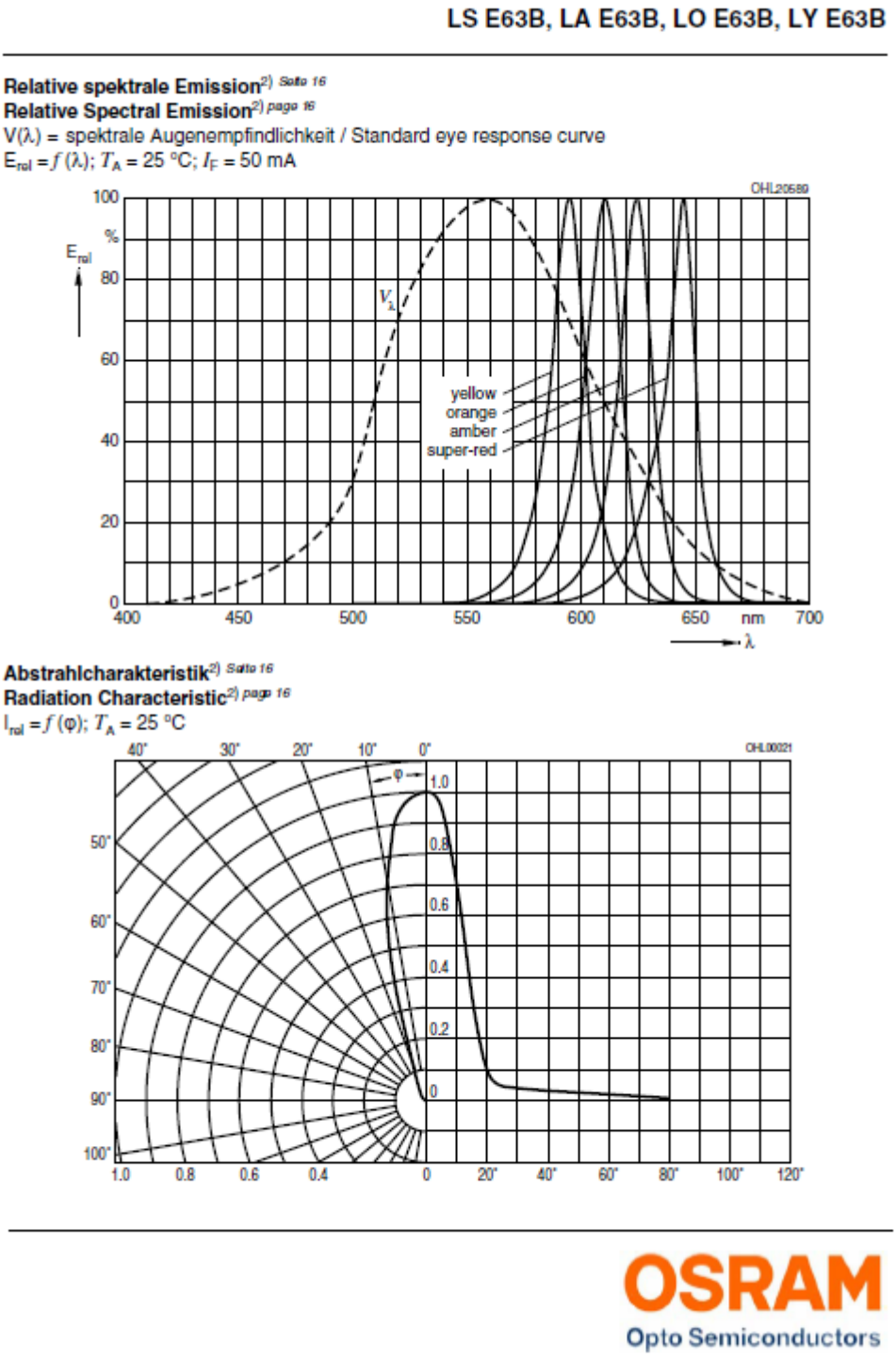

Figure A-2: Spectrum and Radiation Characteristics of LED, LS E63B-BBCB-1-1(2525mcd). This figure is from OSRAM Opto Semiconductors GmbH.

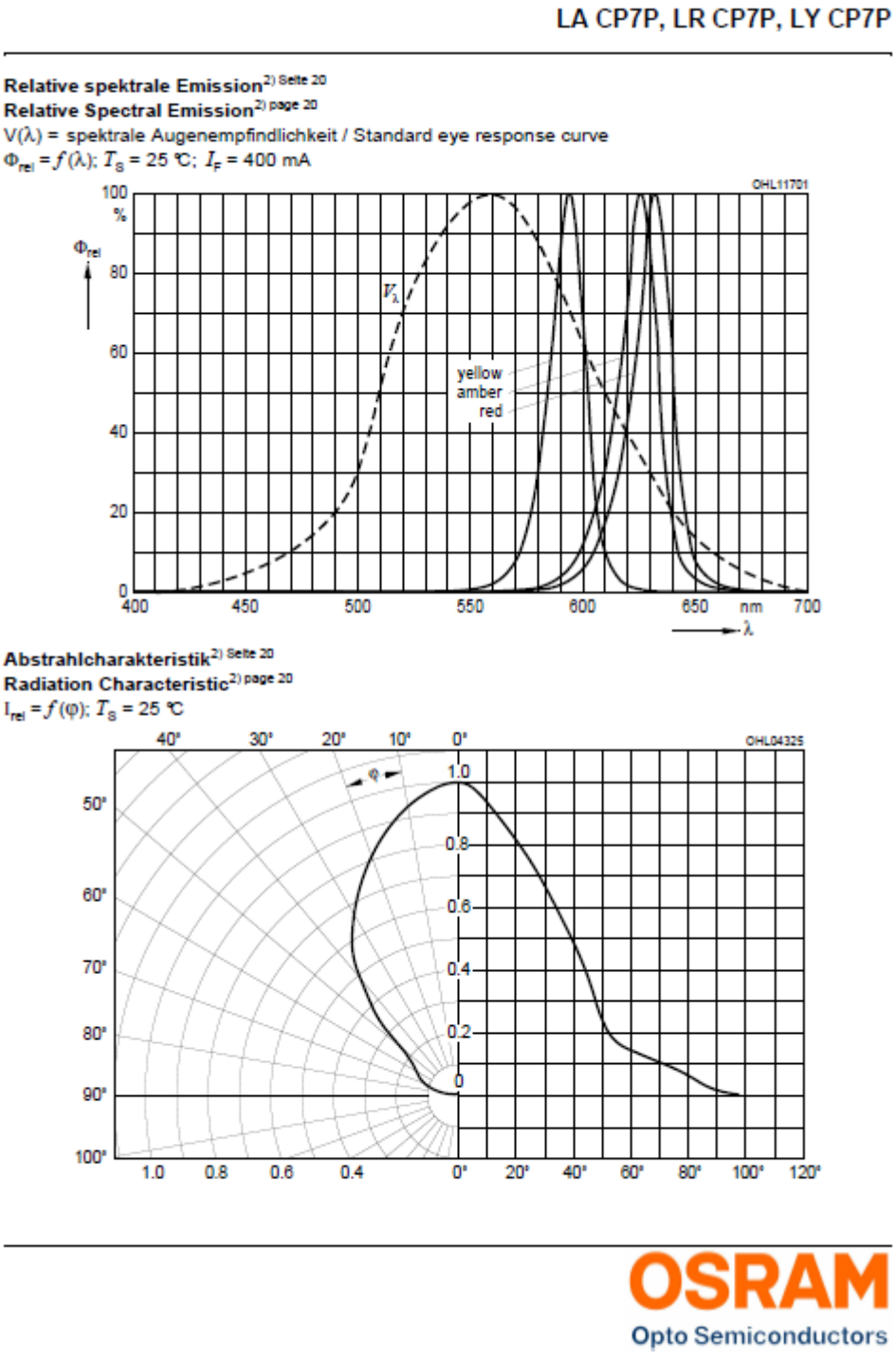

Figure A-3: Spectrum and Radiation Characteristics of LED, LR CP7P-JSJU-1. This figure is from OSRAM Opto Semiconductors GmbH.

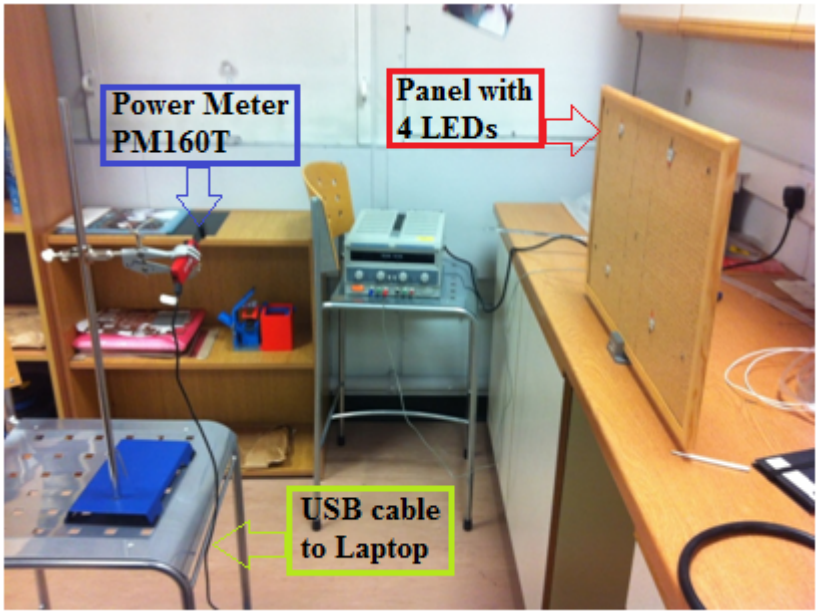

Figure A-4: **Experimental setup to measure output power of LEDs.** 4 LEDs are turned on in the highest intensity as in the Feasibility Experiment. The measuring distance in this setup is 60cm.

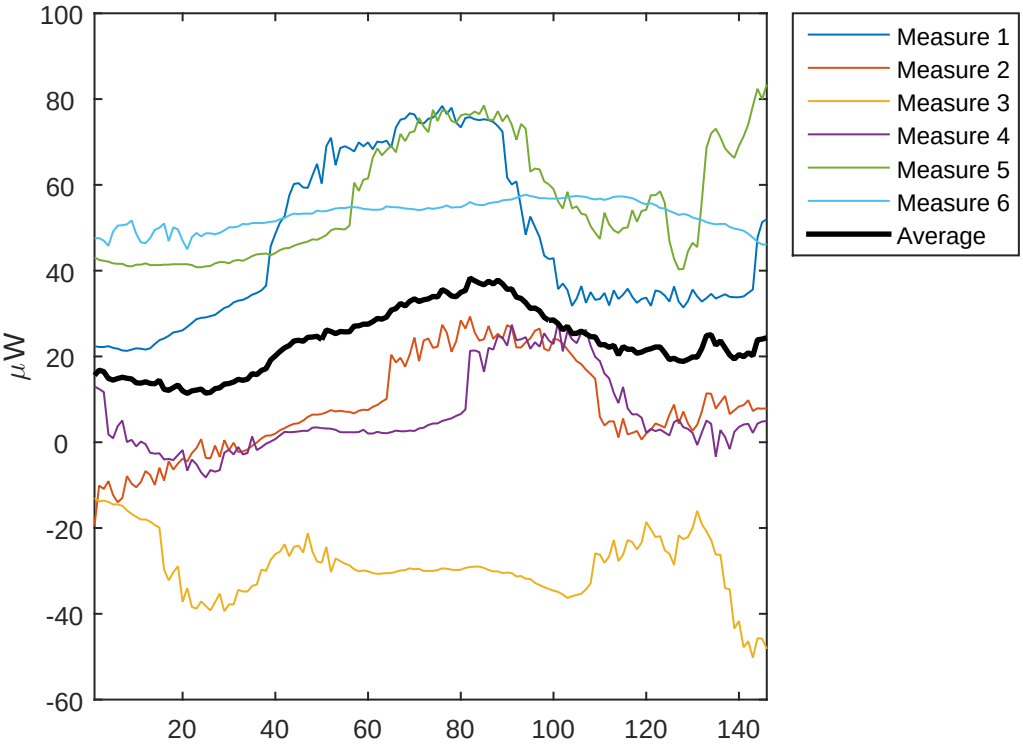

Figure A-5: **LEDs power output of 6 measurements and their average.** x axis of this figure is the data point.

Appendix B

Figures

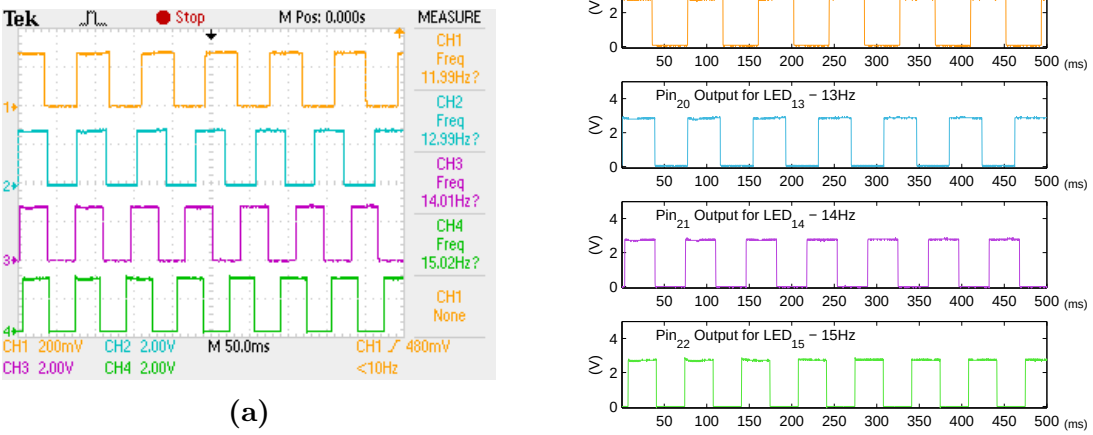

(a) **(b)**

Figure B-1: **Screen shots of 4 stimulating frequencies from Tektronix digital oscilloscope TDS 2014.** (a) The waveforms presented by the colours of orange, cyan, violet and light green, from the top to the bottom, are the square waves with frequencies 12, 13, 14 and 15Hz respectively. (b) waveforms of (a) are re-plotted by Matlab.

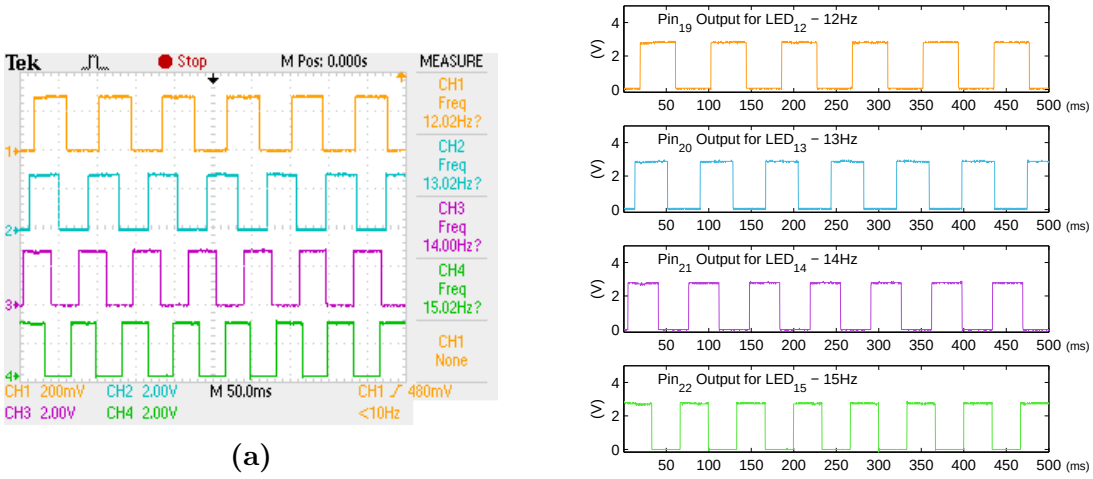

Figure B-2: **Screen shots of 4 stimulating frequencies from Tektronix digital oscilloscope TDS 2014.** (a) The waveforms presented by the colours of orange, cyan, violet and light green, from the top to the bottom, are the square waves with frequencies 12, 13, 14 and 15Hz respectively. (b) waveforms of (a) are re-plotted by Matlab.

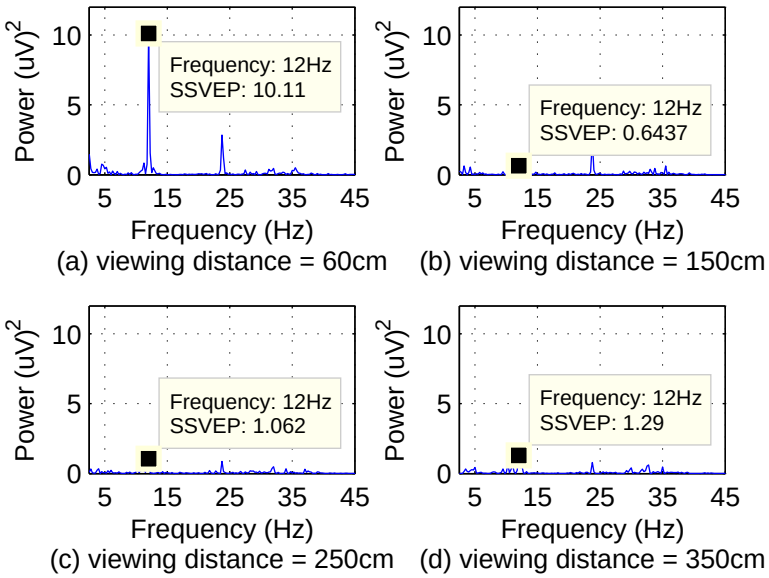

Figure B-3: **FFT power spectrum at four viewing distances without LED intensity compensation. The attended target of this figure is 12Hz.** FFT power spectrum of this figure is the mean of all epochs and electrodes. SSVEP power at the attended frequency decreases as the viewing distances increase without LED intensity compensation. The power at the second harmonics (not labelled) also declined as the viewing distances increase.

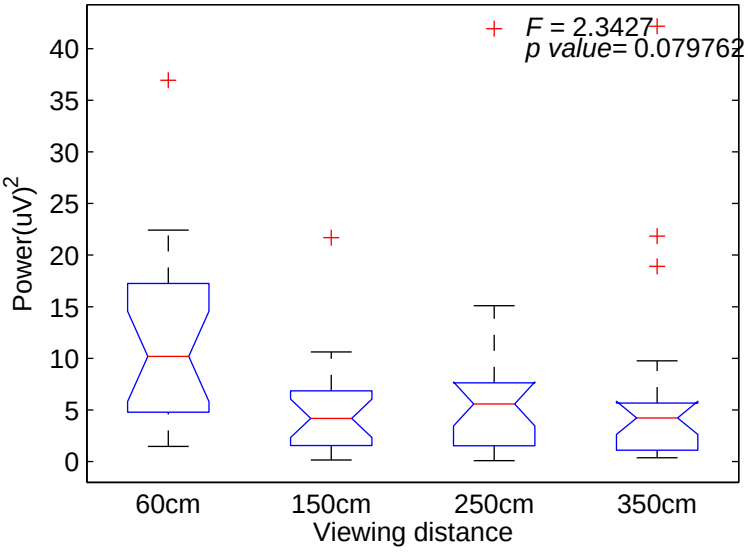

Figure B-4: **Boxplot of SSVEP powers at four viewing distances without LED intensity compensation.** The attended target of this figure is 12Hz. Each viewing distance has 20 epochs.

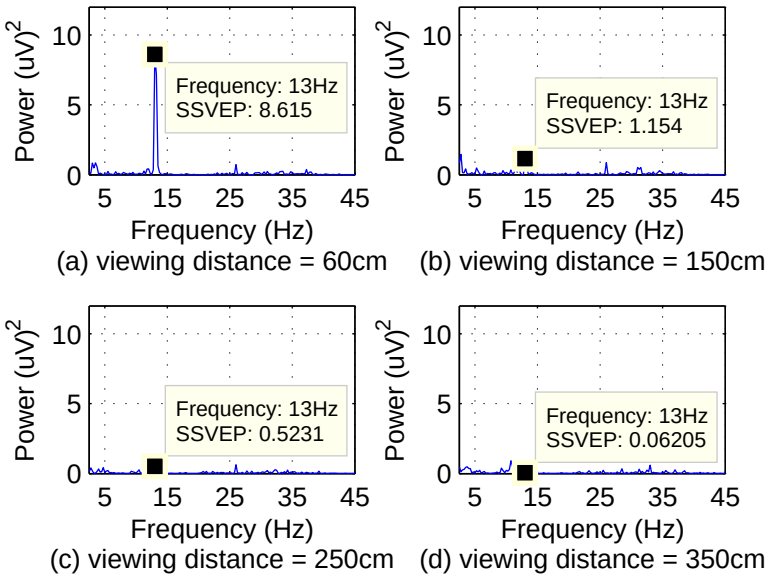

Figure B-5: **FFT power spectrum at four viewing distances without LED intensity compensation.** The attended target of this figure is 13Hz. FFT power spectrum of this figure is the mean of all epochs and electrodes. SSVEP power at the attended frequency decreases as the viewing distances increase without LED intensity compensation. The power at 26Hz (the 2^{nd} harmonics, not labelled) seems stable at all viewing distances compared to the one at 14Hz.

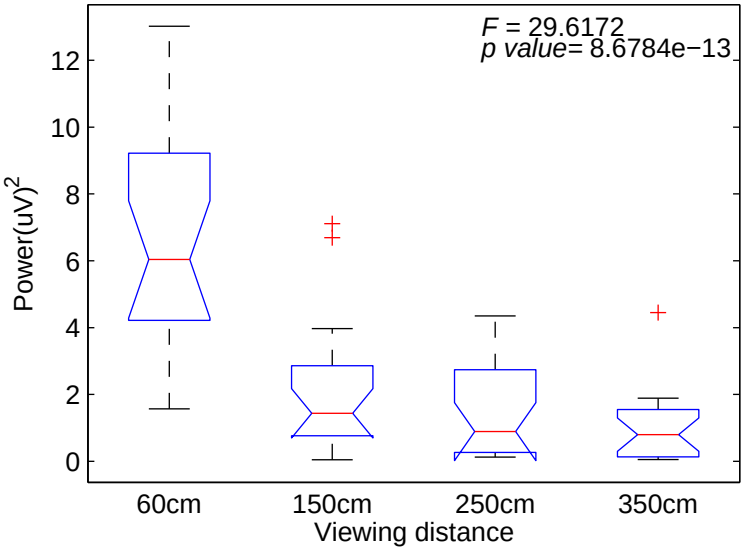

Figure B-6: **Boxplot of SSVEP powers at four viewing distances without LED intensity compensation.** The attended target of this figure is 13Hz. Each viewing distance has 20 epochs.

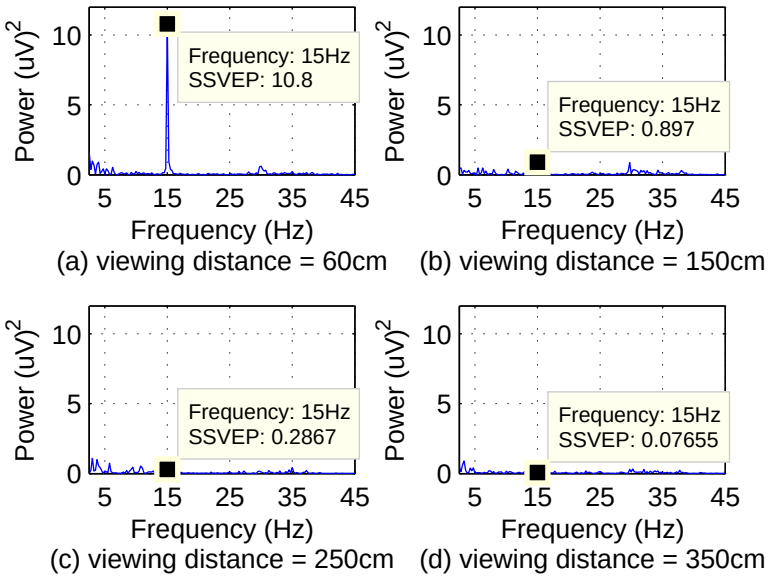

Figure B-7: **FFT power spectrum at four viewing distances without LED intensity compensation.** The attended target of this figure is 15Hz. FFT power spectrum of this figure is the mean of all epochs and electrodes. SSVEP power at the attended frequency decreases as the viewing distances increase without LED intensity compensation. The power at the 30Hz (the 2^{nd} harmonics, not labelled) is not prominent compared to the one at 14Hz.

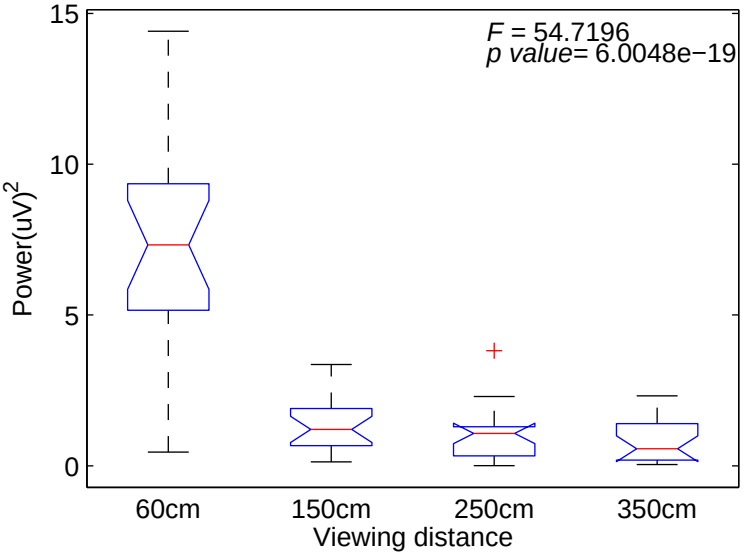

Figure B-8: **Boxplot of SSVEP powers at four viewing distances without LED intensity compensation.** The attended target of this figure is 15Hz. Each viewing distance has 20 epochs.

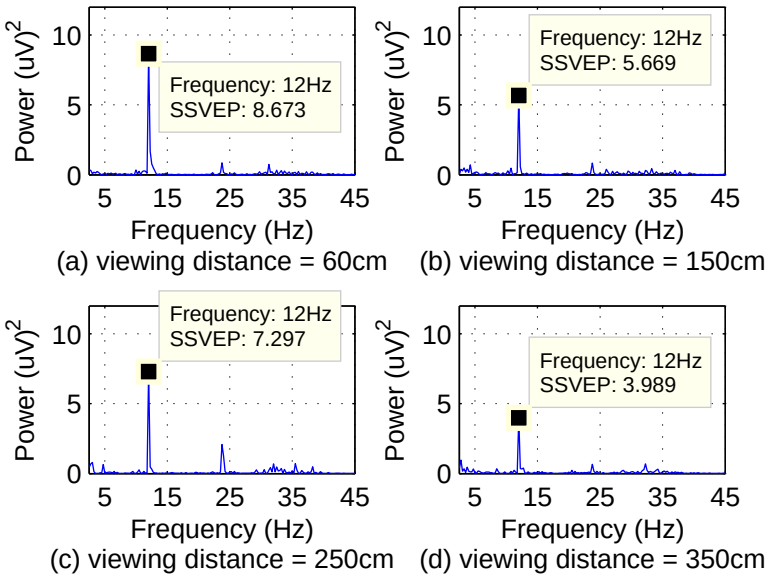

Figure B-9: **FFT power spectrum at four viewing distances with LED intensity compensation.** The attended target of this figure is 12Hz. FFT power spectrum of this figure is the mean of all epochs and electrodes. SSVEP power at the attended frequency remained at the similar level at all viewing distances. The power at longer viewing distance can be larger than the shorter viewing distance.

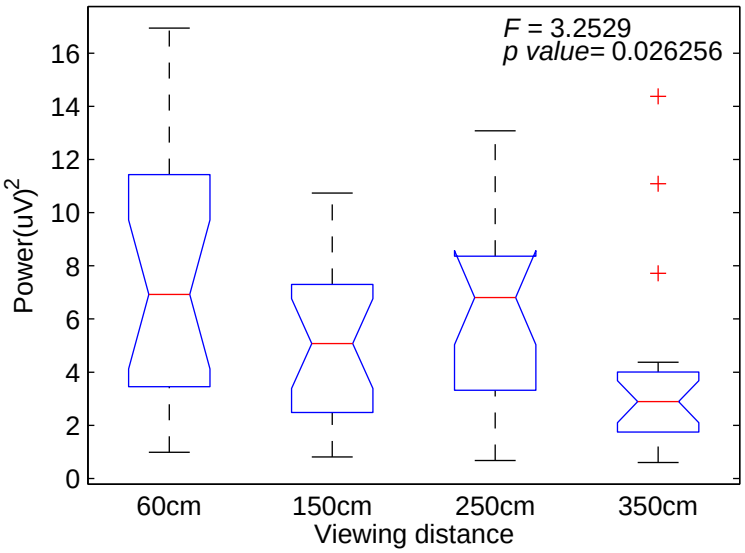

Figure B-10: **Boxplot of SSVEP powers at four viewing distances with LED intensity compensation.** The attended target of this figure is 12Hz. Each viewing distance has 20 epochs.

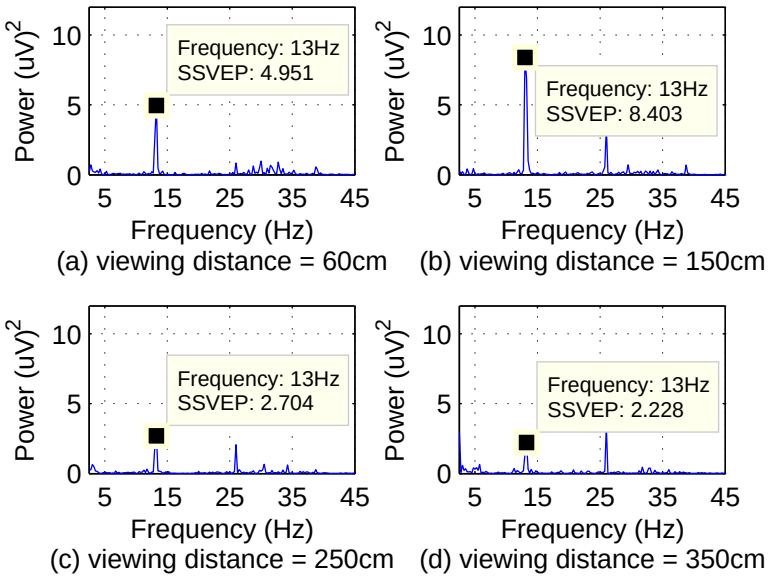

Figure B-11: **FFT power spectrum at four viewing distances with LED intensity compensation.** The attended target of this figure is 13Hz. FFT power spectrum of this figure is the mean of all epochs and electrodes. SSVEP power at the attended frequency remained at the similar level at all viewing distances. The power at longer viewing distance can be larger than the shorter viewing distance.

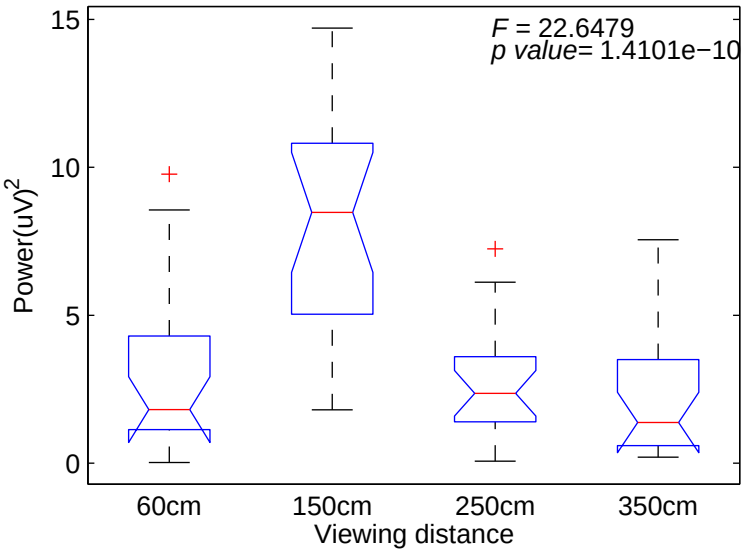

Figure B-12: **Boxplot of SSVEP powers at four viewing distances with LED intensity compensation.** The attended target of this figure is 13Hz. Each viewing distance has 20 epochs.

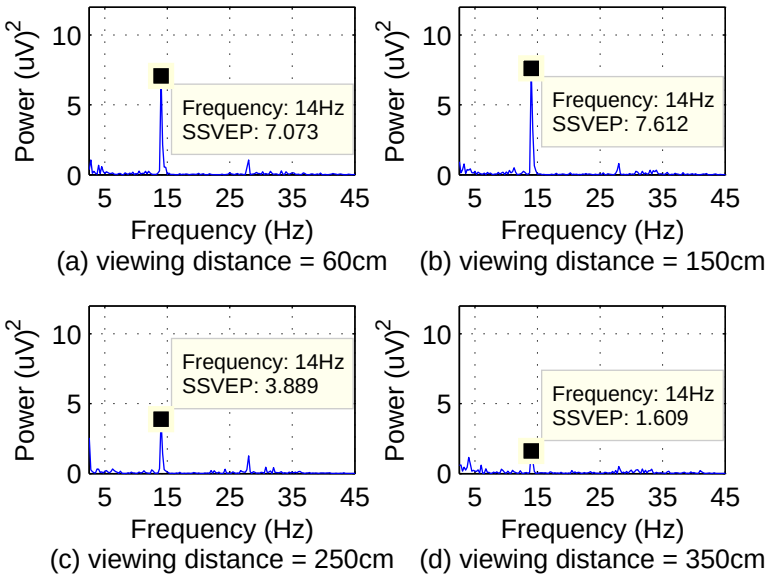

Figure B-13: **FFT power spectrum at four viewing distances with LED intensity compensation.** The attended target of this figure is 14Hz. FFT power spectrum of this figure is the mean of all epochs and electrodes. SSVEP power at the attended frequency remained at the similar level at all viewing distances. The power at longer viewing distance can be larger than the shorter viewing distance.

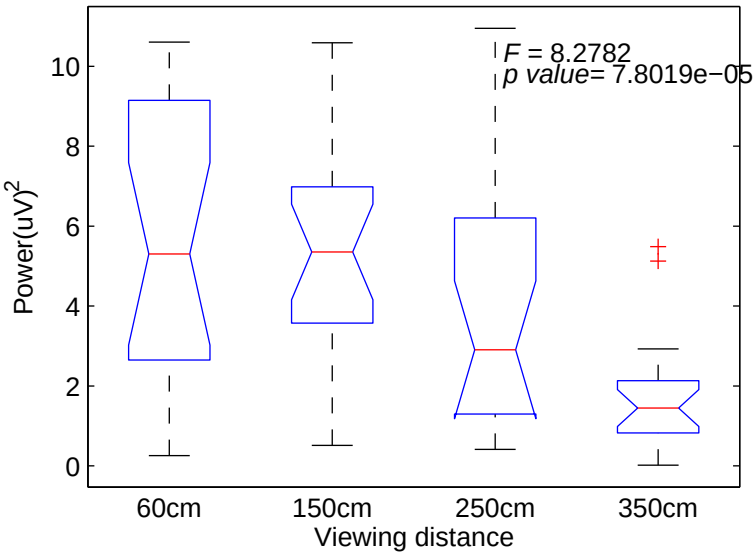

Figure B-14: **Boxplot of SSVEP powers at four viewing distances with LED intensity compensation.** The attended target of this figure is 14Hz. Each viewing distance has 20 epochs.

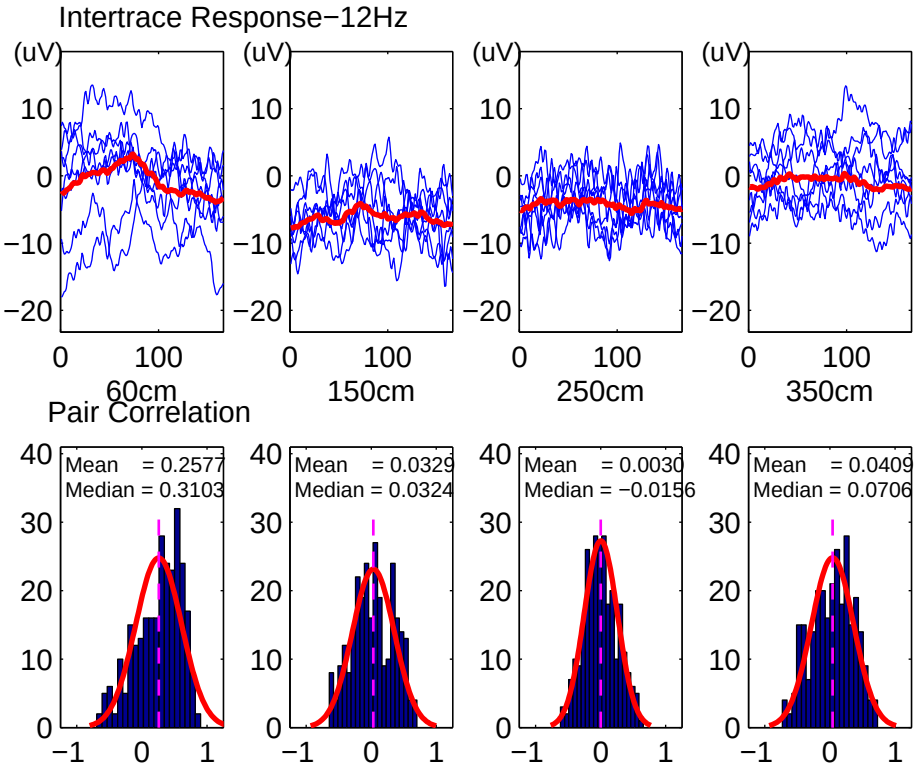

Figure B-15: **EEG inter–traces and histogram of inter–trace correlation coefficients distribution.** First row is the inter–trace EEG in time domain at different viewing distances. Blue thin line is one single inter–trace and red thick line is the average of all inter–traces. The second row is histogram of inter–trace correlation coefficients distribution without LED intensity compensation. LED intensity is the same for all viewing distances. The subject attends 12Hz target.

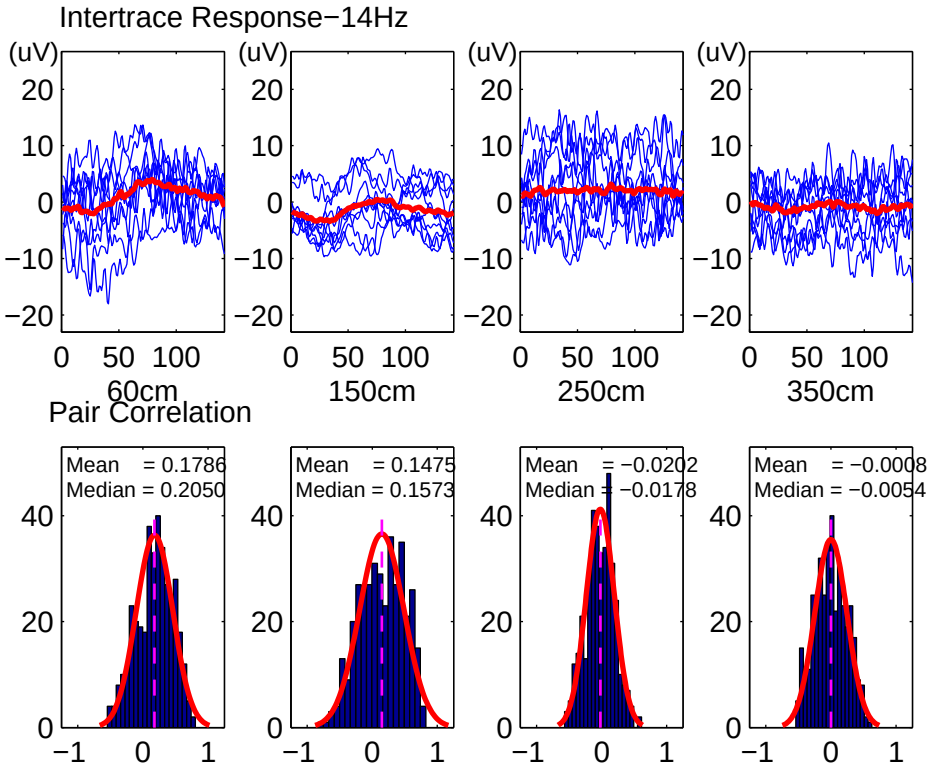

Figure B-16: **EEG inter–traces and histogram of inter–trace correlation coefficients distribution without LED intensity compensation.** First row is the inter–trace EEG in time domain at different viewing distances. Blue thin line is one single inter–trace and red thick line is the average of all inter–traces. The second row is histogram of inter–trace correlation coefficients distribution. LED intensity is the same for all viewing distances. The subject attends 14Hz target.

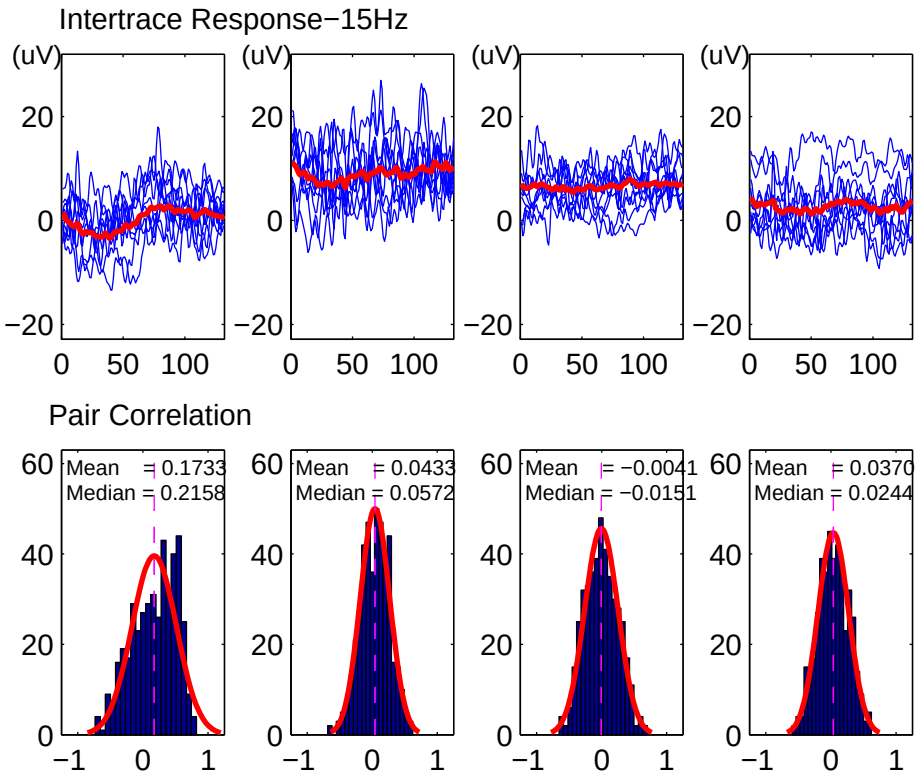

Figure B-17: **EEG inter–traces and histogram of inter–trace correlation coefficients distribution without LED intensity compensation.** First row is the inter–trace EEG in time domain at different viewing distances. Blue thin line is one single inter–trace and red thick line is the average of all inter–traces. The second row is histogram of inter–trace correlation coefficients distribution. LED intensity is the same for all viewing distances. The subject attends 15Hz target.

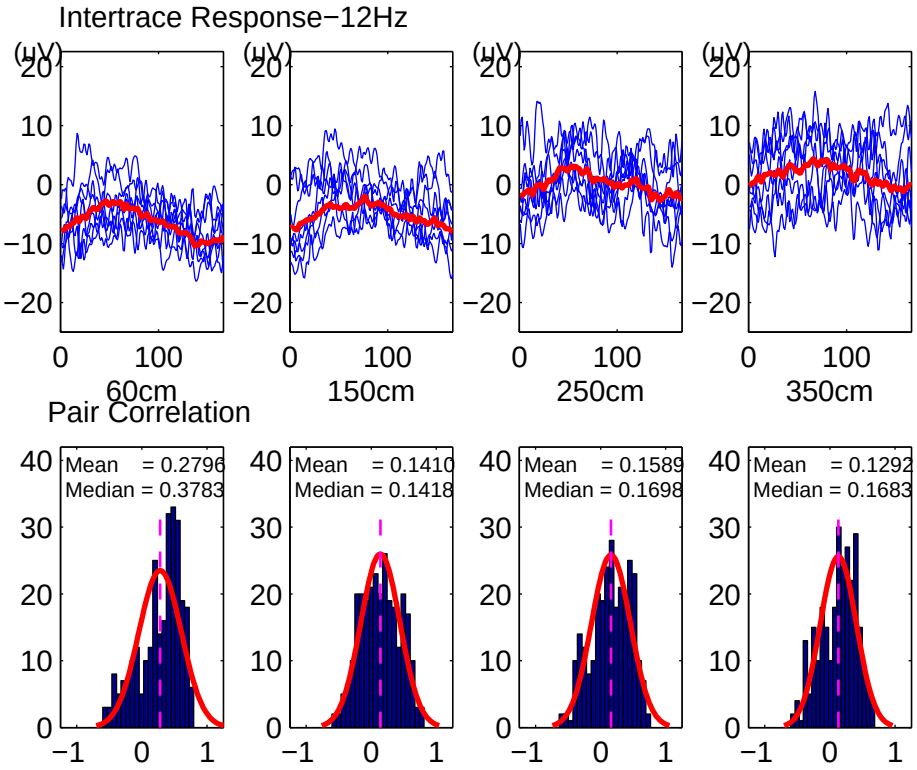

Figure B-18: **EEG inter–traces and histogram of inter–trace correlation coefficients distribution with LED intensity compensation.** First row is the inter–trace EEG in time domain at different viewing distances. Blue thin line is one single inter–trace and red thick line is the average of all inter–traces. The second row is histogram of inter–trace correlation coefficients distribution. LED intensity is compensated to response to the change of the viewing distances. The subject attends 12Hz target.

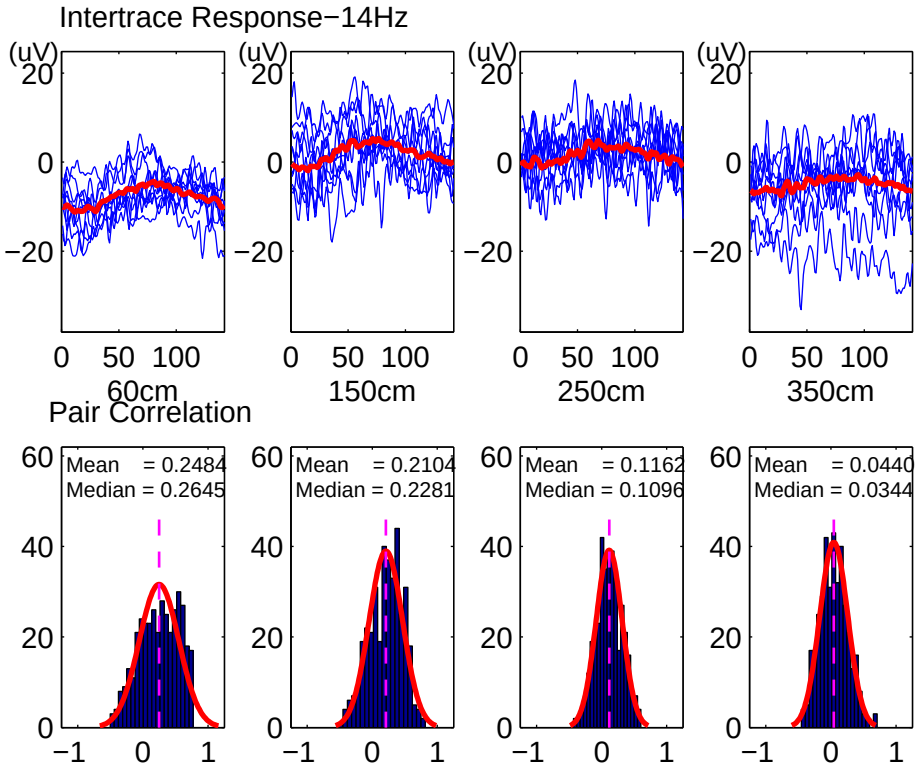

Figure B-19: **EEG inter–traces and histogram of inter–trace correlation coefficients distribution with LED intensity compensation.** First row is the inter–trace EEG in time domain at different viewing distances. Blue thin line is one single inter–trace and red thick line is the average of all inter–traces. The second row is histogram of inter–trace correlation coefficients distribution. LED intensity is compensated to response to the change of the viewing distances. The subject attends 14Hz target.

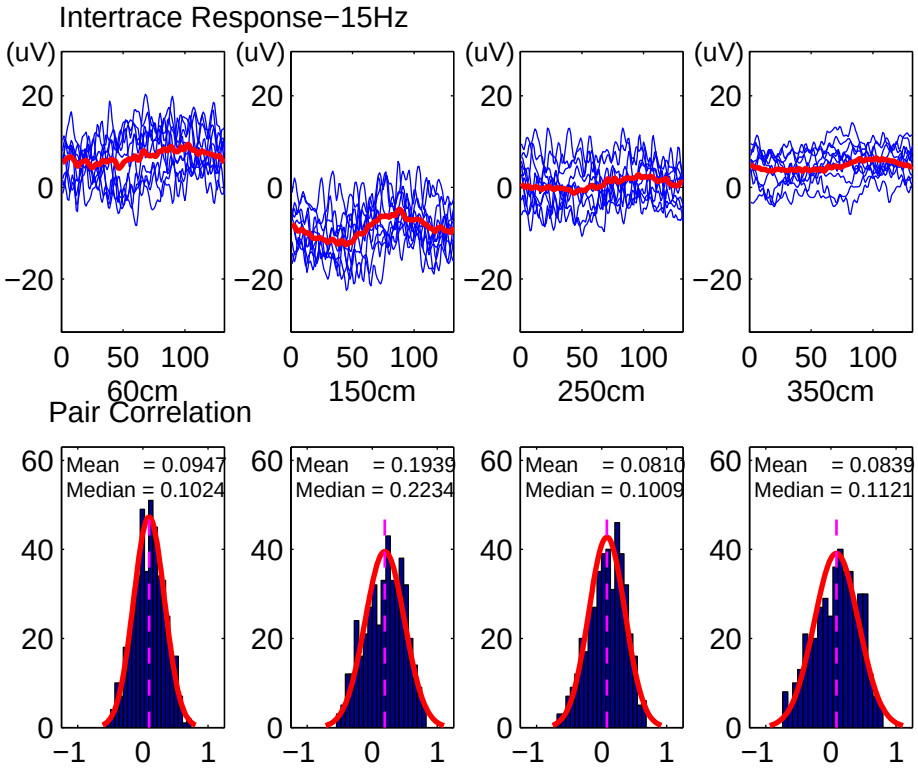

Figure B-20: **EEG inter–traces and histogram of inter–trace correlation coefficients distribution with LED intensity compensation.** First row is the inter–trace EEG in time domain at different viewing distances. Blue thin line is one single inter–trace and red thick line is the average of all inter–traces. The second row is histogram of inter–trace correlation coefficients distribution. LED intensity is compensated to response to the change of the viewing distances. The subject attends 15Hz target.

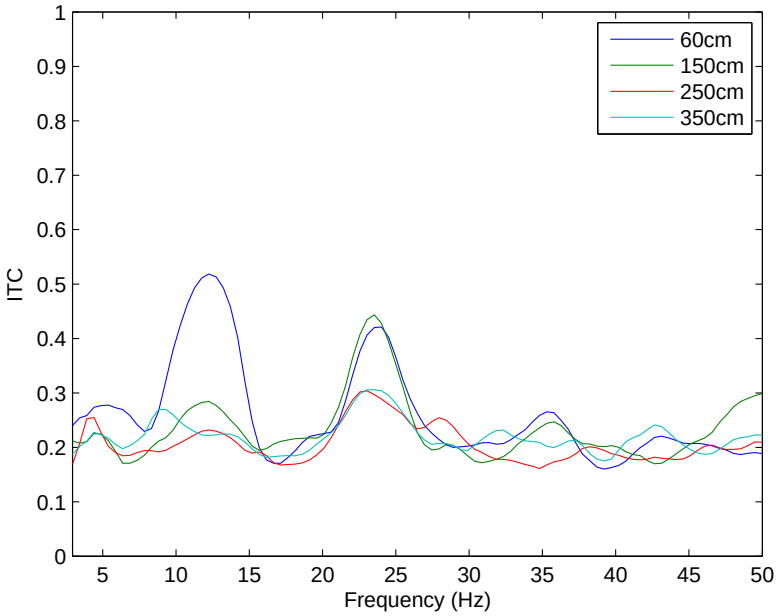

Figure B-21: **ITC at different viewing distances when the subject attended at the target of 12Hz without LED compensation.** ITC at the attended frequency (12Hz) decreases as the viewing distance increases. This decrease can also been seen at the higherharmonics of 12Hz.

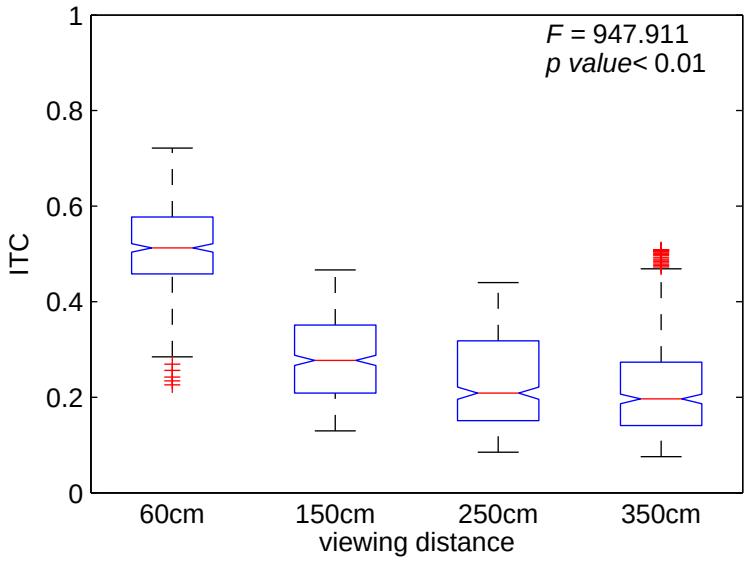

Figure B-22: **Boxplot of ITC when the subject attended at the target of 12Hz at four viewing distances without LED intensity compensation.** This figure shows that ITC at 12Hz decreases as the viewing distance increases. ITC of 12Hz is obtained by linear interpolation of two neighbouring frequencies of 12Hz.

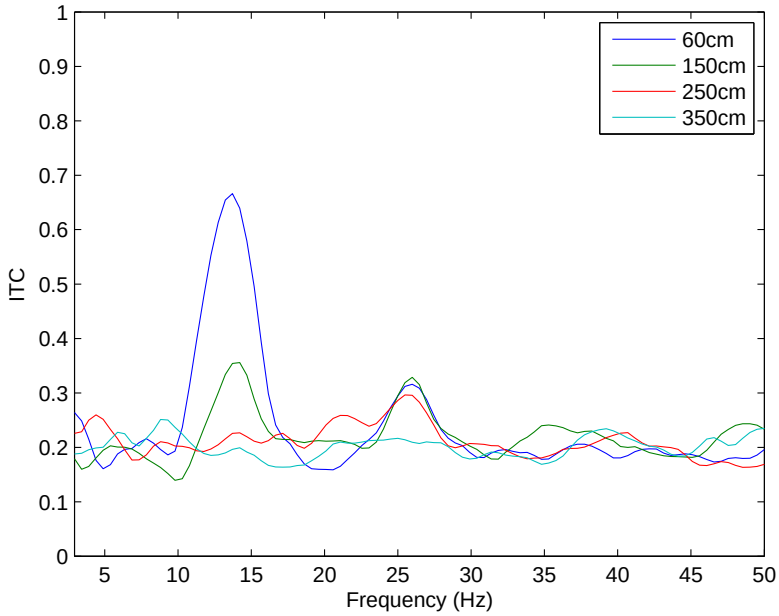

Figure B-23: **ITC at different viewing distances when the subject attended at the target of 13Hz without LED compensation.** ITC at the attended frequency (13Hz) decreases as the viewing distance increases. This decrease can also been seen at the higher harmonics of 13Hz.

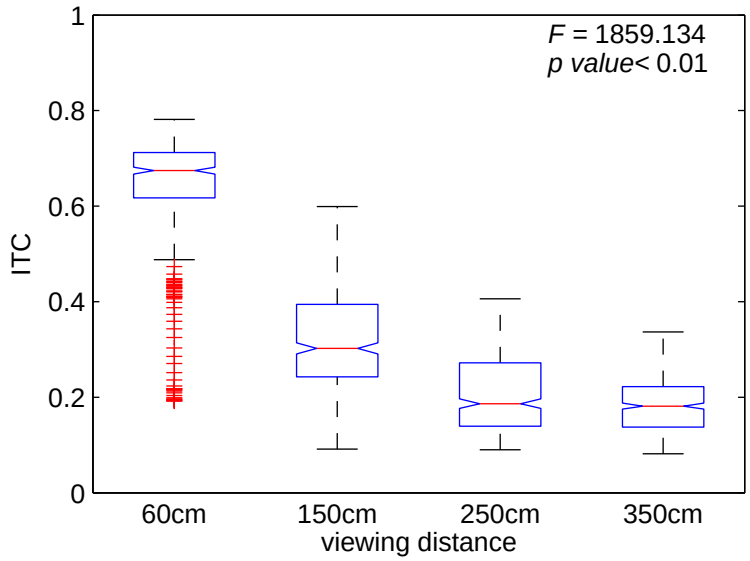

Figure B-24: **Boxplot of ITC when the subject attended at the target of 13Hz at four viewing distances without LED intensity compensation.** This figure shows that ITC at 13Hz decreases as the viewing distance increases. ITC of 13Hz is obtained by linear interpolation of two neighbouring frequencies of 13Hz.

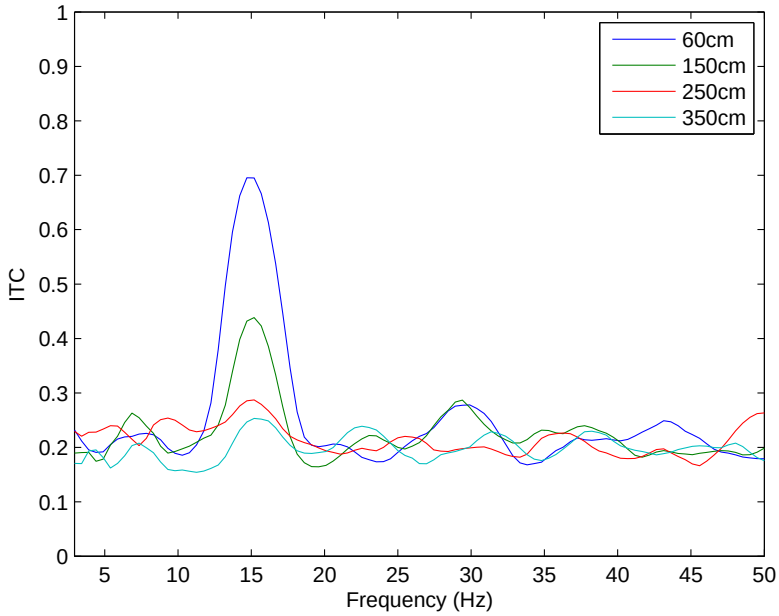

Figure B-25: **ITC at different viewing distances when the subject attended at the target of 15Hz without LED compensation.** ITC at the attended frequency (15Hz) decreases as the viewing distance increases. This decrease can also been seen at the higher harmonics of 15Hz.

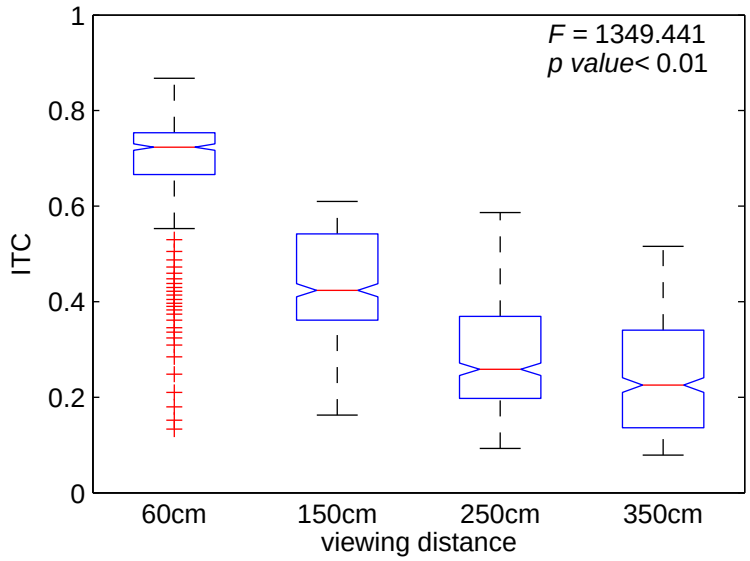

Figure B-26: **Boxplot of ITC when the subject attended at the target of 15Hz at four viewing distances without LED intensity compensation.** This figure shows that ITC at 15Hz decreases as the viewing distance increases. ITC of 15Hz is obtained by linear interpolation of two neighbouring frequencies of 15Hz.

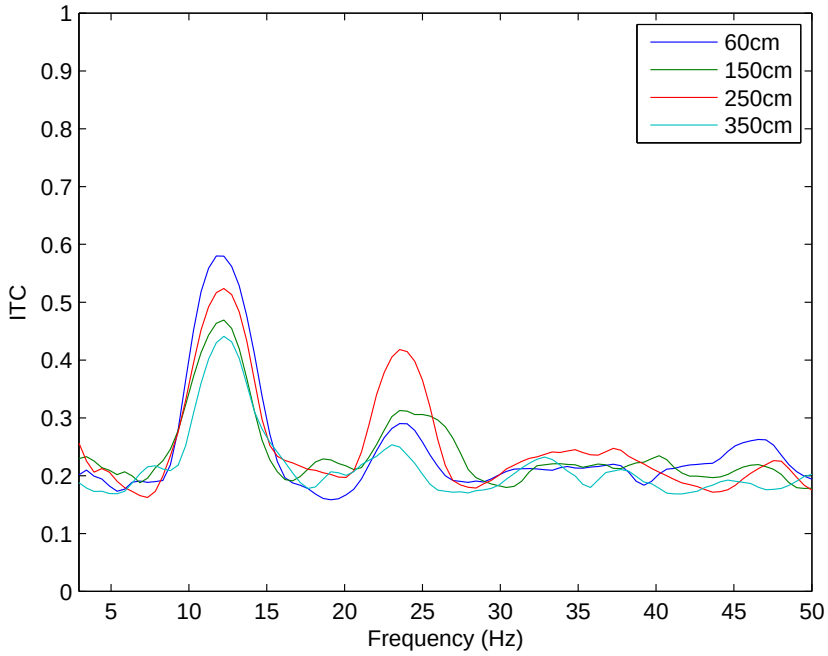

Figure B-27: **ITC at different viewing distances when the subject attended at the target of 12Hz with LED compensation.** With LED intensity compensation, ITC values at attended frequency are more stable compared to the ones without LED intensity compensation (see Figure B-21).

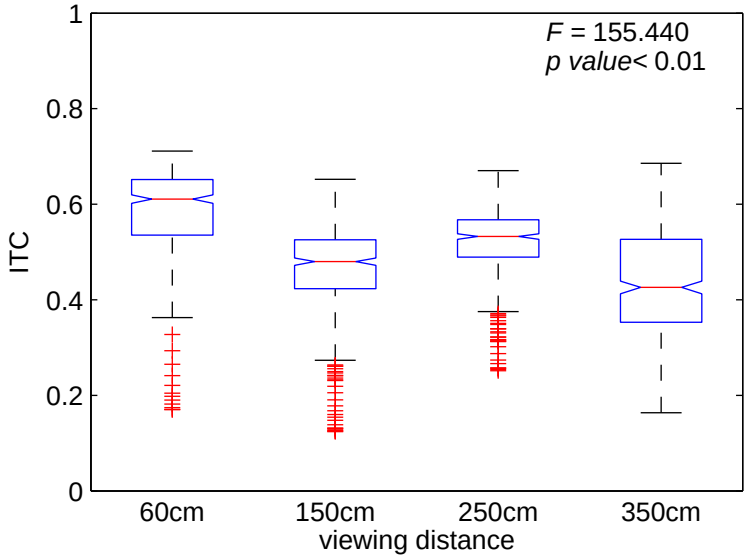

Figure B-28: **Boxplot of ITC when the subject attended at the target of 12Hz at four viewing distances with LED intensity compensation.** This figure shows that ITC at attended frequency, 12Hz is more consistent than without LED compensation (see Figure B-22). ITC of 12Hz is obtained by linear interpolation of two nearest neighbouring frequencies of 12Hz.

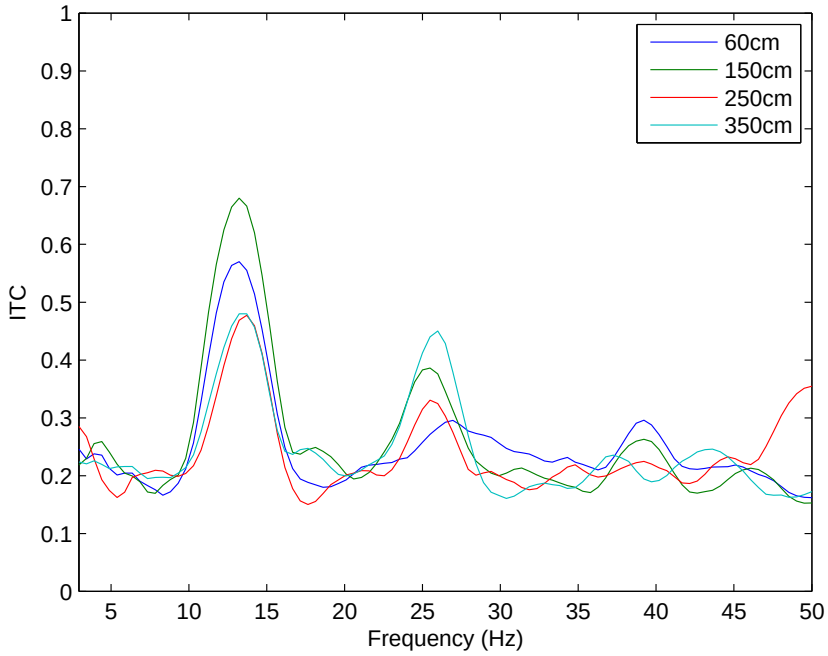

Figure B-29: **ITC at different viewing distances when the subject attended at the target of 13Hz with LED compensation.** With LED intensity compensation, ITC values at attended frequency are more stable compared to the ones without LED intensity compensation (see Figure B-23).

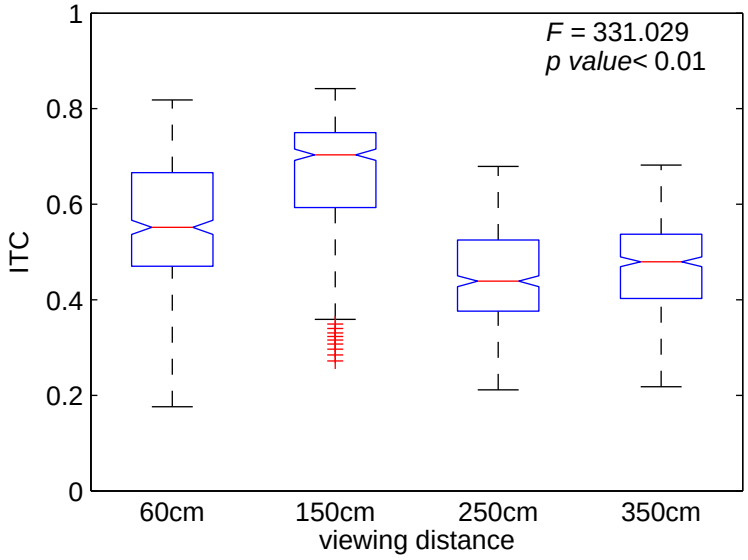

Figure B-30: **Boxplot of ITC when the subject attended at the target of 13Hz at four viewing distances with LED intensity compensation.** This figure shows that ITC at attended frequency, 13Hz is more consistent than without LED compensation (see Figure B-24). ITC of 13Hz is obtained by linear interpolation of two nearest neighbouring frequencies of 13Hz.

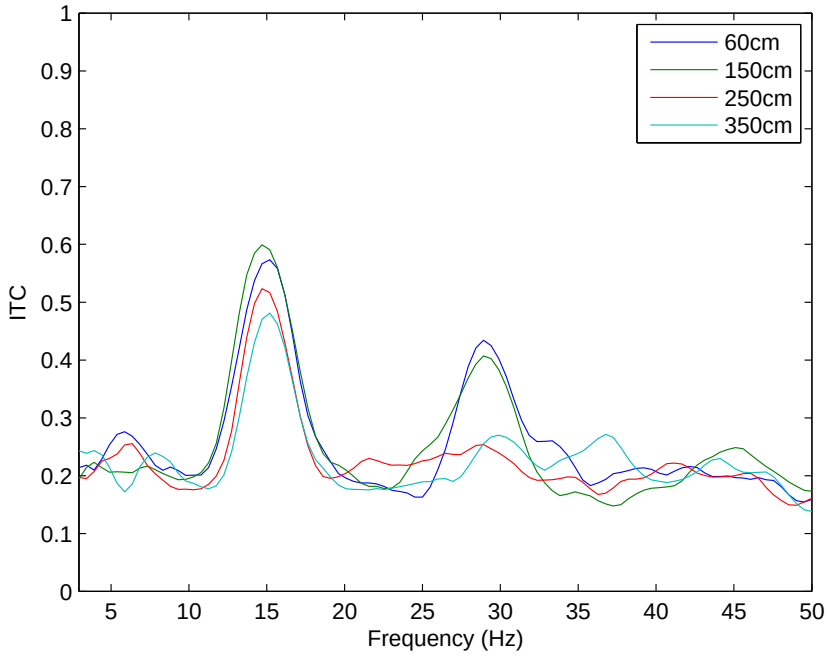

Figure B-31: **ITC at different viewing distances when the subject attended at the target of 15Hz with LED compensation.** With LED intensity compensation, ITC values at attended frequency are more stable compared to the ones without LED intensity compensation (see Figure B-25).

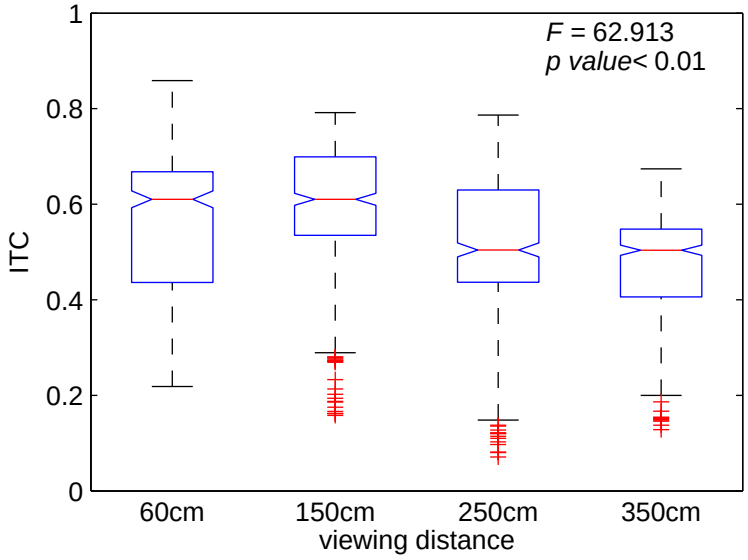

Figure B-32: **Boxplot of ITC when the subject attended at the target of 15Hz at four viewing distances with LED intensity compensation.** This figure shows that ITC at attended frequency, 15Hz is more consistent than without LED compensation (see Figure B-26). ITC of 12Hz is obtained by linear interpolation of two nearest neighbouring frequencies of 15Hz.

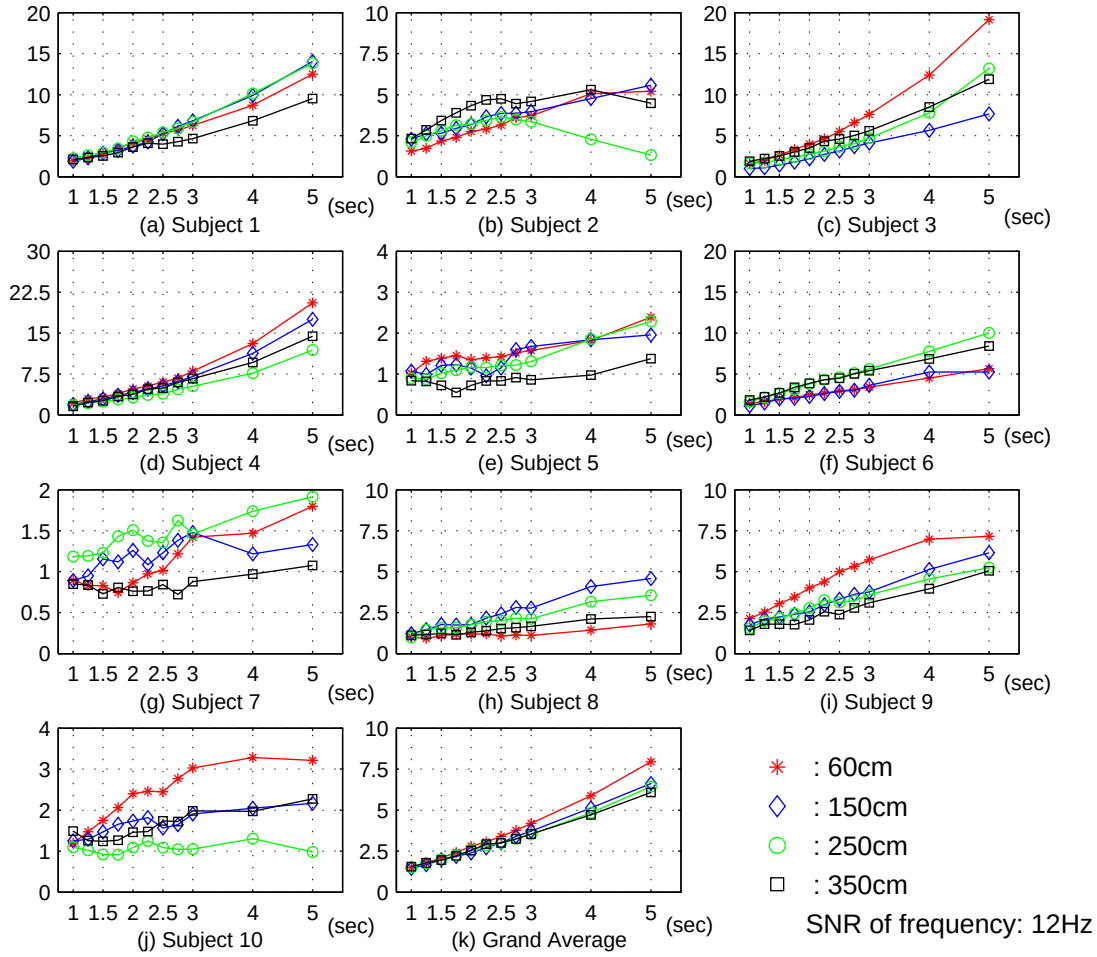

Figure B-33: **SNRs of all subjects when the subjects attend the target of 12Hz at different viewing distance at different EEG TWLs.** For most of the subjects, SNR increases as EEG TWL increases. The SNR scales of the subjects are different.

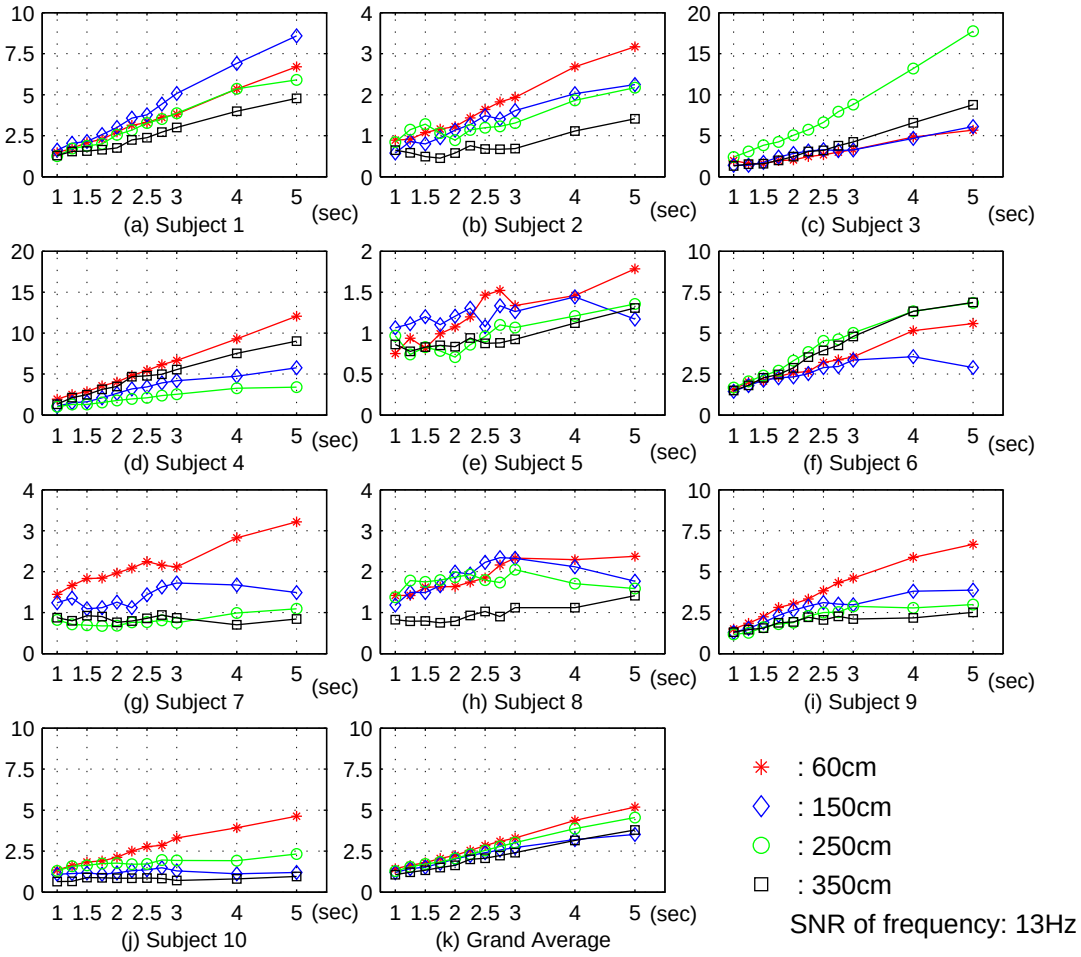

Figure B-34: **SNRs of all subjects when the subjects attend the target of 13Hz at different viewing distance at different EEG TWLs.** For most of the subjects, SNR increases as EEG TWL increases. The SNR scales of the subjects are different.

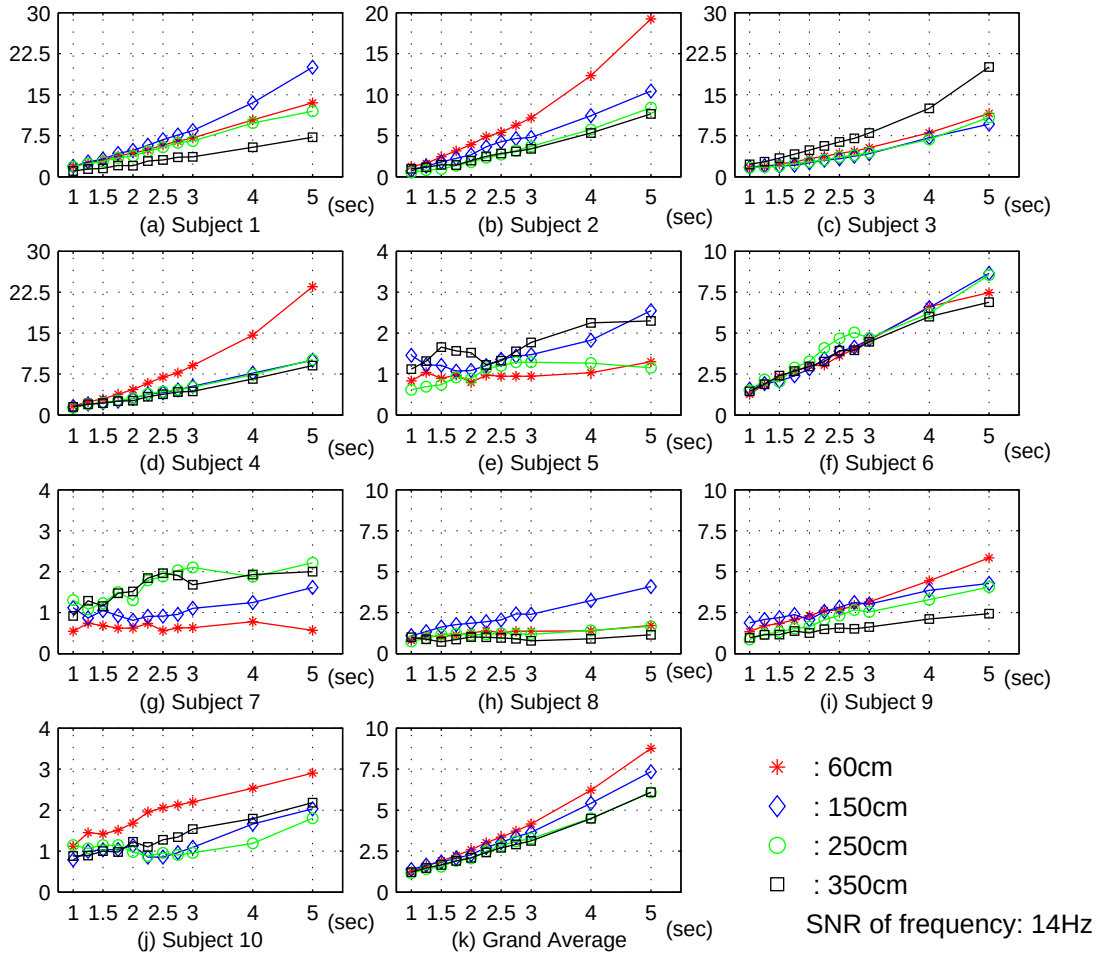

Figure B-35: **SNRs of all subjects when the subjects attend the target of 14Hz at different viewing distance at different EEG TWLs.** For most of the subjects, SNR increases as EEG TWL increases. The SNR scales of the subjects are different.

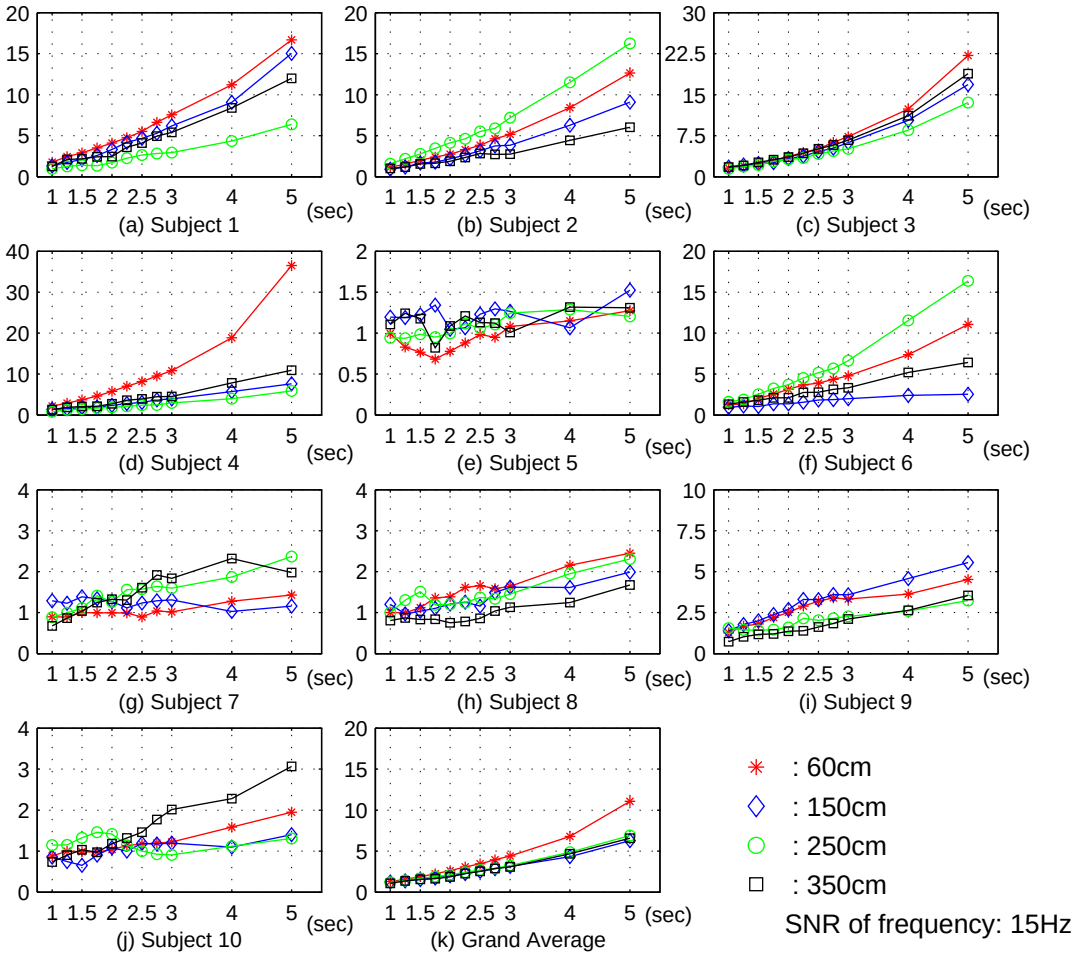

Figure B-36: **SNRs of all subjects when the subjects attend the target of 15Hz at different viewing distance at different EEG TWLs.** For most of the subjects, SNR increases as EEG TWL increases. The SNR scales of the subjects are different.

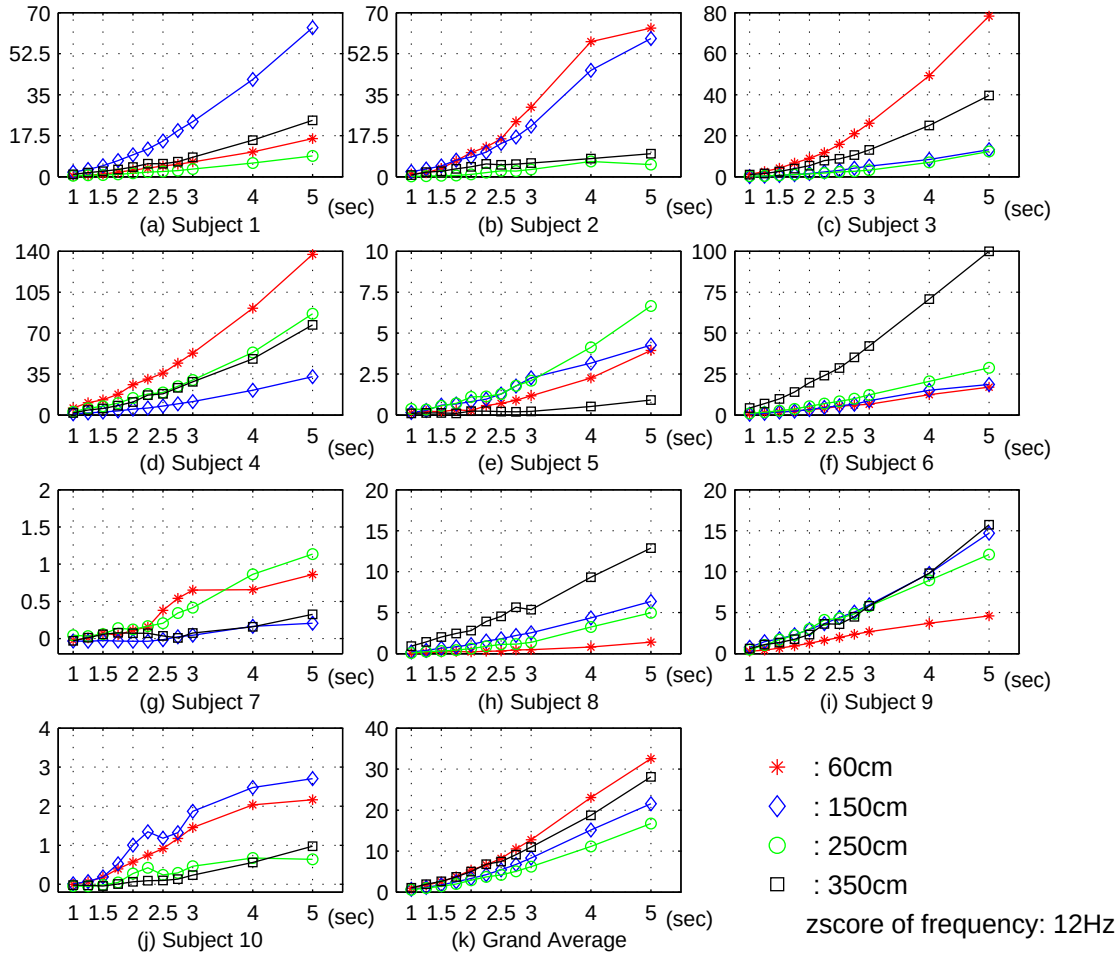

Figure B-37: **z scores of all subjects when the subjects attend the target of 12Hz at different viewing distance at different EEG recording time instances.** For most of the subjects, z scores increased as EEG recording time increased. The z score scales of the subjects are different.

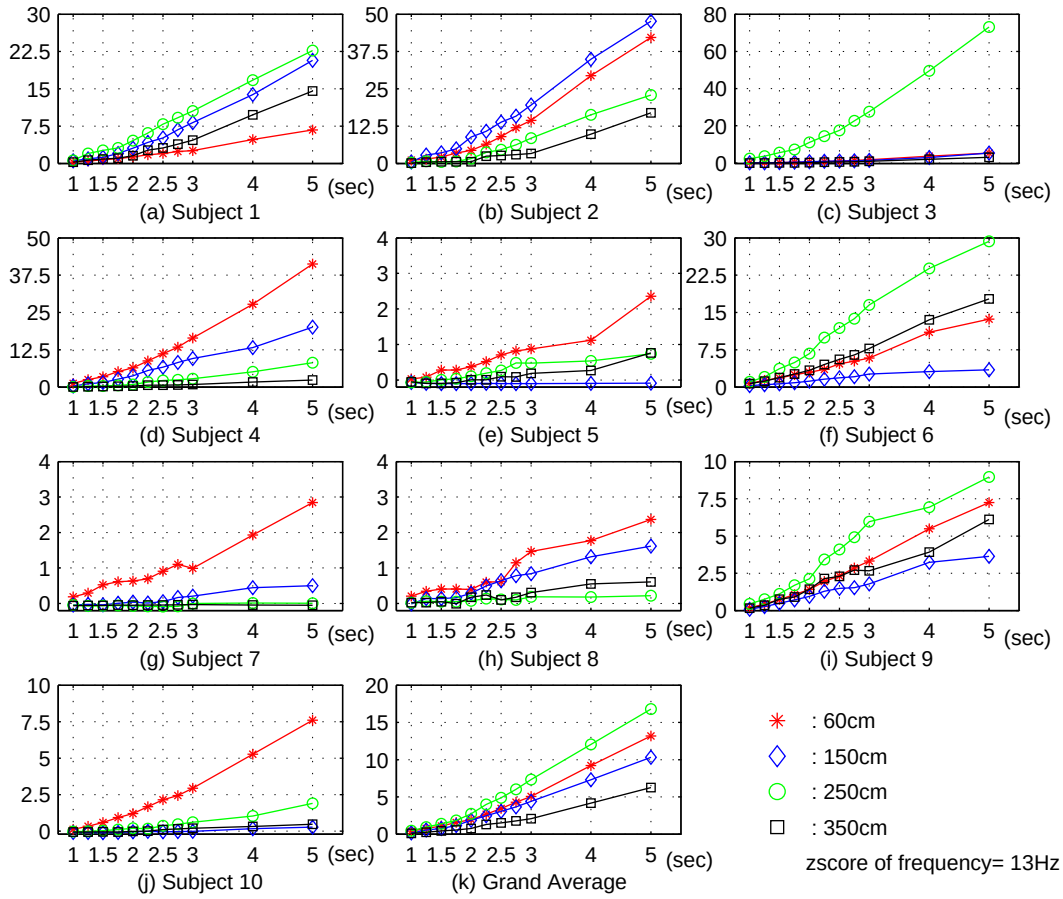

Figure B-38: **z scores of all subjects when the subjects attend the target of 13Hz at different viewing distance at different EEG recording time instances.** For most of the subjects, z scores increased as EEG recording time increased. The z score scales of the subjects are different.

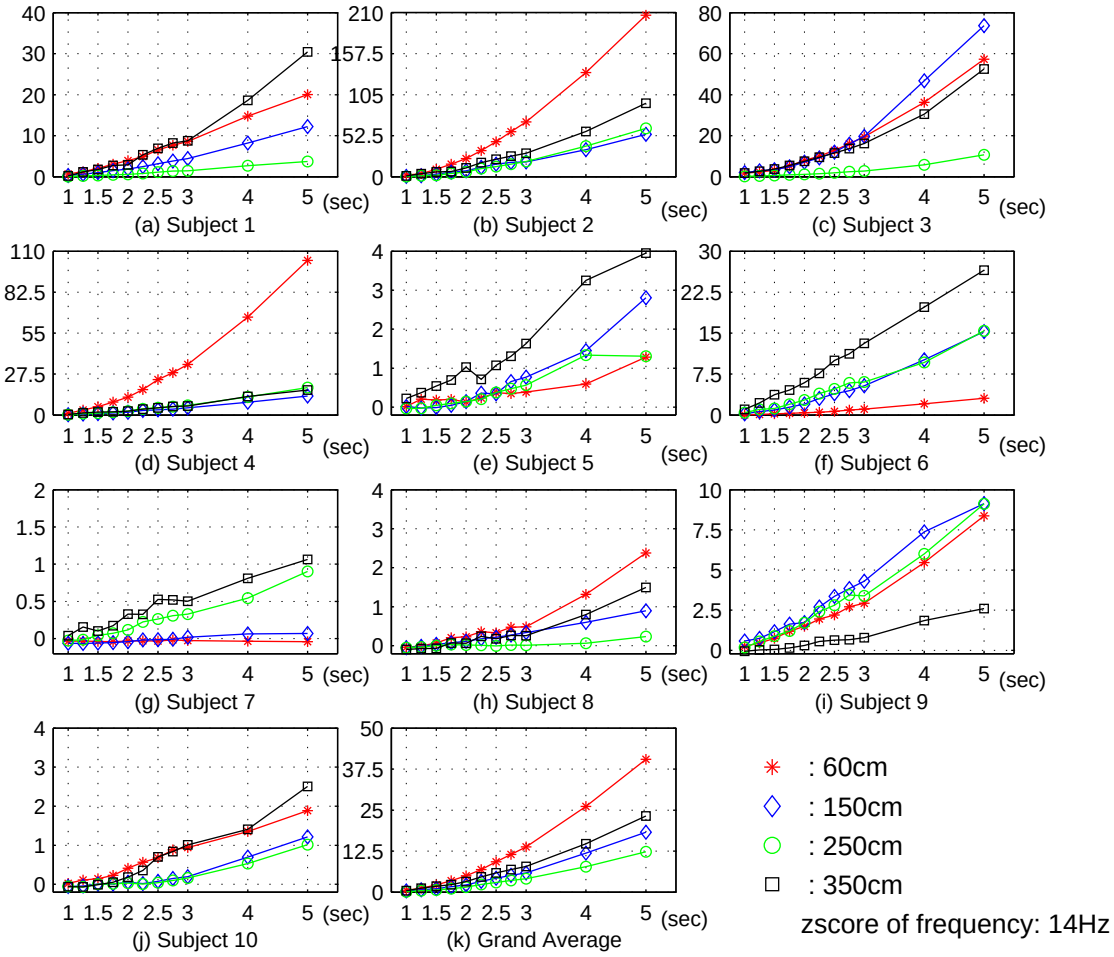

Figure B-39: **z scores of all subjects when the subjects attend the target of 14Hz at different viewing distance at different EEG recording time instances.** For most of the subjects, z scores increased as EEG recording time increased. The z score scales of the subjects are different.

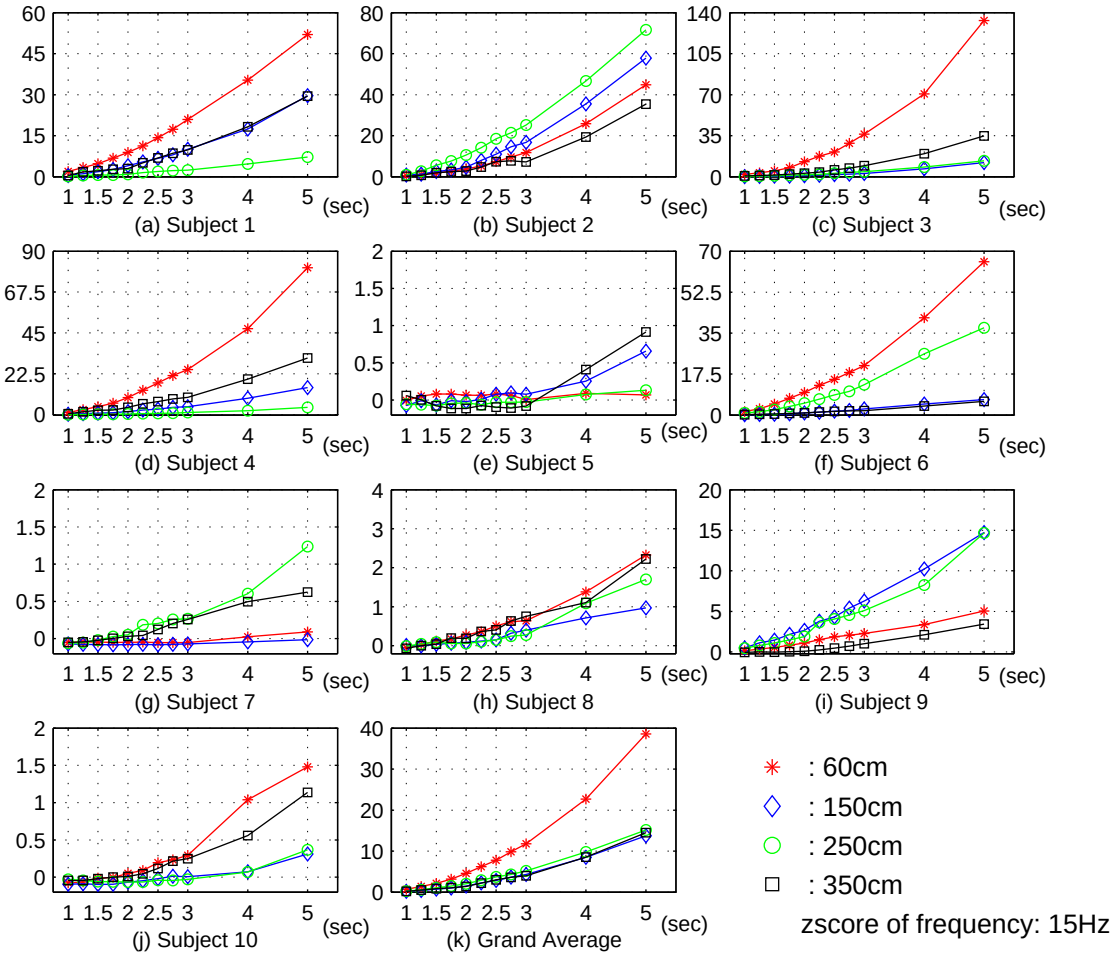

Figure B-40: **z scores of all subjects when the subjects attended the target of 15Hz at different viewing distance at different EEG recording time instances.** For most of the subjects, z scores increased as EEG recording time increased. The z score scales of the subjects are different.

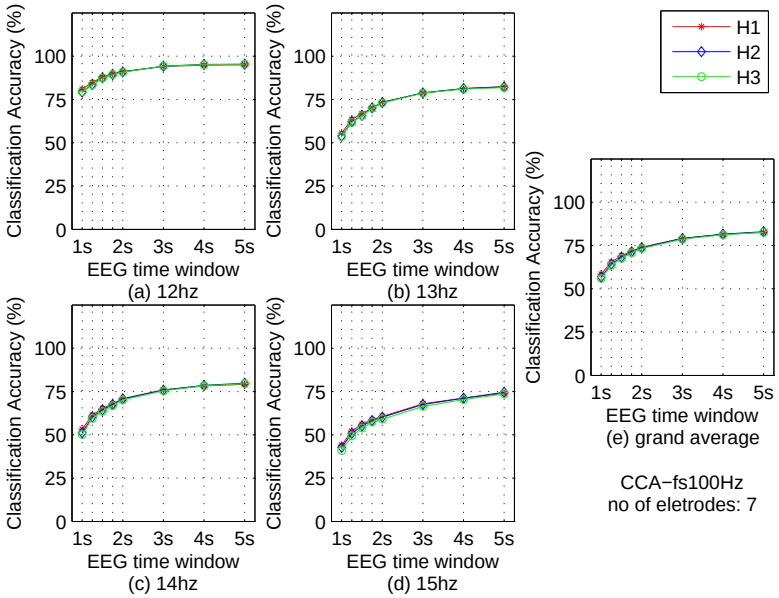

Figure B-41: **Comparison of classification accuracies using different number of SSVEP harmonics.** In this figure, the classification method is CCA and the number of the electrodes is 7. (a) to (d) are the mean classification accuracies across the subjects and the viewing distances of the attended frequency 12Hz, 13Hz, 14Hz and 15Hz respectively. (e) is the mean classification across the subjects, viewing distances and the attended frequencies.

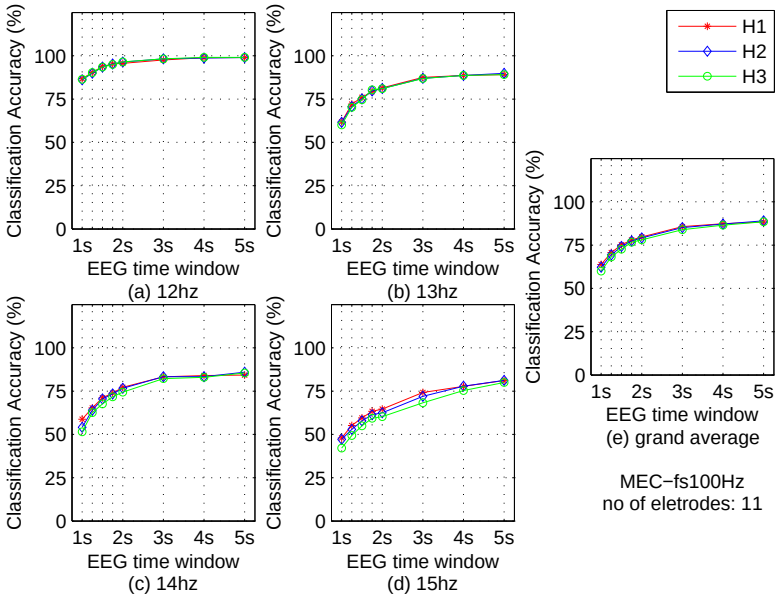

Figure B-42: **Comparison of classification accuracies using different number of SSVEP harmonics using MEC.** In this figure, the classification method is MEC and the number of the electrodes is 11. (a) to (d) are the mean classification accuracies across the subjects and the viewing distances of the attended frequency 12Hz, 13Hz, 14Hz and 15Hz respectively. (e) is the mean classification across the subjects, viewing distances and the attended frequencies.

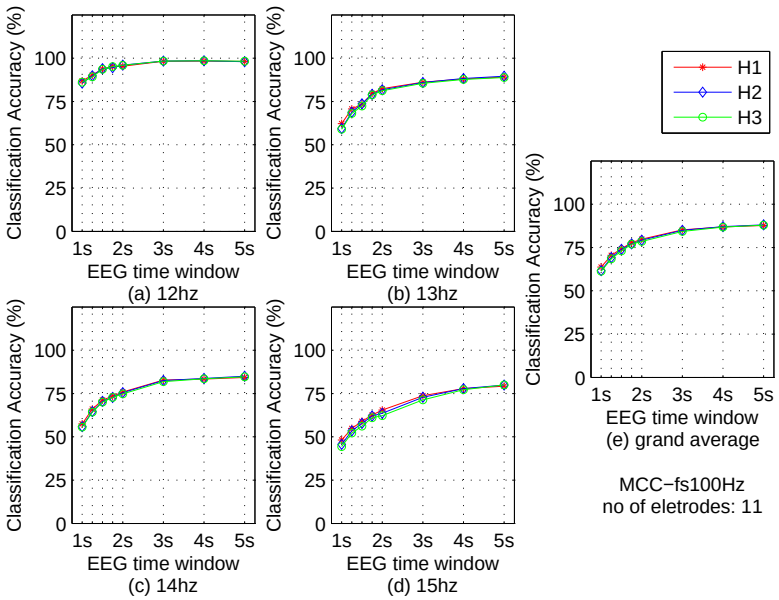

Figure B-43: **Comparison of classification accuracies using different number of SSVEP harmonics using MCC.** In this figure, the classification method is MEC and the number of the electrodes is 11. (a) to (d) are the mean classification accuracies across the subjects and the viewing distances of the attended frequency 12Hz, 13Hz, 14Hz and 15Hz respectively. (e) is the mean classification across the subjects, viewing distances and the attended frequencies.

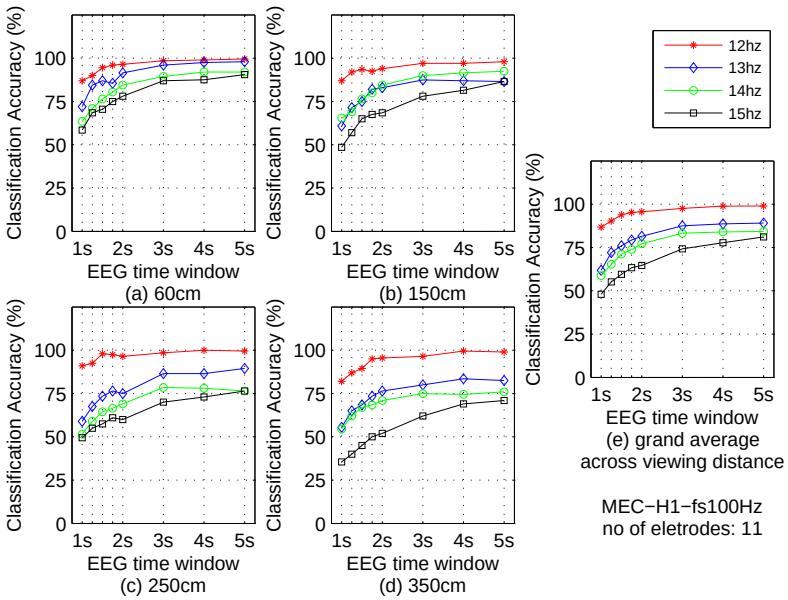

Figure B-44: **Classification accuracies of 4 attended frequencies at different viewing distances. The classification method of this figure is MEC.** (a) to (d) The classification accuracies of each attended frequency at one of the viewing distances. The accuracies are the mean across the subjects. (e) The grand average across the viewing distances of (a) to (d). The number of SSVEP harmonics and electrodes used in this figure are 1 and 11 respectively.

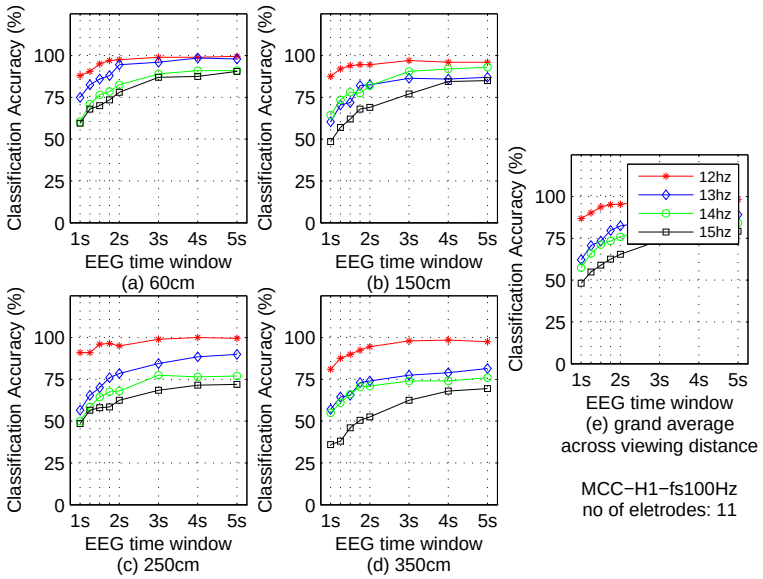

Figure B-45: **Classification accuracies of 4 attended frequencies at different viewing distances. The classification method of this figure is MCC.** (a) to (d) The classification accuracies of each attended frequency at one of the viewing distances. The accuracies are the mean across the subjects. (e) The grand average across the viewing distances of (a) to (d). The number of SSVEP harmonics and electrodes used in this figure are 1 and 11 respectively.

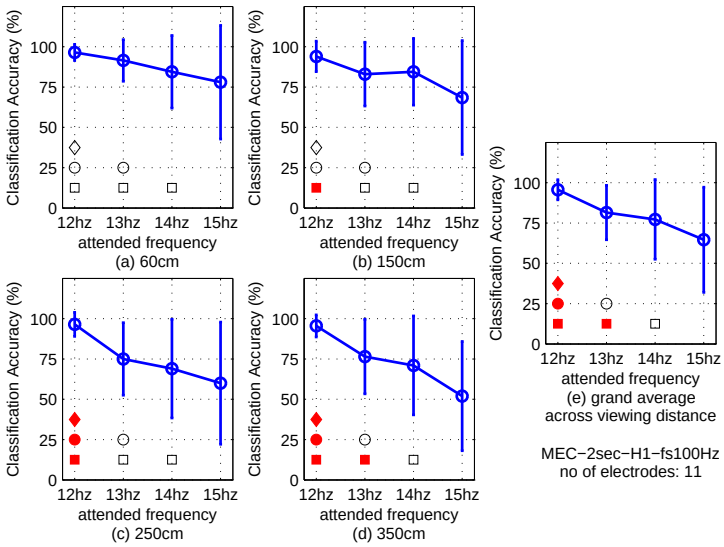

Figure B-46: **Classification accuracies across the subjects of all attended frequencies at different viewing distance and their grand average. The classification method of this figure is MEC.** (a) to (d) The classification accuracies of each attended frequency at one of the viewing distances. The accuracies are the mean across the subjects. (e) The grand average across the viewing distances of (a) to (d). The number of SSVEP harmonics and electrodes used in this figure are 1 and 11 respectively. EEG TWL is 2s.

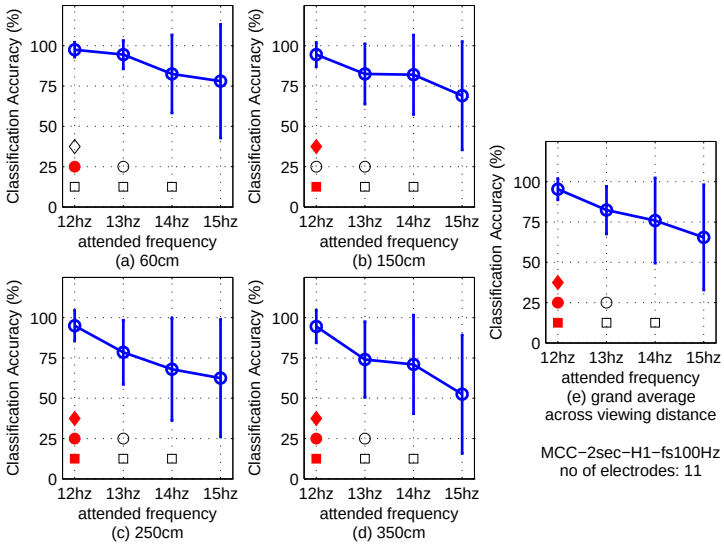

Figure B-47: **Classification accuracies across the subjects of all attended frequencies at different viewing distance and their grand average. The classification method of this figure is MCC.** (a) to (d) The classification accuracies of each attended frequency at one of the viewing distances. The accuracies are the mean across the subjects. (e) The grand average across the viewing distances of (a) to (d). The number of SSVEP harmonics and electrodes used in this figure are 1 and 11 respectively. EEG TWL is 2s.

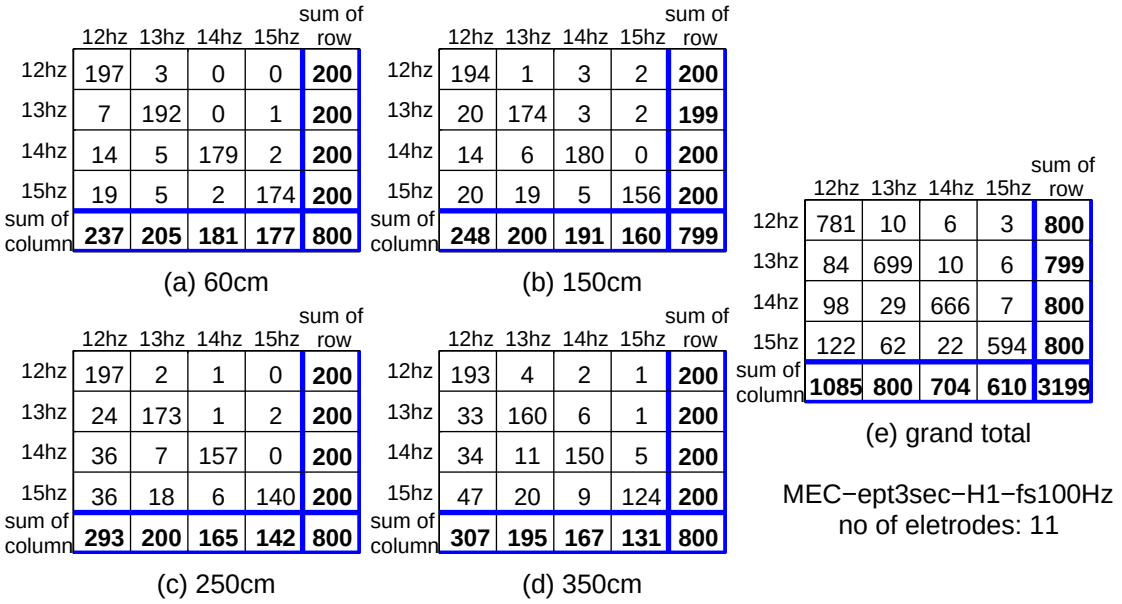

Figure B-48: **Confusion matrix of grand total of all subjects at different viewing distance using MEC.** The confusion matrix of (a) to (d) is the sum of the individual confusion matrix of each subject. (e) is the grand total of (a) to (d). Each number in the cell is the number of class i being classified as class j. The numbers of SSVEP harmonics and electrodes are 1 and 11 in this figure. The classification method is MEC and EEG TWL is 3s.

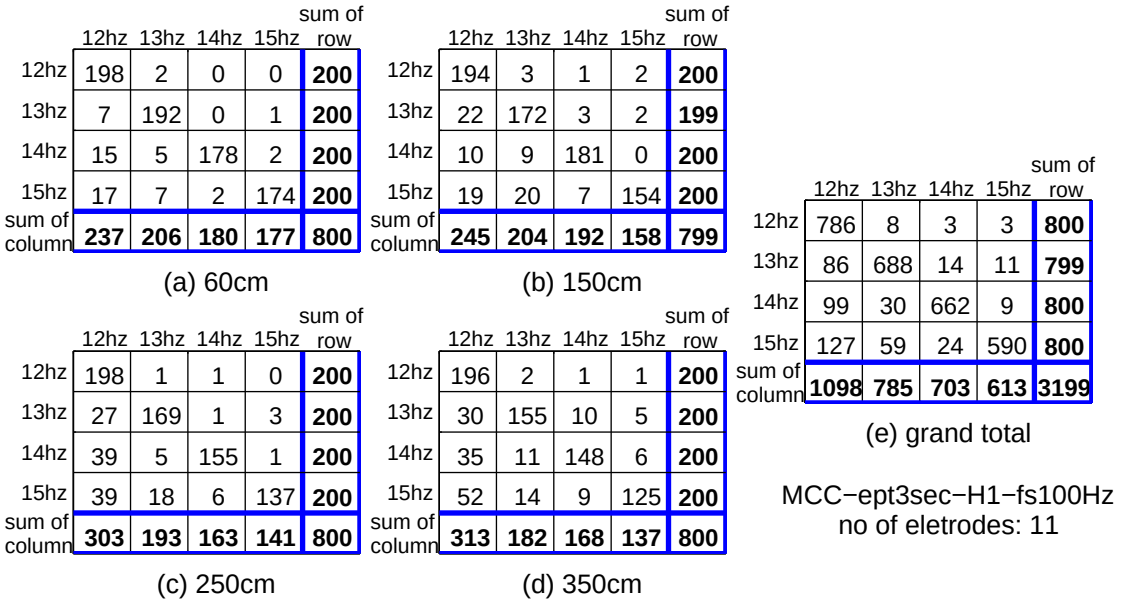

Figure B-49: **Confusion matrix of grand total of all subjects at different viewing distance using MCC.** The confusion matrix of (a) to (d) is the sum of the individual confusion matrix of each subject. (e) is the grand total of (a) to (d). Each number in the cell is the number of class i being classified as class j. The numbers of SSVEP harmonics and electrodes are 1 and 11 in this figure. The classification method is MCC and EEG TWL is 3s.

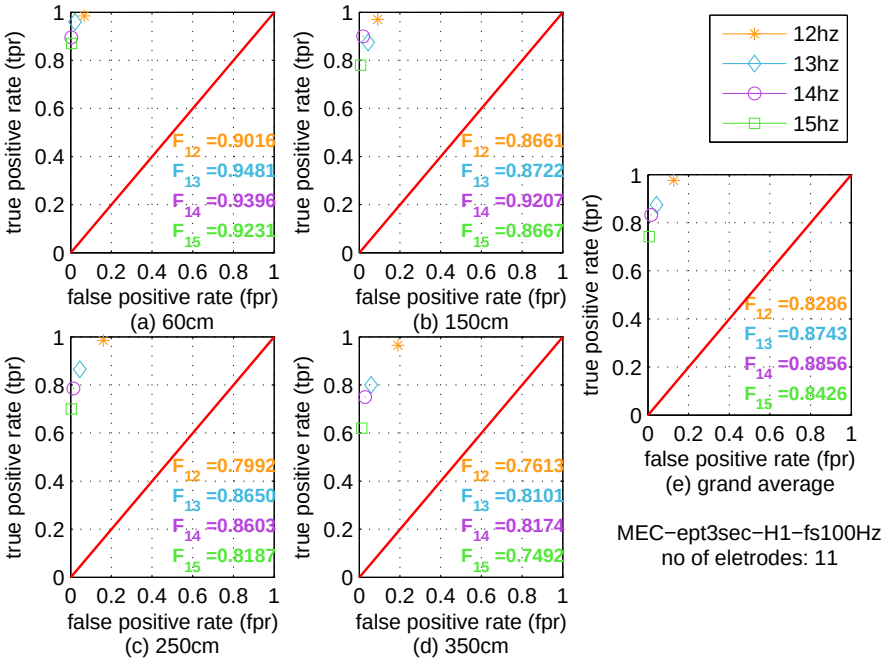

Figure B-50: **ROC plots corresponding to the confusion matrices of Figure B-48 and F measurements.** Each ROC plot (a) to (e) is corresponding to one confusion matrix of Figure B-48 (a) to (e). The classification method and parameters are the same as Figure B-48.

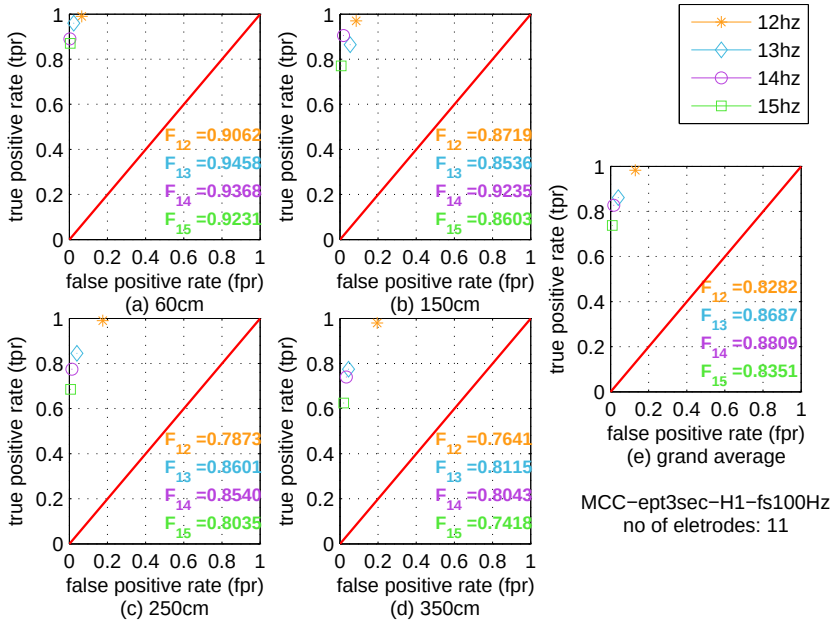

Figure B-51: **ROC plots corresponding to the confusion matrices of Figure B-49 and F measurements.** Each ROC plot (a) to (e) is corresponding to one confusion matrix of Figure B-49 (a) to (e). The classification method and parameters are the same as Figure B-49.

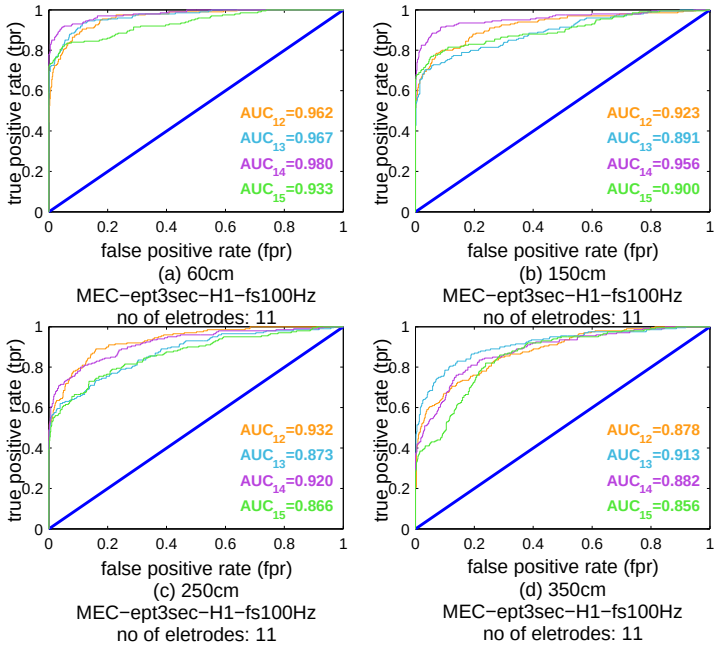

Figure B-52: **Continuous ROC curves of all attended frequencies at different viewing distances.** The subplots of (a) to (d) are for viewing distances of 60cm, 150cm, 250cm and 350cm respectively. This figure is based on classification method MEC. The numbers of SSVEP harmonica and the electrodes are 1 and 11. EEG TWL is 3s.

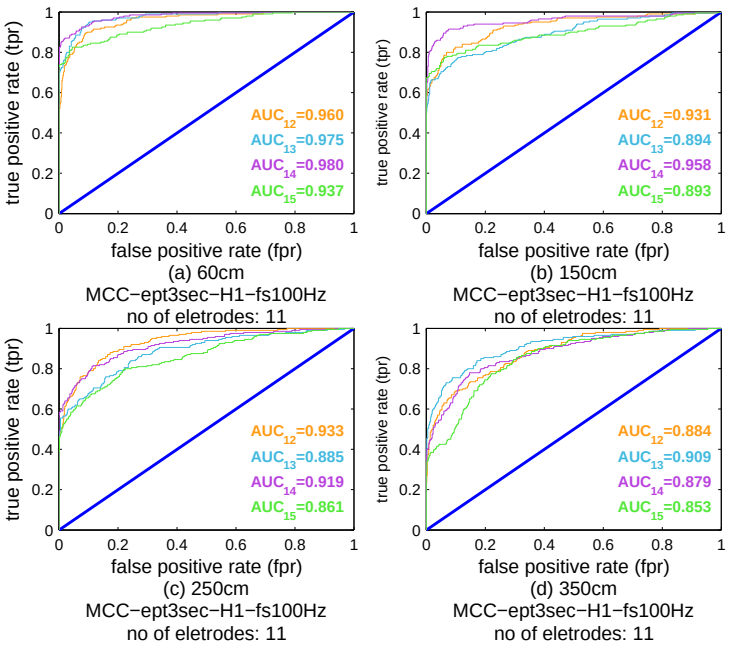

Figure B-53: **Continuous ROC curves of all attended frequencies at different viewing distances.** The subplots of (a) to (d) are for viewing distances of 60cm, 150cm, 250cm and 350cm respectively. This figure is based on classification method MCC. The numbers of SSVEP harmonica and the electrodes are 1 and 11. EEG TWL is 3s.

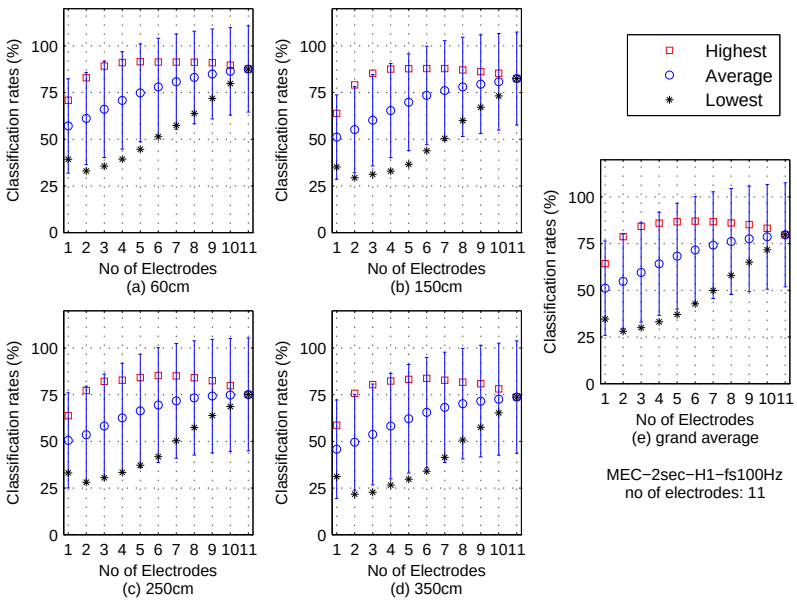

Figure B-54: **The highest, average and lowest classification accuracies and the standard deviation corresponding to the number of the electrodes across the subject and attended frequencies at different viewing distances.** EEG TWL is 2s and the number of SSVEP harmonics is 1 in this figure. The classification method is MEC.

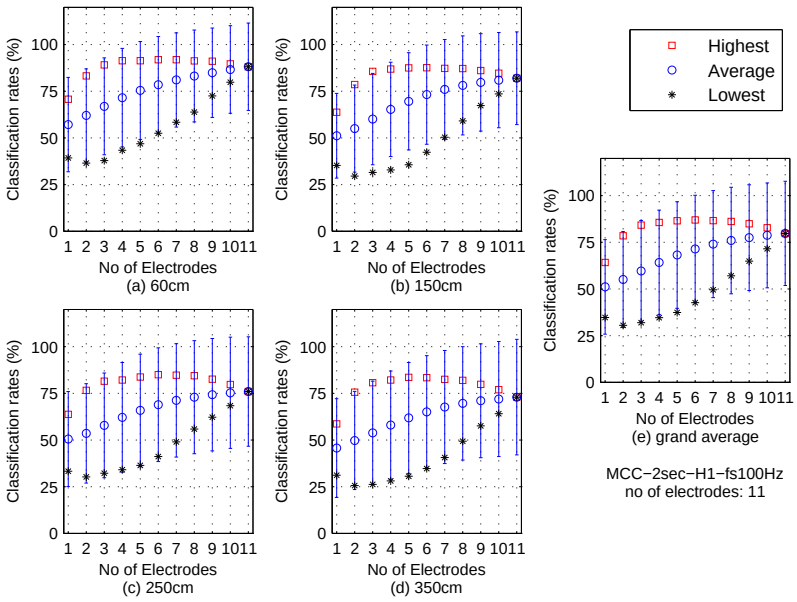

Figure B-55: **The highest, average and lowest classification accuracies and the standard deviation corresponding to the number of the electrodes across the subject and attended frequencies at different viewing distances.** EEG TWL is 2s and the number of SSVEP harmonics is 1 in this figure. The classification method is MCC.

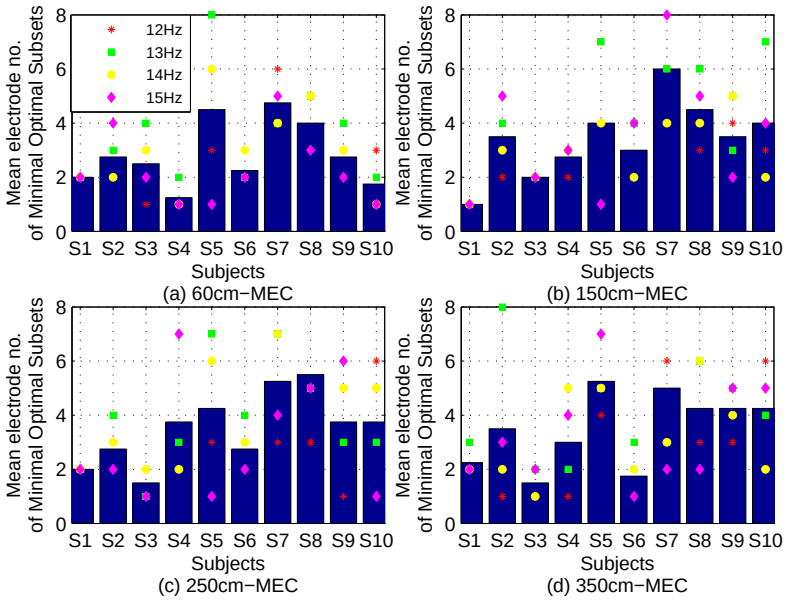

Figure B-56: **Mean electrode number of the minimal optimal electrode subsets for the subjects at different viewing distances.** The blue bar presents the mean electrode number of the minimal optimal electrode subsets for each subject across the attended frequencies. The dot presents the electrode number of one attended frequency at one viewing distance. This figure is based on MEC. EEG TWL is 2s and the number of SSVEP harmonics is 1.

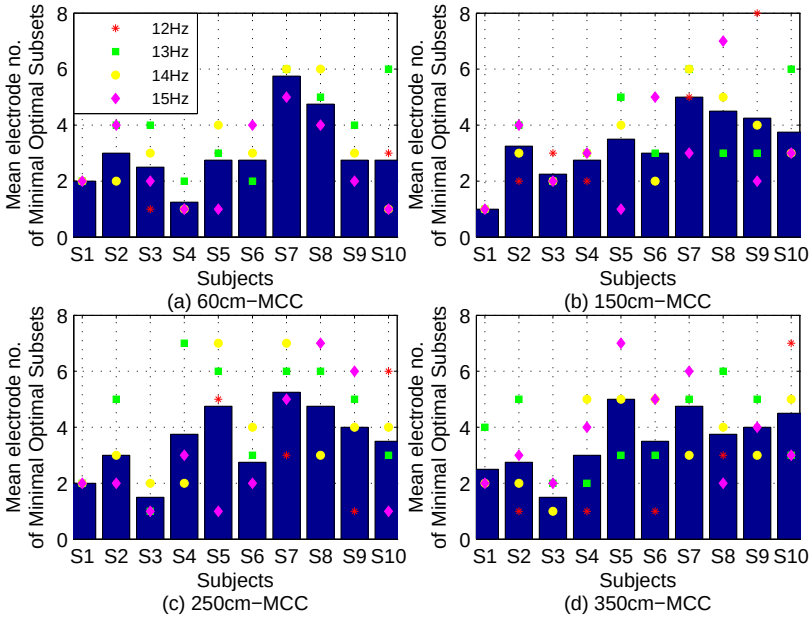

Figure B-57: **Mean electrode number of the minimal optimal electrode subsets for the subjects at different viewing distances.** The blue bar presents the mean electrode number of the minimal optimal electrode subsets for each subject across the attended frequencies. The dot presents the electrode number of one attended frequency at one viewing distance. This figure is based MCC. EEG TWL is 2s and the number of SSVEP harmonics is 1.

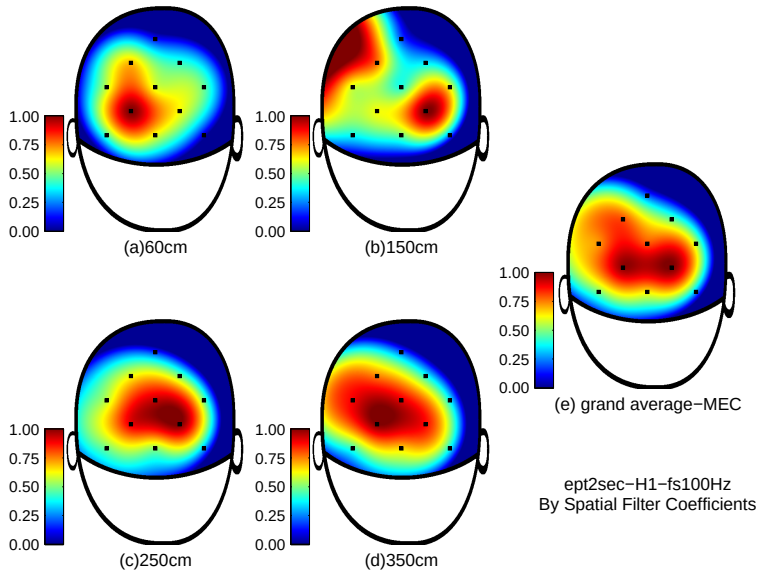

Figure B-58: **Topographies of mean MEC spatial filter coefficients of the electrodes across the subjects and attended frequencies at different viewing distances.** The spatial filter is obtained using the electrode subsets consisting of 11 electrodes in classification. The classification method of this figure is MEC.

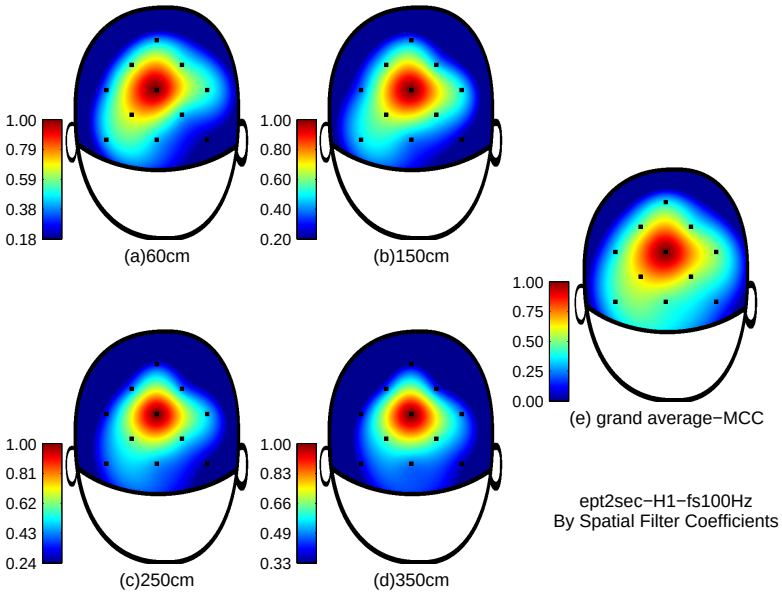

Figure B-59: **Topographies of mean MCC spatial filter coefficients of the electrodes across the subjects and attended frequencies at different viewing distances.** The spatial filter is obtained using the electrode subsets consisting of 11 electrodes in classification. The classification method of this figure is MCC.

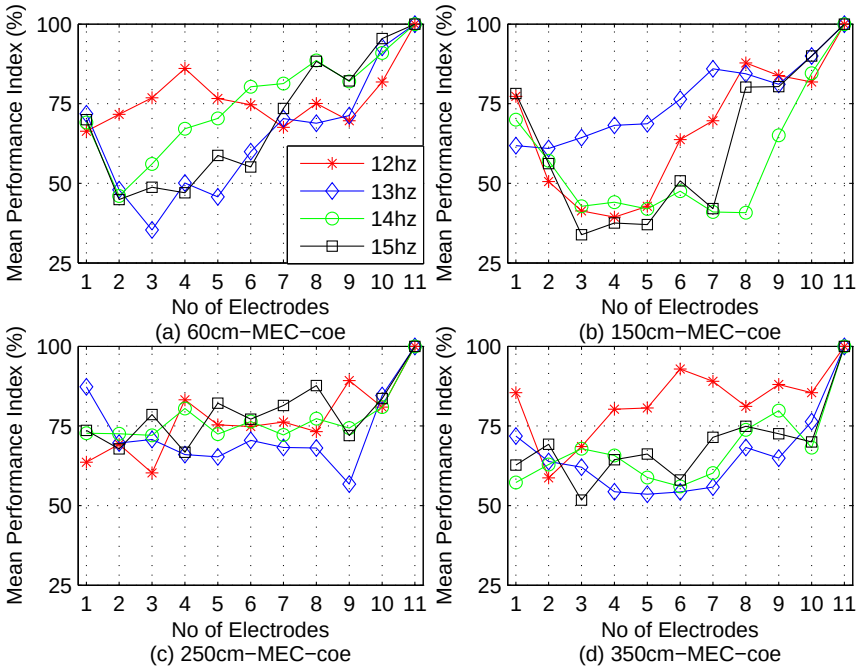

Figure B-60: **Mean PIs across the subjects for each experiment condition. This figure is based on the MEC spatial filter coefficients.** There are more PIs which are lower than 50% compared to Figure 5.15 which employs CCA.

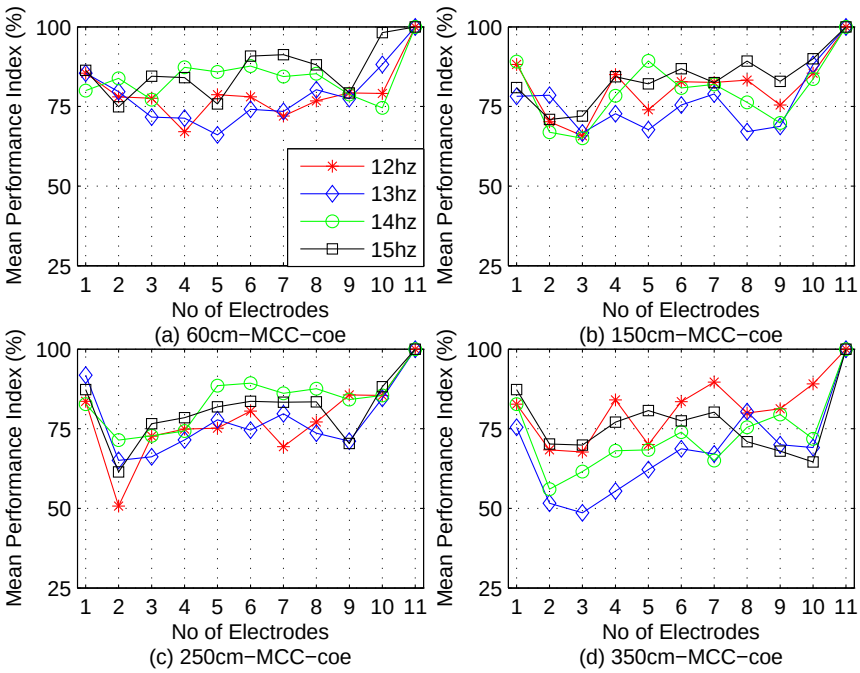

Figure B-61: **Mean PIs across the subjects for each experiment condition. This figure is based on the MCC spatial filter coefficients.** It shows that except one PI is lower than 50%, all PIs are over 50% same as Figure 5.15 which employs CCA.

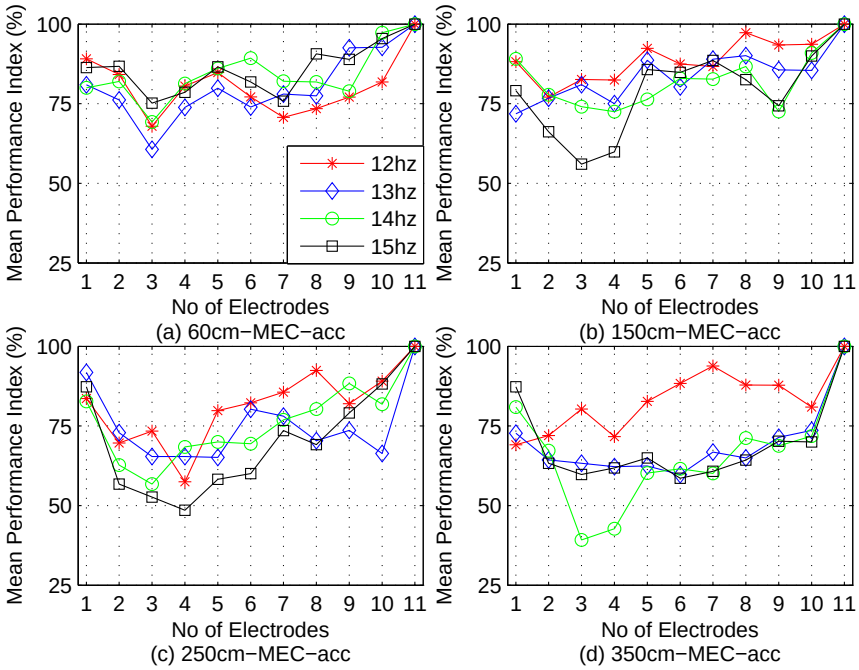

Figure B-62: **Mean PIs across the subjects for each experiment condition based on MEC. PIs of this figure are used as the evaluation metrics of the electrode rankings based on the single electrode classification accuracy.** It also shows that three PIs are lower than 50%, the rest of PIs exceed 50%, the same as seen in Figure 5.17.

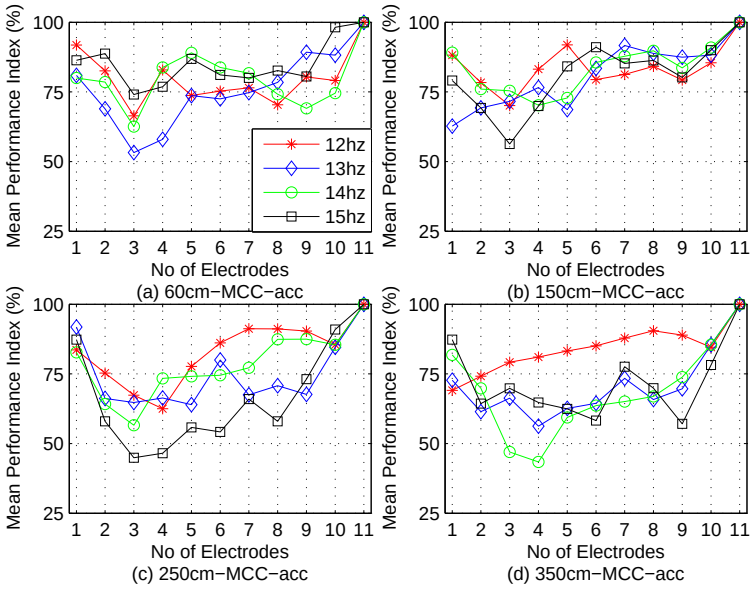

Figure B-63: **Mean PIs across the subjects for each experiment condition based on MCC. PIs of this figure are used as the evaluation metrics of the electrode rankings based on the single electrode classification accuracy.** There are four PIs lower than 50%, which are more than the ones seen in Figure 5.17. The rest of PIs exceed 50%.

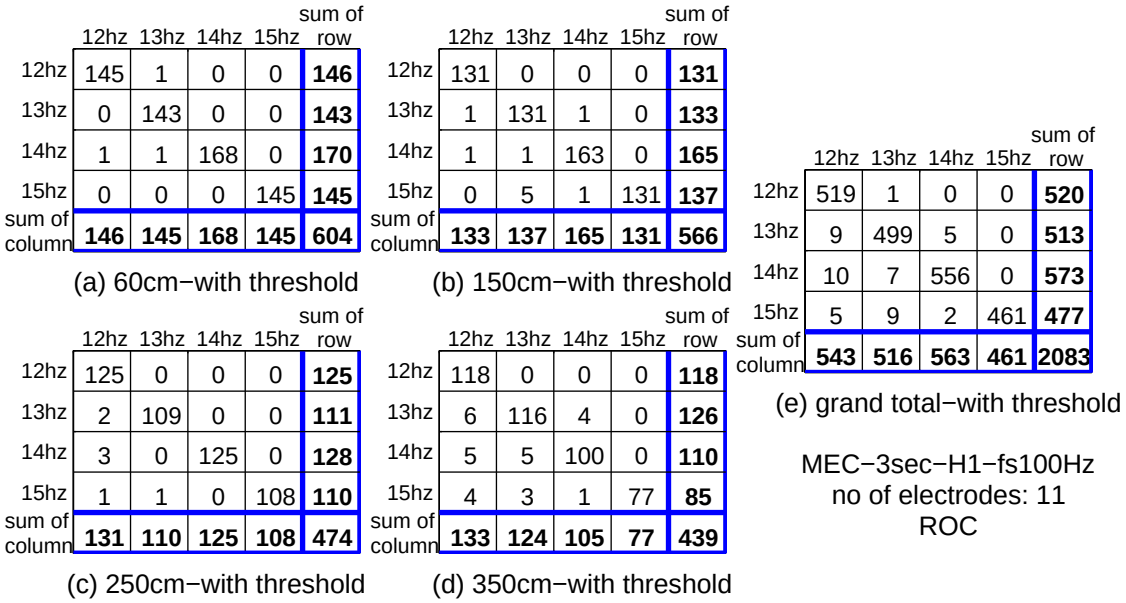

Figure B-64: **Confusion matrix of grand total of all subjects at different viewing distances using MEC with the thresholds applied.** The confusion matrix without applying the thresholds can be found in Figure B-48. The thresholds applied in this figure are the thresholds which maximise the overall accuracy of the equation (3.19) on page 97. The thresholds are different among the experiment conditions but the same for all subjects in one experiment condition. The thresholds, true positive rates and false positives rates used in equation (3.19) are from Figure B-52.

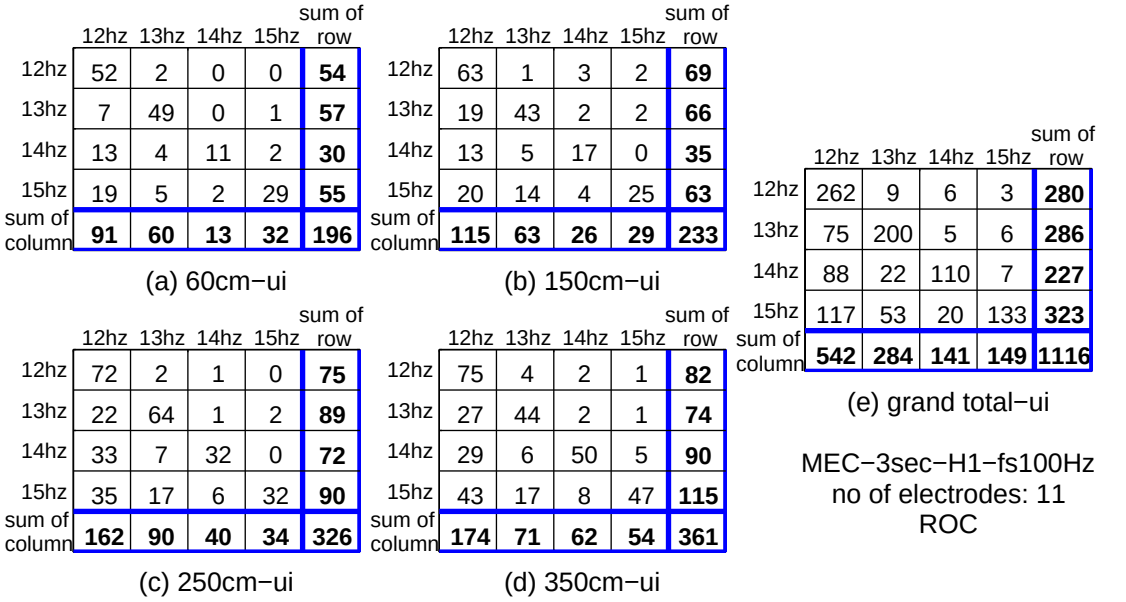

Figure B-65: **Maxtrix of UI class after applying the thresholds on the classification.** Each UI matrix is the difference between the corresponding confusion matrices of Figures B-48, and B-64 in the same subplot. This figure is based on MEC.

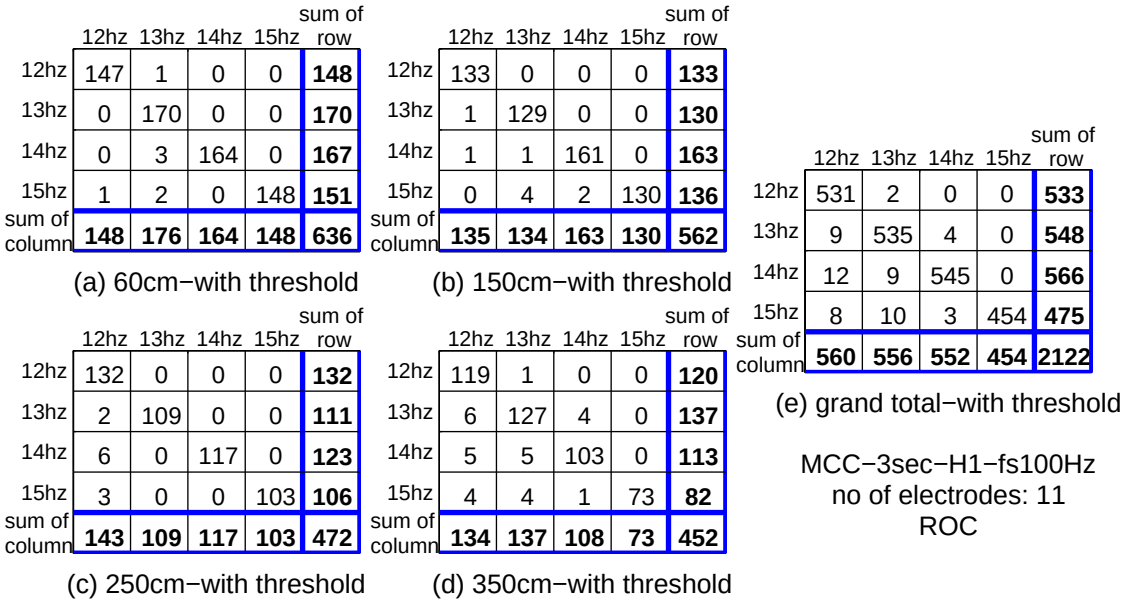

Figure B-66: **Confusion matrix of grand total of all subjects at different viewing distances using MCC with the thresholds applied.** The confusion matrix without applying the thresholds can be found in Figure B-49. The thresholds applied in this figure are the thresholds which maximise the overall accuracy of the equation (3.19) on page 97. The thresholds are different among the experiment conditions but the same for all subjects in one experiment condition. The thresholds, true and false positives rates used in equation (3.19) are from Figure B-53.

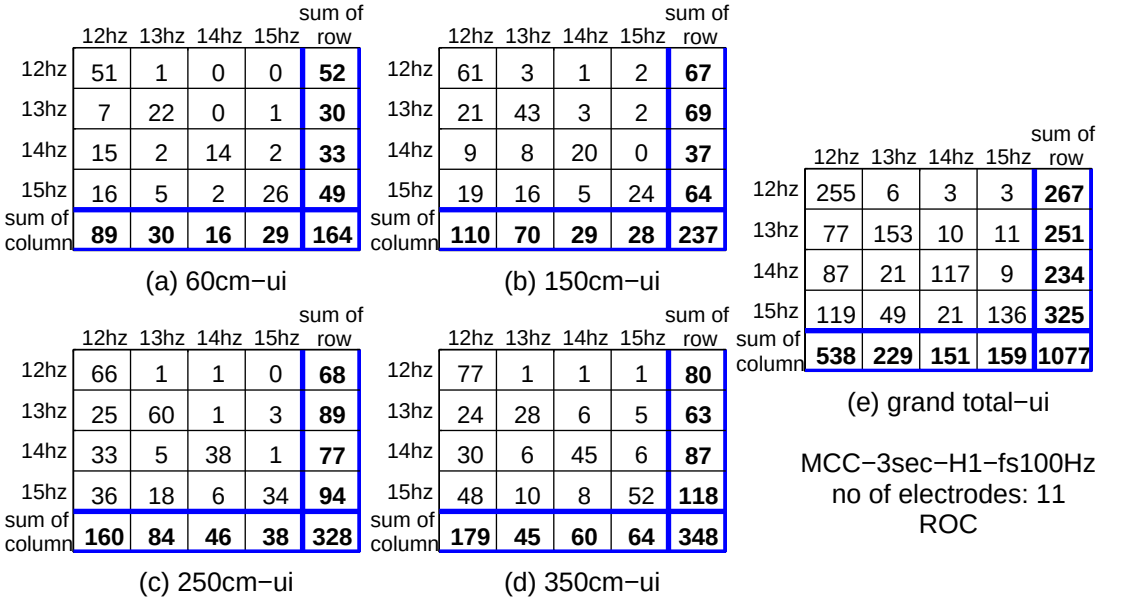

Figure B-67: **Maxtrix of UI class caused after applying the thresholds on the classification.** Each UI matrix is the difference between the corresponding confusion matrices of Figures B-49, and B-66 in the same subplot. This figure is based on MCC.

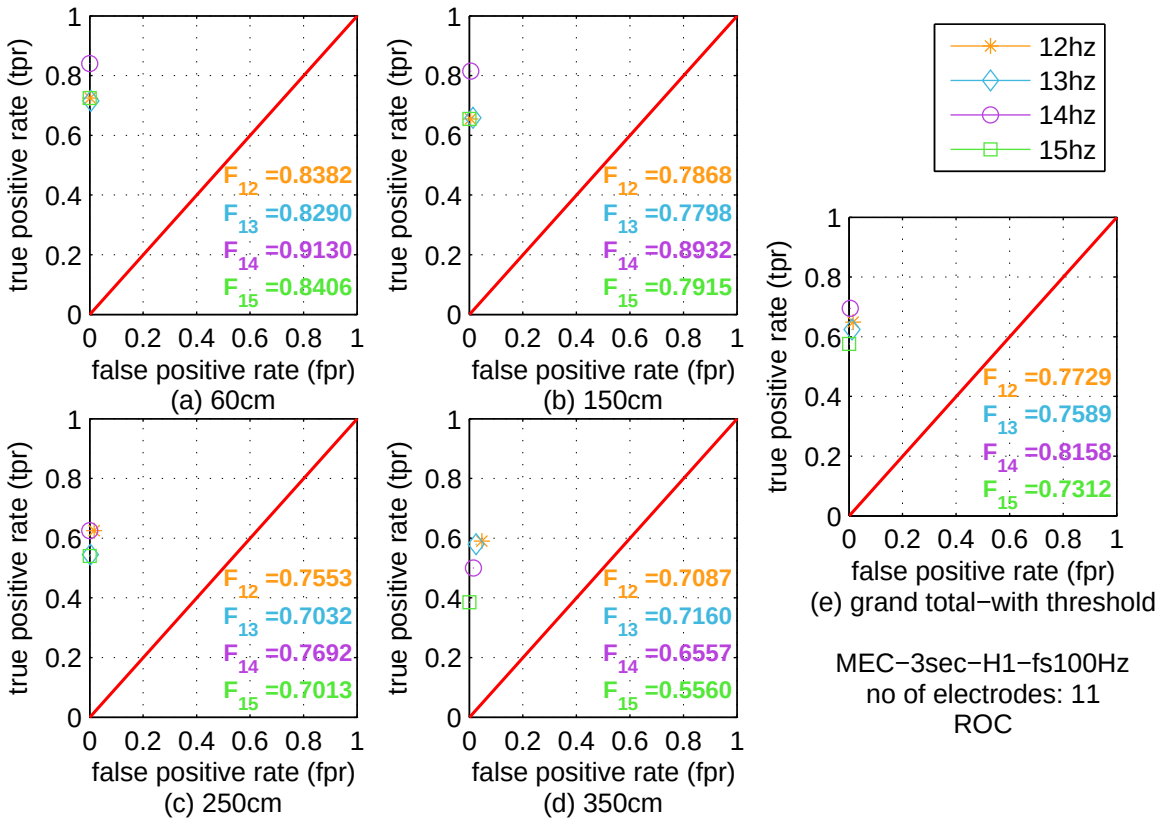

Figure B-68: **Modified ROC plots corresponding to the confusion matrices of Figure B-64 and F measurements when the thresholds applied.** The false positive rate (fpr) in this figure is calculated according to the confusion matrix in Figure B-64. However, to see how the true positive rate (tpr), the accuracies of each frequency, are affected by the thresholds, the total classification number of each row is based on Figure B-48 and the number of the true positives, the number of being classified correctly, of each frequency is based on the Figure B-64. As a result, the true positive rates decrease.

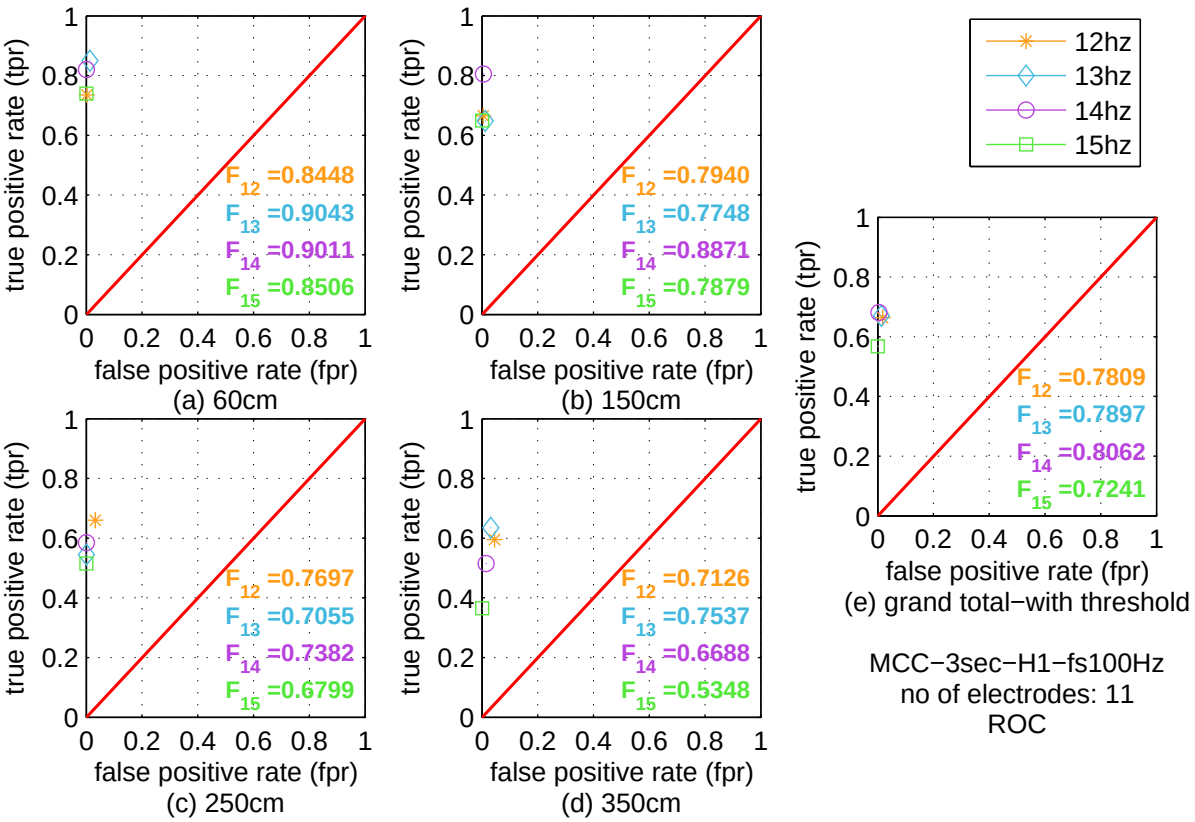

Figure B-69: **Modified ROC plots corresponding to the confusion matrices of Figure B-66 and F measurements when the thresholds applied.** The false positive rate (fpr) in this figure is calculated according to the confusion matrix in Figure B-66. However, to see how the true positive rate (tpr), the accuracies of each frequency, are affected by the thresholds, the total classification number of each row is based on Figure B-49 and the number of the true positives, the number of being classified correctly, of each frequency is based on the Figure B-64. As a result, the true positive rates decrease.

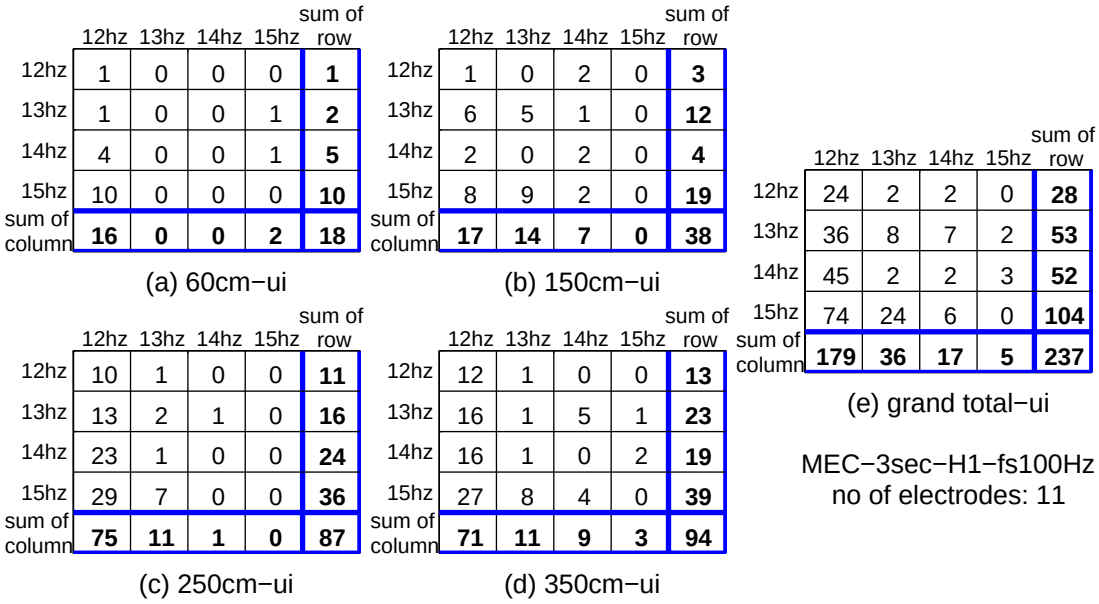

Figure B-70: **UI number of the confusion matrix in Figure B-48 with applied thresholds which maximise *F* measurements.** Each matrix of this figure is the difference between two corresponding matrices in Figures B-48 and Figure B-71.

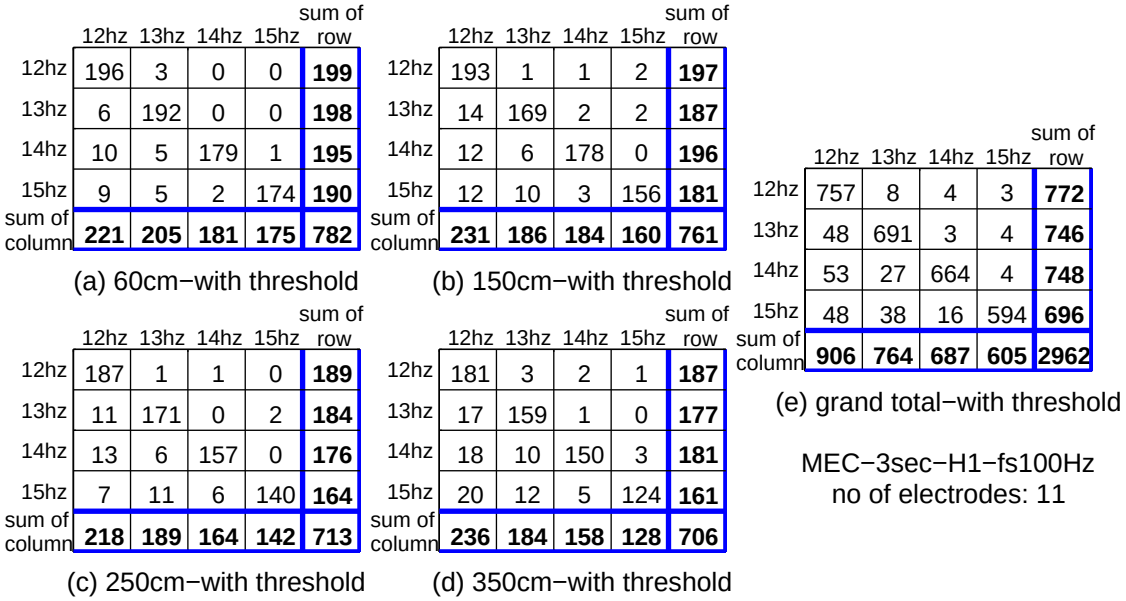

Figure B-71: **Confusion matrix of grand total of all subjects at different viewing distance using MEC.** This figure is corresponding to Figure B-48 in which no thresholds are applied. The thresholds of each subject in each experiment condition are different. The thresholds applied to each subject in different experiment condition maximise F measurement of the corresponding experiment condition. If the feature used as the classification criterion is lower than the thresholds, it is classified as UI class. (a) to (d) is the sum of the individual confusion matrix of each subject. (e) is the grand total of (a) to (d). The numbers of SSVEP harmonics and electrodes are 1 and 11 in this figure. The classification method is CCA and EEG TWL is 3s.

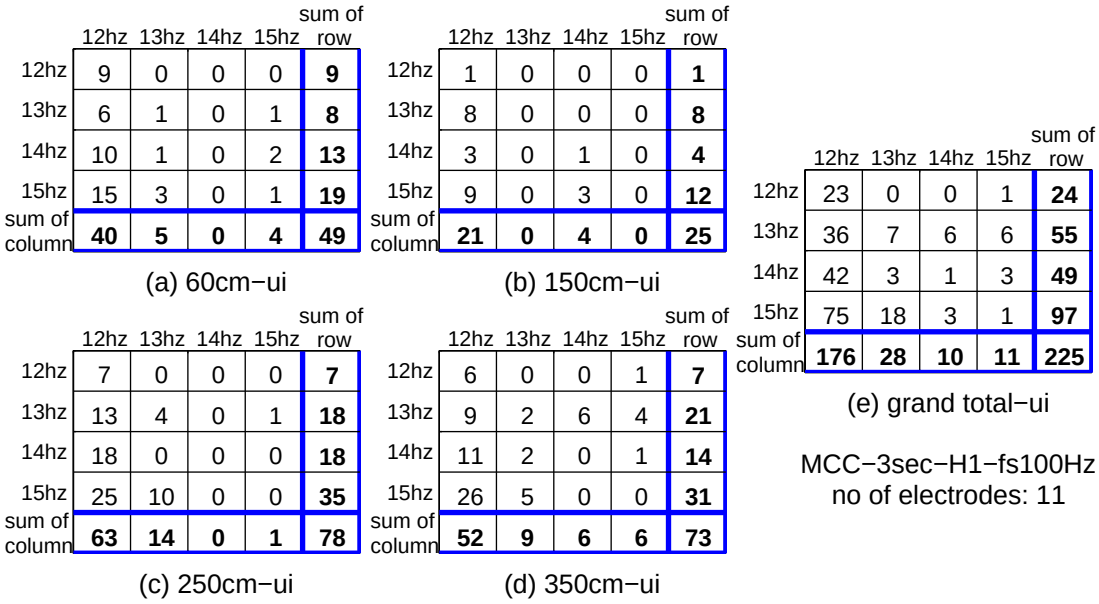

Figure B-72: **UI number of the confusion matrix in Figure B-49 with applied thresholds which maximise *F* measurements.** Each matrix of this figure is the difference between two corresponding matrices in Figures B-49 and Figure B-73.

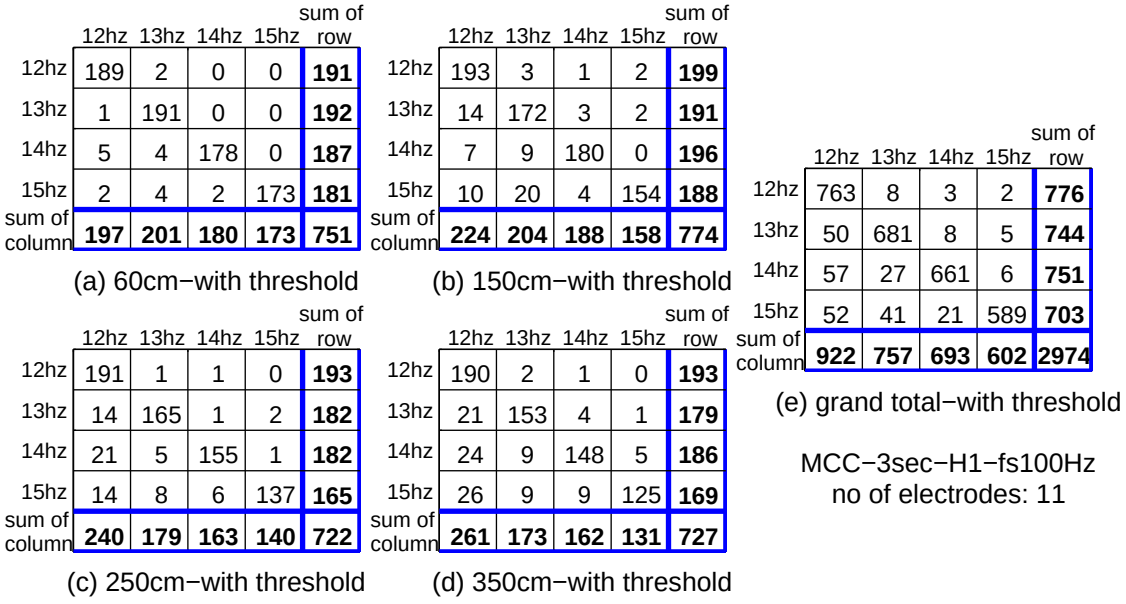

Figure B-73: **Confusion matrix of grand total of all subjects at different viewing distance using MCC.** This figure is corresponding to Figure B-49 in which no thresholds are applied. The thresholds of each subject in each experiment condition are different. The thresholds applied to each subject in different experiment condition maximise F measurement of the corresponding experiment condition. If the feature used as the classification criterion is lower than the thresholds, it is classified as UI class. (a) to (d) is the sum of the individual confusion matrix of each subject. (e) is the grand total of (a) to (d). The numbers of SSVEP harmonics and electrodes are 1 and 11 in this figure. The classification method is MCC and EEG TWL is 3s.

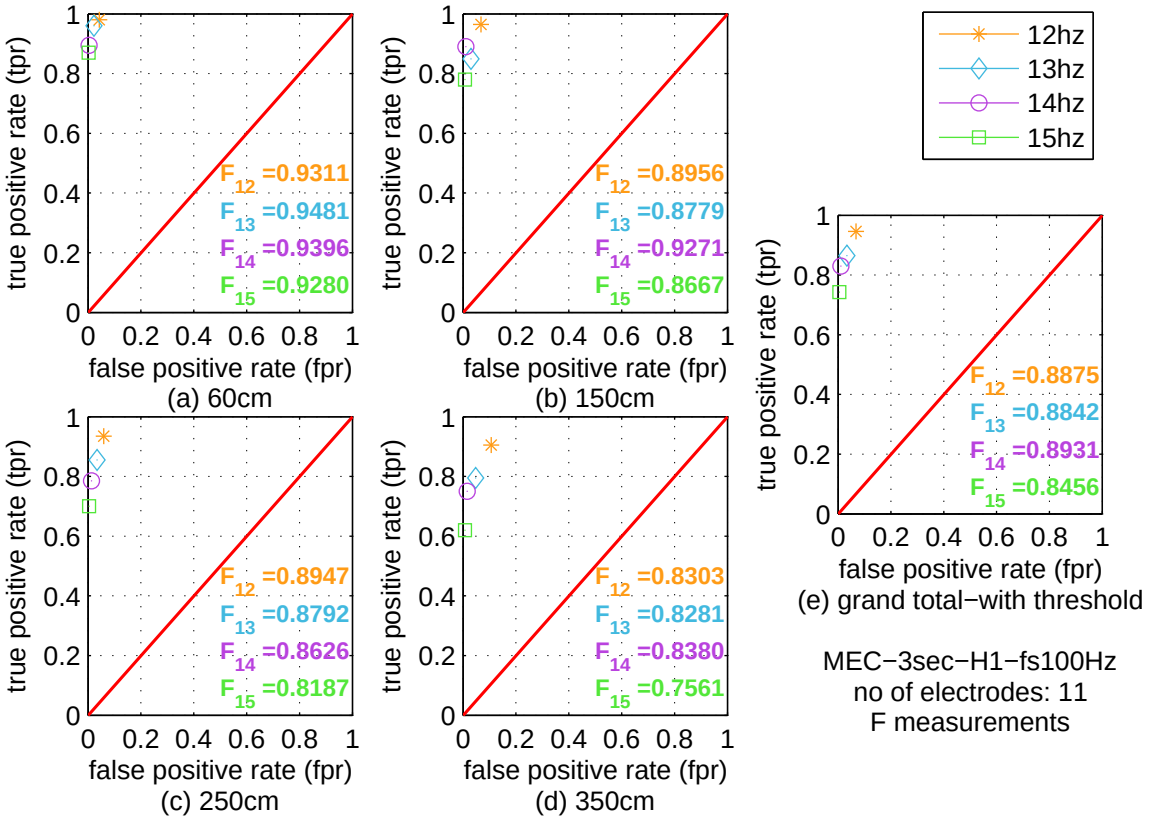

Figure B-74: **Modified ROC plots corresponding to the confusion matrices of Figure B-71 and *F* measurements with the thresholds applied.** ROC plots corresponding to the confusion matrices of Figure B-71 and F measurements. Each ROC plot (a) to (e) is corresponding to one confusion matrix of Figure B-71 (a) to (e). The classification method and parameters are the same as Figure B-48. With the thresholds applied, F measurements are higher or the same compared to Figure B-50.

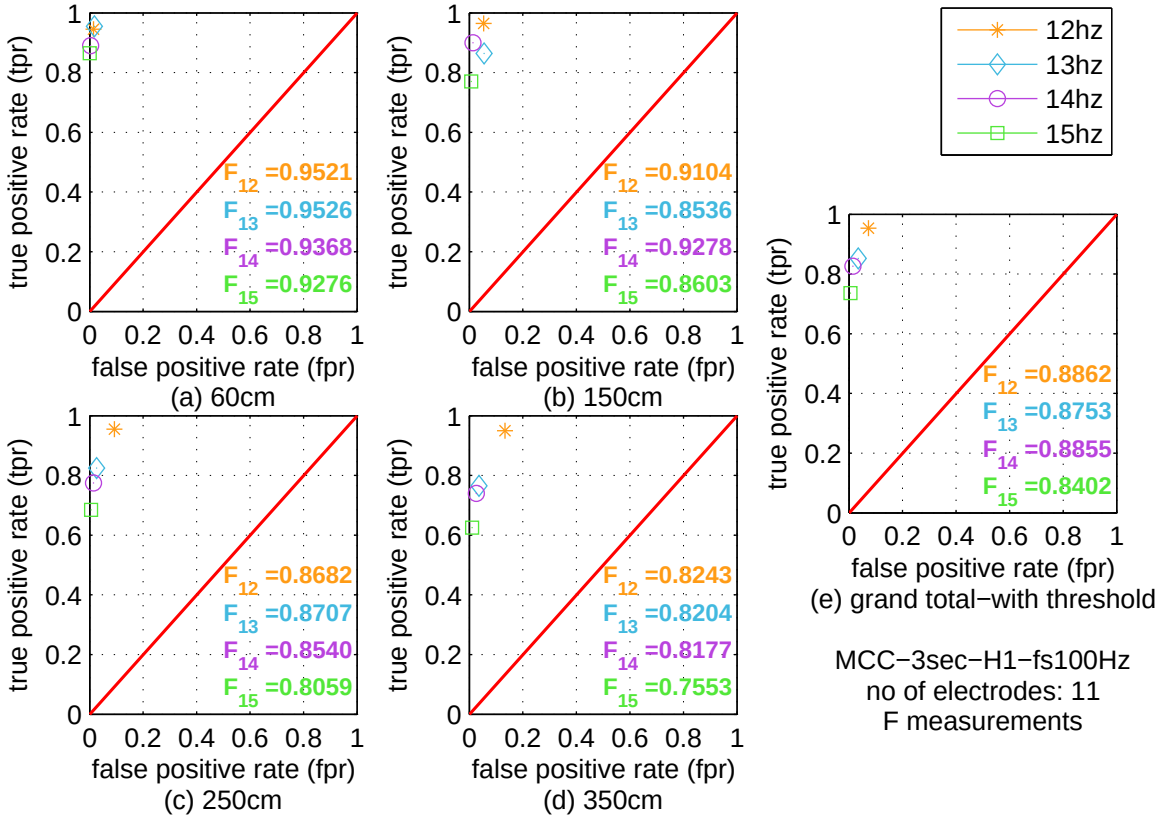

Figure B-75: **Modified ROC plots corresponding to the confusion matrices of Figure B-73 and *F* measurements with the thresholds applied.** ROC plots corresponding to the confusion matrices of Figure B-73 and F measurements. Each ROC plot (a) to (e) is corresponding to one confusion matrix of Figure B-73 (a) to (e). The classification method and parameters are the same as Figure B-49. With the thresholds applied, F measurements are higher compared to Figure B-51.

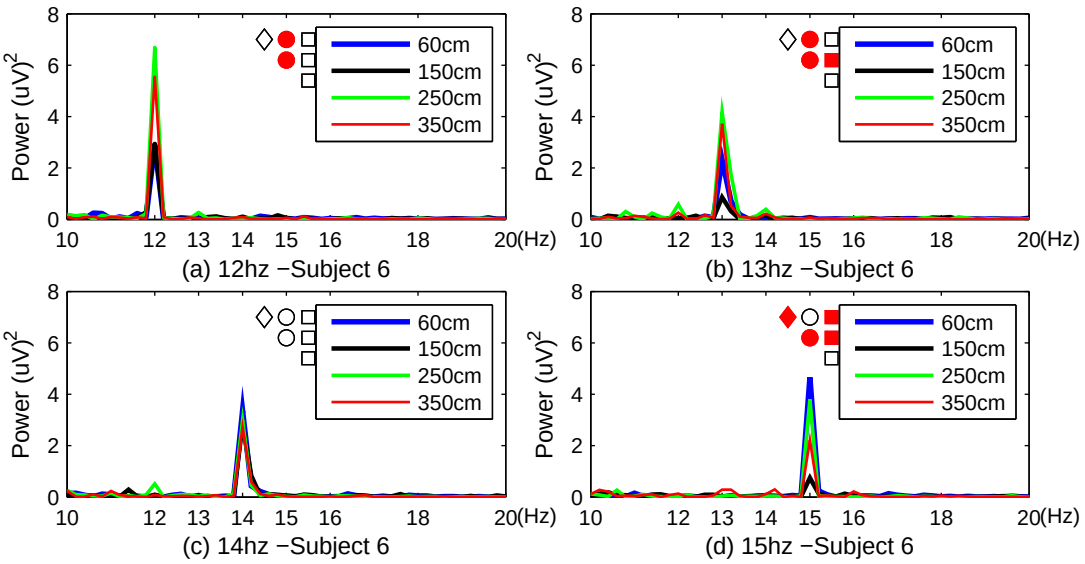

Figure B-76: **Mean SSVEP response of the same attended frequency of subject 6 at different viewing distances and ANOVA test results of SSVEPs of the same attended frequency between different viewing distances.** The presentation of ANOVA test is the same as described in Figure 5.24.

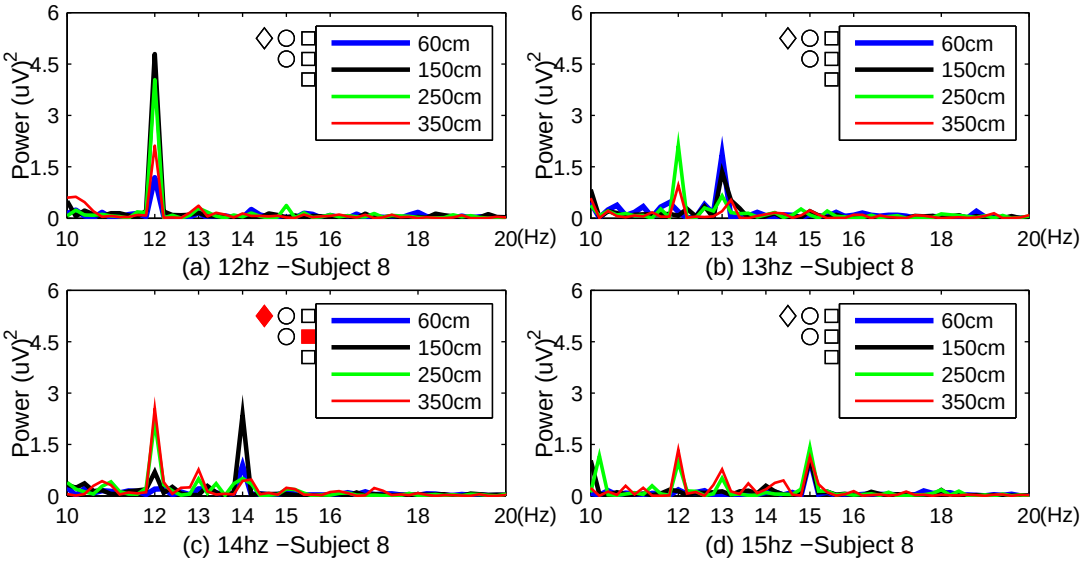

Figure B-77: **Mean SSVEP response of the same attended frequency of subject 8 at different viewing distances and ANOVA test results of SSVEPs of the same attended frequency between different viewing distances.** The presentation of ANOVA test is the same as described in Figure 5.24.

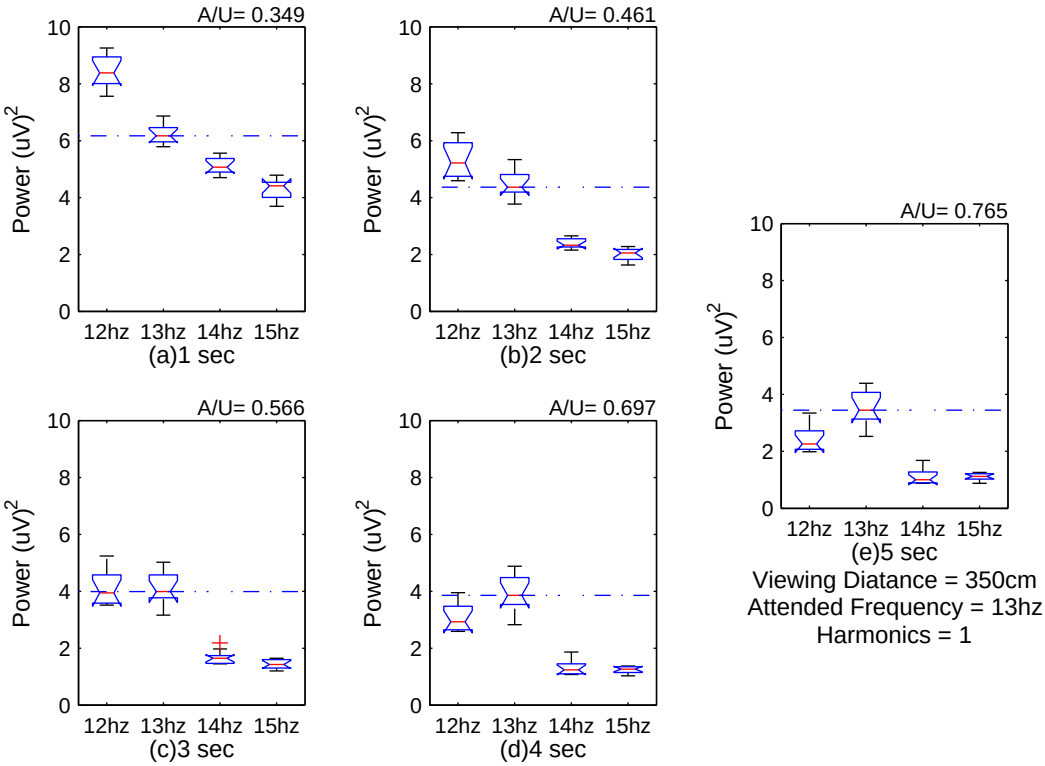

Figure B-78: **Mean SSVEP powers of SSVEPs of the attended frequency and unattended frequencies and its corresponding A/U ratio over time. This figure illustrates SSVEP powers of all stimulating frequencies in (13Hz, 350cm) experiment condition.** This figure illustrates SSVEP powers of all stimulating frequencies in (13Hz, 350cm) experiment condition. A/U ratio increases as the time increases. So do SSVEPs at all stimulating frequencies. It takes more than 3 seconds before the power of attended frequency (13Hz) exceeds the one of 12Hz.

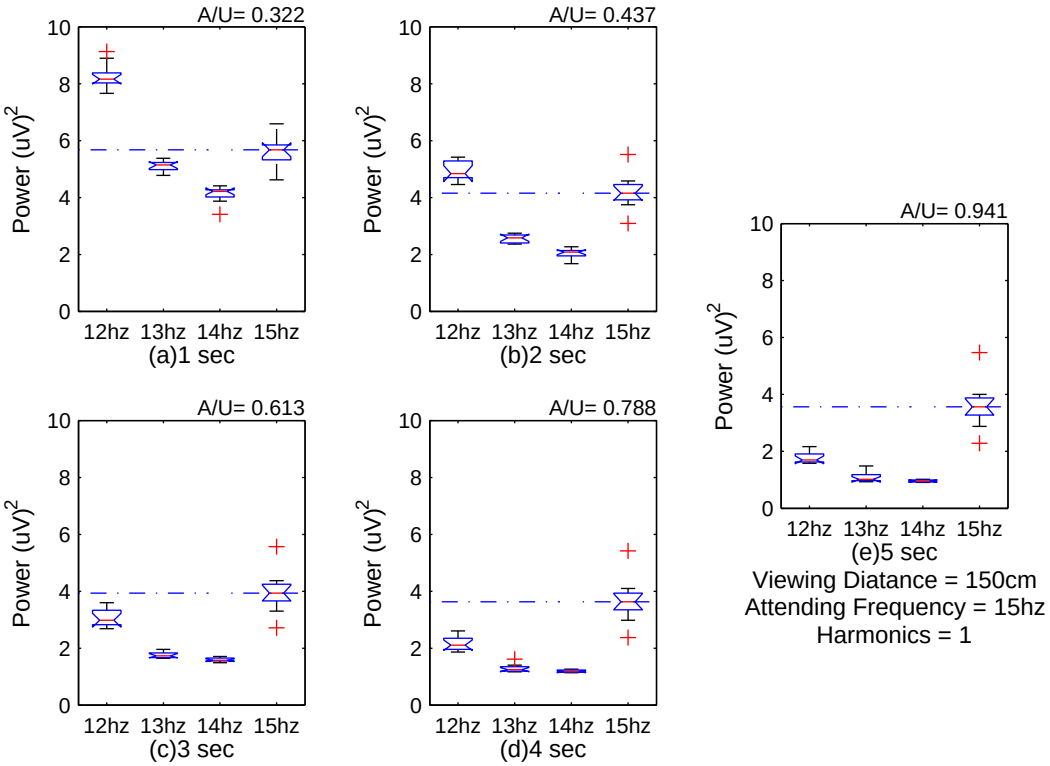

Figure B-79: **Mean SSVEP powers of SSVEPs of the attended frequency and unattended frequencies and its corresponding A/U ratio over time. This figure illustrates SSVEP powers of all stimulating frequencies in (15Hz, 150cm) experiment condition.** This figure illustrates SSVEP powers of all stimulating frequencies in (15Hz, 150cm) experiment condition. A/U ratio increases as the time increases. So do SSVEPs at all stimulating frequencies. It takes more than 2s before the power of attended frequency (15Hz) exceeds the one of 12Hz.

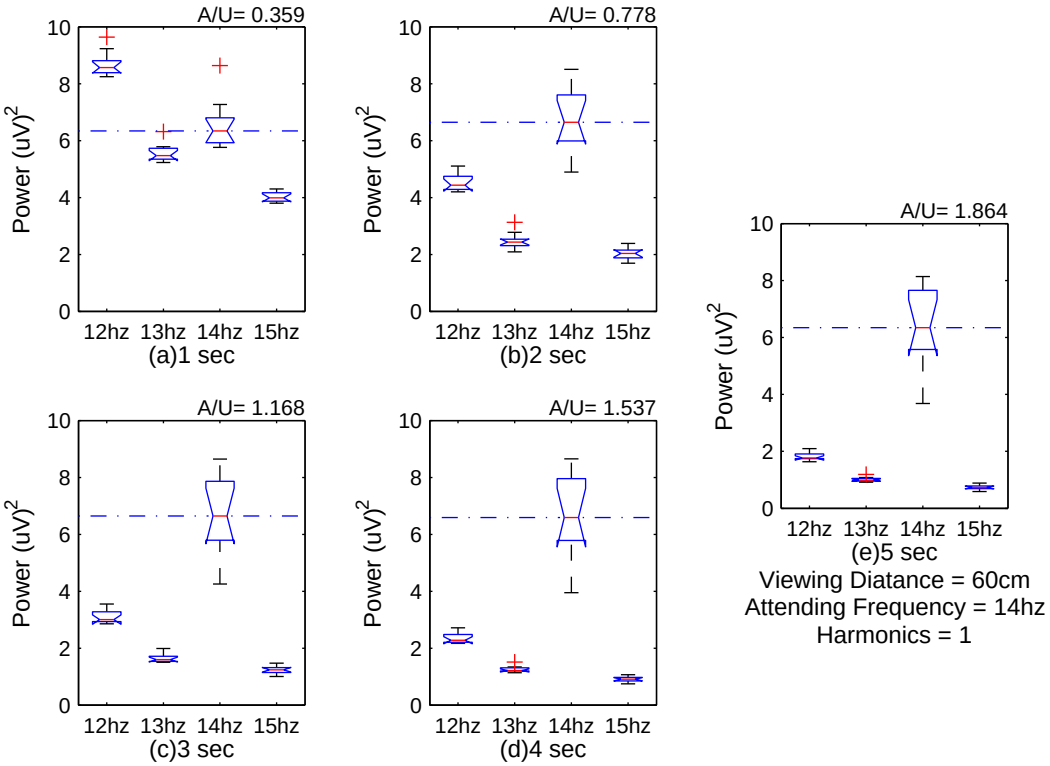

Figure B-80: **Mean SSVEP powers of SSVEPs of the attended frequency and unattended frequencies and its corresponding A/U ratio over time. This figure illustrates SSVEP powers of all stimulating frequencies in (14Hz, 60cm) experiment condition.** This figure illustrates SSVEP powers of all stimulating frequencies in (14Hz, 60cm) experiment condition. A/U ratio increases as the time increases. So do SSVEPs at all stimulating frequencies. It takes more than 1s before the power of attended frequency (14Hz) exceeds the one of 12Hz.

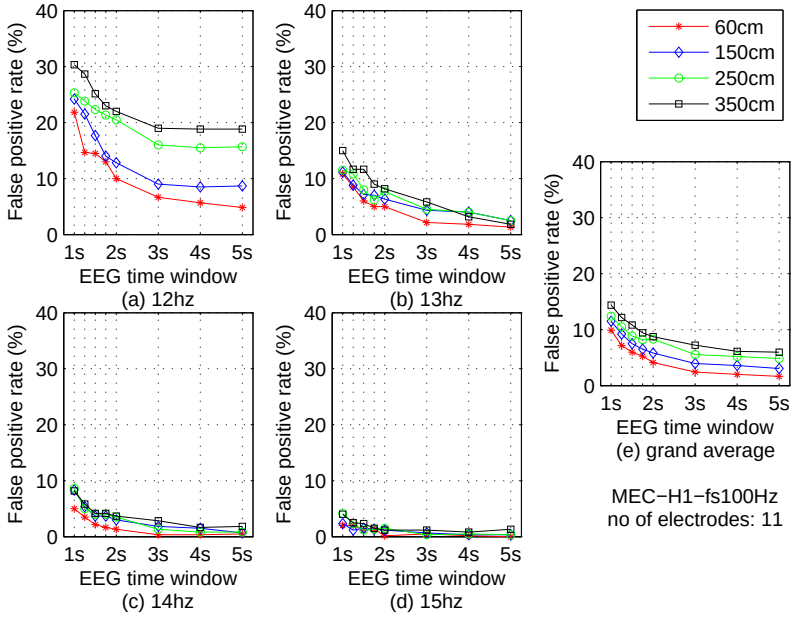

Figure B-81: **False positive rates of different viewing distances of the same attended frequency and their grand average across the attended frequencies over time. This figure is the result of MEC.** Each subplot stands for one attended frequency. Subplots (a) to (d) present the attended frequency 12Hz, 13Hz,14Hz and 15Hz respectively over the time instances from 1s to 5s.

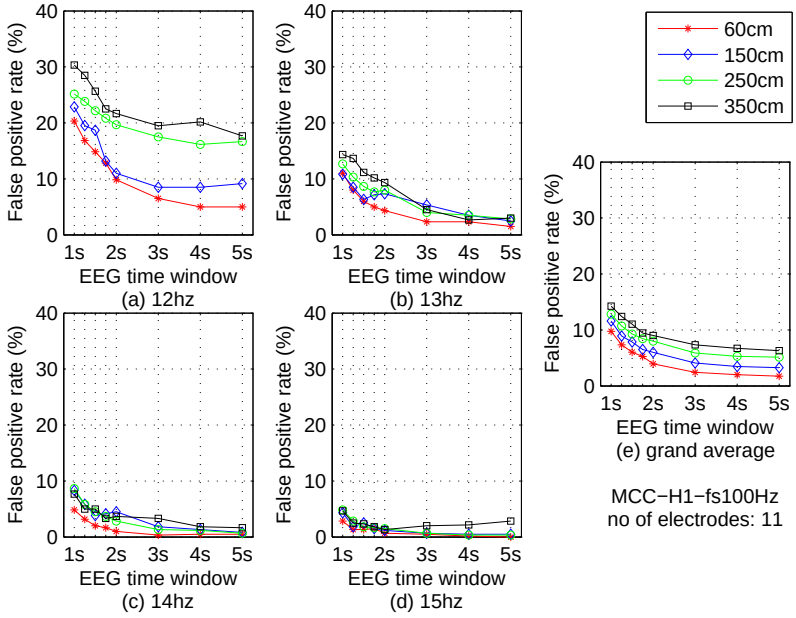

Figure B-82: **False positive rates of different viewing distances of the same attended frequency and their grand average across the attended frequencies over time. This figure is the result of MCC.** Each subplot stands for one attended frequency. Subplots (a) to (d) present the attended frequency 12Hz, 13Hz,14Hz and 15Hz respectively over the time instances from 1s to 5s.

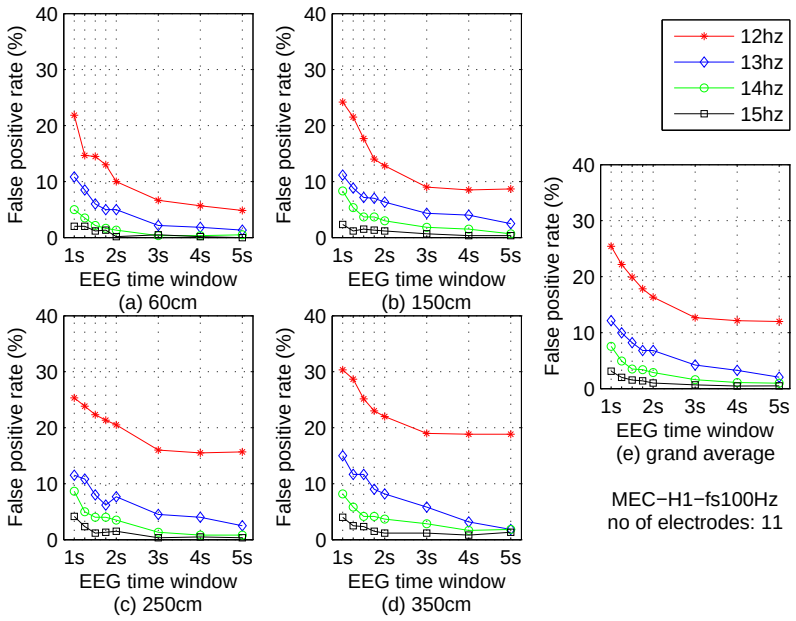

Figure B-83: **False positives rates of different attended frequencies at the same viewing distance and their grand average across the viewing distance over time. This figure is the result of MEC.** Each subplot stands for one viewing distance. Subplots (a) to (d) present the viewing distance 60cm, 150cm, 250cm and 350cm respectively over the time instances from 1s to 5s.

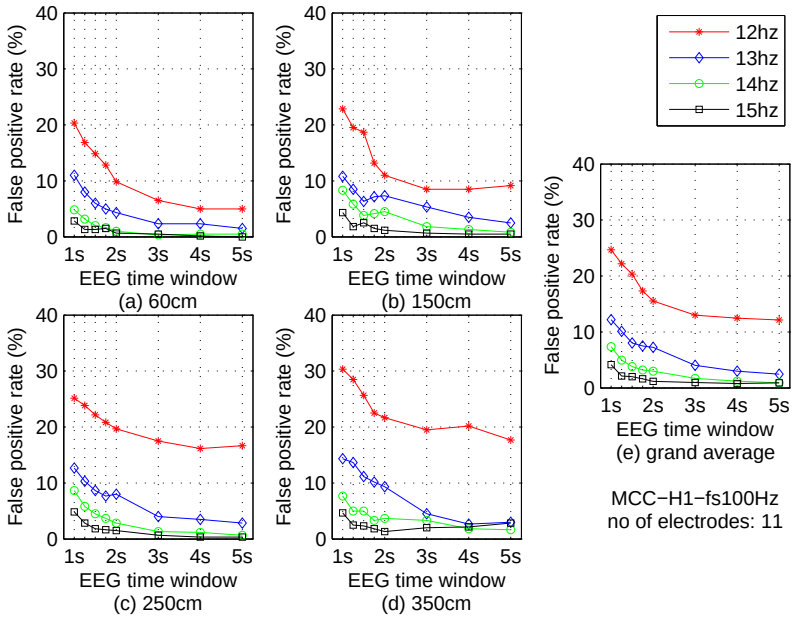

Figure B-84: **False positives rates of different attended frequencies at the same viewing distance and their grand average across the viewing distance over time. This figure is the result of MCC.** Each subplot stands for one viewing distance. Subplots (a) to (d) present the viewing distance 60cm, 150cm, 250cm and 350cm respectively over the time instances from 1s to 5s.

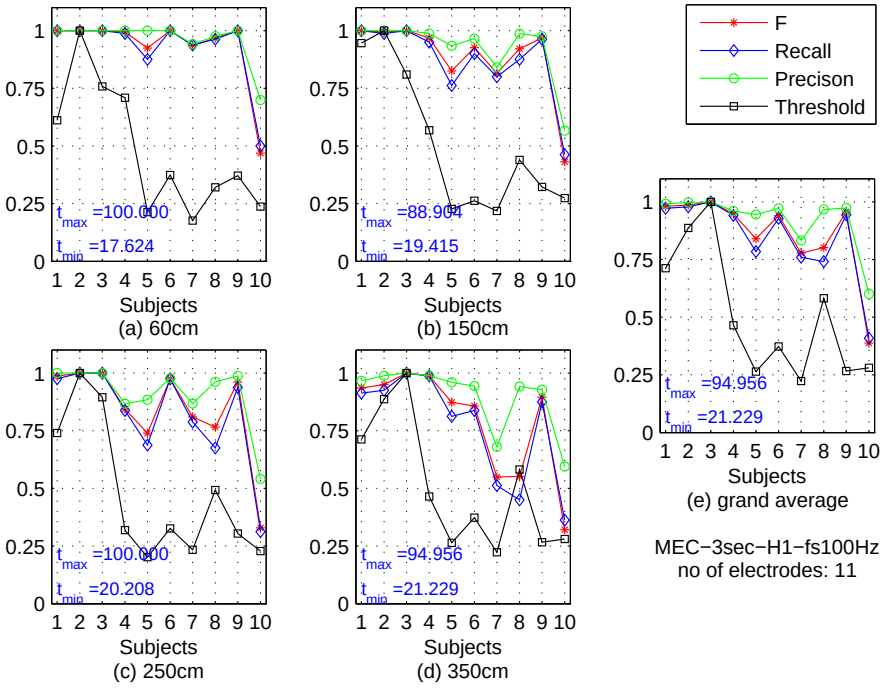

Figure B-85: **Mean optimised thresholds which maximise *F* measurements across the attended frequencies for each subject and the corresponding *F*, recall rates and precision rates.** This figure is based on MEC classification method.

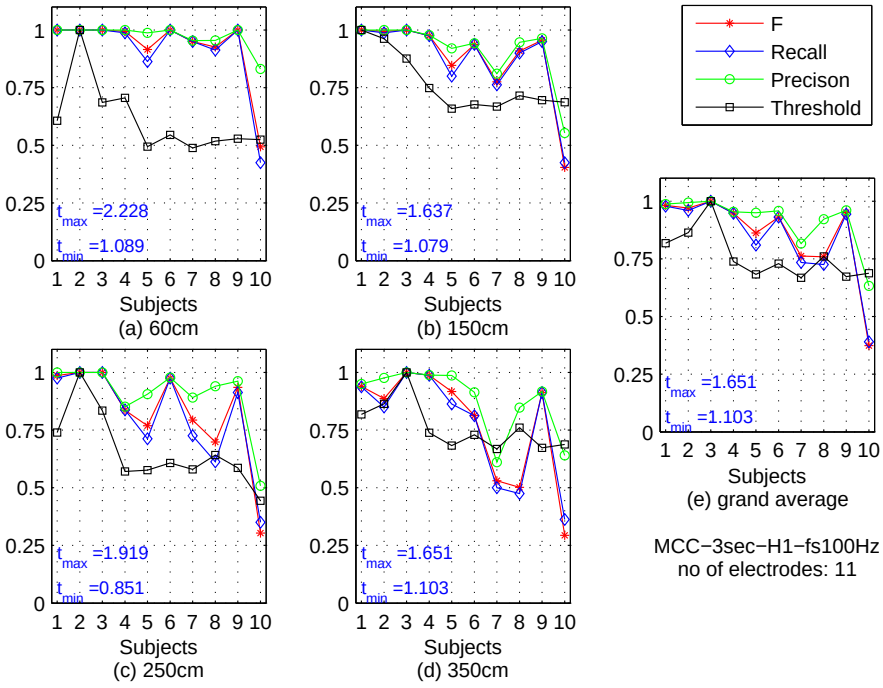

Figure B-86: **Mean optimised thresholds which maximise *F* measurements across the attended frequencies for each subject and the corresponding *F*, recall rates and precision rates.** This figure is based on MCC classification method.

Appendix C

Tables

Table C-1: **Frequency and duty cycle of Figure B-1.** The results of the frequencies and duty cycle are based on the sampling data of Figure B-1 and analysed by Matlab. f and D stand for frequency and duty cycle respectively.

	12Hz		**13Hz**		**14Hz**		**15Hz**	
	f (Hz)	**D (%)**	**f (Hz)**	**D (%)**	**f (Hz)**	**D (%)**	**f (Hz)**	**D (%)**
	11.99	50.12	12.99	50.13	14.01	50.14	15.02	50.15
	12.02	50.00	12.99	50.13	14.01	50.14	14.97	50.00
	12.02	50.00	12.99	50.13	14.01	50.14	14.97	50.00
	12.02	50.00	12.99	50.13	13.97	50.00	14.97	50.00
	12.02	50.00	13.02	50.00	14.01	49.86	14.97	50.00
	12.02	50.00	12.99	49.87	14.01	49.86	15.02	50.15
	12.02	50.00	12.99	49.87	13.97	50.00	15.02	50.15
	12.02	50.00	12.99	49.87	14.01	50.14	14.97	50.00
	12.02	50.00	12.99	49.87	14.01	50.14	14.97	50.00
	12.02	50.00	13.02	50.00	13.97	50.00	14.97	50.00
	-	-	12.99	50.13	14.01	49.86	14.97	50.00
	-	-	-	-	14.01	49.86	14.97	50.00
	-	-	-	-	-	-	14.97	50.00
Mean	**12.02**	**50.01**	**12.99**	**50.01**	**14.00**	**50.01**	**14.98**	**50.03**
SD(%)	**0.08%**	**0.08%**	**0.11%**	**0.25%**	**0.13%**	**0.25%**	**0.13%**	**0.13%**

Table C-2: **Frequency and duty cycle of Figure B-2.** The results of the frequencies and duty cycle are based on the sampling data of Figure B-2 and analysed by Matlab. f and D stand for frequency and duty cycle respectively.

	12Hz		**13Hz**		**14Hz**		**15Hz**	
	f (Hz)	**D (%)**	**f (Hz)**	**D (%)**	**f (Hz)**	**D (%)**	**f (Hz)**	**D (%)**
	12.02	50.00	13.02	50.00	14.01	49.86	15.02	50.15
	12.02	50.00	12.99	49.87	14.01	49.86	15.02	50.15
	12.02	50.00	12.99	49.87	13.97	50.00	14.97	50.00
	12.02	50.00	13.02	50.00	14.01	50.14	14.97	50.00
	12.02	50.00	12.99	50.13	14.01	50.14	14.97	50.00
	12.02	50.00	12.99	50.13	14.01	50.14	14.97	50.00
	12.02	50.00	12.99	50.13	14.01	50.14	15.02	50.15
	12.02	50.00	12.99	50.13	13.97	50.00	15.02	50.15
	11.99	50.12	13.02	50.00	14.01	49.86	14.97	50.00
	11.99	50.12	12.99	49.87	14.01	49.86	14.97	50.00
	-	-	12.99	49.87	13.97	50.00	14.97	50.00
	-	-	-	-	14.01	50.14	14.97	50.00
Mean	**12.01**	**50.02**	**13.00**	**50.00**	**14.00**	**50.01**	**14.99**	**50.05**
SD(%)	**0.08%**	**0.10%**	**0.12%**	**0.23%**	**0.13%**	**0.25%**	**0.15%**	**0.15%**

Table C-3: **Optimal electrode subsets distribution over the number of the electrodes and the highest classification rate of each subject across the attended frequencies and the viewing distances.** The percentage (%) in column 2 to 12 represents the ratio between the number of the optimal electrode subsets which result in the highest classification rate and the total electrode subsets of the corresponding electrode number. The column of column head Highest is the highest classification accuracy in the experiment condition. This table is based on MEC. The number of SSVEP harmonics is 1 and EEG TWL is 2s.

ele #	**1**	**2**	**3**	**4**	**5**	**6**	**7**	**8**	**9**	**10**	**11**	**Highest**
S1	7.95%	15.11%	25.95%	41.08%	55.07%	65.38%	71.57%	74.85%	75.57%	75.57%	75.00%	99.38%
S2	0.57%	4.09%	10.45%	19.96%	29.71%	39.88%	50.36%	60.68%	70.57%	79.55%	87.50%	96.88%
S3	10.80%	17.39%	31.02%	46.36%	59.88%	70.71%	78.41%	83.03%	86.25%	88.64%	93.75%	100.00%
S4	10.80%	10.11%	13.83%	19.17%	25.12%	32.49%	40.23%	47.69%	52.73%	57.39%	50.00%	97.19%
S5	1.70%	0.00%	0.27%	0.70%	2.35%	4.96%	8.84%	13.11%	17.39%	22.16%	25.00%	82.50%
S6	2.27%	5.00%	8.83%	13.75%	18.30%	22.56%	26.74%	29.81%	32.16%	34.09%	37.50%	95.63%
S7	0.00%	0.00%	0.27%	0.21%	0.46%	1.06%	1.89%	3.26%	4.09%	5.11%	6.25%	74.38%
S8	0.00%	0.11%	0.34%	1.46%	3.44%	7.13%	11.63%	17.01%	22.73%	28.98%	37.50%	82.50%
S9	0.57%	4.55%	7.05%	10.11%	13.88%	17.09%	19.70%	22.69%	26.36%	32.39%	37.50%	96.56%
S10	3.41%	0.11%	0.57%	0.70%	0.32%	0.20%	0.19%	0.34%	0.91%	1.70%	6.25%	57.19%

Table C-4: **Optimal electrode subsets distribution over the number of the electrodes and the highest classification rate of each subject across the attended frequencies and the viewing distances.** The percentage (%) in column 2 to 12 represents the ratio between the number of the optimal electrode subsets which result in the highest classification rate and the total electrode subsets of the corresponding electrode number. The column of column head Highest is the highest classification accuracy in the experiment condition. This table is based on MCC. The number of SSVEP harmonics is 1 and EEG TWL is 2s.

ele #	1	2	3	4	5	6	7	8	9	10	11	Highest
S1	7.95%	15.11%	25.95%	41.12%	54.94%	65.25%	71.59%	75.00%	75.57%	75.57%	75.00%	99.38%
S2	0.57%	4.09%	10.45%	19.94%	29.71%	39.88%	50.34%	60.80%	70.68%	80.11%	87.50%	96.88%
S3	11.36%	17.39%	30.91%	46.25%	59.79%	70.66%	78.37%	83.11%	86.36%	88.64%	93.75%	100.00%
S4	10.80%	10.45%	13.67%	19.11%	25.09%	32.54%	40.28%	47.50%	52.84%	57.39%	50.00%	97.19%
S5	1.70%	0.00%	0.27%	0.70%	2.35%	4.87%	8.77%	13.03%	17.05%	22.16%	25.00%	82.50%
S6	2.27%	4.77%	8.90%	13.75%	18.43%	22.77%	26.97%	29.89%	32.50%	34.09%	37.50%	95.63%
S7	0.00%	0.00%	0.27%	0.09%	0.47%	1.06%	1.70%	2.95%	3.98%	5.11%	6.25%	74.69%
S8	0.00%	0.11%	0.38%	1.65%	3.60%	7.41%	11.97%	17.80%	23.98%	31.82%	43.75%	82.50%
S9	0.57%	4.55%	7.20%	10.13%	13.87%	16.99%	19.72%	22.61%	25.91%	31.25%	31.25%	96.56%
S10	2.84%	0.11%	0.57%	0.72%	0.34%	0.20%	0.21%	0.38%	0.91%	1.70%	6.25%	57.19%

Table C-5: **The demographics of the minimal optimal electrodes of the subject across the attended frequencies and the viewing distances.** The number shown in the table presents the number of the corresponding electrodes being one of the electrodes in the minimal optimal electrode subset for the corresponding subject across the attended frequencies and viewing distances. This table is based on MEC with the first harmonics of SSVEP and 2s of EEG TWL.

ele	POz	Oz	Iz	124	125	O1	127	128	O9	O10	O2
S1	3	35	18	18	11	26	21	14	20	21	13
S2	10	52	5	18	19	36	25	9	7	4	36
S3	7	55	7	15	10	15	14	15	12	13	17
S4	10	35	13	12	7	8	10	11	10	8	27
S5	8	27	12	8	16	23	26	25	10	3	12
S6	22	60	18	13	12	16	8	13	12	15	15
S7	24	26	9	30	18	12	7	14	8	5	12
S8	14	21	5	14	6	13	6	11	9	6	17
S9	8	15	21	11	21	14	16	19	41	26	14
S10	12	12	12	8	5	13	11	10	10	11	7
Grand Total	118	**338**	120	147	125	**176**	144	141	139	112	**170**

Table C-6: **The demographics of the minimal optimal electrodes of the subject across the attended frequencies and the viewing distances.** The number shown in the table presents the number of the corresponding electrodes being one of the electrodes in the minimal optimal electrode subset for the corresponding subject across the attended frequencies and viewing distances. This table is based on MCC with the first harmonics of SSVEP and 2s of EEG TWL.

ele	POz	Oz	Iz	124	125	O1	127	128	O9	O10	O2
S1	3	35	18	18	11	26	21	14	20	21	13
S2	10	52	5	18	19	36	25	9	7	4	36
S3	7	55	7	15	10	15	14	15	12	13	17
S4	10	35	13	12	7	8	10	11	10	8	27
S5	8	27	12	8	16	23	26	25	10	3	12
S6	22	60	18	13	12	16	8	13	12	15	15
S7	24	26	9	30	18	12	7	14	8	5	12
S8	14	21	5	14	6	13	6	11	9	6	17
S9	8	15	21	11	21	14	16	19	41	26	14
S10	12	12	12	8	5	13	11	10	10	11	7
Grand Total	118	**338**	120	147	125	**176**	144	141	139	112	**170**

Table C-7: **Electrode Rankings for each subject by using the rule of leave–one–out across the attended frequencies and the viewing distances.** These electrode rankings are based on MEC spatial filter coefficients. The top two ranking are shared by the electrode 127 and 128. The last two rankings are either O10 or POz.

ele ranking	1	2	3	4	5	6	7	8	9	10	11
S1	128	127	Oz	Iz	124	O1	O2	O9	125	O10	POz
S2	127	128	124	O1	Oz	Iz	O2	O9	125	O10	POz
S3	128	127	Oz	Iz	O2	124	O9	125	O1	O10	POz
S4	128	127	124	Oz	O1	O2	125	Iz	O9	O10	POz
S5	128	127	124	Oz	O1	Iz	O2	O9	125	O10	POz
S6	128	127	124	Oz	O1	Iz	O2	O9	125	O10	POz
S7	127	128	124	Oz	O1	Iz	125	O2	O9	O10	POz
S8	127	128	124	O1	Oz	Iz	O2	O9	125	POz	O10
S9	128	127	124	O1	Oz	O2	Iz	O9	125	O10	POz
S10	127	128	124	O1	Oz	Iz	125	O9	O2	O10	POz

Table C-8: **Electrode Rankings for each subject by using the rule of leave–one–out across the attended frequencies and the viewing distances.** These electrode rankings are based on MCC spatial filter coefficients. The electrode rankings have at least two electrodes in the same order, Oz and O2 are the top two rankings and the last two ranking are mainly O1 and O10.

ele ranking	1	2	3	4	5	6	7	8	9	10	11
S1	Oz	O2	128	125	127	POz	O9	Iz	124	O10	O1
S2	Oz	O2	128	125	127	POz	124	O9	Iz	O10	O1
S3	Oz	O2	128	125	127	POz	124	Iz	O1	O9	O10
S4	Oz	O2	128	125	127	POz	Iz	O9	124	O1	O10
S5	Oz	O2	128	125	127	POz	O9	124	Iz	O10	O1
S6	Oz	O2	128	127	125	O9	Iz	124	POz	O10	O1
S7	Oz	O2	125	127	128	POz	124	O9	Iz	O1	O10
S8	Oz	O2	128	125	127	POz	O9	124	Iz	O1	O10
S9	Oz	O2	128	127	125	POz	124	O9	Iz	O10	O1
S10	Oz	O2	125	127	128	POz	O9	124	Iz	O1	O10

Table C-9: **Electrode rankings evaluation results across the subjects and experiment conditions. The electrode rankings are evaluated by comparing the ranked accuracies resulting from the ranked electrode sets and the corresponding highest, average and lowest accuracies of the same electrode number. PIs are listed in the last row of the table.** This table is based on MEC.

ele #	1	2	3	4	5	6	7	8	9	10	11
Ranking accuracies	52.21%	52.25%	57.34%	68.15%	70.53%	73.47%	76.15%	78.25%	77.59%	78.50%	79.75%
Highest	64.28%	78.78%	84.28%	85.97%	86.69%	87.06%	86.78%	86.06%	85.16%	83.25%	79.75%
Average	51.15%	54.84%	59.56%	64.24%	68.28%	71.63%	74.23%	76.17%	77.57%	78.67%	79.75%
Lowest	34.67%	28.02%	30.02%	33.08%	37.05%	42.74%	49.90%	58.00%	65.12%	71.75%	79.75%
PI	66.70%	52.50%	55.23%	70.12%	69.76%	70.88%	75.50%	81.33%	75.40%	79.32%	100.00%

Table C-10: **Electrode rankings evaluation results across the subjects and experiment conditions. The electrode rankings are evaluated by comparing the ranked accuracies resulting from the ranked electrode sets and the corresponding highest, average and lowest accuracies of the same electrode number. PIs are listed in the last row of the table.** This table is based on MCC.

ele #	1	2	3	4	5	6	7	8	9	10	11
Ranking accuracies	57.89%	60.34%	62.96%	68.59%	72.71%	76.75%	77.12%	77.34%	77.34%	79.59%	79.78%
Highest	64.21%	78.53%	84.25%	85.63%	86.56%	86.97%	86.59%	86.22%	84.94%	82.75%	79.78%
Average	51.14%	55.09%	59.67%	64.24%	68.18%	71.45%	74.01%	75.97%	77.51%	78.73%	79.78%
Lowest	34.73%	30.48%	31.96%	34.61%	37.36%	42.68%	49.59%	57.06%	64.93%	71.50%	79.78%
PI	84.20%	69.15%	66.94%	72.01%	75.55%	82.63%	80.89%	78.42%	73.50%	85.17%	100.00%

Table C-11: **PIs of individual subject corresponding to one electrode number when using the leave–one–out electrode rankings.** This table expands PIs of Table C-9 from the mean values to the details of each subject. The classification data of this table are based on MEC.

ele #	1	2	3	4	5	6	7	8	9	10	11
S1	63.07%	**37.50%**	89.43%	90.23%	78.10%	77.22%	86.95%	96.33%	93.98%	96.59%	100.00%
S2	69.89%	57.84%	**34.58%**	68.94%	80.07%	79.72%	94.41%	92.23%	86.93%	82.95%	100.00%
S3	72.16%	**34.66%**	90.08%	82.65%	86.92%	97.62%	88.98%	93.48%	92.50%	94.32%	100.00%
S4	71.02%	63.86%	**46.82%**	70.13%	71.27%	88.91%	87.23%	79.43%	73.18%	77.27%	100.00%
S5	65.91%	62.95%	**49.89%**	79.51%	77.07%	79.52%	84.28%	89.89%	83.75%	82.39%	100.00%
S6	**49.43%**	**44.43%**	53.37%	83.52%	83.02%	75.54%	81.67%	78.22%	82.61%	77.84%	100.00%
S7	69.89%	56.02%	67.35%	79.79%	73.63%	73.01%	65.17%	61.10%	57.27%	35.23%	100.00%
S8	70.45%	66.36%	**38.98%**	60.64%	71.86%	64.95%	80.30%	83.60%	56.59%	90.91%	100.00%
S9	63.64%	**41.48%**	**24.13%**	**19.68%**	**9.42%**	**8.06%**	**17.25%**	70.72%	77.05%	91.48%	100.00%
S10	71.59%	59.89%	57.69%	66.14%	66.29%	64.20%	68.71%	68.30%	50.11%	64.20%	100.00%

Table C-12: **PIs of individual subject corresponding to one electrode number when using the leave–one–out electrode rankings.** This table expands PIs of Table C-10 from the mean values to the details of each subject. The classification data of this table are based on MCC.

ele #	1	2	3	4	5	6	7	8	9	10	11
S1	94.32%	87.39%	87.77%	80.55%	97.36%	82.59%	87.71%	90.38%	93.30%	96.59%	100.00%
S2	87.50%	89.77%	77.80%	74.81%	94.05%	98.71%	98.01%	98.90%	100.00%	100.00%	100.00%
S3	97.73%	95.23%	91.06%	85.53%	90.79%	99.78%	99.51%	99.17%	98.07%	92.05%	100.00%
S4	94.89%	98.75%	93.67%	94.68%	92.90%	94.86%	92.65%	94.43%	95.34%	88.07%	100.00%
S5	79.55%	86.93%	75.95%	73.35%	76.83%	74.39%	68.79%	65.80%	71.59%	57.95%	100.00%
S6	97.73%	83.86%	83.07%	94.17%	85.54%	78.27%	78.26%	78.98%	82.39%	85.23%	100.00%
S7	64.77%	62.73%	67.12%	60.49%	52.23%	45.85%	87.14%	74.89%	76.59%	79.55%	100.00%
S8	73.86%	61.59%	57.05%	**30.70%**	**42.74%**	80.18%	70.53%	70.42%	65.57%	83.52%	100.00%
S9	76.14%	**26.14%**	**32.08%**	**16.19%**	**28.98%**	**41.59%**	**44.53%**	72.80%	63.52%	79.55%	100.00%
S10	75.57%	64.55%	58.48%	66.40%	56.25%	57.82%	65.98%	**47.27%**	66.70%	75.00%	100.00%

Table C-13: **PIs of individual subject corresponding to one electrode number using the leave–one–out electrode rankings of Table 5.7.** This table shows detail PIs of MEC in Table 5.8 from the mean values to the values of each subject.

ele #	1	2	3	4	5	6	7	8	9	10	11
S1	63.07%	**41.25%**	88.11%	87.16%	78.10%	77.22%	86.95%	96.33%	93.98%	96.59%	100.00%
S2	73.86%	60.11%	**40.19%**	68.94%	80.07%	79.72%	94.41%	92.23%	86.93%	82.95%	100.00%
S3	72.16%	**37.05%**	90.08%	82.65%	82.91%	92.42%	88.98%	93.48%	92.50%	94.32%	100.00%
S4	71.02%	65.57%	**46.82%**	74.72%	71.27%	88.91%	87.23%	79.43%	73.18%	77.27%	100.00%
S5	68.18%	60.57%	50.68%	77.29%	77.07%	77.22%	80.97%	85.87%	83.75%	82.39%	100.00%
S6	52.84%	**46.93%**	53.37%	83.52%	83.02%	75.54%	81.67%	73.56%	77.27%	77.84%	100.00%
S7	72.73%	61.25%	67.80%	79.58%	73.63%	73.01%	65.89%	61.10%	57.27%	**35.80%**	100.00%
S8	73.30%	71.14%	**43.52%**	63.62%	71.19%	66.04%	82.22%	86.82%	61.14%	90.91%	100.00%
S9	66.48%	**40.57%**	**23.07%**	**19.68%**	**11.32%**	**8.58%**	**17.25%**	66.63%	77.05%	87.50%	100.00%
S10	71.59%	58.64%	60.23%	69.64%	68.13%	68.17%	70.13%	68.30%	55.57%	67.05%	100.00%

Table C-14: **PIs of individual subject corresponding to one electrode number using the leave–one–out electrode rankings of Table 5.7.** This table shows detail PIs of MCC in Table 5.8 from the mean values to the values of each subject.

ele #	1	2	3	4	5	6	7	8	9	10	11
S1	94.32%	77.27%	85.87%	86.65%	74.70%	81.34%	93.54%	91.97%	92.16%	93.75%	100.00%
S2	87.50%	88.18%	76.36%	87.84%	96.35%	92.22%	87.97%	91.25%	88.30%	95.45%	100.00%
S3	97.73%	97.73%	91.02%	91.82%	99.85%	95.16%	99.51%	87.12%	88.52%	92.05%	100.00%
S4	94.89%	62.27%	81.93%	91.89%	92.14%	92.55%	87.84%	84.32%	78.86%	88.07%	100.00%
S5	79.55%	**46.82%**	**42.12%**	68.09%	78.58%	80.93%	83.73%	76.74%	84.66%	86.36%	100.00%
S6	97.73%	85.91%	89.09%	83.43%	90.87%	90.71%	83.88%	78.98%	77.05%	84.66%	100.00%
S7	64.77%	51.59%	58.90%	78.83%	72.04%	67.25%	66.86%	63.26%	56.14%	79.55%	100.00%
S8	73.86%	77.95%	62.54%	61.86%	90.71%	90.04%	72.61%	73.45%	70.57%	83.52%	100.00%
S9	76.14%	**29.89%**	**25.83%**	**16.19%**	**8.56%**	60.35%	65.61%	70.45%	60.57%	73.30%	100.00%
S10	75.57%	73.98%	62.65%	50.53%	56.60%	65.73%	61.57%	59.09%	**45.57%**	75.00%	100.00%